

The Propulsive Small Expendable Deployer System (ProSEDS)

NASA Grant NAG8-1605

Final Report

For the period 1 March 1999 through 31 December 2003

Principal Investigator

Enrico C. Lorenzini

December 2003

Prepared for

National Aeronautics and Space Administration
Marshall Space Flight Center, Alabama 35812

Smithsonian Institution
Astrophysical Observatory
Cambridge, Massachusetts 02138

The Smithsonian Astrophysical Observatory
is a member of the
Harvard-Smithsonian Center for Astrophysics

The Propulsive Small Expendable Deployer System (ProSEDS)

NASA Grant NAG8-1605

Final Report

For the period 1 March 1999 through 31 December 2003

Principal Investigator

Enrico C. Lorenzini

Co-Investigators

Mario L. Cosmo

Robert D. Estes

Collaborators

Juan Sanmartin

Jesus Peláez

Manuel Ruiz

December 2003

Prepared for

National Aeronautics and Space Administration

Marshall Space Flight Center, Alabama 35812

Smithsonian Institution

Astrophysical Observatory

Cambridge, Massachusetts 02138

The Smithsonian Astrophysical Observatory

is a member of the

Harvard-Smithsonian Center for Astrophysics

TABLE OF CONTENTS

LIST OF FIGURES 4

LIST OF TABLES..... 7

SCOPE 8

SUMMARY..... 9

1. BRIEF DESCRIPTION OF PROSEDS..... 12

 1.1 SYSTEM OVERVIEW..... 12

 1.2 EXPECTED RESULTS..... 13

2. MISSION ANALYSIS..... 17

 2.1 DEFINITION OF THE ORBIT 17

 2.2 TETHER-GENERATED POWER 25

3. DYNAMICS REFERENCE MISSION..... 27

 3.1 SIMULATION MODEL..... 27

 3.2 DISCRETIZATION AND VIBRATIONAL MODES..... 27

 3.3 REFERENCE MISSION SIMULATION..... 29

 3.4 CONCLUDING REMARKS..... 42

4. DYNAMICS STABILITY..... 43

 4.1 DUMBBELL TETHER SYSTEM SUBJECTED TO ED FORCES..... 43

 4.1 PROSEDS-TYPE SYSTEM SUBJECTED TO ED FORCES 46

 4.3 CONCLUDING REMARKS..... 47

5. DEPLOYMENT CONTROL..... 49

 5.1 CONTROL LAW 49

 5.2 REFERENCE PROFILES 54

 5.3 MITIGATION OF TENSION SPIKE AT END OF DEPLOYMENT 63

 5.4 CONCLUDING REMARKS..... 65

6. UPDATED SYSTEM PERFORMANCE..... 66

 6.1 INTRODUCTION..... 66

 6.2 UPDATED VALUES OF DECAY RATES..... 66

7. UPDATED MISSION ANALYSIS..... 68

 7.1 EFFECTS OF A LOWER ORBIT..... 68

 7.2 ATOMIC OXYGEN TETHER EROSION..... 70

8. UPDATED DYNAMICS REFERENCE MISSION..... 73

 8.1 REFERENCE MISSION SIMULATION..... 73

 8.2 EXTREME CASES 82

 8.3 CONCLUDING REMARKS..... 85

9. UPDATED DEPLOYMENT CONTROL PROFILES AND SIMULATIONS..... 86

 9.1 INTRODUCTION..... 86

 9.2 FRICTION PARAMETERS..... 87

9.3 CONTROL PARAMETERS.....	89
9.4 REFERENCE TABLES.....	90
9.5 VALIDATION PROCESS.....	99
9.4 CONCLUDING REMARKS.....	126
10. UPDATED REFERENCE MISSION.....	127
10.1 INTRODUCTORY REMARKS.....	127
10.2 NEW MISSION PARAMETERS AND CURRENT OPERATING CYCLES.....	127
10.3 APPLICABILITY OF RESULTS TO LATER LAUNCH DATES.....	135
10.4 EXTREME ELECTRODYNAMIC FORCING.....	137
10.5 CONCLUDING REMARKS.....	143
11. EVALUATION OF POWER DELIVERED BY THE TETHER.....	144
11.1 INTRODUCTION.....	144
11.2 NUMERICAL RESULTS.....	144
11.3 CONCLUDING REMARKS.....	145
12. DEPLOYMENT CONTROL PROFILE REF. #78 AND SIMULATIONS.....	146
12.1 INTRODUCTION.....	146
12.2 FRICTION MODEL.....	146
12.3 FLIGHT REFERENCE TABLE.....	148
12.4 FLIGHT CONTROL LAW BACKUP MODES AND PARAMETERS.....	153
12.5 SENSITIVITY OF CONTROL LAW TO FRICTION PARAMETERS.....	156
12.6 CONCLUDING REMARKS.....	163
13. KALMAN FILTERS FOR MISSION ESTIMATION.....	164
13.1 INTRODUCTION.....	164
13.2 MAGNETOMETER DATA KALMAN FILTER.....	164
13.3 POSITION/CURRENT DATA KALMAN FILTER.....	167
14. ANALYSIS/ESTIMATION OF DEPLOYMENT FLIGHT DATA.....	170
14.1 INTRODUCTION.....	170
14.2 NUMERICAL RESULTS.....	171
14.3 CONCLUDING REMARKS.....	172
15. COMPARISON OF ED TETHERS AND ELECTRICAL THRUSTERS.....	173
15.1 INTRODUCTION.....	173
15.2 COMPARISONS.....	173
15.3 CONCLUSIONS.....	175
16. DYNAMICS ANALYSIS FOR MISSION STARTING AT LOWER ALTITUDE	176
16.1 INTRODUCTORY REMARKS.....	176
16.2 DYNAMICS ANALYSIS.....	176
16.2 CONCLUDING REMARKS.....	180
17. DEPLOYMENT PERFORMANCE AT A LOWER ALTITUDE.....	181
17.1 DEPLOYMENT ANALYSIS.....	181
17.2 CONCLUDING REMARKS.....	182
18. SATELLITE ORBIT AFTER TETHER CUT.....	183
18.1 INTRODUCTORY REMARKS.....	183
18.2 NUMERICAL CASES.....	183
18.3 CONCLUDING REMARKS.....	186

19. DEPLOYMENT WITH SHORTER DYNEEMA TETHER LENGTH.....	187
19.1 INTRODUCTORY REMARKS.....	187
19.2 DEPLOYMENT PROFILES FOR SHORTER TETHER LENGTHES	187
19.3 CONCLUDING REMARKS.....	192
20. INTERACTIVE SOFTWARE FOR ED TETHERS.....	193
20.1 GOALS	193
20.2 BRIEF DESCRIPTION.....	193
20.2 DELIVERED SOFTWARE	197
20.3 BRIEF DESCRIPTION OF FINAL PRODUCT	197
PAPERS PUBLISHED OR PRESENTED AT CONFERENCES.....	200
REFERENCES.....	202

LIST OF FIGURES

Figure 1 ProSEDS schematic12

Figure 2 Reentry time vs. average tether current for F10.7 with 50% percentile ionospheric density in August 2000 and a starting altitude of 400 km15

Figure 3 Decay profiles for Delta stage with and without ProSEDS.....16

Figure 4 ProSEDS Descending Node Orbits for Different Values of Probability of Achieving Orbit (PCS) [The Boeing Company]18

Figure 5 ProSEDS Ascending Node Orbits for Different PCS Values of Probability of Achieving Orbit (PCS) [The Boeing Company]19

Figure 6 Results for descending node orbit 340x600 km – Case 1 (Min. Solar).....21

Figure 7 Results for descending node orbit 400x650 km – Case 2 (Min. Solar).....22

Figure 8 Results for ascending node orbit 375x410 km – Case 3 (Min. Solar).....23

Figure 9 Results for ascending node orbit 400x400 km – Case 4 (Min. Solar).....24

Figure 10 Tether average current for the descending node cases compared to the reference case 4 during one week (Solar Min.)26

Figure 11 Smoothed shapes of first 4 eigenvectors (lateral dynamics).....28

Figure 12 EPT Sequence 1 (60-sec cycle) - Operation on Primary Battery.30

Figure 13 EPT Sequence 2 (80-sec cycle) - Operation on Secondary Battery.30

Figure 14 Ground trace of preliminary Delta 7925 Block IIR trajectory [The Boeing Company].....32

Figure 15 Results for day-launch and circularization burn over Antigua.....33

Figure 16 Results for day-launch and circularization burn over Antigua.....34

Figure 17 Results for day-launch and circularization burn over Antigua.....35

Figure 18 Results for day-launch and circularization burn over Antigua.....36

Figure 19 Results for night-launch and circularization burn over Antigua37

Figure 20 Results for night-launch and circularization burn over Antigua38

Figure 21 Results for night-launch and circularization burn over Antigua39

Figure 22 Results for night-launch and circularization burn over Antigua40

Figure 23 3-D trajectory of endmass of a dumbbell tether system undergoing a librational instability44

Figure 24 State-space trajectory in the potential surface. The in-plane angle θ (rad) and out-of-plane angle ϕ (rad) are on the x and y axes. The out-of-plane angle grows large and forces an in-plane libration instability45

Figure 25 Effect of increasing orbital inclination on the trajectory of the tip of the wire and the endmass. For increasing inclination the amplitude of the ED-forced-motion (eight-shaped trajectories) increases.....46

Figure 26 Effect of increasing ED-force/gravity-gradient ratio on the trajectory of the tip of the wire and endmass. For increasing values of the ratio the amplitude of the ED-forced-motion (eight-shaped trajectories) increases47

Figure 27 Diagram of deployment closed-loop control system.....52

Figure 28 Deployment Reference Profile #9.....56

Figure 29 Deployment Reference Profile #18.....57

Figure 30 Deployment Reference Profile #21.....58

Figure 31 Deployment Reference Profile #26.....59

Figure 32 Final libration amplitude vs. T_0 (leader tether) for selected deployment profiles60

Figure 33 Sensitivity of deployment dynamics to T_0 (Ref#26)61

Figure 34 Sensitivity of tether tension to minimum tension (Ref#26).....62

Figure 35 Tension vs time following a hard stop at 15-km tether length (EA = 15,000 N) .63

Figure 36 Braking profile for tension spike mitigation64

Figure 37 13-month smoothed F10.7 radio flux [from MSAFE NASA/MSFC].....66

Figure 38 Decay rates of ProSEDS for various altitude and operational scenarios with a launch in August 2001	69
Figure 39 Ratio of average electro/aero forces vs. altitude.....	70
Figure 40 Atomic oxygen density (number-of-atoms/m ³) vs. mission time for nominal atmospheric conditions.....	71
Figure 41 AO mass flux integrated over mission time (start altitude = 400 km)	71
Figure 42 Ground trace of (August 2001) Delta 7925 Block IIR trajectory [adapted from The Boeing Company].....	76
Figure 43 Results for day-launch with launch date on 16 August 2001.....	77
Figure 44 Results for day-launch with launch date on 16 August 2001.....	78
Figure 45 Results for day-launch with launch date on 16 August 2001.....	79
Figure 46 Results for day-launch with launch date on 16 August 2001.....	80
Figure 47 Results for day-launch with launch date on 16 August 2001.....	81
Figure 48 System decay and geographic position (latitude and longitude) for double the nominal plasma density on 16 August 2001.....	83
Figure 49 System decay and geographic position (latitude and longitude) without any electrodynamic forces for a launch on 16 August 2001.....	84
Figure 50 Reference profile Ref#47 (without slow down maneuver).....	92
Figure 51 Reference profile Ref#55 (without slow down maneuver).....	93
Figure 52 Deployment dynamics for Ref#55 for T ₀ = 0 mN.....	95
Figure 53 Deployment dynamics for Ref#55 for T ₀ = 10 mN (nominal).....	96
Figure 54 Deployment dynamics for Ref#55 for T ₀ = 20 mN.....	97
Figure 55 Final libration amplitude vs. T ₀ for selected deployment profiles.....	98
Figure 56 Nominal minimum tension T ₀ = 10 mN.....	100
Figure 57 Nominal minimum tension T ₀ = 10 mN (MASTER vs. DUMBELL).....	101
Figure 58 Nominal minimum tension T ₀ = 10 mN.....	102
Figure 59 Nominal minimum tension T ₀ = 10 mN.....	103
Figure 60 Nominal minimum tension T ₀ = 10 mN.....	104
Figure 61 Nominal minimum tension T ₀ = 10 mN.....	105
Figure 62 Nominal minimum tension T ₀ = 10 mN.....	106
Figure 63 Minimum tension T ₀ = 5 mN (MASTER vs. DUMBELL).....	107
Figure 64 Minimum tension T ₀ = 5 mN.....	108
Figure 65 Minimum tension T ₀ = 5 mN.....	109
Figure 66 Minimum tension T ₀ = 20 mN.....	110
Figure 67 Minimum tension T ₀ = 20 mN (MASTER vs. DUMBELL).....	111
Figure 68 Minimum tension T ₀ = 20 mN.....	112
Figure 69 Minimum tension T ₀ = 20 mN.....	113
Figure 70 No brake is activated throughout deployment.....	114
Figure 71 No brake is activated throughout deployment.....	115
Figure 72 Wire inertia multiplier = 2.5.....	117
Figure 73 Wire inertia multiplier = 2.5.....	118
Figure 74 Wire inertia multiplier = 2.5.....	119
Figure 75 Wire inertia multiplier = 2.5.....	120
Figure 76 Wire inertia multiplier = 2.5.....	121
Figure 77 Wire inertia multiplier = 3.5.....	122
Figure 78 Wire inertia multiplier = 3.5.....	123
Figure 79 Wire inertia multiplier = 3.5.....	124
Figure 80 Wire inertia multiplier = 3.5.....	125
Figure 81 Wire inertia multiplier = 3.5.....	126
Figure 82 Operating cycle #1 (60-sec cycle) - Operation on Primary Battery.....	128
Figure 83 New operating cycle #2 (80-sec cycle) - Operation on Secondary Battery.....	128
Figure 84 Simulation results for Summer 2002 launch; nominal solar condition.....	130
Figure 85 Simulation results for Summer 2002 launch; nominal solar condition.....	131
Figure 86 Simulation results for Summer 2002 launch; nominal solar condition.....	132

Figure 87 Simulation results for Summer 2002 launch; nominal solar condition.....	133
Figure 88 Simulation results for Summer 2002 launch; nominal solar condition.....	134
Figure 89 Sunspot number predictions [NASA MSFC].....	136
Figure 90 Ionospheric Global Index (IG) prediction [Rutherford Appleton laboratory]....	136
Figure 91 Results for Summer 2002 launch, plasma density twice nominal.....	138
Figure 92 Results for Summer 2002 launch, plasma density twice nominal.....	139
Figure 93 Results for Summer 2002 launch, plasma density twice nominal.....	140
Figure 94 Results for Summer 2002 launch, plasma density twice nominal.....	141
Figure 95 Results for Summer 2002 launch, plasma density twice nominal.....	142
Figure 96 Tether current during battery charging mode: instant value and 12-hour average	144
Figure 97 Control law Reference Profile #78.....	153
Figure 98 Deployment dynamics for Ref#78 and $T_0 = 5$ mN.....	158
Figure 99 Deployment dynamics for Ref#78 and $T_0 = 10$ mN.....	159
Figure 100 Deployment dynamics for Ref#78 and $T_0 = 20$ mN (reference).....	160
Figure 101 Deployment dynamics for $T_0 = 20$ mN with $\pm 50\%$ tension white noise.....	161
Figure 102 Deployment trajectory of the endmass with respect to the Delta stage.....	162
Figure 103 Final libration amplitude vs. T_0 with control (Ref. #78) and without control..	163
Figure 104 Estimated Bias Components (SEDS-1 Flight Data).....	165
Figure 105 Magnetometer Y Component - Estimated vs. Measured (SEDS-I Flight Data)	166
Figure 106 Estimated vs. Actual Proseds Semi-major Axis (MASTER simulation).....	168
Figure 107 Estimated Average vs. Current Measured at Delta (MASTER simulation).....	168
Figure 108 Estimated Proseds EMF (MASTER simulation).....	169
Figure 109 Deployment trajectory of endmass: estimated from noisy turn counter data (solid line); and original data (dotted line).....	171
Figure 110 Comparison of EDT (a, b) and Electrical Thrusters (c, d) with Dedicated Solar Power System.....	174
Figure 111 Comparison of EDT (a, b) and Electrical Thrusters (c, d) without Dedicated Solar Power System.....	175
Figure 112 ProSEDS decay with atmospheric and ED drag.....	177
Figure 113 ProSEDS decay with atmospheric drag only.....	177
Figure 114 Comparison of atmospheric and ED forces acting on ProSEDS.....	178
Figure 115 Comparison of orbit-average atmospheric and ED forces on ProSEDS.....	178
Figure 116 Neutral density vs. time.....	179
Figure 117 Atomic oxygen vs. time.....	179
Figure 118 Final libration amplitude vs. Dyneema minimum tension.....	182
Figure 119 Effect of a tether cut for a circular orbit.....	184
Figure 120 Effect of a tether cut at apogee for the max. expected eccentricity.....	185
Figure 121 Effect of a tether cut at preigee for the max. expected eccentricity.....	185
Figure 122 Deployemnt reference profile for an overall tether length of 12 km.....	188
Figure 123 Deployemnt reference profile for an overall tether length of 11 km.....	189
Figure 124 Deployemnt reference profile for an overall tether length of 10 km.....	190
Figure 125 Deployemnt reference profile for an overall tether length of 8 km.....	191
Figure 126 The simulation setup window for defining the system.....	194
Figure 127 Starting orbit setup window with boost system setup in background.....	195
Figure 128 An orbit raising simulation showing altitude in km versus days.....	196
Figure 129 The simulation setup window for defining the system.....	198
Figure 130 Starting orbit setup window with boost system setup in background.....	199

LIST OF TABLES

Table 1 ProSEDS Success Criteria.....	14
Table 2 First-week decay rate for Cases 1-4 (Solar Min.).....	20
Table 3 First-week tether average current for Cases 1-4 (Solar Min.).....	25
Table 4 First 12 eigenvalues of ProSEDS (linearized system).....	28
Table 5 Characteristics of selected reference profiles.....	55
Table 6 Decay rates for different launch dates.....	67
Table 7 ProSEDS position errors after 24 hours.....	82
Table 8 Characteristics of selected reference profiles.....	94
Table 9 Updated control parameters for Reference Profile #78.....	155

SCOPE

This is the Final Report for Grant NAG8-1605 entitled "The Propulsive Small Expendable Deployer System (ProSEDS)" prepared by the Smithsonian Astrophysical Observatory for NASA Marshall Space Flight Center. The technical officer for this grant is Randy Baggett; the Program Manager for the ProSEDS project is Leslie Curtis. The Final Report covers the period of activity from 1 March 1999 through 31 December 2003.

SUMMARY

This Final Report covers the following main topics:

1. Brief Description of ProSEDS

Short introduction to the ProSEDS system with a discussion of the criteria for success, the expected results and the expected performance.

2. Mission Analysis

Analysis to define a suitable orbit for ProSEDS based on the probability of achieving the orbit (determined by Boeing) with the goal of evaluating the system dynamics, stability and the power generated by the tether for various orbital options under worst case ionospheric conditions.

3. Dynamics Reference Mission

The reference ProSEDS mission is evaluated for two different launch times (day launch and night launch). Simulations are run for nominal solar activity condition at the time of launch. Simulations include the dynamics of the system, the electrodynamics of the bare tether, the neutral atmosphere and the thermal response of the tether inclusive of all the relevant thermal inputs and outputs.

4. Dynamics Stability

The stability of an electrodynamic (ED) tethered satellite, either with a single ED tether or with the ProSEDS configuration, is analyzed in general terms to identify the parameters that drive the long-term instability and the rate of growth.

5. Deployment Control

The control law for ProSEDS deployment is described inclusive of its closed-loop portion (leader tether) and open-loop portion (insulated tether). The performance of a

selection of reference profiles, for different values of endmass ejection velocity, is shown together with expected tension spikes at the end of deployment with and without mitigation.

6. Updated System Performance

Comparative analysis of the decay rate expected for ProSEDS for various launch dates.

7. Updated Mission Analysis

Analysis to define the effect of a lower orbital altitude on the environmental forces acting on ProSEDS. Evaluation of the altitude at which the atomic oxygen is expected to damage the Dyneema tether.

8. Updated Dynamics Reference Mission

The reference ProSEDS mission is evaluated for the updated launch date. Simulations are run for nominal solar activity condition at the time of launch. Simulations include the dynamics of the system, the electrodynamics of the bare tether, the neutral atmosphere and the thermal response of the tether.

9. Updated Deployment Control Profiles and Simulations

Selected deployment profiles are compared in terms of their deployment performance. The flight profile is derived based on the latest friction characteristics obtained from deployment tests.

10. Updated Reference Mission

The reference ProSEDS mission is evaluated for an updated launch date in the Summer of 2002 and for the new 80-s current operating cycle. Simulations are run for nominal solar activity condition at the time of launch and for extreme conditions of dynamic forcing. Simulations include the dynamics of the system, the electrodynamics of the bare tether, the neutral atmosphere and the thermal response of the tether.

11. Evaluation of power delivered by the tether

The power delivered by the tethered system during the battery charging mode is computed under the assumption of minimum solar activity for the new launch date.

12. Deployment Control Profile Ref. #78 and Simulations

The flight deployment profile (Ref. #78) is derived based on the friction characteristics obtained from deployment tests of the F-1 tether ($L = 15$ km). Results of computer simulations are shown to demonstrate the robustness of the control law.

13. Kalman filters for mission estimation

Development of two Kalman filters for estimation of system position from GPS data and attitude from magnetometer data.

14. Analysis/estimation of deployment flight data

A process was developed to estimate the deployment trajectory of the endmass with respect to the Delta and the final libration amplitude from the data of the deployer turn counters. This software was tested successfully during the ProSEDS mission simulation at MSFC EDAC.

15. Comparison of ED tethers and electrical thrusters

A comparison between electrical thrusters and electrodynamic bare tethers which takes into account the energy conversion efficiency and the mass of the hardware involved.

16. Dynamics Analysis for Mission Starting at a Lower Altitude

Analysis of the decay rate of ProSEDS when starting the mission at a lower altitude.

17. Deployment Performance at a Lower Altitude

Analysis of the deployment control law performance when deploying at a lower altitude.

18. Satellite orbit after a tether cut

Evaluation of the satellite orbit after a tether cut occurring at different orbital locations.

19. Deployment with shorter Dyneema tether length

Derivation of four different reference profiles for lengths shorter than 15 km.

20. Interactive software for ED tethers

The development process and features of the software delivered to NASA are briefly described.

1. BRIEF DESCRIPTION OF PROSEDS

1.1 System Overview

As presently planned, ProSEDS will be carried into a 400 km orbit as a Delta-II secondary payload. It will use a SEDS deployer to deploy upward a tether made up of two main parts (see Fig. 1): the non-conductive leader tether and the metallic bare tether. First a 10 km nonconductive leader tether with an endmass will be deployed followed by the 5 km of bare metallic tether, which is used to collect electrons. A hollow cathode will maintain electrical connection with the plasma at the Delta platform.

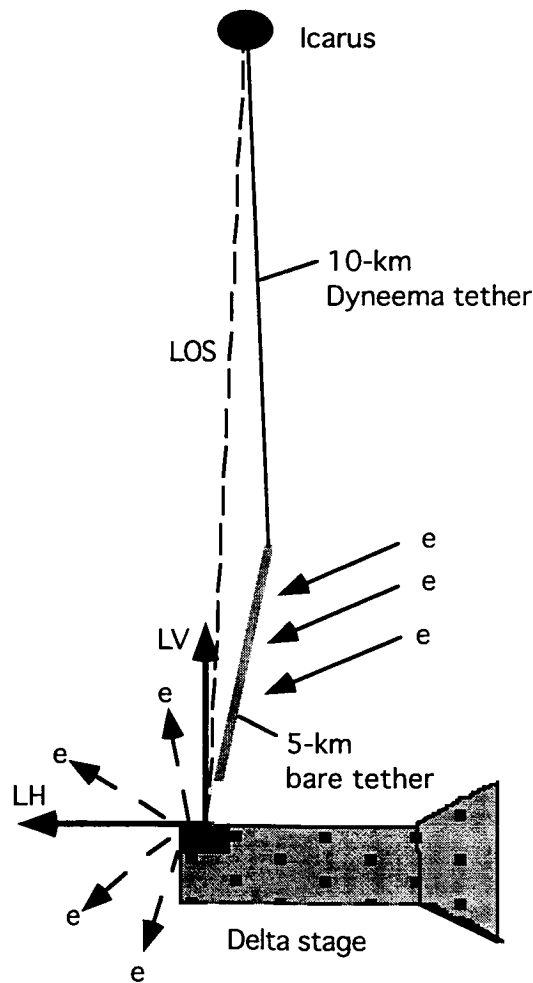


Figure 1 ProSEDS schematic

ProSEDS flies as secondary payload on a Delta II rocket carrying a GPS satellite as primary payload. The total mass allowed for secondary payloads on a GPS Delta mission is only 102 kg (225 lb). The volume is also limited to the annular space between the Delta 2nd stage and its outer fairing. ProSEDS utilizes the already-built SEDS deployer which has a volume of about 10,160 cc for the tether spool. The volume and mass constraint associated with the characteristics of the SEDS deployer makes the system and the tether design rather challenging.

ProSEDS will use a bare tether as the anode to collect the ionospheric electrons. From theoretical estimates and plasma chamber tests it appears that a bare tether can collect a much higher current per unit of collecting area than the spherical termination anode (like those adopted in the TSS program). References^{1 2 3 4 5} should be consulted for the fundamentals of current collections by a bare tether anode.

1.2 Expected Results

The goals of the mission are to demonstrate high current collection by a bare tether to accelerate significantly the orbital decay of the Delta stage through the electrodynamic drag.

The success of ProSEDS will mainly be judged on whether or not it sets new standards in current collection by an electrodynamic tethered system. It is not necessary that the experiment attain current levels that would directly be useful in the ultimate applications, but ProSEDS should attain current levels closely approaching the theoretical predictions of orbital motion limited (OML) current collection by a thin wire. Or, if there are deviations from the predictions, there should be sufficient data on plasma and magnetic conditions to determine where modifications to the theory need to be made, so that reasonable estimates for system performance for useful applications can be made. There must in the end be a convincing case for proceeding to the next level of development of the bare tether concept.

One of the primary success criteria of ProSEDS (see Table 1) is for the Delta stage with ProSEDS attached to attain a decay rate greater than 5 km/day. Another success criteria is for the ProSEDS tether to generate enough power to keep the system going, in a self-sustaining mode, after the lifetime of the primary batteries has been exhausted. The complete set of success criteria is shown in Table 1.

Table 1 ProSEDS Success Criteria

OBJECTIVES	CRITERIA FOR SUCCESS	MSMT REQUIRED	INSTRUMENTS REQUIRED
(Primary) Demonstrate significant, measurable electrodynamic tether thrust in space.	Demonstrate an orbital decay rate of 5 km per day.	Change Of Orbital Position.	Ground RADAR Ground telescopes (GPS)
(Primary) Measure the current collection performance of the bare electrodynamic tether under varied ionospheric conditions and determine its scalability to future applications.	Obtain data over 16 orbits. (Obtain continuous data for the first 3 orbits and sampling over the remaining 13.)	Voltage Current Magnetic Field Orientation Spacecraft Potential Plasma Density Ambient Electron Temperature Absolute position of Delta Relative position of Tether (estimation)	Voltmeter Ammeter Aspect Magnetometer Langmuir Probe, DIFP Langmuir Probe, DIFP Langmuir Probe Ground RADAR Turns Counter*
(Secondary) Demonstrate the regulation, storage and use of tether generated electrical power	Battery recharging.	Battery Temperature Voltage Current	Thermistor Voltmeter Ammeter
(Secondary) Determine system performance during the extended mission phase (begins after orbit 16).	Collect available tether performance data.	Telemetry (if available) Change of Orbital Position	All functioning instruments Ground RADAR Ground Telescopes
(Secondary) Assess tether survivability in Atomic Oxygen, meteoroid and orbital debris environment.	Observe tether integrity.	Tether observation(s) Voltage Current	Ground RADAR & telescopes Voltmeter** Ammeter**

* Provides Deployment Rate. Deployment provides tether orientation in order to calibrate EMF measurement.
EMF acts as a tether relative position sensor.

** If functioning (especially during extended mission phase)

Figure 2 shows the effect of the tether current on the reentry time of the Delta 2nd stage. The estimated reentry time is plotted vs. the *average current along the tether* which, for a tether like ProSEDS, is about 30% lower than the tether current measured at the Delta. The present estimate of ProSEDS tether current measured at the Delta is slightly more than 0.8 Amp which corresponds to an average current along the tether of 0.55 Amp.

Figure 3 shows a comparison of the reentry profiles of the Delta 2nd stage with and without ProSEDS for a system mass of about 1100 kg. In this computation it was assumed, rather optimistically, that the ProSEDS non-conductive tether would survive the Atomic Oxygen erosion at altitudes below 200-250 km during the extended mission phase. The full reentry of the Delta stage is not a mission goal. In general, we can say that ProSEDS will strongly accelerate the reentry of the Delta 2nd stage. At the start altitude of 400 km, the electrodynamic force overpowers the atmospheric drag by a factor greater than 10. The electrodynamic forces will dominate the reentry down to an altitude of roughly 250 km where the ProSEDS tether is no longer expected to survive. ProSEDS is in fact a demonstrator of the bare tether anode and its ability to collect electrons at a much higher rate than an equivalent-area spherical termination.

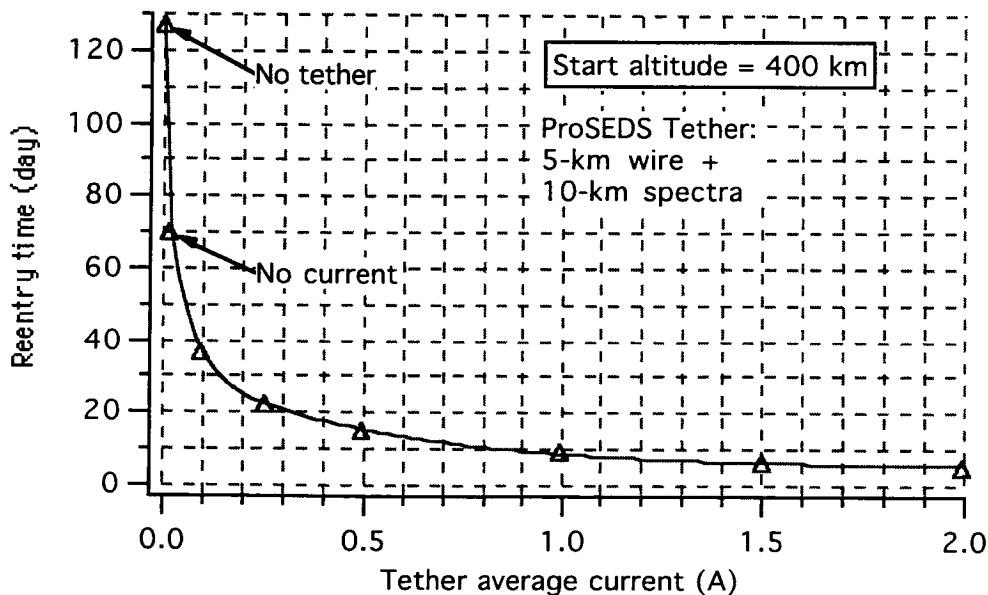


Figure 2 Reentry time vs. average tether current for F10.7 with 50% percentile ionospheric density in August 2000 and a starting altitude of 400 km

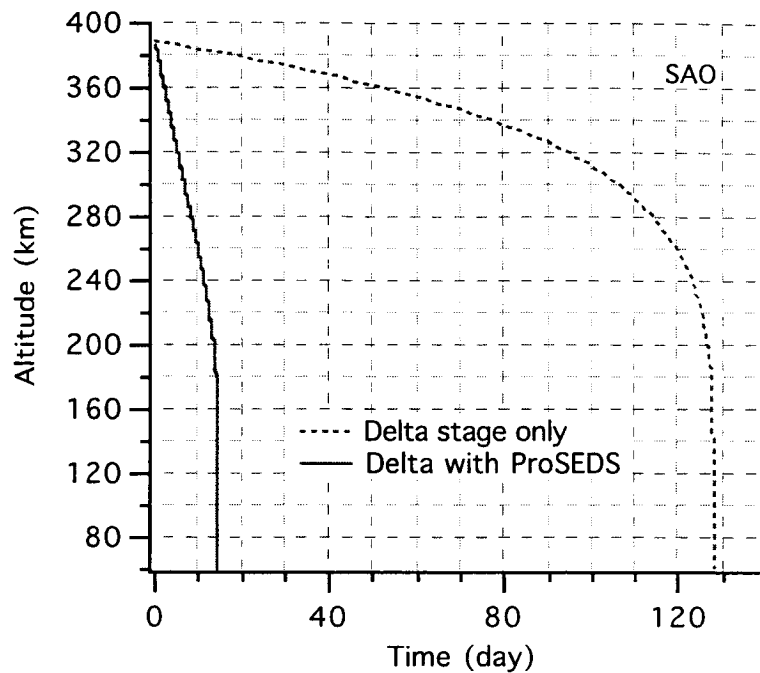


Figure 3 Decay profiles for Delta stage with and without ProSEDS

The main measure of ProSEDS success will be the decay rate of the Delta stage which is increased by an order of magnitude with respect to the Delta stage natural decay. As said previously, the success criteria for the Delta stage with ProSEDS sets a value for the decay rate greater than 5 km/day.

2. MISSION ANALYSIS

2.1 Definition of the Orbit

The power (and decay rate) produced by a tethered system depends on the plasma density which in turn depends on the orbital altitude and the position of the spacecraft with respect to the Sun. The orbital parameters of ProSEDS must be chosen in a way to enable the tether to produce enough current (per orbit) for recharging the secondary batteries to supply electrical power to the on-board equipment.

From an analysis done by The Boeing Company on the probabilities (PCS) of delivering the secondary payload to the desired orbit, it appears that the descending node orbits have $PCS < 90\%$ while the ascending node orbits have $PCS > 90\%$. A few descending node cases and ascending node cases have been simulated in order to assess the system dynamics, decay rates and power budgets.

The descending node case analyzed are elliptical orbits which have values of $PCS > 95\%$ (the circular and low-eccentricity orbits do not meet the level of acceptable probability). The ascending node cases are either low-eccentricity or circular orbits which also have values of $PCS > 99\%$. The cases in questions are as follows:

Descending-node cases (PCS > 95%)

Case 1: 340x600 km orbit

Case 2: 400x650 km orbit

Ascending-node cases (PCS > 99%)

Case 3: 375x410 km orbit

Case 4: 400x400 km orbit

Figures 4-5 (courtesy of Boeing) show the probabilities of the secondary payload to achieve orbit (PCS) for descending and ascending node orbits, respectively. The descending node cases with $PCS > 95\%$ (not shown in Fig. 2) are all orbits with relatively high eccentricity while the ascending node cases with $PCS > 99\%$ can be low-eccentricity or circular orbits.

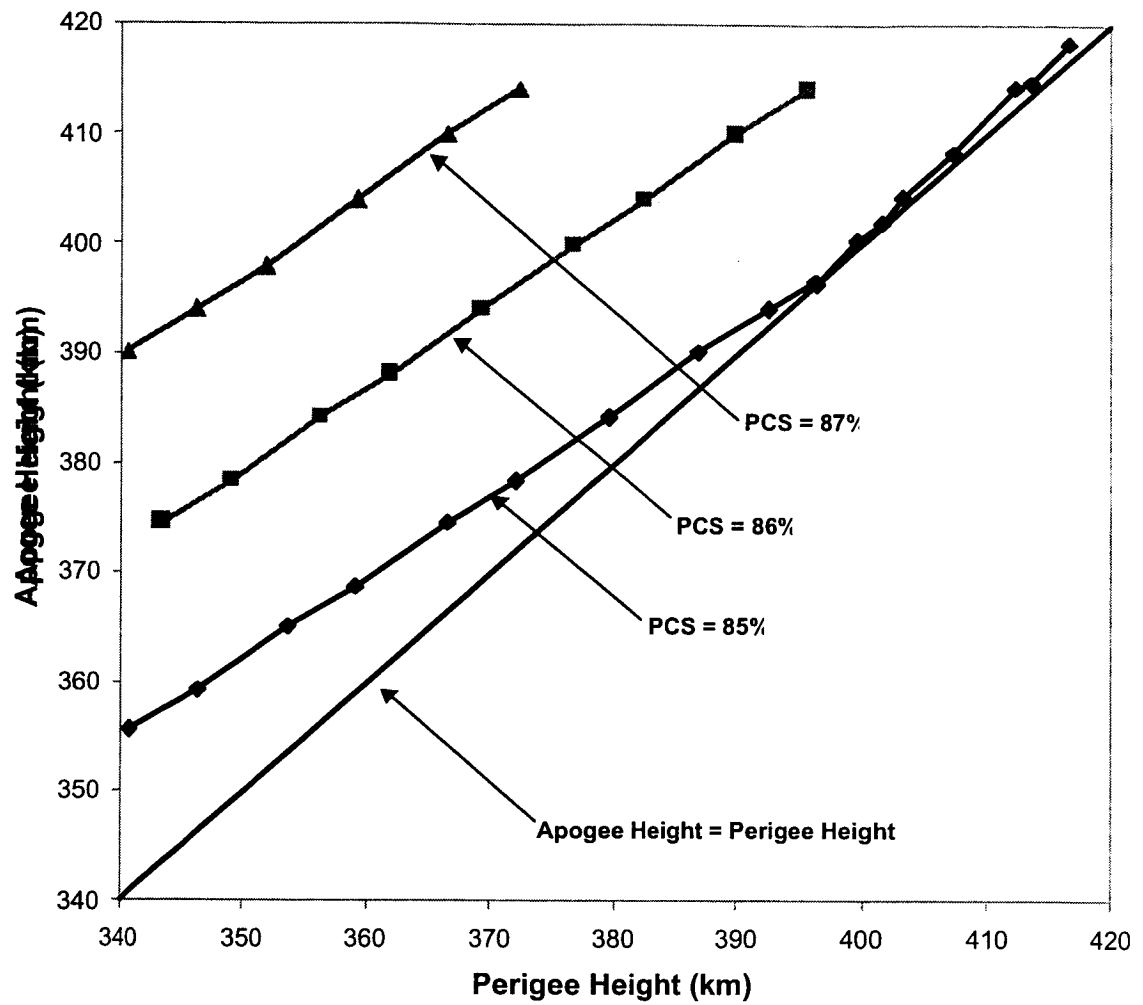


Figure 4 ProSEDS Descending Node Orbits for Different Values of Probability of Achieving Orbit (PCS) [The Boeing Company]

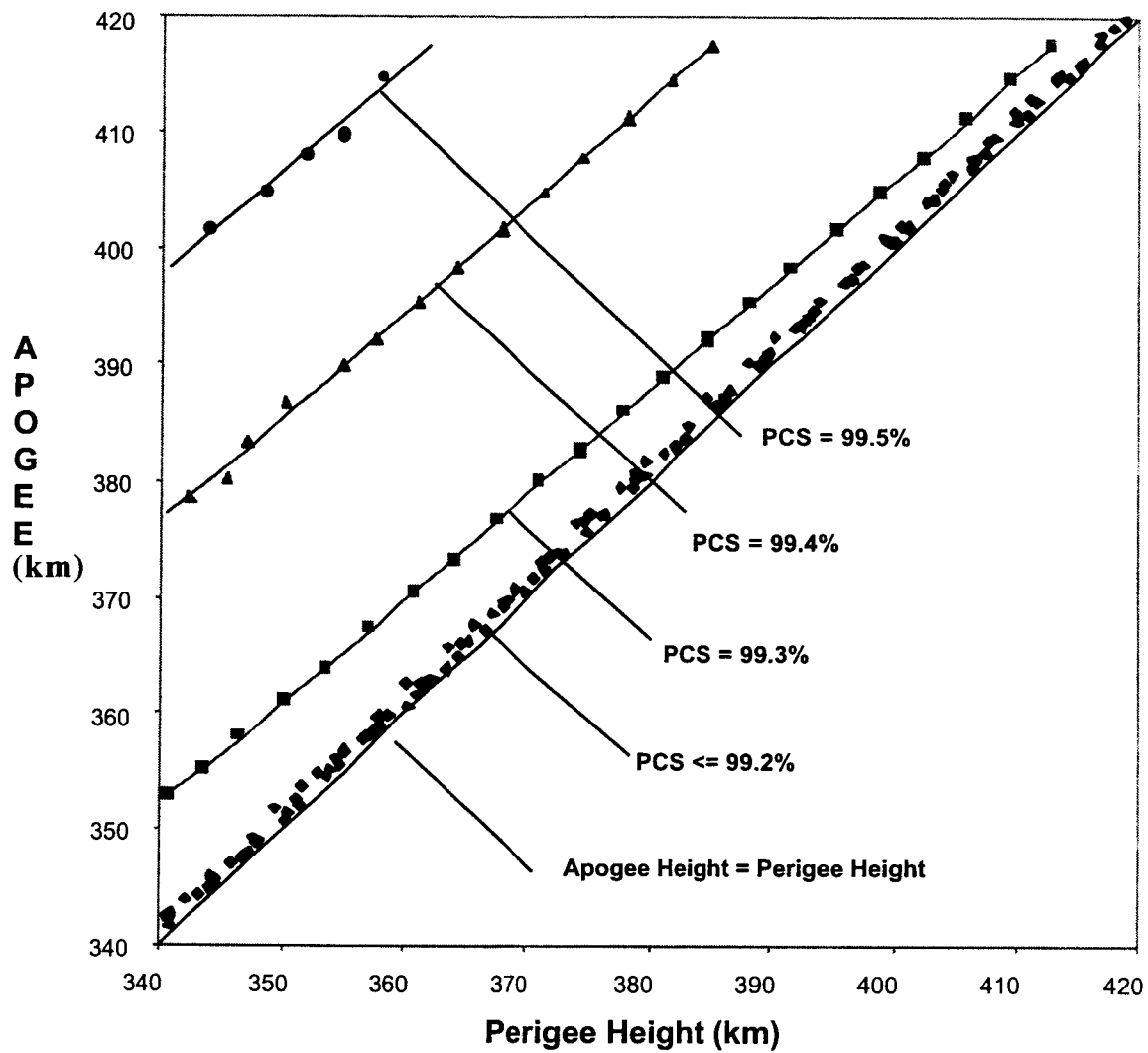


Figure 5 ProSEDS Ascending Node Orbits for Different PCS Values of Probability of Achieving Orbit (PCS) [The Boeing Company]

A summary of the results for the four cases listed above is shown in Figs. 6-9. We remind the reader that these simulations were run for conditions of minimum solar activity, that is with a ionospheric density in the 5% (percentile). Consequently, these simulations represent worst case scenarios with respect to the tether power budgets and orbital decay rates. Table 2 summarizes the decay rate (during the first week) and the average tether current for the four cases.

Table 2 First-week decay rate for Cases 1-4 (Solar Min.)

Case	Orbit (kmxkm)	Decay rate (km/day)
1 (descending)	340x600	7.8
2 (descending)	400x650	7.3
3 (ascending)	375x410	11.5
4 (ascending)	400x400	11.0

Case 4, which is the reference orbit mission, will be analyzed in more details later. In conclusion, the ascending node orbits are preferred for the higher values of probability to achieve the desired orbit and also for the higher values of decay rates.

ProSEDS 265 ohm@20 C, 340x600 km orbit, min. solar, sec. batt. cycle, August 2000

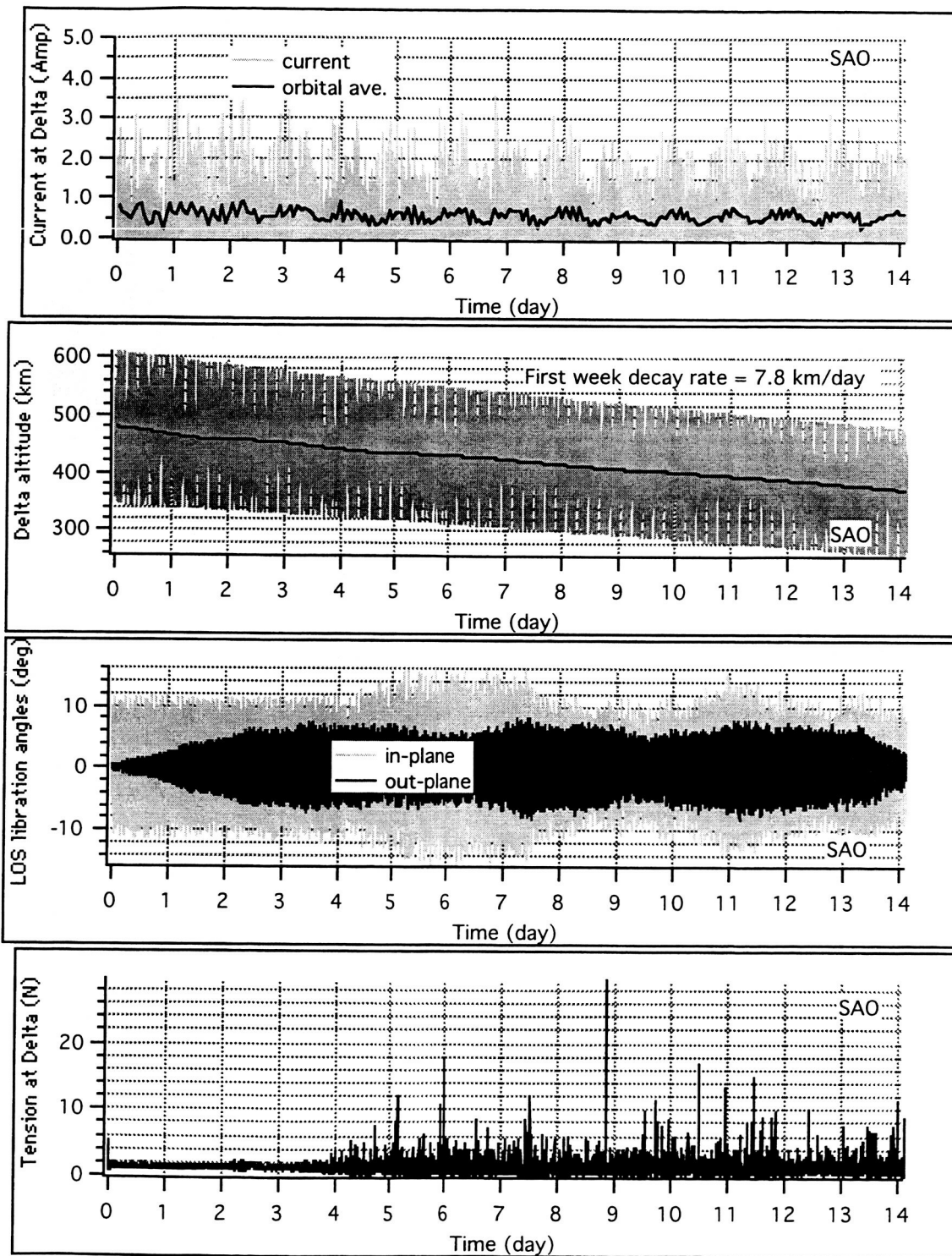


Figure 6 Results for descending node orbit 340x600 km – Case 1 (Min. Solar)

ProSEDS 265 ohm@20 C, 400x650 km orbit, min. solar, sec. batt. cycle, August 2000

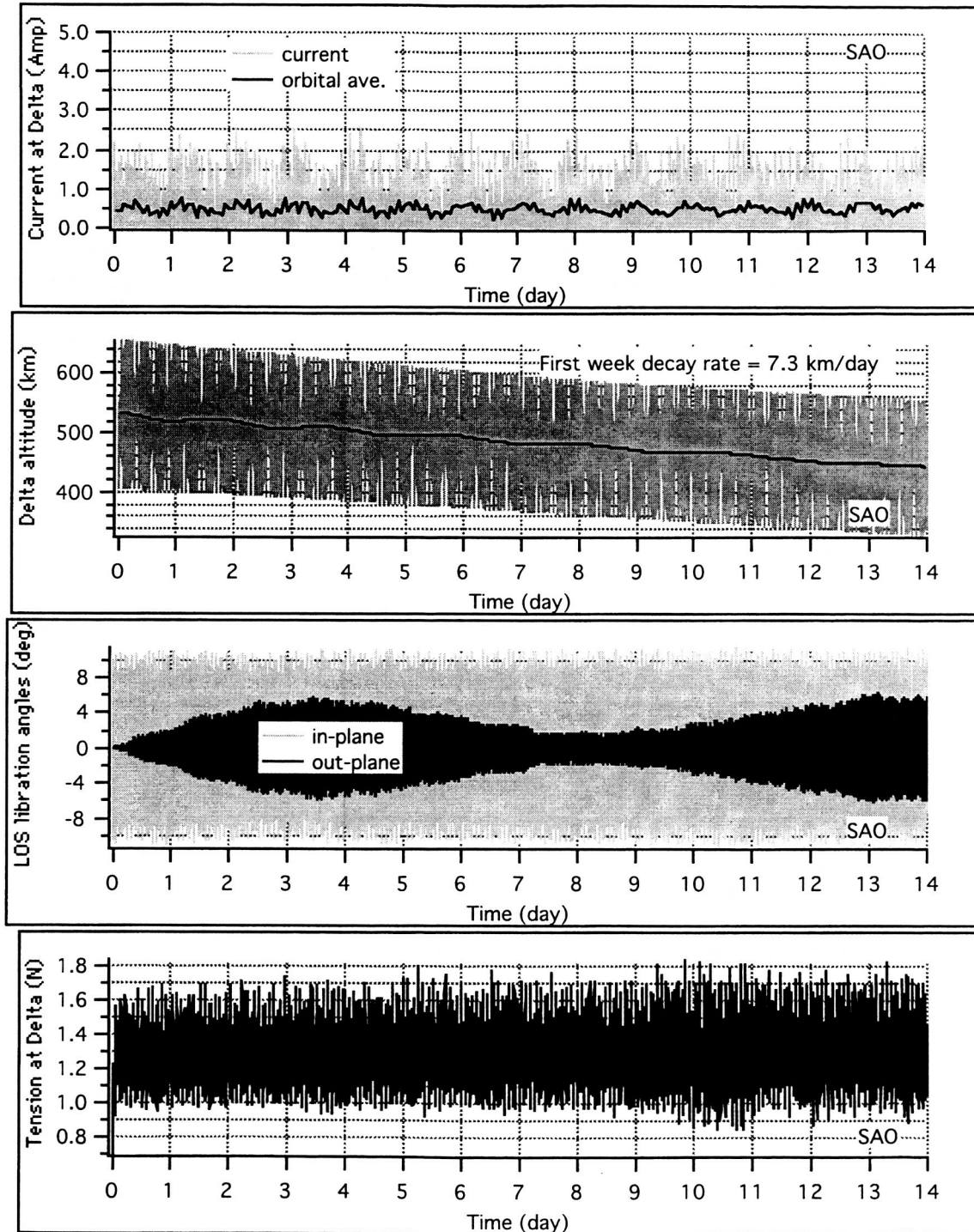


Figure 7 Results for descending node orbit 400x650 km – Case 2 (Min. Solar)

ProSEDS 265 ohm@20 C, 375x410km, min. solar, August 2000

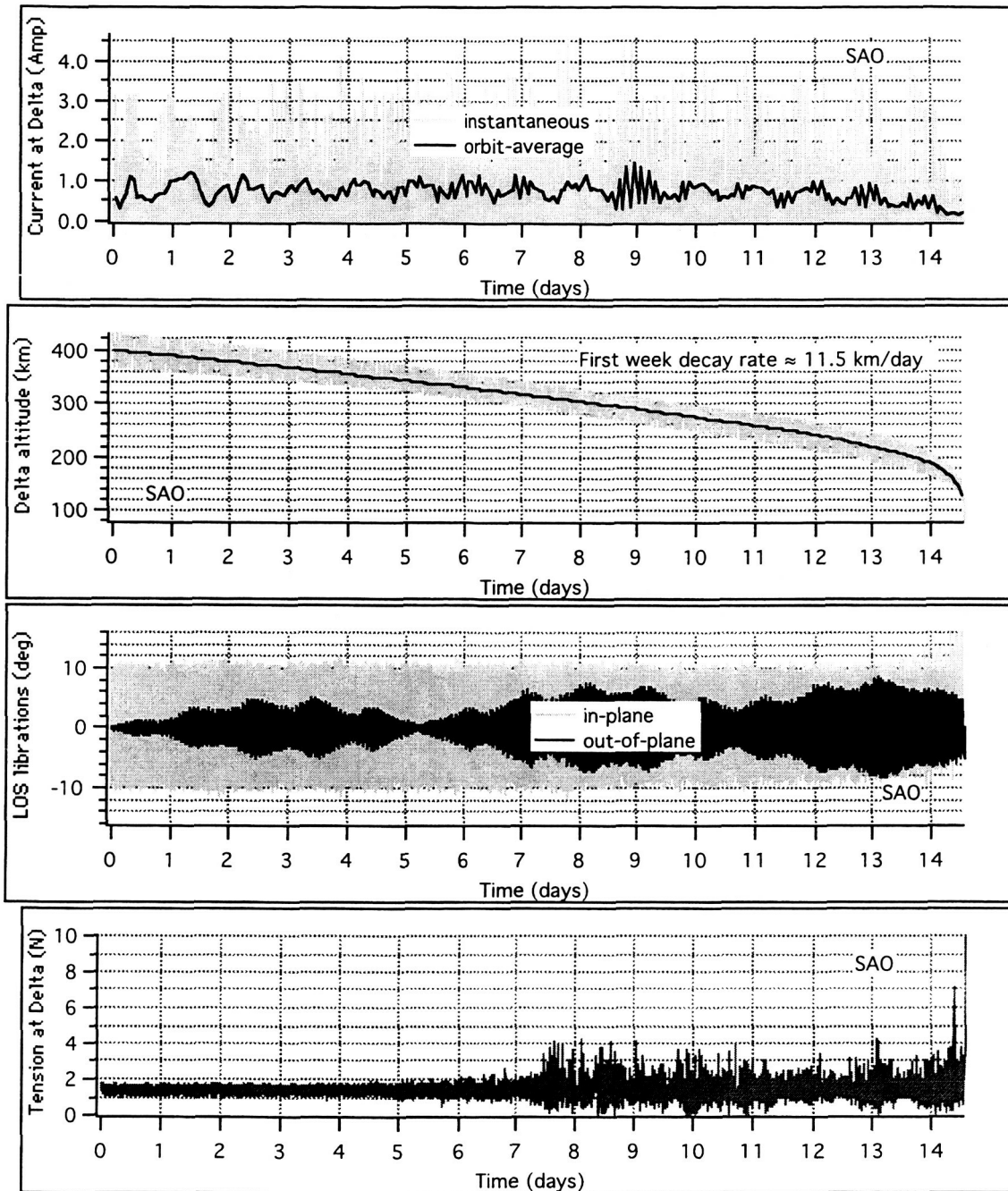


Figure 8 Results for ascending node orbit 375x410 km – Case 3 (Min. Solar)

ProSEDS 265 ohm@20 C, 400x400km, min. solar, August 2000

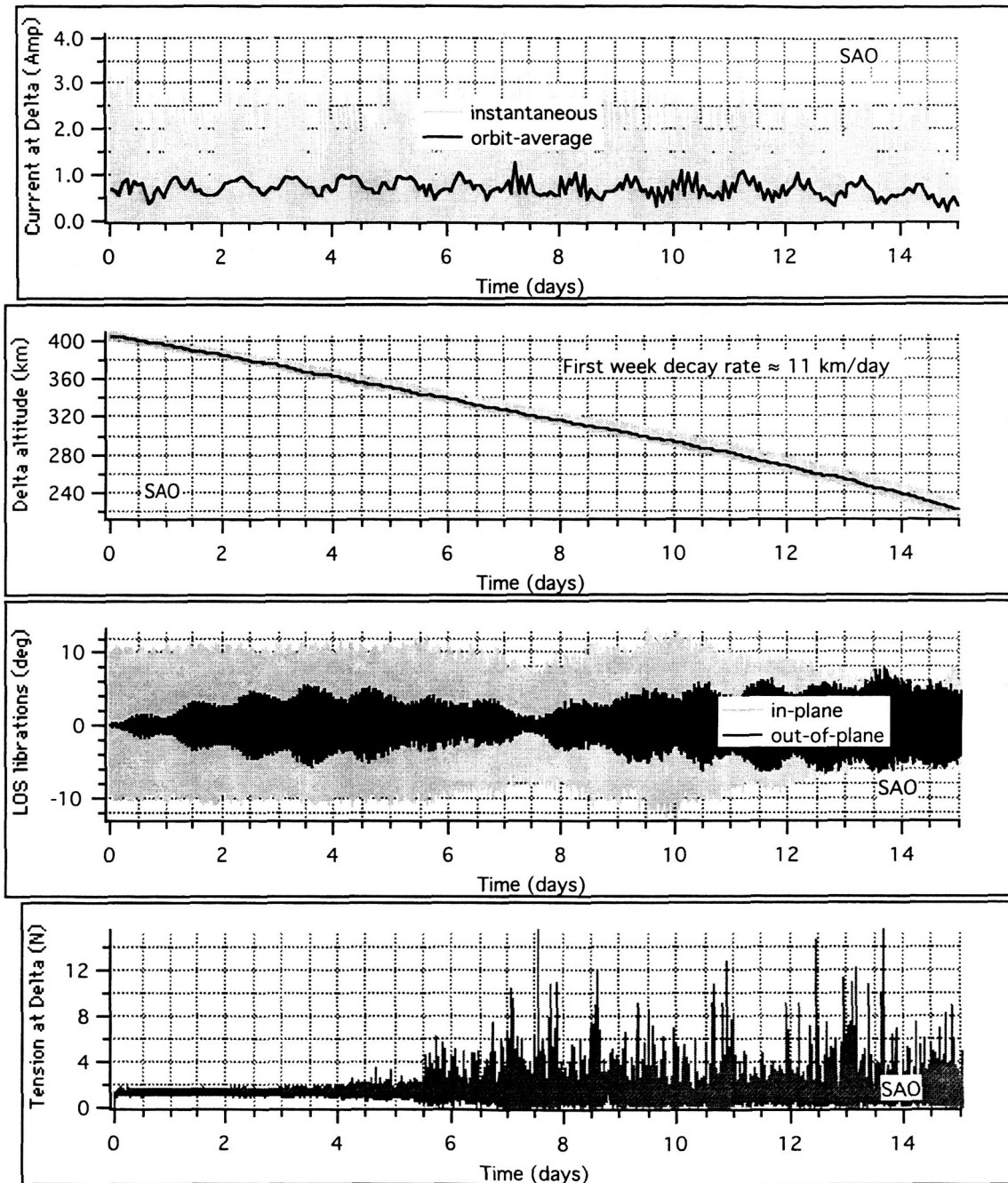


Figure 9 Results for ascending node orbit 400x400 km – Case 4 (Min. Solar)

2.2 Tether-Generated Power

We remind the reader that the orbits of descending node cases with a PCS > 95% all have a relatively high eccentricity. Because of the eccentricity, the decay rates and the values of the average electrical power is substantially reduced with respect to the low eccentricity orbits that are attainable in the ascending node cases with higher reliability of orbit delivery (PCS > 99%).

Specifically, the reduction of decay rate and average power with respect to the ascending node reference Case 4 is about 20% for Case 1 and about 25% for Case 2. Consequently, the descending node cases tax the electrical power provided by the tether to the secondary batteries and reduce substantially the decay rate of the Delta second stage. At the end it was decided to run ProSEDS on an ascending node GPS mission. Moreover, the ProSEDS team decided to adopt an orbit as close to circular as possible (400x400 km) because in a circular orbit, the performance of the system is no longer dependent of the position of the perigee in the ionosphere which introduces an additional variable that affects the mission performance. Table 3 shows the values of the first-week average current for the cases analyzed. The values of average power during the first day of operation are only slightly lower than the values reported in the table.

Table 3 First-week tether average current for Cases 1-4 (Solar Min.)

Cases	Orbit (kmxkm)	Average current (Amp) during first week
1 (descending)	340x600	0.56
2 (descending)	400x650	0.52
3 (ascending)	375x410	0.82
4 (ascending)	400x400	0.80

Figure 10 shows the average current vs. time for the two descending node cases and for the reference case 4 (all for minimum solar activity conditions).

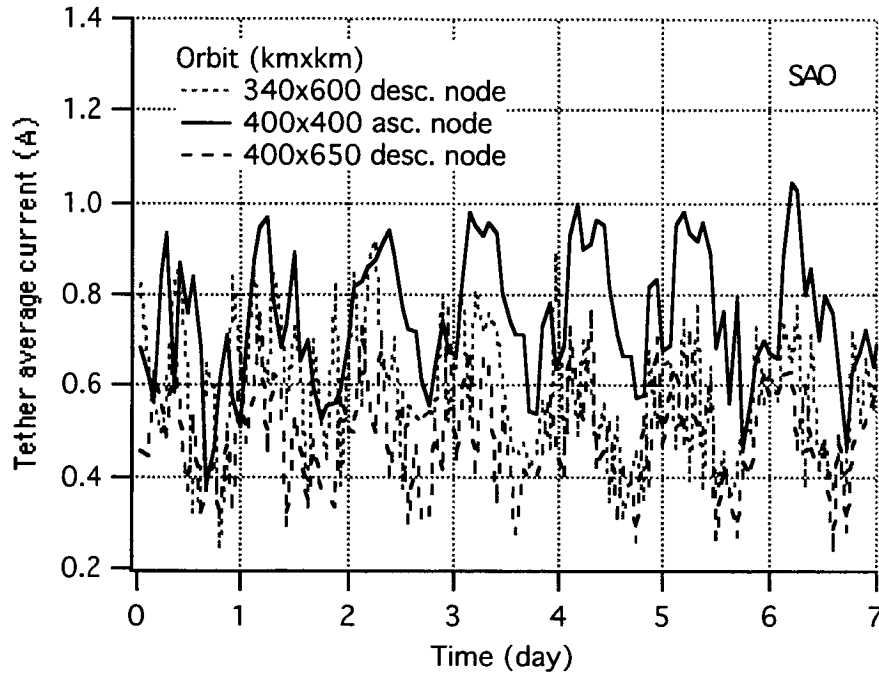


Figure 10 Tether average current for the descending node cases compared to the reference case 4 during one week (Solar Min.)

The power available from the tether is key to extending the mission duration of ProSEDS beyond the primary mission phase. The current from the tether, in fact, provides the electrical power to recharge the secondary batteries once the primary batteries are exhausted. The analysis of the descending-node orbits vs. the ascending-node orbits led to the conclusion that the former orbits do not provide enough current for recharging the secondary batteries during the extended mission phase under worst case conditions.

3. DYNAMICS REFERENCE MISSION

3.1 Simulation Model

As pointed out in Ref⁶, ProSEDS exhibits features that are unlike any other space vehicle for what concerns the strong coupling among dynamics, electrodynamics and thermodynamics of the system. In fact, the tether temperature changes significantly the electrical conductivity of the wire that, in turn, affects the tether current and, consequently, the dynamic of the system. The dynamics itself couples into the current collection ability through changes in the tip-to-tip EMF acting on the tether and, through the Joule heating, into the tether temperature. Consequently, the accurate simulation of ProSEDS requires a computer code that combines dynamics, electrodynamics and thermodynamics of the system.

The simulation code that has been used to estimate the dynamics reference mission is the SAO code MASTER which has been tested on data of previous tether missions (TSS-1, TSS-1R, SEDS-I, SEDS-II and TiPS). The code has the following characteristics:

Lumped-mass model of the tether (discretization most widely used in tether simulators)

Attitude dynamics of endmasses

Gravity field: $J_0 + J_2$

Atmospheric density: MSIS '86

Plasma density: IRI '95

Magnetic field: IGRF '85

Collection model: Orbital Motion Limited (OML) for any tether shape and amounts of insulation

Tether thermal model: Earth's IR, solar illumination, emitted radiation, thermal capacity, ohmic heating

3.2 Discretization and Vibrational Modes

For the design reference mission, ProSEDS was modeled with 9 lumps as follows: 1 for the Delta, 4 for the wire, 3 for the leader tether and 1 for the endmass.

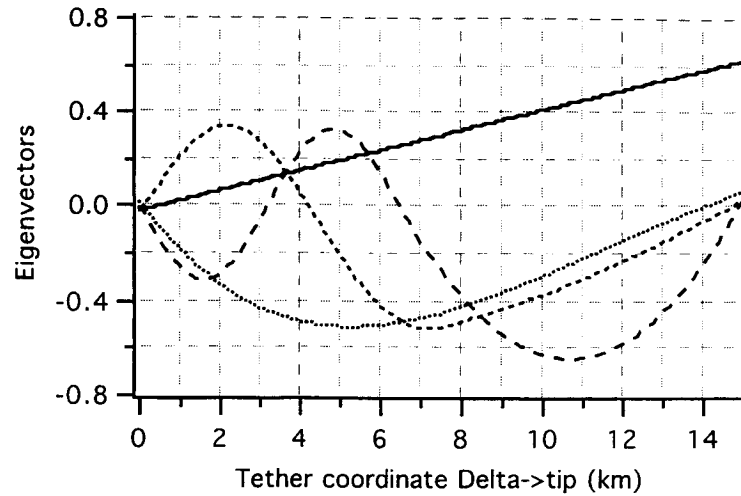


Figure 11 Smoothed shapes of first 4 eigenvectors (lateral dynamics).

Table 4 First 12 eigenvalues of ProSEDS (linearized system).

No.	Freq. (mHz)	Freq. (f = orb. freq)	Period (s)	Type
1	0.317	$\sqrt{3}f$	3156	In-plane librat.
2	1.32	7.2f	759	1 st in-plane lat.
3	2.99	16.3f	335	2 nd in-plane lat.
4	3.82	20.9f	262	3 rd in-plane lat.
5	0.366	2f	2732	Out-plane librat.
6	1.33	7.3f	752	1 st out-plane lat.
7	2.99	16.3f	335	2 nd out-plane lat.
8	3.82	20.9f	262	3 rd out-plane lat.
9	20.0	109f	50	1 st longitudinal
10	81.3	455f	12.3	2 nd longitudinal
11	185.1	1012f	5.4	3 rd longitudinal
12	238.1	1301f	4.2	4 th longitudinal

Figure 11 shows the shape of the first 4 eigenvectors for the lateral dynamics. The librational eigenvectors (in-plane and out-of-plane) are rectilinear and independent of the tether density distribution. The first 12 eigenfrequencies of ProSEDS (linearized system) are shown in Table 4.

3.3 Reference Mission Simulation

The orbital and system parameters for the reference mission are as follows:

Orbit: 400 km circular

Inclination: 36 deg

Launch date: August 2000

Ascending node for: (a) launch close to 10:00A EST and (b) launch close to 10:00P.

Ionosphere/Atmosphere: nominal (50 percentile) solar activity at time of launch

Delta mass: 994 kg

Endmass: 20.4 kg

Tether linear densities: 0.2 kg/km (leader); 2 kg/km (wire)

Tether optical properties:

Spectra - $\alpha_s = 0.1$, $\epsilon_{IR} = 0.5$;

C-COR coated wire - $\alpha_s = 0.9$, $\epsilon_{IR} = 0.8$.

Tether mechanical properties: $EA = 15,000$ N; $E'A \approx 2000$ Ns.

Tether electrical resistance: 265 ohm at 20 °C.

Operating modes: 3 orbits with primary mode and the remainder with secondary mode.

The current is controlled according to duty cycles that repeat themselves throughout the mission duration. Two duty cycles are adopted during the mission. The first one is the primary battery duty cycle that is utilized only during the first 3 orbits when the system is powered by the primary batteries. The second one is the secondary battery duty cycle that is utilized after the first 3 orbits till the end of the mission. The battery duty cycles are shown in Figs. 12 and 13.

In a recent update the number of orbits on primary batteries has been extended to 7 and the launch date has been postponed to mid 2001. However, these change will have only

minimal effects on the system dynamics. Once the new launch date is assigned, we will rerun an updated dynamics reference mission.

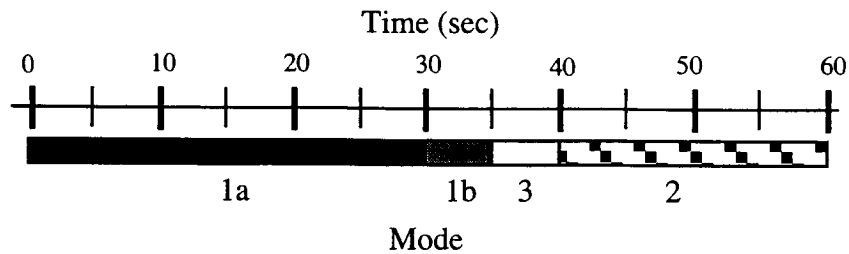


Figure 12 EPT Sequence 1 (60-sec cycle) - Operation on Primary Battery.

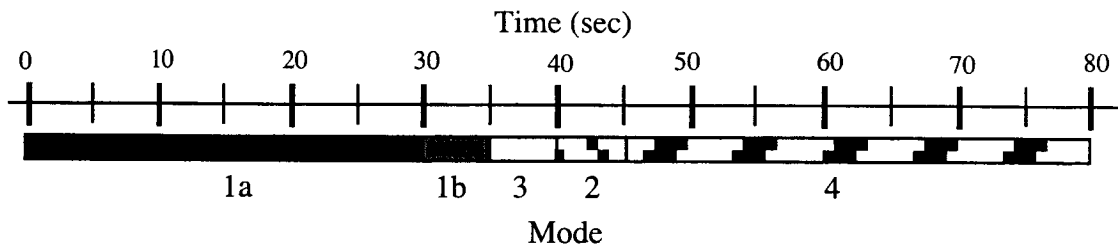


Figure 13¹ EPT Sequence 2 (80-sec cycle) - Operation on Secondary Battery.

Mode 1a is open circuit, plasma contactor OFF

Mode 1b is open circuit, plasma contactor ON

Mode 2 is SHUNT mode

Mode 3 is RESISTOR mode

Mode 4 is BATTERY CHARGE mode

EPT Sequence 1 is for primary battery use only (first 3 orbits).

The time of launch will affect the phasing between the magnetic field (corotating with the Earth) and the plasma field which is mostly driven by the position of the Sun. After considering that the time of launch is not yet known for the Delta rocket, simulation have been run for a day launch which sets the deployment of ProSEDS close to 10:00AM EST and a night launch which sets the deployment close to 10:00PM EST. The ground trace of the orbit is unaffected by the time of launch. The preliminary trajectory ground trace (computed by The Boeing Company) is shown in Fig. 14.

¹ Contributed by NASA/MSFC.

The results of the day-launch simulation are shown in Figs. 15-18 over the extended mission duration of over 2 weeks. The results of the night-launch simulation are shown in Figs. 19-22 over the primary mission duration of 1 day (~15 orbits).

(ESTAR Min. for T/M Sites = 2.00 deg)

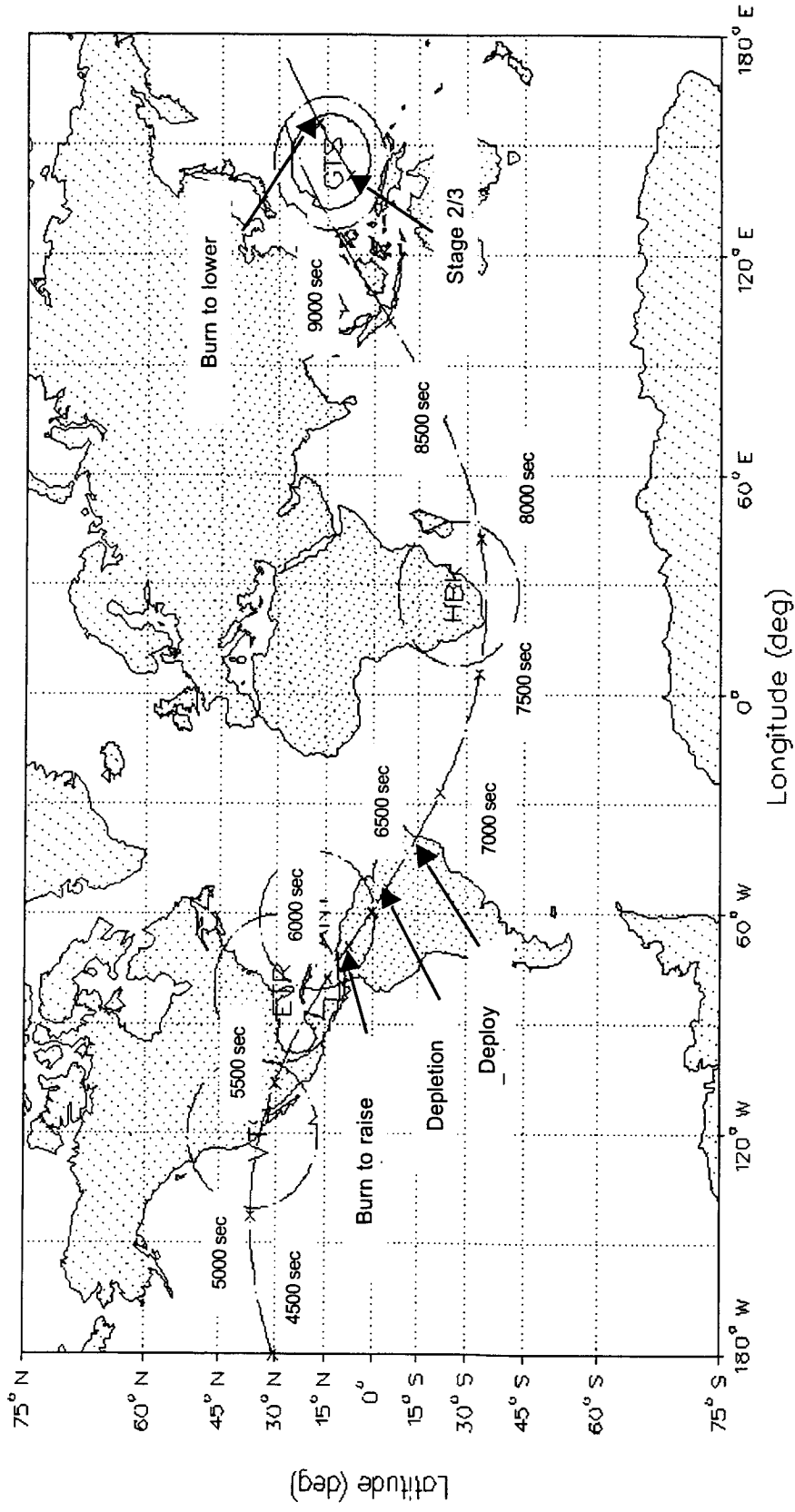


Figure 14 Ground trace of preliminary Delta 7925 Block IIR trajectory [The Boeing Company]

ProSEDS 265 ohm@20 C, 400x400km, nom. solar, day launch, Antigua burn

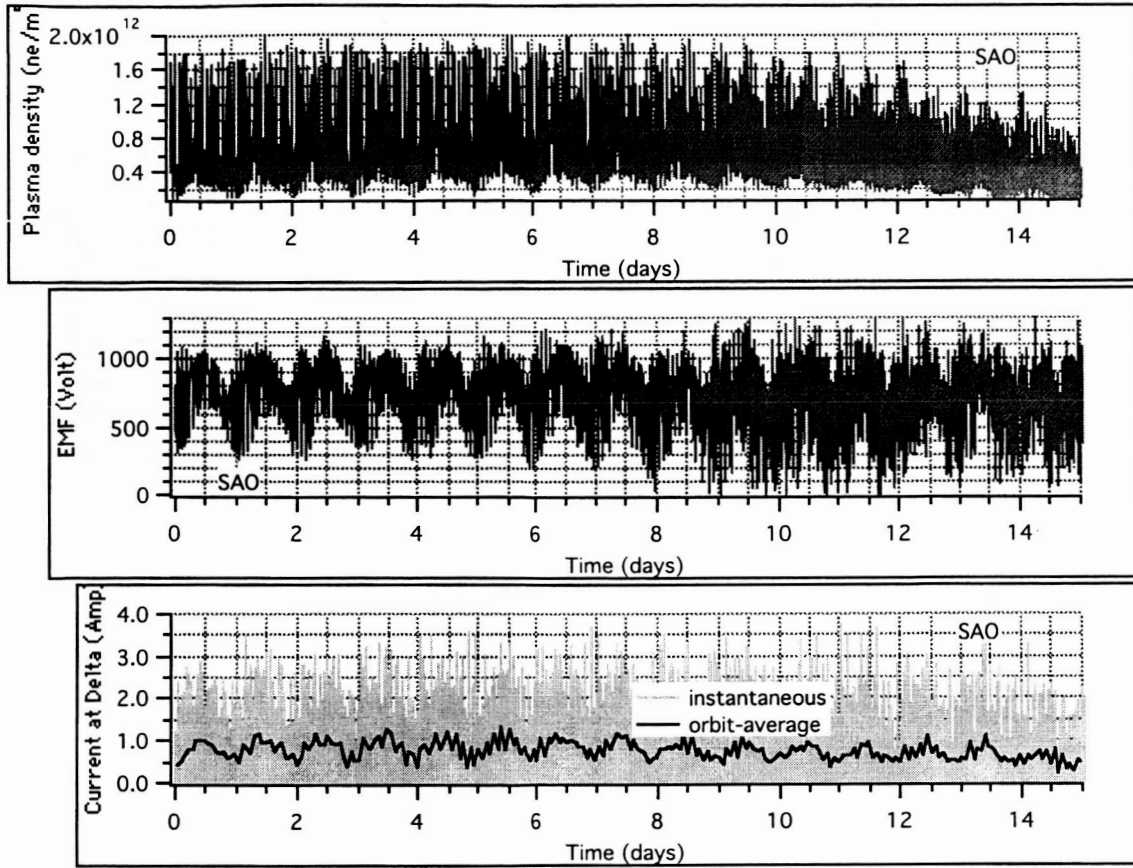


Figure 15 Results for day-launch and circularization burn over Antigua

ProSEDS 265 ohm@20 C, 400x400km, nom. solar, day launch, Antigua burn

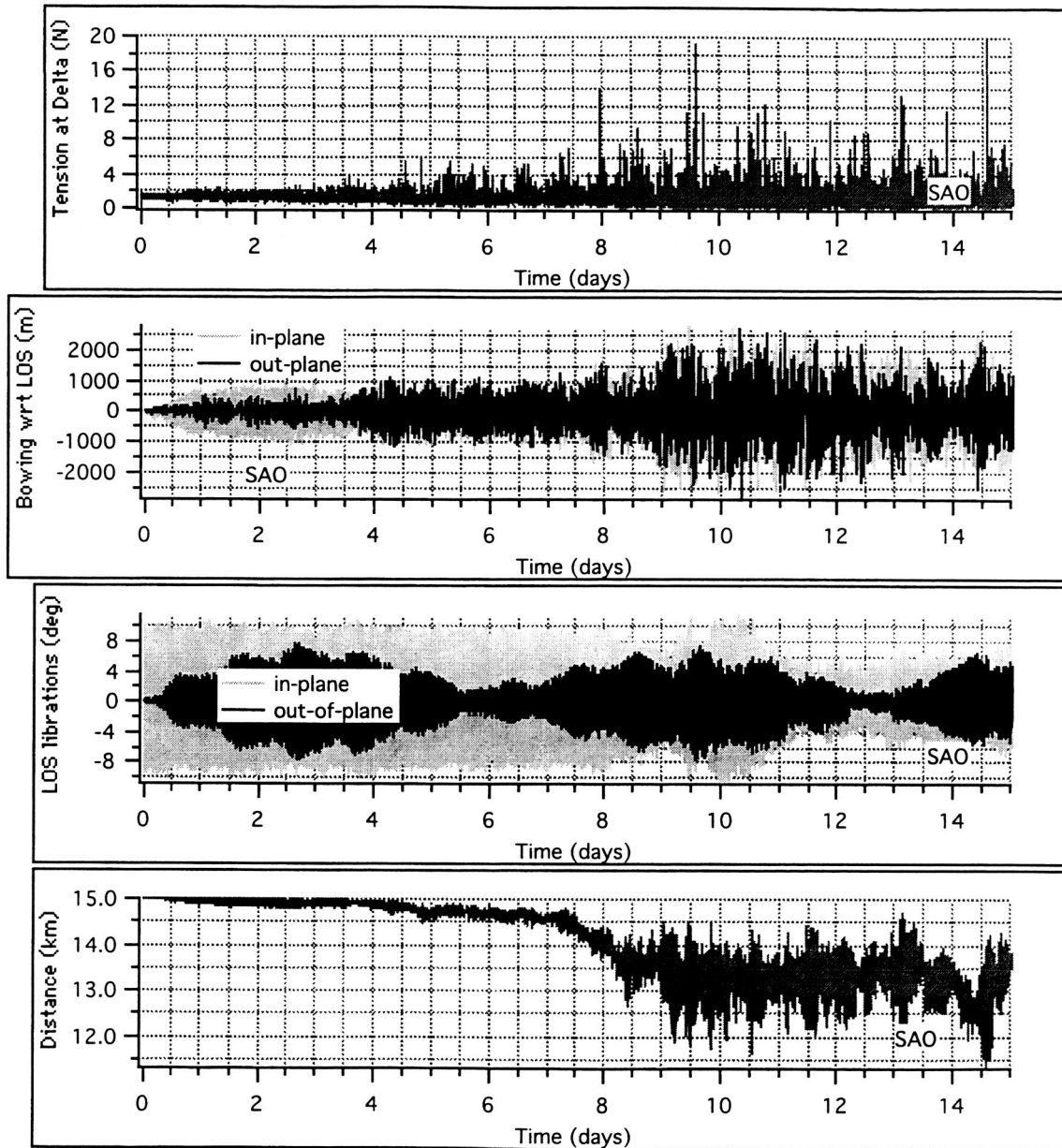


Figure 16 Results for day-launch and circularization burn over Antigua

ProSEDS 265 ohm@20 C, 400x400km, nom. solar, day launch, Antigua burn

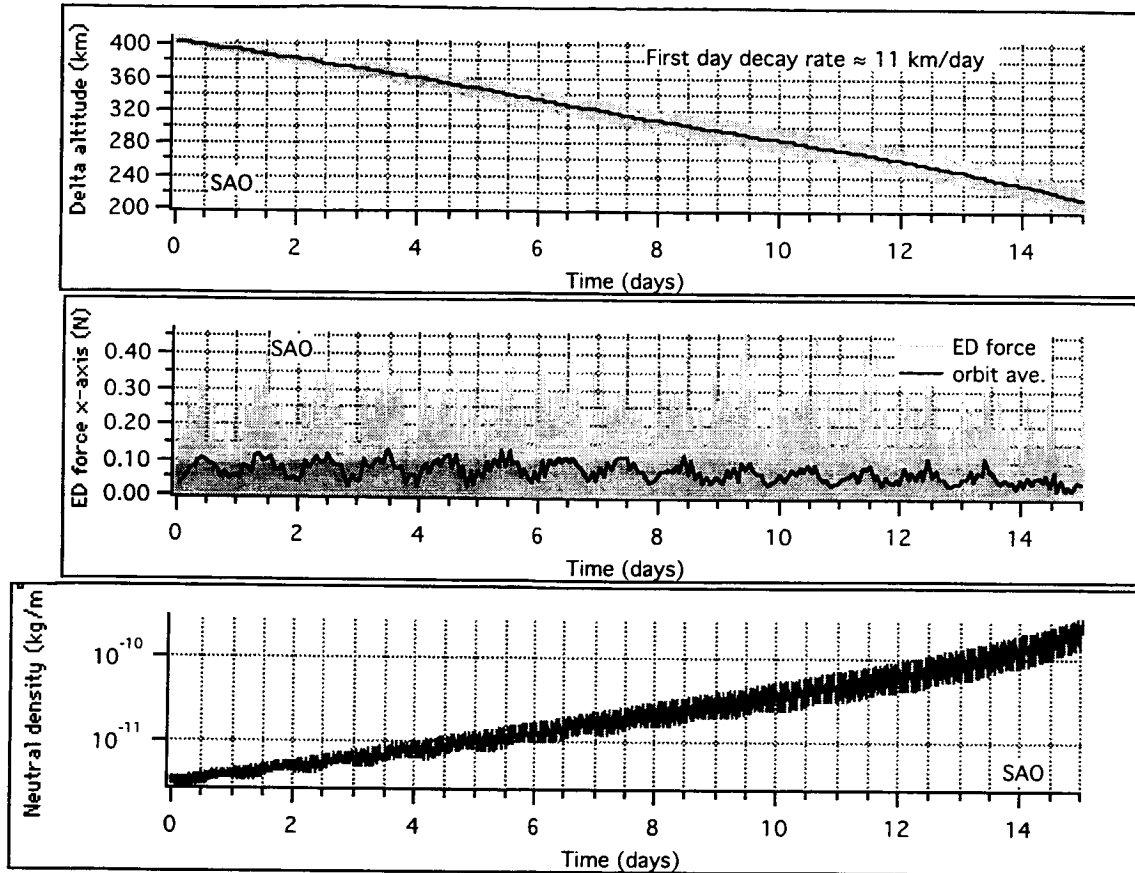


Figure 17 Results for day-launch and circularization burn over Antigua

ProSEDS 265 ohm@20 C, 400x400km, nom. solar, day launch, Antigua burn

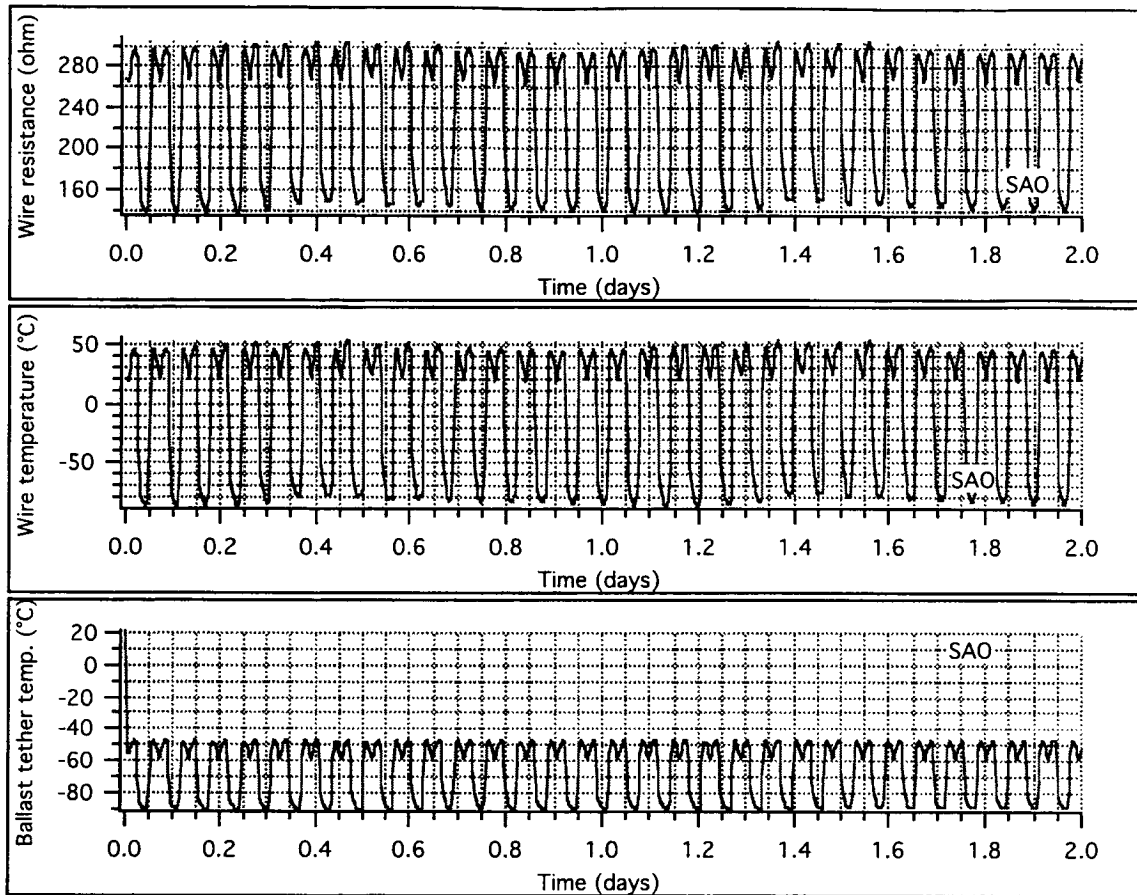


Figure 18 Results for day-launch and circularization burn over Antigua

ProSEDS 265 ohm@20 C, 400x400km, nom. solar, night launch, Antigua burn

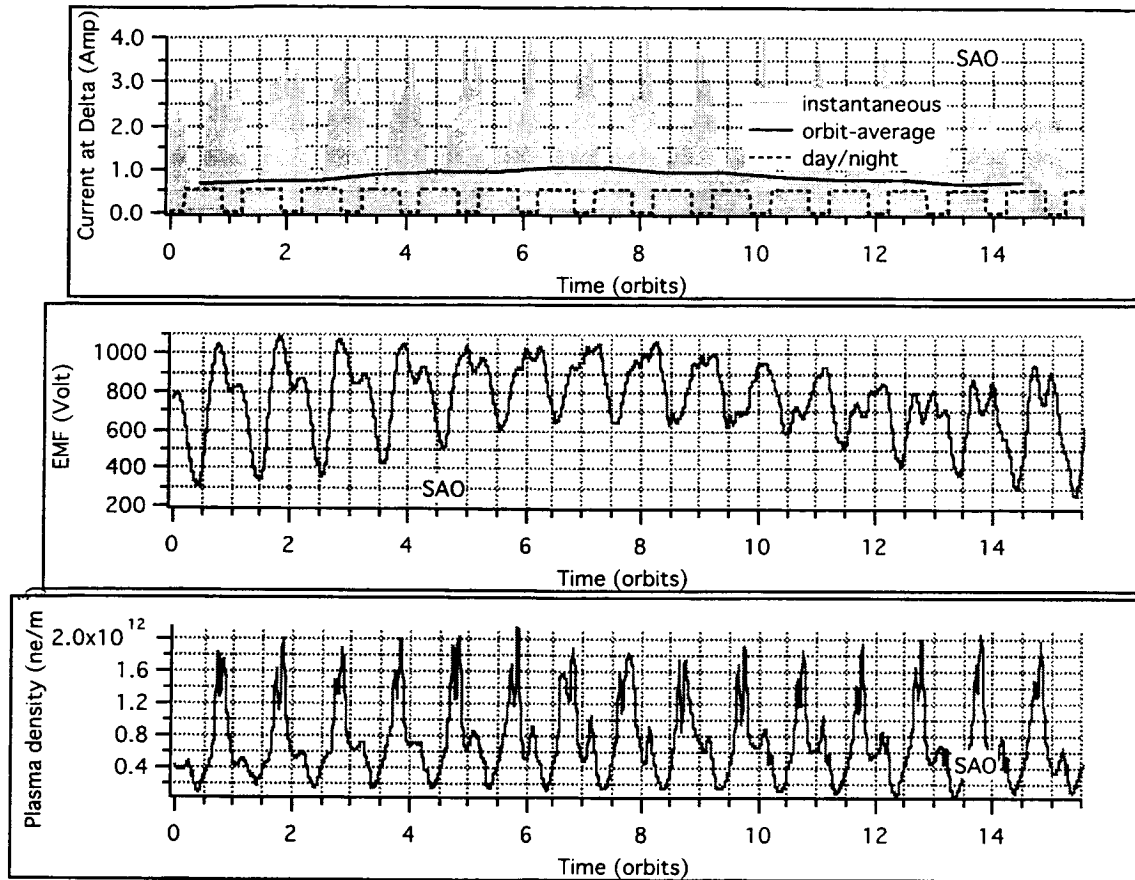


Figure 19 Results for night-launch and circularization burn over Antigua

ProSEDS 265 ohm@20 C, 400x400km, nom. solar, night launch, Antigua burn

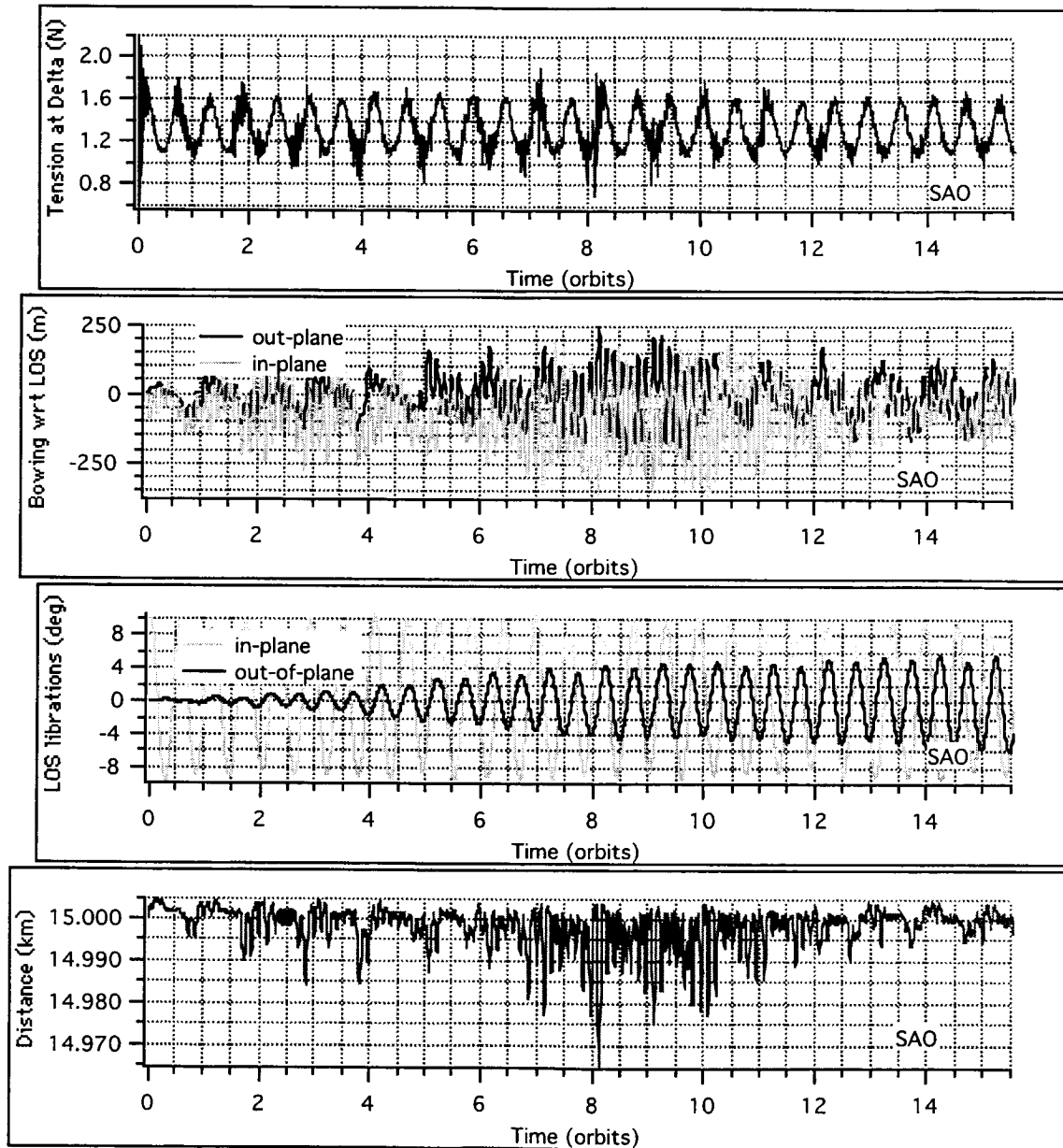


Figure 20 Results for night-launch and circularization burn over Antigua

ProSEDS 265 ohm@20 C, 400x400km, nom. solar, night launch, Antigua burn

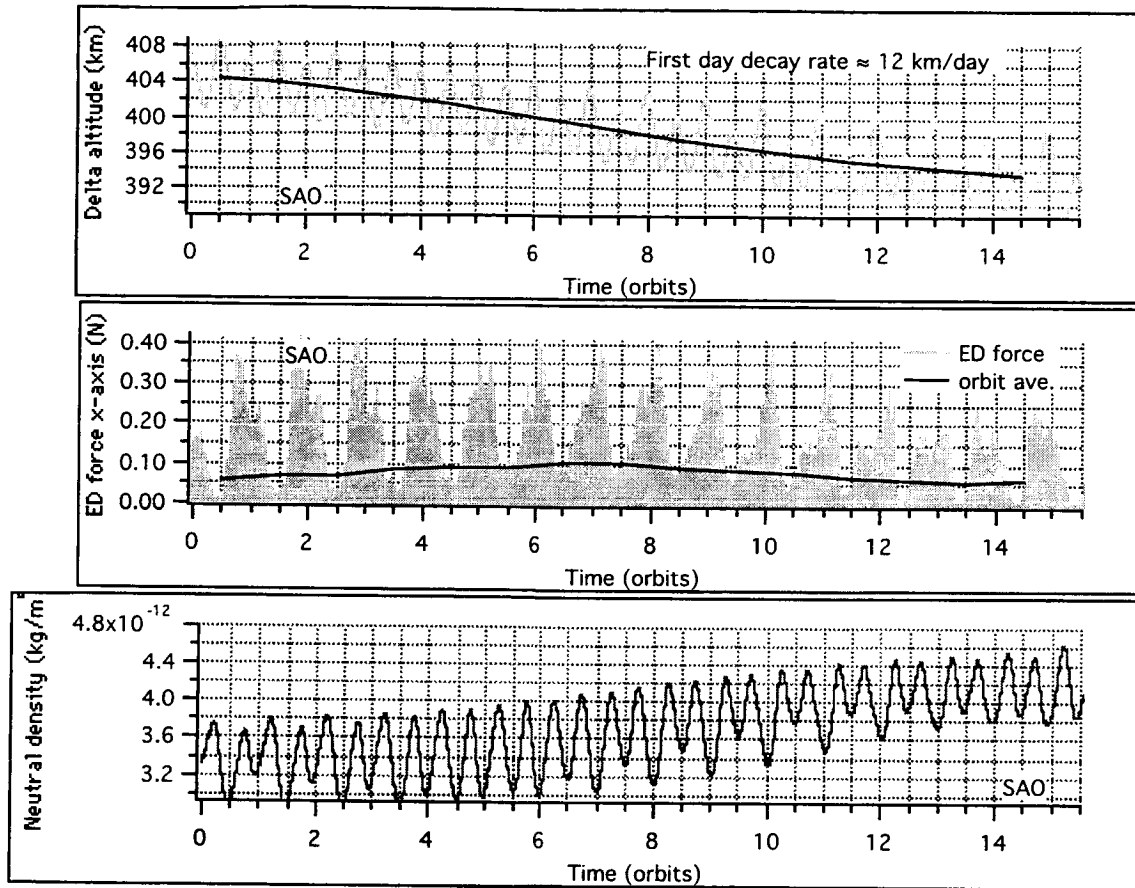


Figure 21 Results for night-launch and circularization burn over Antigua

ProSEDS 265 ohm@20 C, 400x400km, nom. solar, night launch, Antigua burn

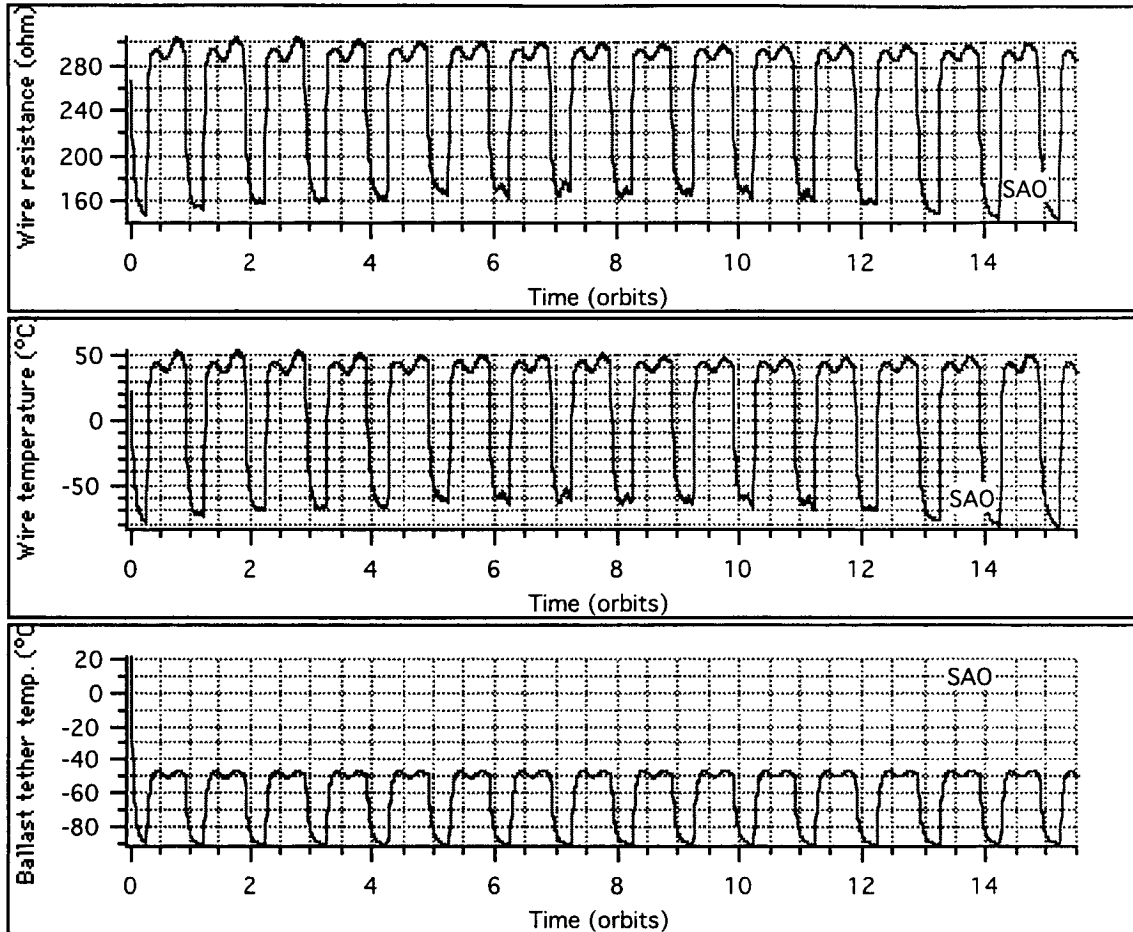


Figure 22 Results for night-launch and circularization burn over Antigua

The main conclusions from the analysis of the reference mission are as follows:

The decay rate during the first day (primary mission) is about 11 km/day and 12 km/day for the day and night launches, respectively. These values exceed the minimum value of 5 km/day established as a success criteria for ProSEDS. It is also worth reminding that the decay rate of ProSEDS is mostly constrained by the current control cycle which limit the current flowing (for science data gathering reasons) in the tether to about 50% of the available time.

The orbit-average current produced by the tether are as follows:

Day launch:

0.8 Amp (over entire current cycle)

1.5 Amp (during battery charging)

Night launch

0.85 Amp (over entire current cycle)

1.6 Amp (during battery charging)

The minimum and maximum tether temperatures for the Spectra tether and the C-COR wire are:

Spectra: from $-90\text{ }^{\circ}\text{C}$ to $-47\text{ }^{\circ}\text{C}$;

C-COR: from $-87\text{ }^{\circ}\text{C}$ to $+54\text{ }^{\circ}\text{C}$.

The tether temperatures are within the allowable limits for the two tether types.

The system dynamics is stable and rather well-behaved over the extended mission lifetime of over two weeks. Because of the relatively low ratio of absorptivity/emissivity ($\alpha/\epsilon \approx 1.1$) provided by the latest formulation of C-COR, the wire temperature is rather low as it ranges from $-87\text{ }^{\circ}\text{C}$ to $+54\text{ }^{\circ}\text{C}$. Consequently, the electrical resistance of the wire ranges from 150 ohm to 300 ohm. This is a fairly good range of electrical resistance for a 15-km tether with a total mass of less than 12 kg.

It is worth reminding that a purely bare aluminum tether would have had an $\alpha/\epsilon \approx 8$ which would have reduced the decay rate by approximately 40% with respect to the rates obtained with the coated wire.

3.4 Concluding Remarks

The accurate simulation of ProSEDS requires the combination of dynamics, electrodynamics and thermal models of the tether. The interplay among dynamics, electrodynamics and thermodynamics is crucial in explaining the performance of the system. The changing tether temperature and, consequently, electrical resistance of the wire has a positive effect on the current profile over the day/night cycles and ultimately on the dynamics and stability of the system.

Another important conclusion of the analysis carried out is that an uncoated metal wire would attain high maximum temperatures that are strongly undesirable from the points of view of system performance and mechanical strength of the tether. Consequently, the α/ϵ (absorptance/emittance) ratio of the metal was decreased (while preserving its ability to collect electrons) by using an appropriate coating with the final goal of keeping the temperature of the wire well below 100 °C. The coating is necessary for a thin and light tether like ProSEDS in which the electrical resistance becomes detrimental at high temperatures. The design of the ProSEDS tether was driven by the very stringent limitations of mass and volume available to a Delta secondary payload and by the characteristics of the SEDS deployer.

The wire coating will not be strictly necessary for all-metal, thick tethers with much higher mass because the electrical resistance could be, in those cases, negligible and its increase with temperature might be not strong enough to create problems. Moreover, the ProSEDS wire must have a relatively low maximum temperature because higher temperatures weaken the Kevlar core. Here again the Kevlar core is necessary in ProSEDS for obtaining a light and mechanically strong tether. Attempts made to use a higher temperature material like PBO did not succeed in producing a tether that could be wound on the SEDS deployer.

The present estimate of the orbital decay rate during the first week of the mission is about 11-12 km/day for 50% (percentile) solar conditions during the mission.

4. DYNAMICS STABILITY

4.1 Dumbbell Tether System Subjected to ED Forces

The dynamics of electrodynamic tethers whether bare or insulated with conductive termination is dominated by the electrodynamic (perturbing) forces and torques which are counteracted by the gravity gradient restoring forces and torques. The magnitude of the electrodynamic force varies widely over the orbit because of variation of plasma density, emf, and orientation of the vectors involved. The direction of the electrodynamic forces also varies and it can not be made to change at will because it simply depends on the direction of the magnetic field and the orientation of the tether with respect to it. On the other hand, the main gravity gradient restoring torque only depends on the system libration and the orbital eccentricity and, consequently, its behavior can be considered predictable (the influence of the higher order harmonics of the gravity field on the restoring torque are negligible). As a consequence, under realistic conditions (i.e., realistic magnetic and plasma density models) we can not balance the gravity gradient torque with the electro-dynamic torque continually and keep the system attitude at a desired static position as the system moves around the orbit. Dynamics plays an important role in electrodynamic tethers.

A striking feature of the dynamics of electrodynamic tethers on an inclined orbit is the appearance of energy exchanges between degrees of freedom that would be otherwise decoupled and of a continuous input of energy into these degrees of freedoms by the electrodynamic forces. In a system with a light tether for example (in which the contribution of the tether skip-rope can be neglected), the main energy exchange can result from a coupling between the in-plane and out-of-plane librations even at relatively small angles (where these degrees of freedom would be otherwise decoupled).

The coupling in electrodynamic tether is produced by the component of the magnetic field aligned along the local vertical. This component produces torques that are proportional either to the in-plane or the out-of-plane angles but that affect those angles in reverse order. Consequently, these torques generate coupling terms in the equations of motion that give rise to the energy exchange between degrees of freedom. The coupling, combined with the energy input from the lateral electrodynamic forces will eventually lead to instabilities if no damping is present in the system and the mission is relatively long. This topic is treated in details in a paper by Pelaez, Lorenzini, Loper-Rebollal and Ruiz⁷. In the following, we

briefly summarize some of the results of that paper referring the reader to the paper itself for a more in-depth analysis.

The study of the dynamics stability is rather involved because the non-linear equations of motions with periodic coefficients must be analyzed. This was accomplished by finding, through series expansion, periodic solutions of the non-linear equations and then utilizing the Floquet theory to analyze the stability of those solutions.

The result of interest is that the growth of the instability can be made to be very slow by an appropriate selection of the system electrical and mass characteristics. The instability growth depends on the ratio ϵ of the maximum value of the lateral magnetic force (for a dipole magnetic model and constant current) to the gravity gradient force along the local vertical. Consequently, short systems with low-resistance wire and high currents (whether bare or not) that have a high value of the ϵ ratio exhibit a faster instability growth than ballasted systems (like the ProSEDS configuration) with higher-resistance wire and lower currents. The instability growth depends on the cube of the above mentioned ratio which implies that it can be made to be very slow. Moreover, the instability growth increases with the orbital inclination, which increases the vertical component, up to a point, of the magnetic field.

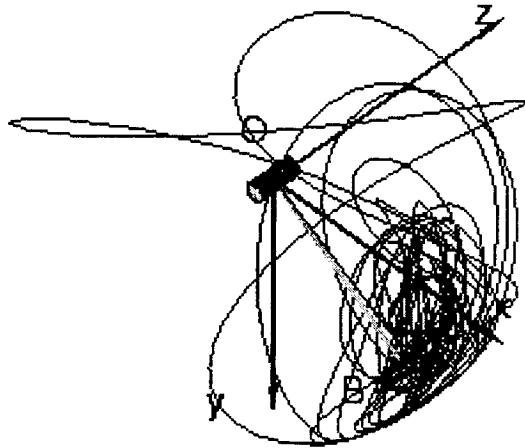


Figure 23 3-D trajectory of endmass of a dumbbell tether system undergoing a librational instability

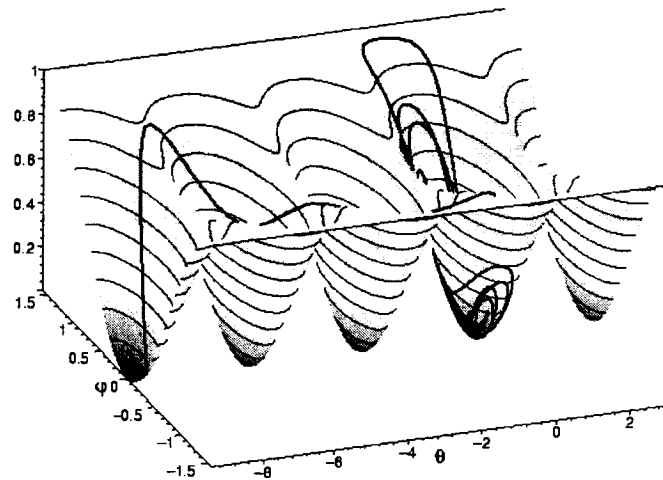


Figure 24 State-space trajectory in the potential surface. The in-plane angle θ (rad) and out-of-plane angle ϕ (rad) are on the x and y axes. The out-of-plane angle grows large and forces an in-plane libration instability

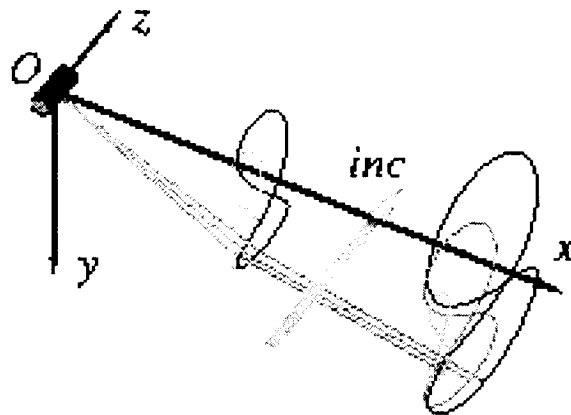
Figures 23 and 24 show clearly the behavior of a system that is driven unstable by electrodynamic forces. The system under consideration is modeled as a dumbbell (rigid-bar) tether system. The state-space trajectory on the potential surface of Fig. 24 (the potential surface is the sum of the gravitational energy and kinetic energy with respect to the orbiting reference frame) shows a system that swings in a stable manner inside the potential well at first. Subsequently, the out-of-plane libration grows large driven by the electrodynamic forces which eventually forces an in-plane libration instability (the system starts spinning close to the orbital plane). As it can be inferred from the shape of the potential well, the in-plane degree of freedom has less stability margin than the out-of-plane degree of freedom and, consequently, the in-plane libration instability is more likely to occur eventually.

In ProSEDS, the ratio of the lateral magnetic force to the vertical gravity gradient is sufficiently low that the instability does not occur during the mission lifetime. In lighter systems, the electrodynamic forces can lead to a librational instability (the system topples

over) in comparatively short times. More work is needed to devise passive energy dissipation or an active control strategy to impede the relatively rapid growth of the instability in light systems.

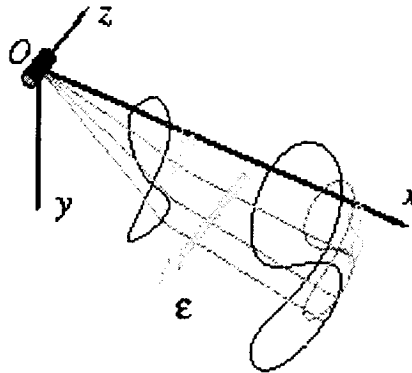
4.1 ProSEDS-type System Subjected to ED Forces

Far more complicated is to analyze the tether motion itself and the role it plays in the general instability of the system. Reference ⁸ treats this topic in some details. In this paper, we evaluated this effect in a fairly general way by modeling the tethered system as two rigid bars articulated at their joint. Although the model is simplified, the stability analysis becomes very complex. Figures 25 and 26 show the trajectories of the tip of the wire (at first aligned along the local vertical x while z is along the flight direction) and the endmass for different values of the orbital inclination and ratio of ED-force/gravity-gradient (ϵ_0). The trajectories shown in Figures 25 and 26 are the result of the motion forced solely by the ED forces (that is, they are the purely non-homogeneous solutions to the equations of motion).



$$i = 25^\circ, 50^\circ, 75^\circ; \epsilon_0 = 0.75$$

Figure 25 Effect of increasing orbital inclination on the trajectory of the tip of the wire and the endmass. For increasing inclination the amplitude of the ED-forced-motion (eight-shaped trajectories) increases.



$$\epsilon_0 = 0.4, 0.8, 1.2; i = 45^\circ$$

Figure 26 Effect of increasing ED-force/gravity-gradient ratio on the trajectory of the tip of the wire and endmass. For increasing values of the ratio the amplitude of the ED-forced-motion (eight-shaped trajectories) increases

As the amplitude of the oscillations increase with the increase of the orbital inclination or the ϵ_0 ratio, the state-space trajectory reaches higher toward the edges of the potential well and the stability margin is reduced. Moreover, the instability growth rate vs. time increases with the increase of ϵ_0 . The addition of more degrees of freedom lead to the appearance of another unstable eigenvalue. The model still exhibits the weak librational instability observed in the previous dumbbell tether model and, in addition, it exhibits a stronger instability associated with the ratio of the tether mass to the end masses. The dependence of this stronger instability on the mass ratio is very complex and its functional dependence upon the system parameters is still under investigation.

4.3 Concluding Remarks

The stability analysis of electrodynamic tethers is complex because the non-linear equations must be considered for obtaining meaningful results. To this end, two models have been adopted for investigating the stability in a rather general way: (a) a dumbbell tether model and (b) a two-bar tether model. Periodic solutions have been found to the non-homogeneous (and non-linear) equations through series expansions. The stability of these periodic solutions was investigated by utilizing the Floquet theory. A number of general conclusions have been reached as follows:

ED tethers (either with bare tether or spherical termination anodes) are subjected to a librational instability caused by the electrodynamic forces. The instability depends on the ratio of the out-of-plane electrodynamic force over the vertical gravity gradient force and, consequently, the instability increases with the orbital inclination for constant tether current. In reality, the current also depends on the inclination in ways that are different for different modes of operations so that the maximum instability is reached at values of inclination which are intermediate between equatorial and polar.

The role played by the motion of the tether itself is involved. So far we have analyzed the role played by the first lateral harmonics of the tether motion and we have established a few preliminary conclusions. The lateral motion of the tether brings about another unstable eigenvalue. The growth of this other instability is also slow for low value of the tether current but the growth can become much quicker than the growth of the librational instability for values of the current which are above a critical value. The dependency of the critical value of the current on the ratio of tether mass to endmass and on the orbital inclination is complex and this work is still in progress.

5. DEPLOYMENT CONTROL

5.1 Control law

The non-linear deployment control law^{9 10} that deployed successfully SEDS-II was adopted for ProSEDS deployment.

The mathematical model of the deployer friction model is due to Joe Carroll and it is best explained in Ref. [□] (Glaese, 1992). This tension law was derived for cylindrical non-conductive tethers. Consequently, adjustments will be necessary for the flat-braid non-conductive tether and possibly for the conductive wire.

The tension model used so far is as follows:

$$T = \left(T_0 + I \cdot \rho \cdot \dot{L}^2 \cdot A_{rel}^E \right) \cdot e^{f \cdot |\theta_0 - \theta|} \quad (1)$$

where:

A_{rel}	=	$1 - A_{sol} \cdot L / L_{fin}$
A_{sol}	=	annulus solidity of tether
L	=	length of tether deployed
L_{fin}	=	final length of tether
B	=	$2\pi f n$ (n is the number of tether turns wrapped around the brake post)
T_0	=	minimum tension
ρ	=	linear density of tether
I	=	inertia multiplier
\dot{L}	=	tether exit speed
θ	=	tether's exit angle with respect to the local vertical
θ_0	=	tether deployment null angle (orientation of the longitudinal axis of deployer with respect to the local vertical)
f	=	friction coefficient.

In case of the ProSEDS non-conductive tether (where the deployment control law is applied), we have the following numerical values:

$A_{sol} = 0.3375$ (for leader tether based on an overall tether length of 15 km); $L_{fin} = 15$ km; $f = 0.14$; $\theta_0 = 1.1345$ rad (65°); $I = 5$; $\rho = 0.2$ kg/km; $T_0 = 5-30$ mN.

In summary, the control law consists of a static part (T_0) that dominates the behavior at low exit speeds and a dynamic part (the second term in parentheses) that dominates the behavior at higher speed. These two tension terms are then multiplied by the two exponential terms: the brake multiplier and the exit-guide multiplier.

Because T_{\min} has a high variability, the control law must be designed for robustness against large changes in the minimum tension. Moreover, the system dynamics and the actuator (brake) are strongly non-linear. The control law developed at SAO and flight-tested with SEDS-II utilizes the strategy of input-output linearization in order to eliminate the strong non-linearities associated with the SEDS deployer and the system dynamics. The equations of motion are as follow:

$$\ddot{\theta} + 2\frac{\dot{L}}{L}(\dot{\theta} - \Omega) + \frac{3}{2}\Omega^2 \sin(2\theta) = 0 \quad (2.1)$$

$$\ddot{L} - L\left[(\dot{\theta} - \Omega)^2 + \Omega^2(3\cos^2(\theta) - 1)\right] = -\frac{1}{m}\left(\tau_1 \cdot T_0 + \tau_2 \cdot I\rho L^2 A_{rel}^E\right)e^{B+f|\theta_0 - \theta|} \quad (2.2)$$

where $A_{rel} = 1 - A_{sol} L/L_{full}$ and τ_1 and τ_2 are uncertainty coefficients that are equal to unity for reference conditions.

The non-linearities of the system response are eliminated by solving the non-linear control equations numerically for given initial conditions (initial state) and desired final state for reference values of the friction profile. This reference solution, which includes the deployment length L_{ref} , length rate \dot{L}_{ref} and brake profile B_{ref} is then fed forward to the controller. The optimal profile B_{ref} is the nominal control of the brake. This profile steers the system along the reference state trajectory $L_{ref}(t)$, \dot{L}_{ref} (note that θ_{ref} and $\dot{\theta}_{ref}$ are not feedback variables) that accomplishes the control goal under reference conditions. In an actual situation in which disturbances and uncertainties are present, a local regulator is needed to force the system to follow the reference trajectory. The regulator increases the stability of the dynamic response and provide robustness to the control law. We adopted as regulator a locally-linear feedback control with terms proportional to the departures of L and \dot{L} from L_{ref} and \dot{L}_{ref} respectively.

In a departure from classic feedback linearization, the linear feedback is not simply added to the reference brake profile but rather B_{ref} is used as the weighting function as follows:

$$B = B_{ref}(1 + F) \quad (3)$$

where the feedback F is as follows:

$$F = K_1(L - L_{ref}) + K_2(\dot{L} - \dot{L}_{ref}) \quad (4)$$

The use of B_{ref} as the scheduling function of the control gains K_1 and K_2 has resulted in a robust yet simple control law. As said previously, the in-plane angle and angular rate are not feedback parameters simply because of lack of sensors that observe those variables. The control law, therefore, only uses a partial knowledge of the system state to control deployment. A control law that take advantage of the knowledge of the full state would have been even more robust.

The solution to the control equations, i.e., the reference profile in state space, is found by an iterative process aimed at minimizing a cost function which is a function of the differences between the actual (subscript end) and desired final (subscript goal) states as follows:

$$F = C_1(L_{end} - L_{goal})^2 + C_2(\dot{L}_{end} - \dot{L}_{goal})^2 + C_3(\theta_{end} - \theta_{goal})^2 + C_4(\dot{\theta}_{end} - \dot{\theta}_{goal})^2 + G \quad (5)$$

where $(L_{end}, \dot{L}_{end}, \theta_{end}, \dot{\theta}_{end})$ is the final state of a generic trajectory, C_i , $i = 1, \dots, 4$, are positive real constants, and G is a real and positive function.

The minimization process parameterizes the brake profile by means of a small number of fiducial values which are the support points of cubic splines. These support points are modified by the minimization routine after each iteration utilizing a convergence criteria in order to reduce, possibly at each step, the value of the cost function.

Block Diagram

The flight control software is based on an outer loop sampled at every 8 seconds and an inner loop sampled at every 1 second. The output of the turn counter (see Fig.27), sampled at every second, is filtered by a recursive filter and the turn count rate is computed by taking the numerical derivative of the filtered turn counts over 8-s intervals. This process provides a smooth turn count rate despite the high noise level of the turn count signal. At every 8-s, the smoothed turn count and turn rates are compared to the reference turn count and rate for computing the correction (feedback) to apply to the reference brake B_{ref} profile in order to track the reference length and rate profiles.

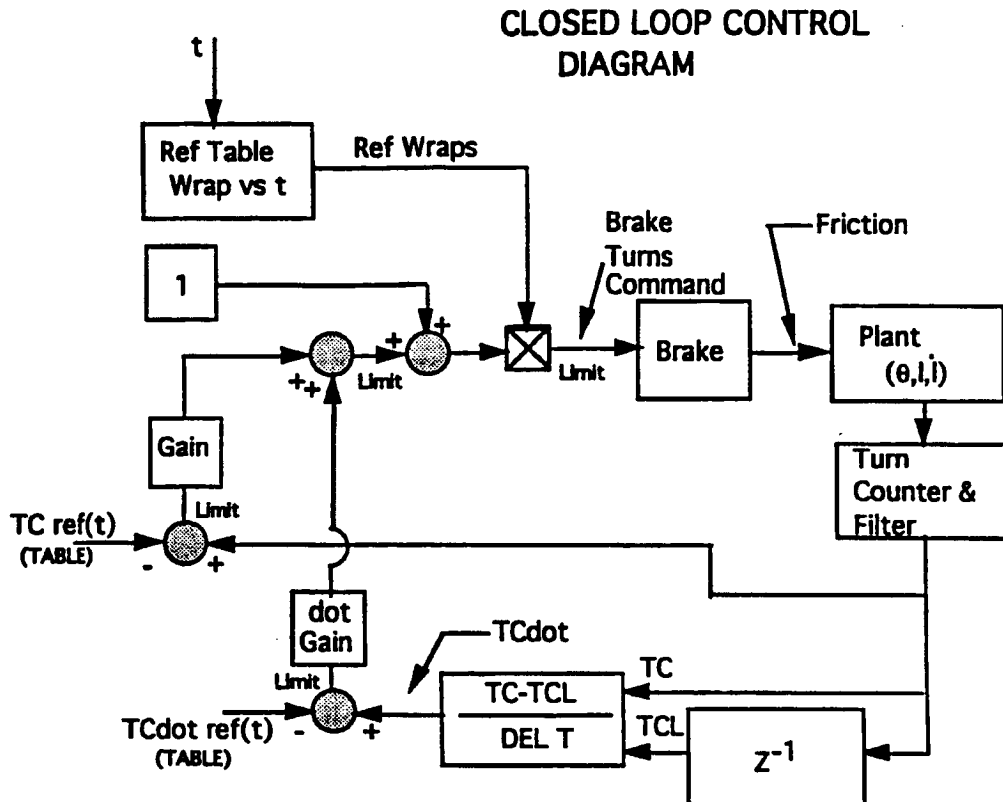


Figure 27 Diagram of deployment closed-loop control system

Unlike SEDS-II, the deployment of ProSEDS is controlled only while paying out the non-conductive tether, i.e., over 10 km out of the 15 km total length. This is because of the concern that debris from the conductive wire may jam the delicate brake mechanism. This limitation is implemented into the minimization process as an additional constraint imposed on the reference brake profile. Additional constraints are also imposed in order to obtain a reference brake profile that does not force undesired situations during deployment. The exit velocity is constrained to be above 1 m/s during deployment of the non-conductive tether and above 3 m/s during deployment of the wire. The function G in the *cost function* is used to implement the speed constraints. The velocity limitations ensure that the satellite has enough kinetic energy to overcome unexpected discontinuities along the tether. G is a constraint function that penalizes the trajectories with rate values smaller than the predetermined minimal rate values.

The desired final state at the end of deployment is for the system to be aligned and swingless with respect to the local vertical with a residual longitudinal velocity greater than 3 m/s before the beginning of the insulated portion of the wire (last 160 m of tether). As explained later on, the residual velocity is then reduced by a final activation of the brake triggered on by the brake enabler sensor which detects the beginning of the insulated wire.

Because of all the constraints imposed on the minimization routine, the process of deriving a good reference profile is tedious. The process requires a large number of trials. In many of them the routine is unable to converge properly to a cost function which is within the specified accuracy. In many other cases, the process produce a reference profile but some characteristics of the reference profile are not desirable such as sharp gradients in the brake actuation or in the exit velocity profile. Many attempts must be made and once a good reference profile is found it must be tested in the simulator for assessing its robustness vs. variations in the tension model parameters.

All in all, 26 valid profiles (out of a much larger number of trials) have been derived for this first edition of the ProSEDS control law (Reference profile #26). Some of these profiles differ in the selection of reference values of the tension model. In others, the same reference values have produced substantially different reference profiles depending on the different initialization of the minimization routine. The final selection of a flight control profile is then made on the basis of: (1) its robustness to variations of the parameters of the tension model and (2) the closeness of the reference friction parameters to the values obtained in the deployment tests.

The most uncertain and also most influential parameter (during the early and most critical phase of deployment) of the tension model is T_0 . The minimum tension of the ProSEDS leader tether (which dominates the final state at the end of deployment) has already been measured in deployment tests on the ground under different temperatures to vary between 5 mN and 30 mN. Consequently, the control law must provide a residual libration at the end of deployment of less than 20° (which stems from the mission requirements) within the measured range of variability of the minimum tension.

The deployment reference profiles depend on the initial conditions at endmass ejection. These initial conditions have changed during the development of ProSEDS as the selection of the ejection springs has changed through the project development.

5.2 Reference Profiles

A selected set of reference profiles is shown in Fig. 28. In general, the control law can tolerate without a significant decay in performance a value of the non-conductive tether minimum tension as follows: $5 \text{ mN} < T_0 \leq 30 \text{ mN}$.

For $30 \text{ mN} < T_0 < 50 \text{ mN}$, the libration at end of deployment increases rapidly from 5 deg to 15 deg (valid for Reference #26). For $T_0 \geq 80 \text{ mN}$, the deployment stops at a distance of about 500 m because of excessive friction and without any role being played by the control law. The critical value of 80 mN for the minimum tension is determined by the ejection velocity which with the present ejection system is equal to 2.8 m/s. It is, therefore, very important that the flight leader tether satisfies the critical constraint.

The most recent parameters adopted for the reference profile (Reference #26) are as follows

Orbital and ejection parameters

Orbit: 400x400 km

Orbital inclination: 32 deg

Ejection velocity = 2.8 m/s

Ejection angle = 5 deg (forward of LV with an upward deployment)

System parameters

Satellite mass = 20.4 kg

Delta-II Mass = 911 kg (2008 lb)

Tether lengths: 10 km (non conductive) and 5 km (conductive)

Tether linear densities: 0.2 kg/km (Non-conductive) and 2 kg/km (Conductive)

Reference minimum tension:

$T_0 = 30 \text{ mN}$ (leader tether)

$T_{\text{wire}} = 200 \text{ mN}$ (conductive wire)

Friction coefficient:

$f = 0.14$ (Leader tether)

$f = 0.20$ (Conductive wire)

Inertia multiplier:

$I = 5$ (leader tether)

$I = 5$ (conductive wire)

Annulus Solidity (based on an overall tether length of 15 km)

$$A_{sol} = 0.3375 \text{ (leader tether)}$$

$$A_{sol} = 0.94 \text{ (preliminary value of wire)}$$

Area exponent

$$E = -0.6 \text{ (leader tether)}$$

$$E = -0.6 \text{ (preliminary value for wire)}$$

A number of different reference profiles have been selected out of the 26 valid profiles to show the consequent differences in deployment performance. These profiles differ primarily for the ejection velocity of the endmass and the reference minimum tension. They were derived to reflect the changes in the ejection velocity of the endmass and the different estimates of the minimum tension of the leader tether that took place throughout the development of the ProSEDS project. Table 5 summarizes the key features of these profiles.

Table 5 Characteristics of selected reference profiles

Profile	ΔV (m/s)	T_0 (mN)	
		Leader	Wire
#9	1.85	20	300
#18	2.5	20	300
#21	2.8	20	200
#26	2.8	30	200

Figures 28-31 depict the reference variables for the selected reference profiles. The in-plane angle is not part of the control and it is shown only for the sake of completeness. Figure 32 shows the amplitude of the residual libration at the end of deployment vs. the minimum tension T_0 of the leader tether for the selected profiles. The final libration amplitude is very sensitive to the leader tether T_0 and it is quite insensitive to the value of the wire T_{wire} . Values of T_{wire} wire of 100-300 mN have been explored with very good deployment dynamics. Values as high as 500 mN are tolerable for the minimum tension of the wire.

ProSEDS Reference 9

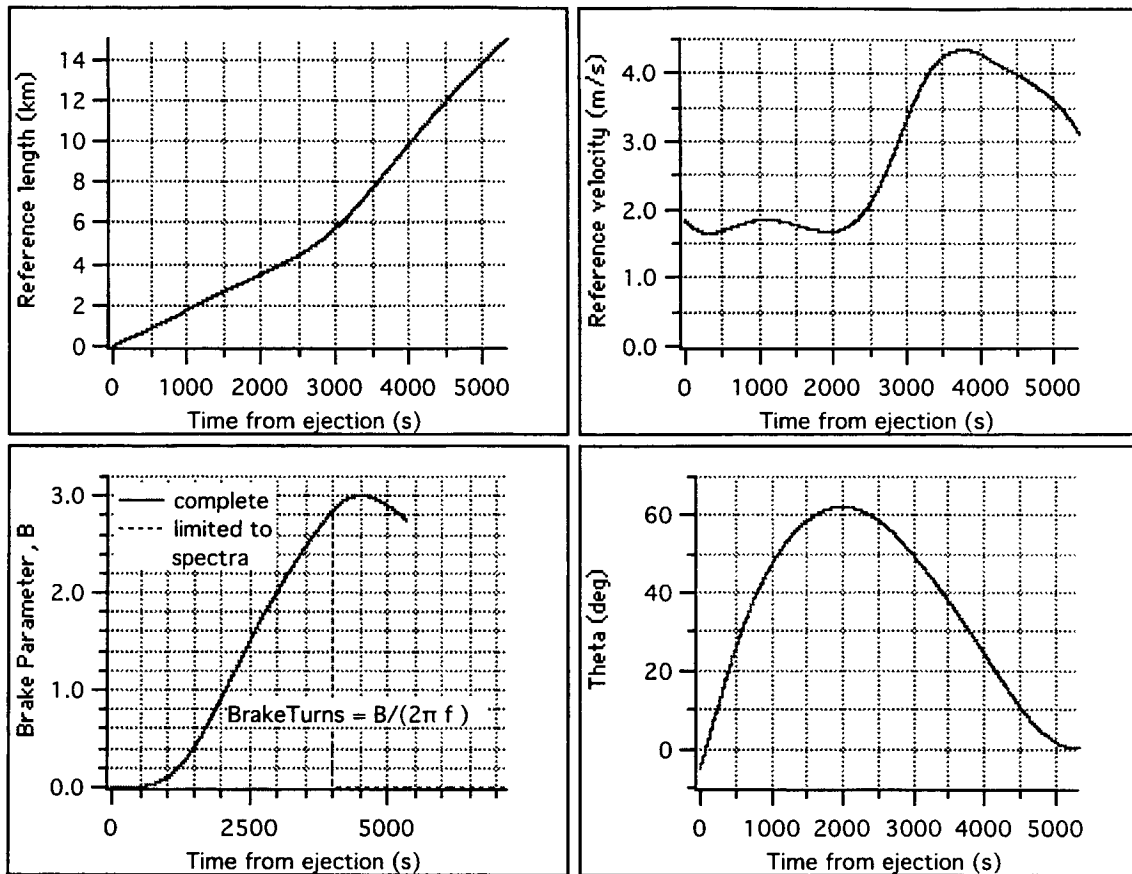


Figure 28 Deployment Reference Profile #9

Reference Profile #18

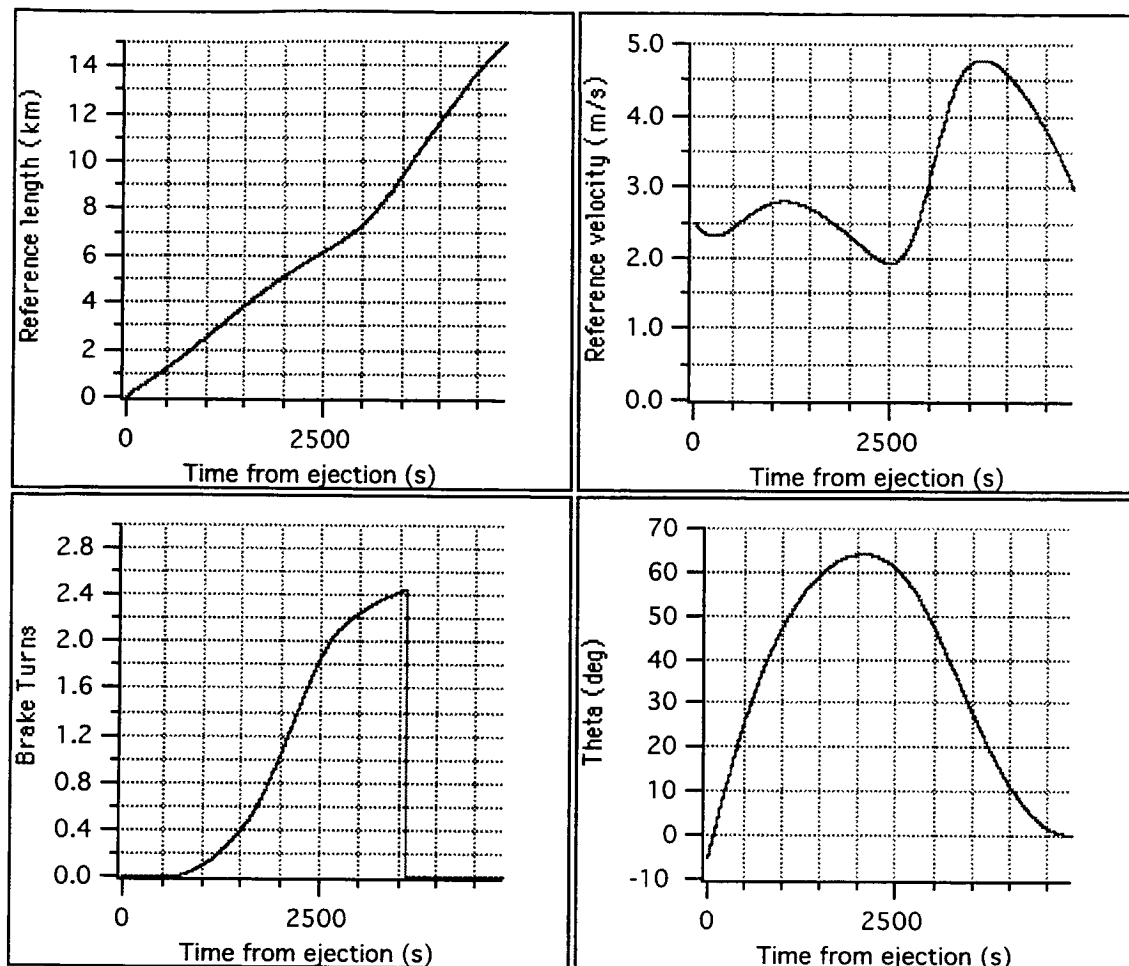


Figure 29 Deployment Reference Profile #18

Reference Profile #21

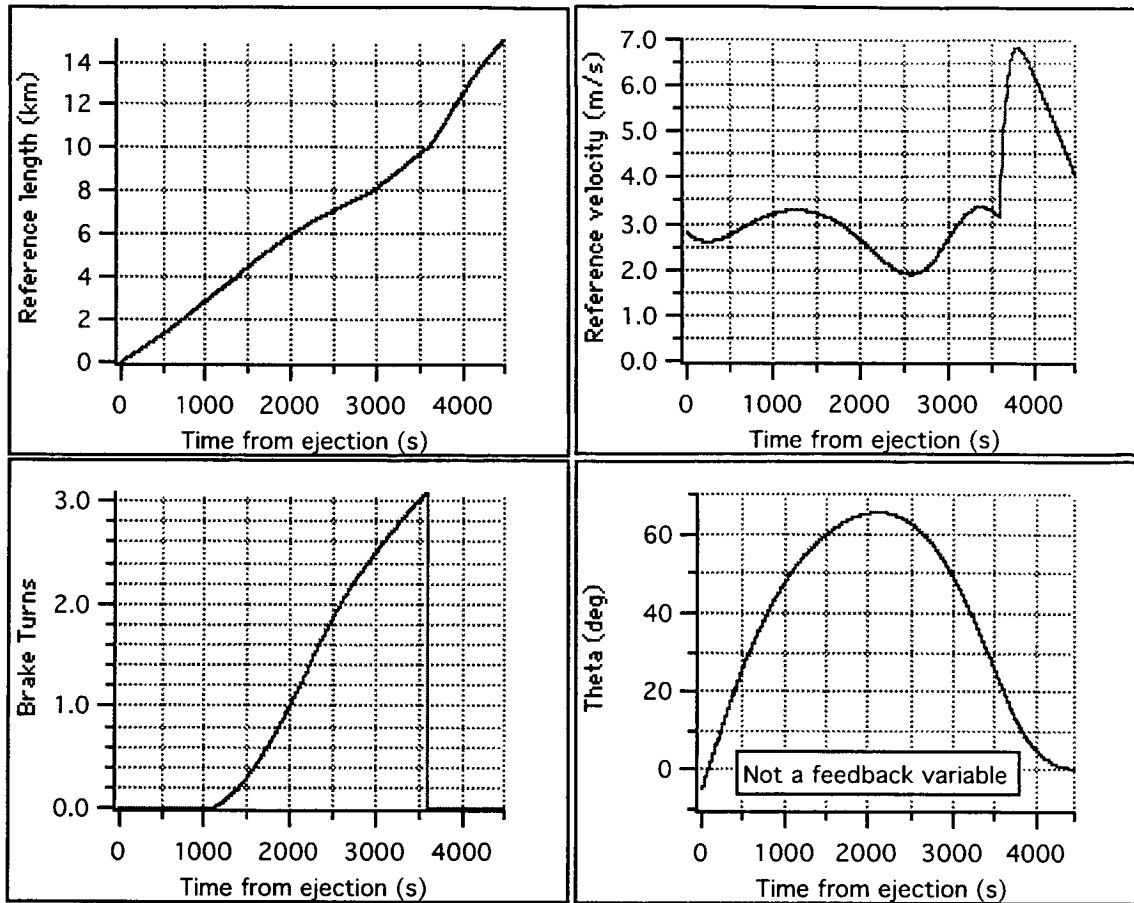


Figure 30 Deployment Reference Profile #21

Reference Profile #26

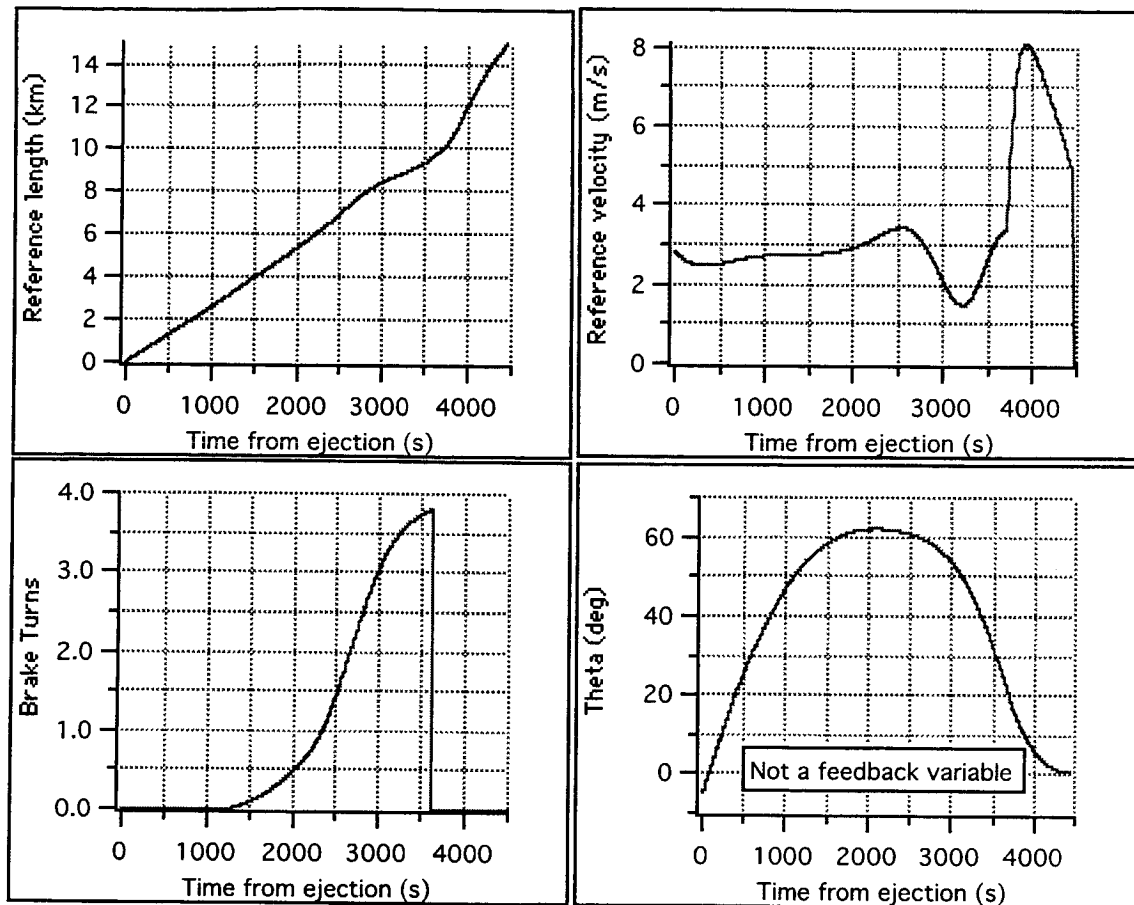


Figure 31 Deployment Reference Profile #26

It is clear from Fig. 32 that a higher ejection velocity has a very beneficial effects as follows: (a) it allows for a smaller residual libration amplitude and (b) it makes deployment much more tolerant of friction in the leader tether. Consequently, the ProSEDS team adopted the maximum ejection velocity allowable by the ejection system of 2.8 m/s (for an endmass of 20.4 kg). This ejection velocity makes ProSEDS deployable within specs for a T_0 of the leader tether as high as 60 mN (with a hard stop of deployment at short range for $T_0 = 80$ mN).

Figure 32 also shows that for a given value of ejection velocity, the libration performance associated with a reference profile can change depending on the values of the friction parameters as shown by the differences between Ref.#21 and Ref. #26.

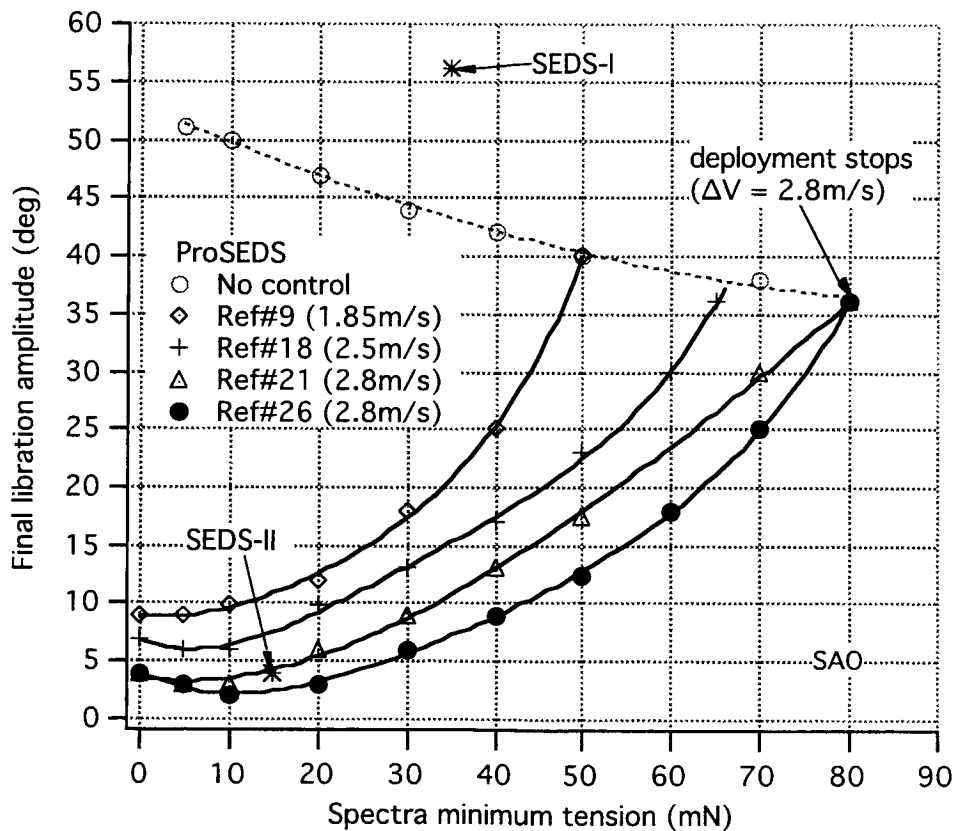


Figure 32 Final libration amplitude vs. T_0 (leader tether) for selected deployment profiles

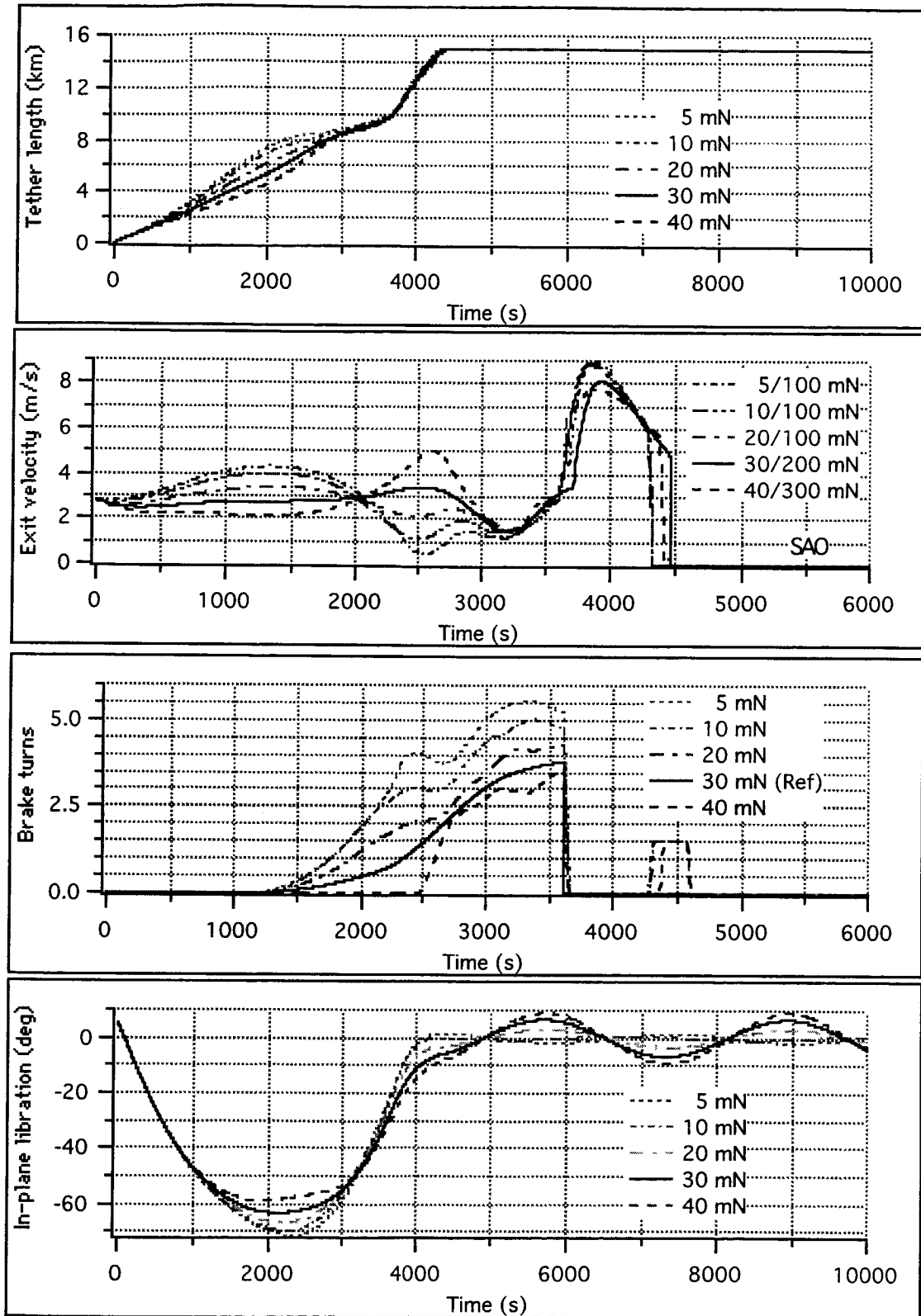


Figure 33 Sensitivity of deployment dynamics to T_0 (Ref#26)

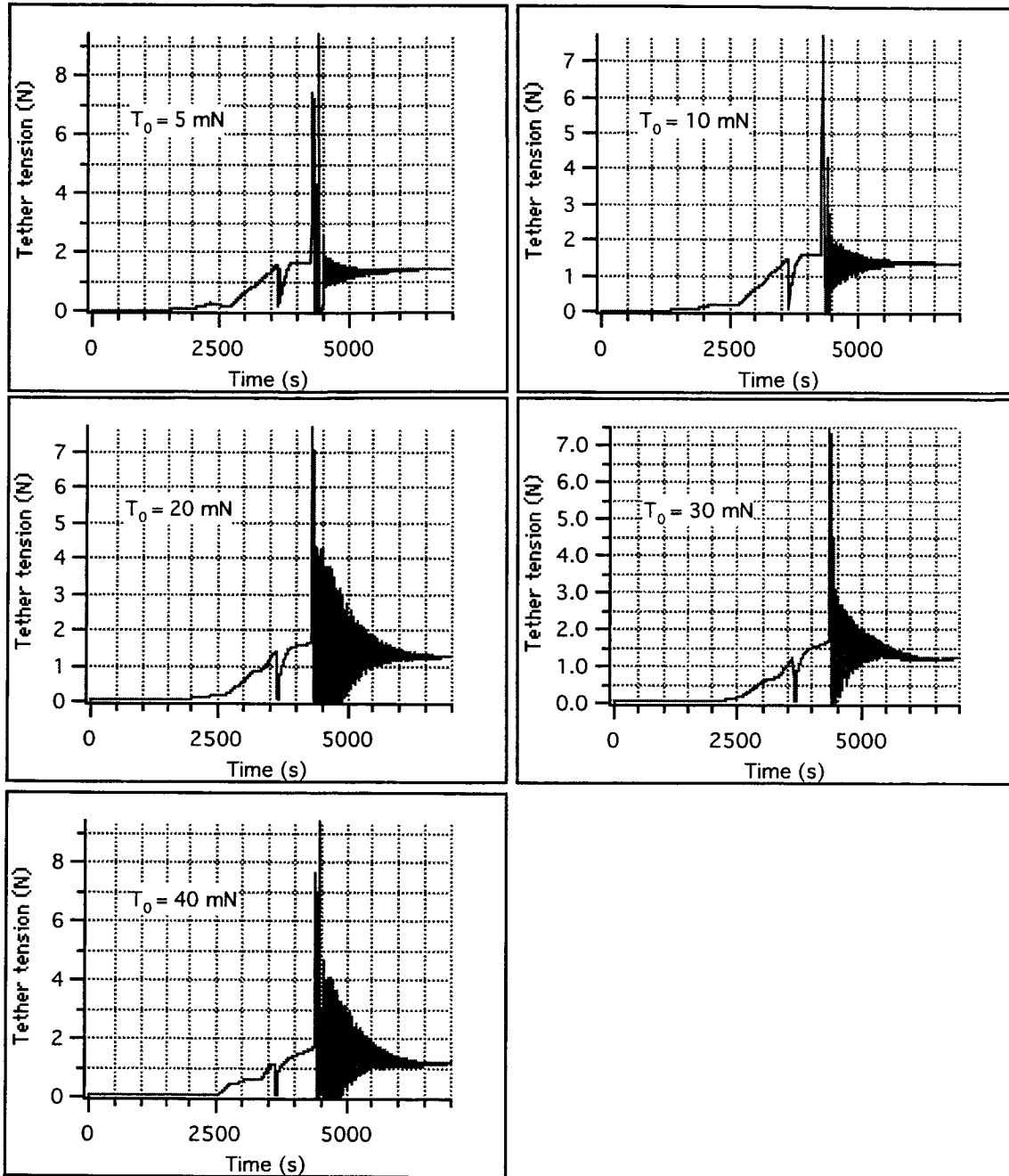


Figure 34 Sensitivity of tether tension to minimum tension (Ref#26)

Simulation results of ProSEDS deployment for Ref. #26 are shown in Figs. 33-34 for different values of the minimum tensions. The dynamic response is well within the required 20 deg maximum residual amplitude for rather conservative ranges of the minimum tension of the leader and wire tethers.

5.3 Mitigation of Tension Spike at End of Deployment

As shown in Fig. 33, the brake is actuated again (this time in an open-loop fashion) before the very end of deployment. There is, in fact, a need to mitigate the tension spike at the end of deployment which, if unmitigated, causes problems with the attitude of the Delta stage after deployment. The Delta stage will be without power well before the end of ProSEDS deployment and, consequently, it will be unable to damp out actively the attitude perturbations generated by the tether tension.

If the brake is not actuated before the end of deployment, the value of the exit velocity can be as high as 6 m/s. Upon reaching the end of the run at non-zero speed, a tension wave propagates through the tether with a maximum peak estimated at less than 50 N for a tether longitudinal stiffness $EA = 15,000$ N.

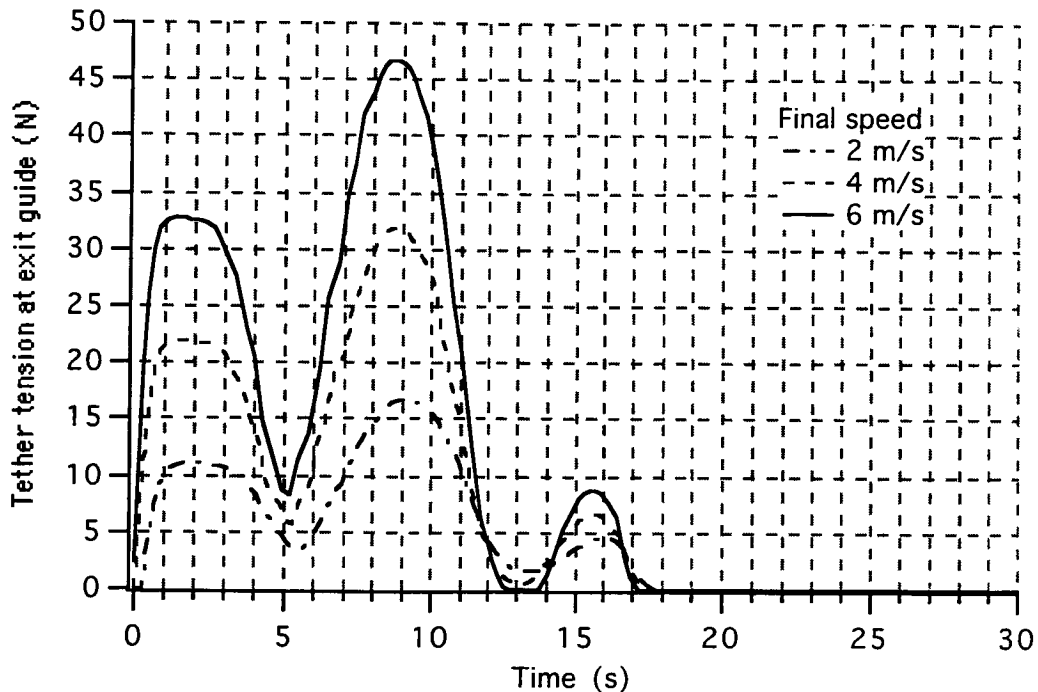


Figure 35 Tension vs time following a hard stop at 15-km tether length ($EA = 15,000$ N)

The actuation of the brake before the end of deployment can not be done during the wire deployment because of the risk of stopping deployment before the insulated portion of the tether has exited the deployer. Consequently, we decided to take advantage of the brake

enabler sensor that is positioned at (and can detect) the beginning of the insulated tether portion. The insulated tether portion is (currently) only 160 m long which implies that the time available for the slowdown maneuver is short. Moreover, the final tether portion deploys in a noisy frictional mode when little tether is left in the deployment canister. For the reasons above an open loop control strategy was selected for the brake actuation before the end of deployment. The actuation takes place according to the braking profile shown in Figure 36.

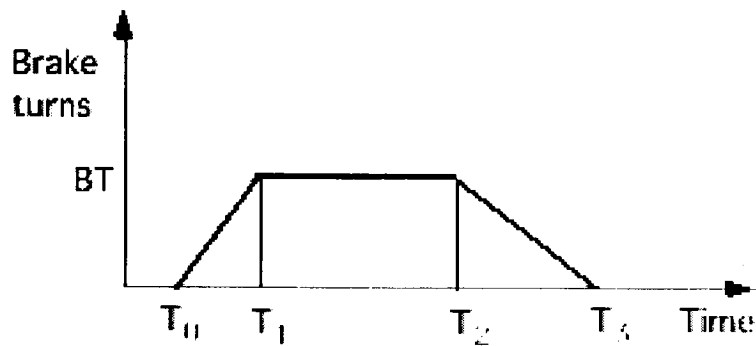


Figure 36 Braking profile for tension spike mitigation

The control parameters are as follows:

BT = number of brake turns for slow down

T_0 = start time defined by brake enable switch

T_1 = end of ramp up time

T_2 = start of ramp down time

T_3 = end of ramp down time

$$\Delta T_1 = T_1 - T_0$$

$$\Delta T_2 = T_3 - T_2$$

T_0 (time and not tension) is determined by the brake enabler switch, T_3 is a predefined time measured from the beginning of deployment (endmass ejection), ΔT_1 and ΔT_2 are predefined time intervals.

Values of the slow down parameters that were used in the previous simulations are as follows: $T_3 = 4520$ s, $\Delta T_1 = 25$ s, $\Delta T_2 = 25$ s and $BT = 1.5$ turns. These values of the slowdown parameters need to be fine tuned (before freezing the design of the flight control software) based on new results from deployment tests on the ground.

5.4 Concluding Remarks

The deployment reference profiles were progressively improved thanks in large part to the increased ejection velocity and also to the improved knowledge of the frictional characteristics of the tether. The present reference profile #26 is rather robust as it can tolerate relatively large changes in the minimum tensions of the leader tether and the wire. Within a realistic range of the minimum tension for the leader tether, i.e., 0-40 mN reference #26 provides a final libration amplitude of less than 10° . The same profile meets the requirement of a maximum libration of 20° for values of the minimum tension of the leader tether for a minimum tension less than 60 mN. The deployment control law is not affected by the minimum tension of the wire as the control law is not activated during the wire deployment. The final libration itself is negligibly affected by the minimum tension of the wire for values between 100-300 mN. The deployment of the wire is well behaved for values of the minimum tension up to 500 mN. Modifications to the deployment reference profile will be made in the future depending on new results from deployment tests on the ground.

6. UPDATED SYSTEM PERFORMANCE

6.1 Introduction

The performance of ProSEDS will be assessed on the basis of the decay rate of the Delta stage which is affected mostly by the plasma conditions at the time of launch. The launch date of ProSEDS has changed with respect to the performance analysis carried out in the early time of this project and reported in the previous sections. For this reason it is important to update the analysis and to compare those results.

6.2 Updated Values of Decay Rates

We are presently in the solar cycle 23 during which the solar activity peaked in April-June 2000. Consequently, the solar activity and the plasma density (that is a function of the solar activity) will likely decrease over the next few years (see Fig. 38).

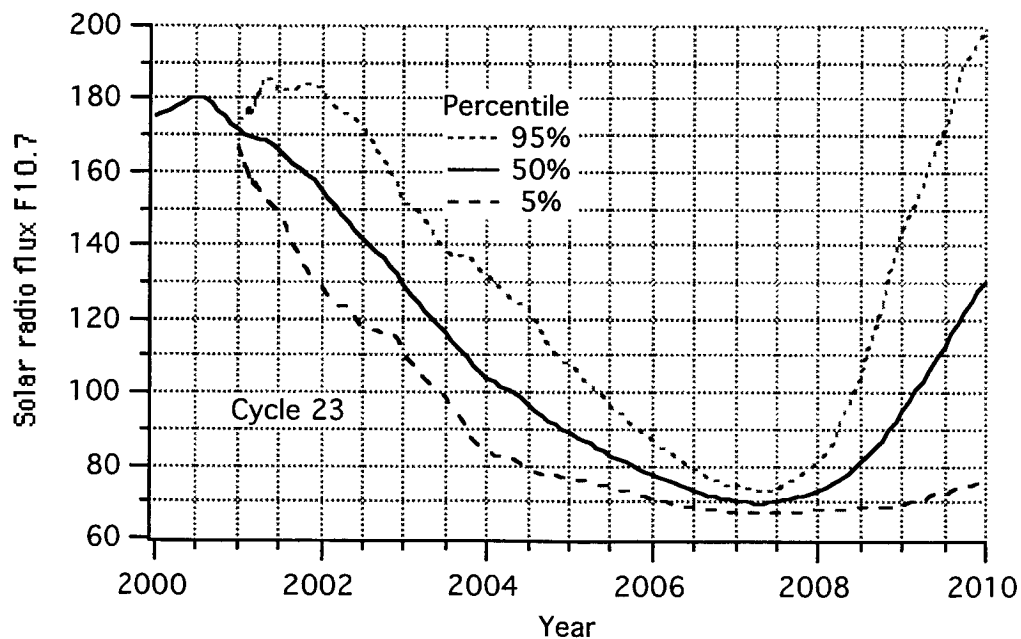


Figure 37 13-month smoothed F10.7 radio flux [from MSAFE NASA/MSFC]

In other words, we should expect that a mission launched in August 2001 or later will exhibit a slower decay rate than a mission launched in August 2000. The later the mission will take place during the next few years, the slower the decay rate because of the reduced plasma density.

We have produced an updated reference mission for nominal (50% percentile) solar activity and according to the updated mission sequence with 7 orbits (instead of the previous 3) operating under the primary operating cycle. The goal of this analysis is to estimate the orbital decay rate during the first day (primary mission phase) and the first week (extended mission phase). The launch time (not yet known) influences the position of the plasma field with respect to the magnetic field and, hence, affects the decay rate because of the phase of the maxima of the magnetic field with respect to the maxima of the plasma density. If we consider two mission start times, one close to local noon and after to midnight, the difference in decay rates is less than 10% in favor of the night launch.

Table 6 Decay rates for different launch dates

Launch date	Orbit (kmxkm)	1 st day decay rate (km/day)	1 st week decay rate (km/day)
April 2000 ^o	400x400	12.5*	14.3
August 2000 [#]	400x400	10.6*	12.0
August 2001 [#]	400x400	9.4	11.8

* The primary cycle was limited to 3 orbits in 2000 as opposed to 7 in 2001 resulting in a first-day decay rate which is closer to the weekly decay rate than in the 2001 scenario

^o night launch

[#] day launch

The main measure of ProSEDS success will be the decay rate of the Delta stage which is increased by more than an order of magnitude with respect to the Delta stage natural decay. The success criteria for ProSEDS specify a decay rate of at least 5 km/day. Assuming the worst possible condition that ProSEDS will operate only for the primary mission phase of 1 day, it is clear from Table 6 that the margin on the success criteria (now slightly less than two) is decreasing and it will decrease a bit more if the launch is postponed further (see later on).

7. UPDATED MISSION ANALYSIS

7.1 Effects of a lower orbit

Another issue that is essential for the success of ProSEDS is that the decay rate must be dominated by the electrodynamic forces rather than the drag due to the neutral density. In other words, the ratio of the electrodynamic forces over the atmospheric forces must be large. One related problem is, however, the determination of the (neutral) drag area of ProSEDS. We have to consider that the Delta stage is not 3-axis stabilized and the 10-km-long, non-conductive tether is flat and likely randomly twisted. The 5-km-long conductive tether is cylindrical and, consequently, unaffected by the twist.

The Delta stage will be hanging from the tether with a torque equilibrium angle (TEA) of about 35° . The stage will be fairly close to the local vertical and rotating about the tether axis, that is, its drag area will be $A_{\text{Delta}} = A_{\text{max}} \cos(\text{TEA})$ where A_{max} is the lateral drag area of the Delta. For $A_{\text{max}} \approx 12 \text{ m}^2$ and $\text{TEA} = 35^\circ$, $A_{\text{Delta}} \approx 10 \text{ m}^2$. However, later during the mission the Delta stage develops large attitude oscillation and its effective drag area can not be estimated accurately.

The flat tether has a close to rectangular cross section of $0.2\text{mm} \times 1.2\text{mm}$. If we assume that the tether will have many twists so that its orientation with respect to the ram follows an 'ABS(cosine)' law we can estimate the drag area as $A_{\text{ncTether}} = (2/\pi) \times W \times L$ where W and L are the width and length of the non-conductive tether. For $L = 10 \text{ km}$ and $W = 1.2 \text{ mm}$, $A_{\text{ncTether}} \approx 7.7 \text{ m}^2$. Finally, after adding the cross section of the $1.2\text{mm} \times 5\text{km}$ conductive tether, we obtain $A_{\text{Drag}} \approx 23.7 \text{ m}^2$ for the total drag area of the system.

Figure 39 shows estimated deorbit rates for ProSEDS assuming nominal operating cycle starting from 400 km and 360 km compared with those from neutral drag on ProSEDS system with no current. Neutral drag is included in all cases. Actual ProSEDS deorbit rate would likely be greater than what is shown in Fig. 39 due to extended periods of battery charging. Simulations assume OML current collection and constant 220 ohm resistance for tether. A satellite without a tether would deorbit more slowly than a tethered system without current.

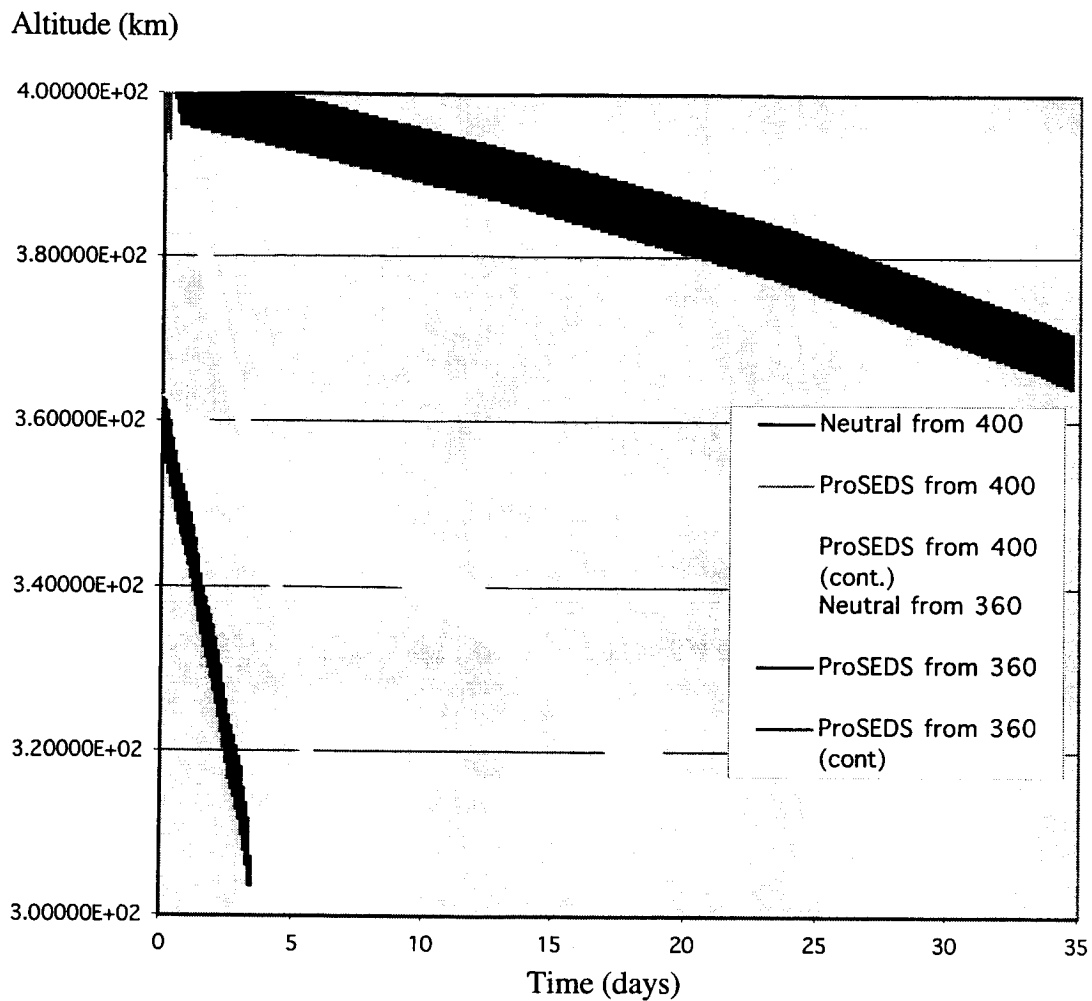


Figure 38 Decay rates of ProSEDS for various altitude and operational scenarios with a launch in August 2001

The ratio of electrodynamic forces to atmospheric (i.e., neutral density) drag forces was estimated by computing the orbit-average magnitude of those forces acting on ProSEDS at various altitudes for a launch in August 2001. An error band on the ratio between electrodynamic and neutral drag forces was also computed based on estimates of the

variability of the plasma and neutral densities for 5 and 95 percentile probabilities as shown in Fig. 40.

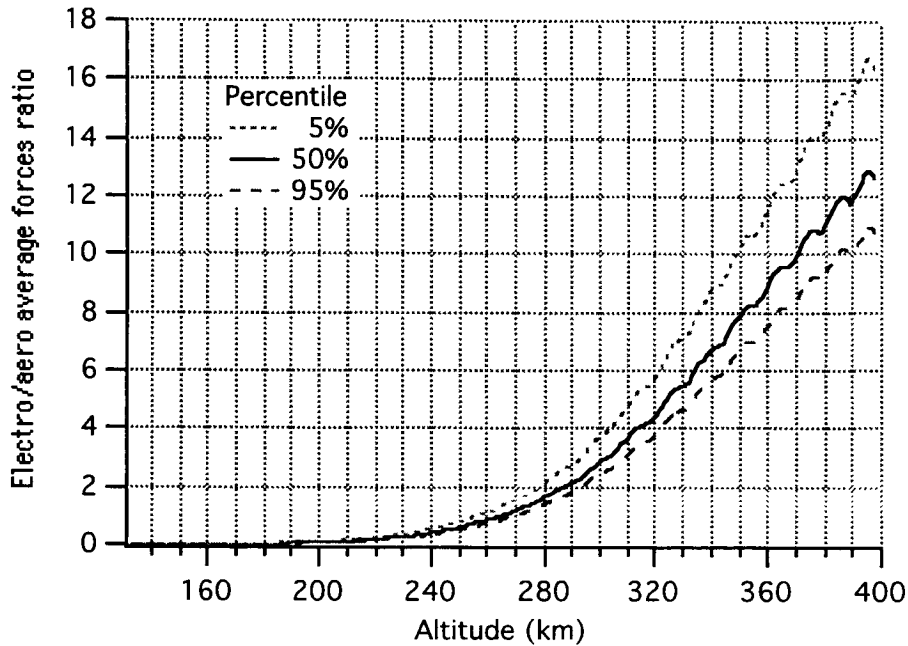


Figure 39 Ratio of average electro/aero forces vs. altitude

In summary, the electrodynamic forces overpower the neutral drag forces under nominal conditions (at 50% percentile probability) by a factor of 13 at 400-km of altitude and a factor of 9 at 360 km of altitude. Under the most conservative conditions (at 95% percentile probability), the ratio of the two forces is approximately equal to 11 and 8 at 400 km and 360 km of altitude, respectively.

7.2 Atomic Oxygen Tether Erosion

The lifetime of the ProSEDS tether is affected by two major factors: (1) micrometeoroids and orbital debris (M/OD) impacts and (2) erosion by atomic oxygen (AO). It was computed by NASA/MSFC that the tether of ProSEDS has about a 82% probability of surviving M/OD hits over a period of 14 days¹². Conversely, the probability of a fatal hit over 14 days is about 18% (ie, 1.3% per day probability of failure).

The rate of erosion of the Dyneema by AO is more deterministic than the M/OD impact risk. This rate can be computed by integrating the flux of AO impinging on the tether over the altitude profile during the orbital decay. The AO density is derived from the MSIS'86

atmospheric model that is part of the SAO tether dynamic simulator. The critical value of the integrated AO mass flux that makes the tether fails depends on the tether design and internal structure.

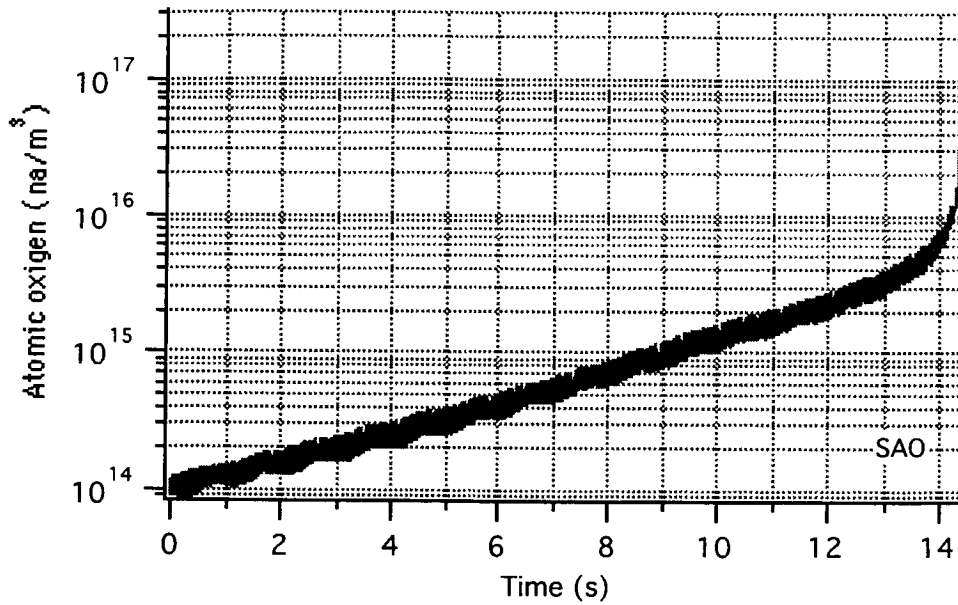


Figure 40 Atomic oxygen density (number-of-atoms/m³) vs. mission time for nominal atmospheric conditions.

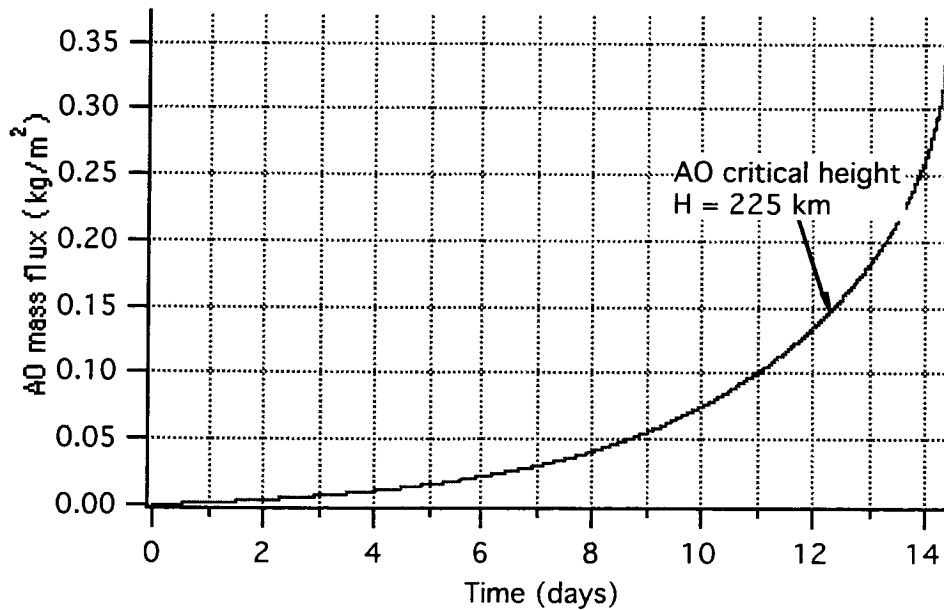


Figure 41 AO mass flux integrated over mission time (start altitude = 400 km)

For a flat braided tether like ProSEDS, it is reasonable to assume that the tether fails once the AO has chewed away a layer of tether as thick as the fibers that constitute the braided tether. With this assumption, the critical value of the integrated AO mass flux is = 0.15 kg/m^2 . Figure 40 shows the AO density which increases as the orbit of ProSEDS moves lower. Figure 41 shows the AO mass flux (vs. time) integrated over the trajectory spanned by ProSEDS.

If we assume nominal atmospheric density conditions (at 50% probability), a launch date in August 2001 and a starting altitude of 400 km, the critical altitude where the Dyneema tether fails due to AO is equal to 225 km, which occurs (for simulated conditions) after about 12 days from the mission start.

8. UPDATED DYNAMICS REFERENCE MISSION

8.1 Reference Mission Simulation

The orbital and system parameters for the reference mission are as follows:

Orbit: 400 km circular

Inclination: 36 deg

Launch date: 16 August 2001

Ascending node for: (a) day launch at about 10:00AM EST and (b) night launch at about 10:00PM EST

Ionosphere/Atmosphere: nominal (50 percentile) solar activity at time of launch

Delta mass: 994 kg

Endmass: 21.4 kg

Tether linear densities: 0.15 kg/km (Dyneema); 2 kg/km (wire).

Tether optical properties:

Dyneema: $\alpha_s = 0.1$, $\epsilon_{IR} = 0.5$;

C-COR coated wire: $\alpha_s = 0.9$, $\epsilon_{IR} = 0.8$.

Tether mechanical properties: $EA = 15,000$ N; $E'A \approx 2000$ Ns.

Tether electrical resistance: 265 ohm at 20 °C.

Operating modes¹³: 7 orbits according to the primary mode and the remainder according to the secondary mode. The first operating cycle starts approximately when the Delta stage crosses the Atlantic coast of South America (see Fig. 43).

The time of launch affects the phasing between the magnetic field (corotating with the Earth) and the plasma field which is mostly driven by the position of the Sun. Because the time of launch is not yet known for the Delta rocket, simulation have been run for a day launch which sets the deployment of ProSEDS close to 10:00AM EST and a night launch

which sets the deployment close to 10:00PM EST. The ground trace of the orbit is unaffected by the time of launch but is shown again in Fig. 42 (provided by The Boeing Company) because the time of deployment start (and its orbital location) has changed with respect to the previous analysis.

The results of the day-launch simulation August 2001 are shown in Figs. 43-48 over the extended mission duration of over 2 weeks. The system response (not show here) for a night launch is similar to the day launch with the notable difference of a 6% increase in the decay rate and average current with respect to the day-launch case.

The main conclusions from the analysis of the reference mission are as follows:

The decay rate during the first day (primary mission) is about 9.4 km/day and 10 km/day for the day and night launches, respectively. These values exceed the minimum value of 5 km/day established as a success criteria for ProSEDS but the margin for errors has been reduced substantially with respect to the cases with a launch in August 2000.

The orbit-average current produced by the tether and the decay rates are as follows:

Day launch:

Orbit-average current = 0.8 Amp (over entire current cycle)

Orbit-average current = 1.5 Amp (during battery charging)

1st day decay rate = 9.4 km/day

1st week decay rate = 11.8 km/day

Night launch

Orbit-average current = 0.85 Amp (over entire current cycle)

Orbit-average current = 1.6 Amp (during battery charging)

1st day decay rate = 10 km/day

1st week decay rate = 12.4 km/day

The minimum and maximum tether temperatures for the Dyneema tether and the C-COR wire are:

Dyneema: from -90 °C to -45 °C;

C-COR: from -86 °C to +53 °C.

The tether temperatures are within the allowable limits for the two tether types.

The system dynamics is stable and rather well-behaved (like for a launch in August 2000) over the extended mission lifetime of over two weeks. Because of the relatively low ratio of absorptivity/emissivity ($\alpha/\epsilon \approx 1.1$) provided by the latest formulation of C-COR, the wire temperature is rather low as it ranges from -86 °C to +53 °C. Consequently, the electrical resistance of the wire ranges from 150 ohm to 300 ohm.

(ESTAR Min. for T/M Sites = 2.00 deg)

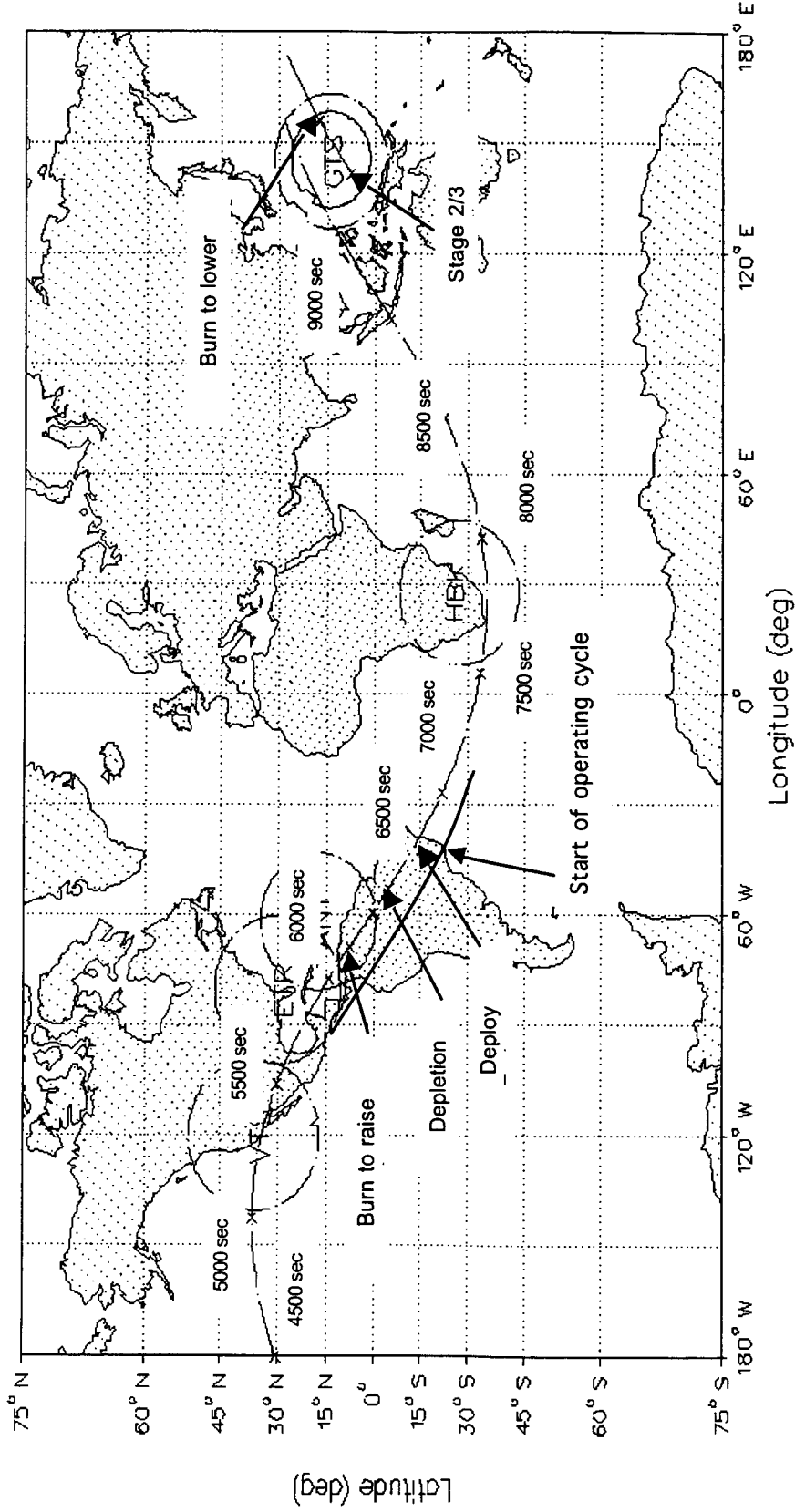


Figure 42 Ground trace of (August 2001) Delta 7925 Block IIR trajectory [adapted from The Boeing Company]

ProSEDS 265 ohm@20 C, 400x400km, nom. solar, day launch, Antigua burn, 16 August 2001

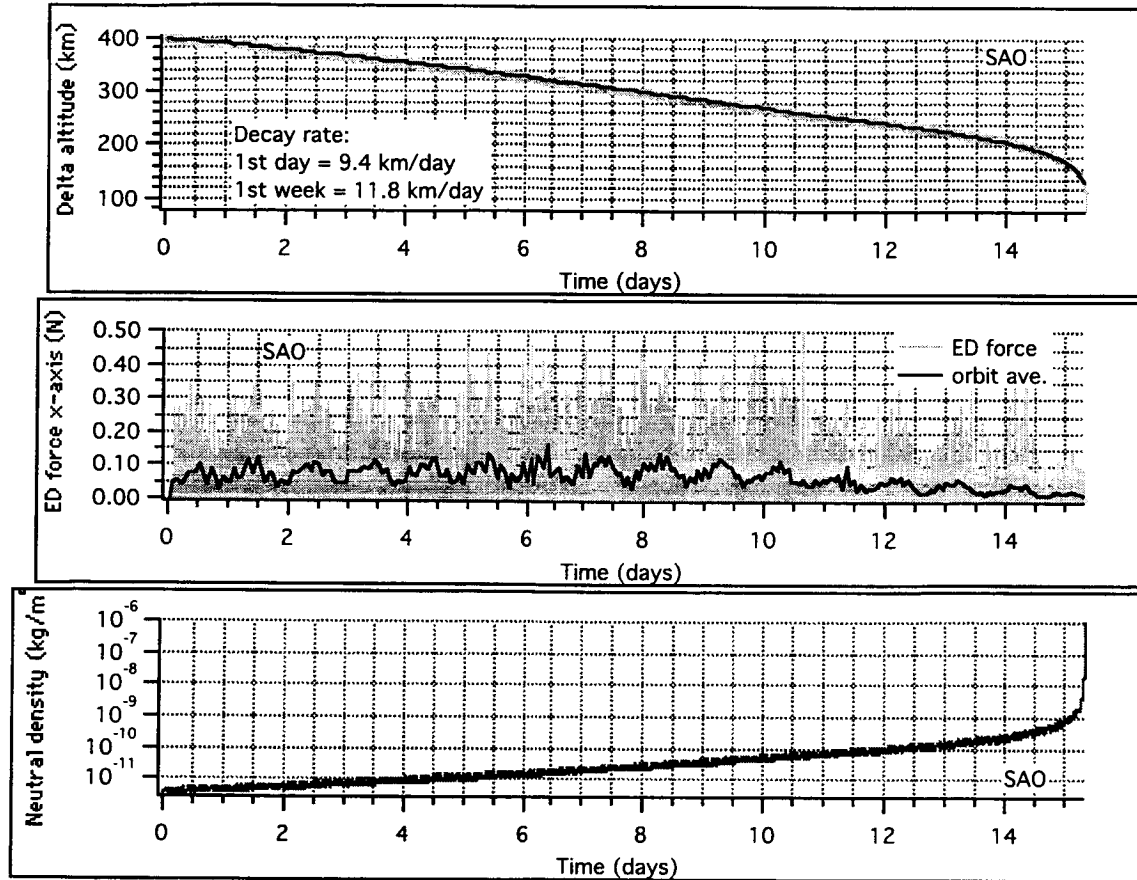


Figure 43 Results for day-launch with launch date on 16 August 2001.

ProSEDS 265 ohm@20 C, 400x400km, nom. solar, day launch, Antigua burn, 16 August 2001

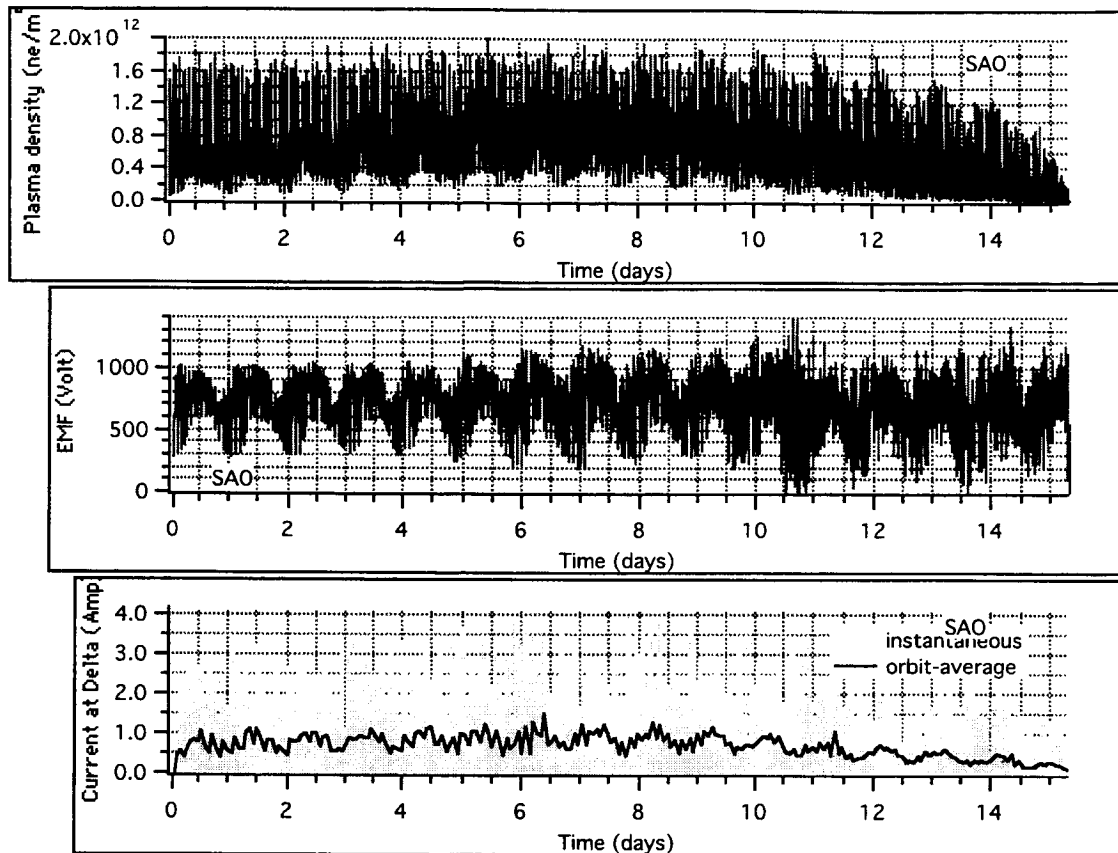


Figure 44 Results for day-launch with launch date on 16 August 2001.

ProSEDS 265 ohm@20 C, 400x400km, nom. solar, day launch, Antigua burn, 16 August 2001

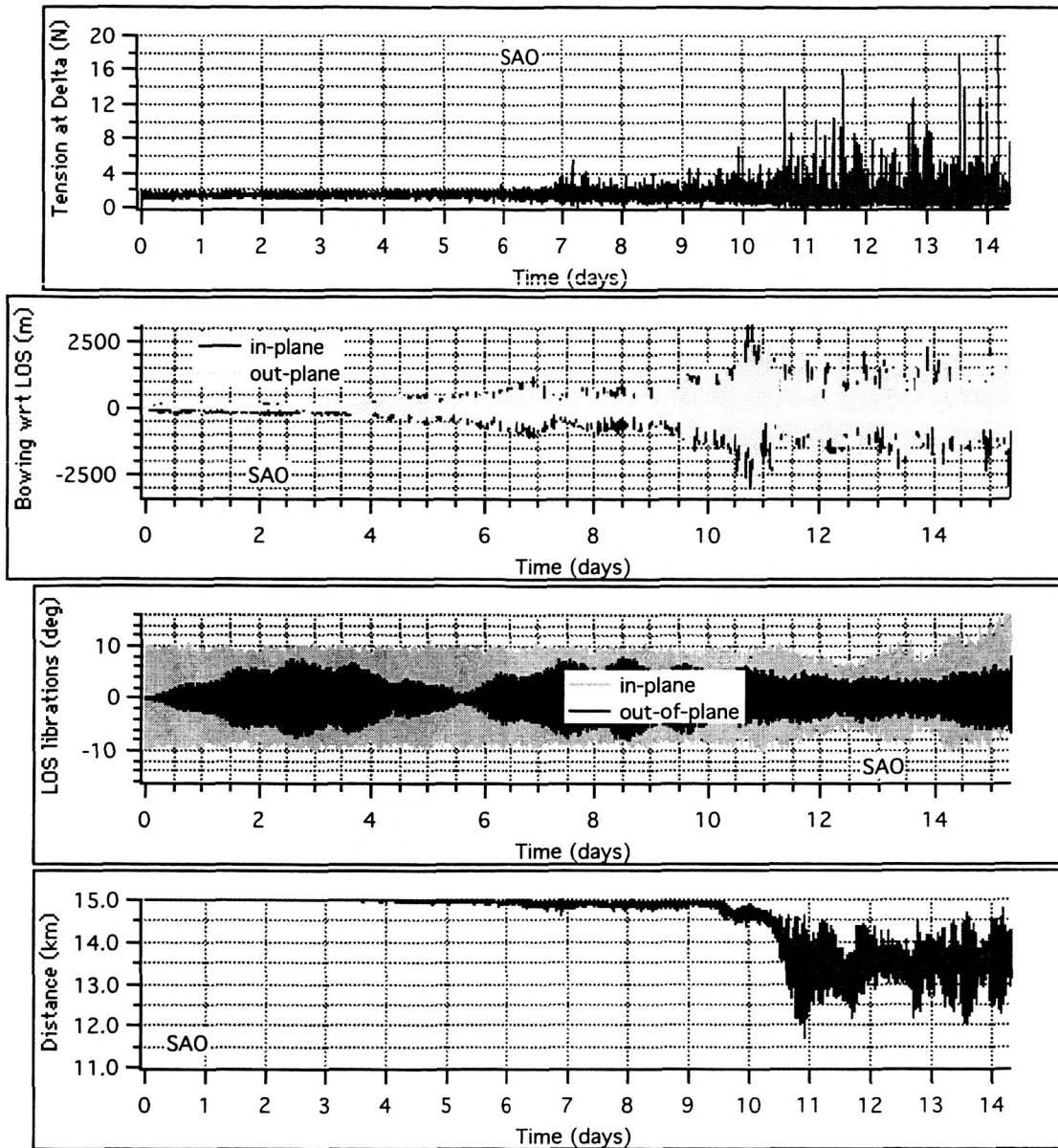


Figure 45 Results for day-launch with launch date on 16 August 2001

ProSEDS 265 ohm@20 C, 400x400km, nom. solar, day launch, Antigua burn, 16 August 2001

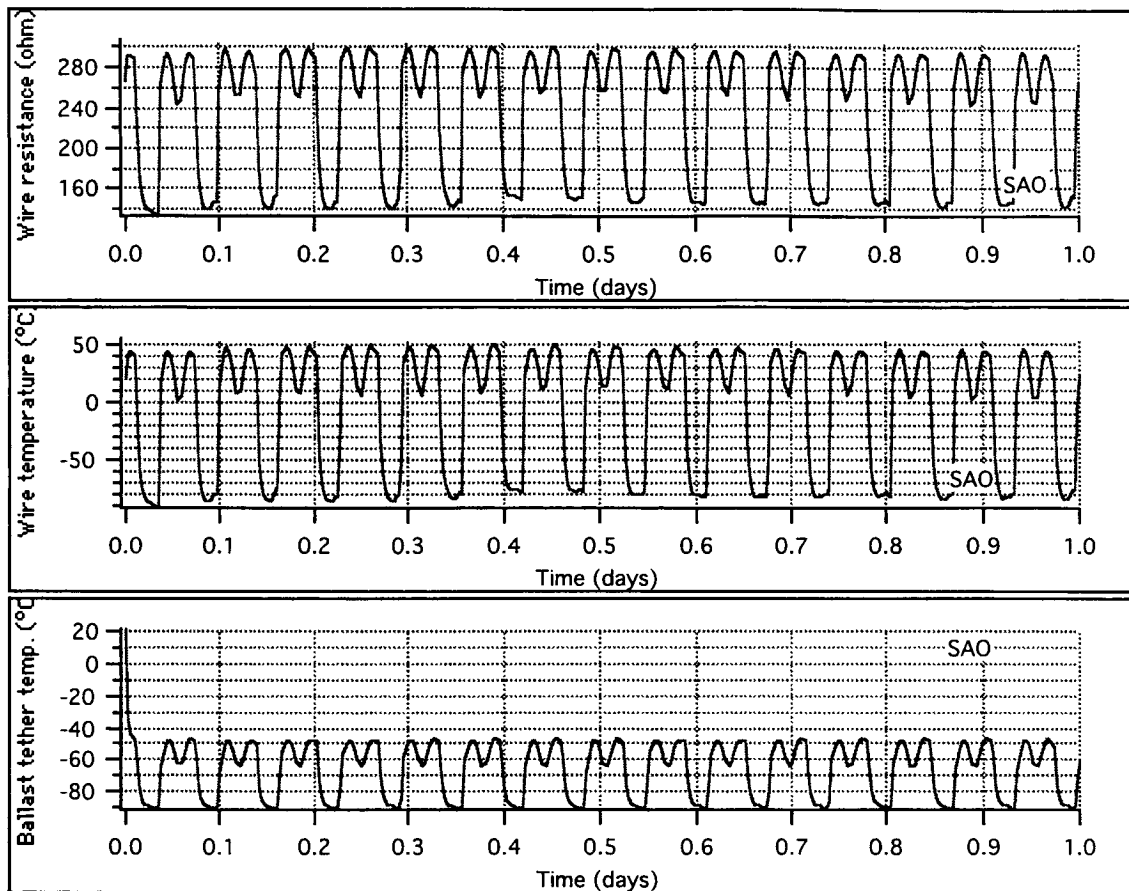


Figure 46 Results for day-launch with launch date on 16 August 2001

ProSEDS 265 ohm@20 C, 400x400km, nom. solar, day launch, Antigua burn, 16 August 2001

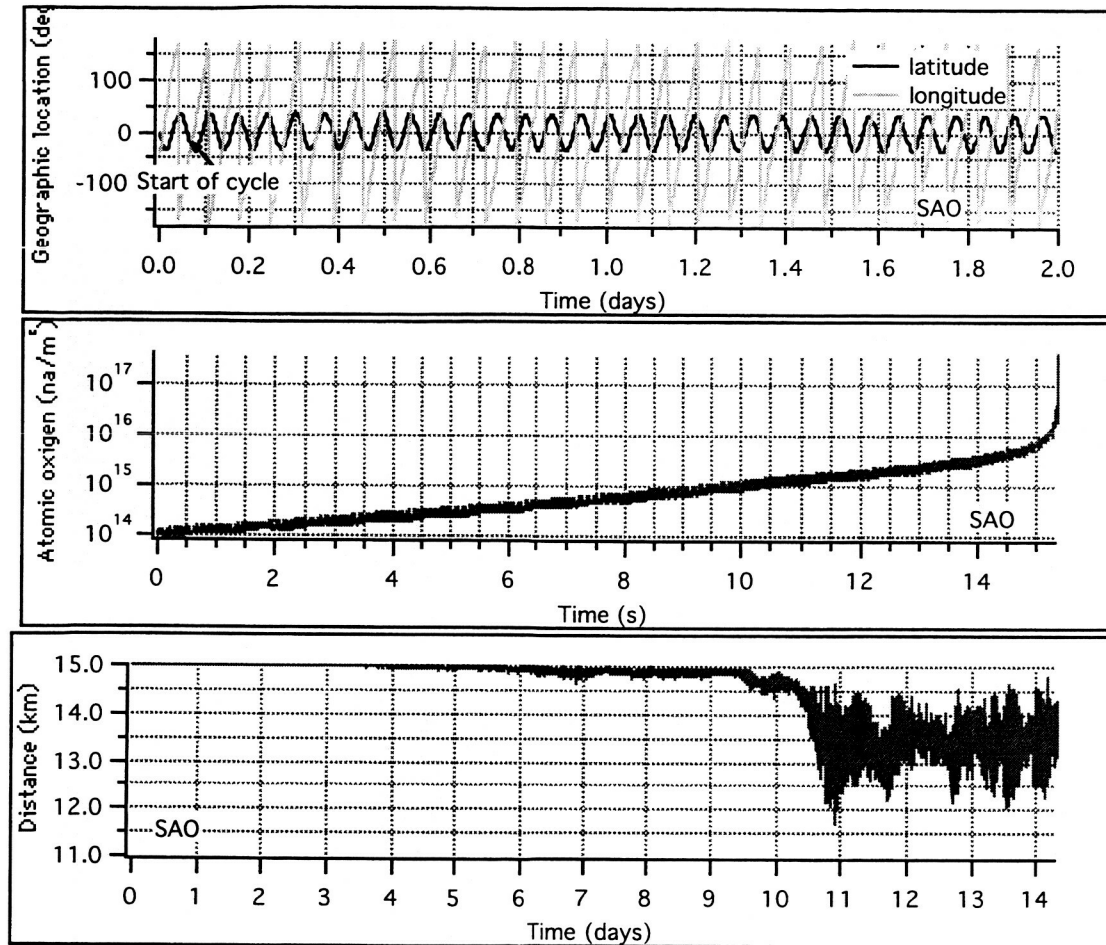


Figure 47 Results for day-launch with launch date on 16 August 2001

8.2 Extreme Cases

For the purpose of evaluating the system behavior under extreme conditions, cases were also run for: (1) a plasma density that is (artificially) twice the plasma density under nominal conditions and (2) without any electrodynamic force. These simulations were run for a 5 day mission duration as the MSFC project team was interested in estimating ProSEDS position under worst case scenarios and, hence, evaluating the risk posed by this system to other spacecraft operating at the same altitude.

The double plasma density increases the decay rate to 16.5 km/day averaged over a week (and hence the error in the pre-flight estimate of the position). Fig. 48 shows the plasma density, altitude and geographic position (latitude and longitude) of the system. The latitude and longitude are shown over a period of only 2 days for increasing the display clarity. It is notable that the decay rate does not double with respect to the baseline case thanks to the ability of the bare tether to adjust in part to changing plasma conditions.

The case without electrodynamic forces provides the largest difference in ProSEDS position with respect to the nominal estimate because the decay rate is reduced by more than a factor of 10 with respect to the baseline case (with nominal electrodynamic forces) when the electrodynamic forces vanish. Figure 49 shows the plasma density, altitude and geographic position of the system for this case.

The position errors after 1 day of mission elapsed time are shown in Table 7. The latitude and longitude angular errors have been converted to kilometers assuming an orbital altitude of 400 km. The distance is the magnitude of the position error vector. The errors grow approximately linearly with mission time.

Table 7 ProSEDS position errors after 24 hours

	Altitude error (km)	Latitude error (km)	Longitude error (km)	Distance (km)
No current	+7.3	-208	-614	648 (lag)
Double plasma	-2.3	+68	+222	232 (lead)

ProSEDS 265 ohm@20 C, 400x400km, 2xnominal plasma density, day launch, 16 August 2001

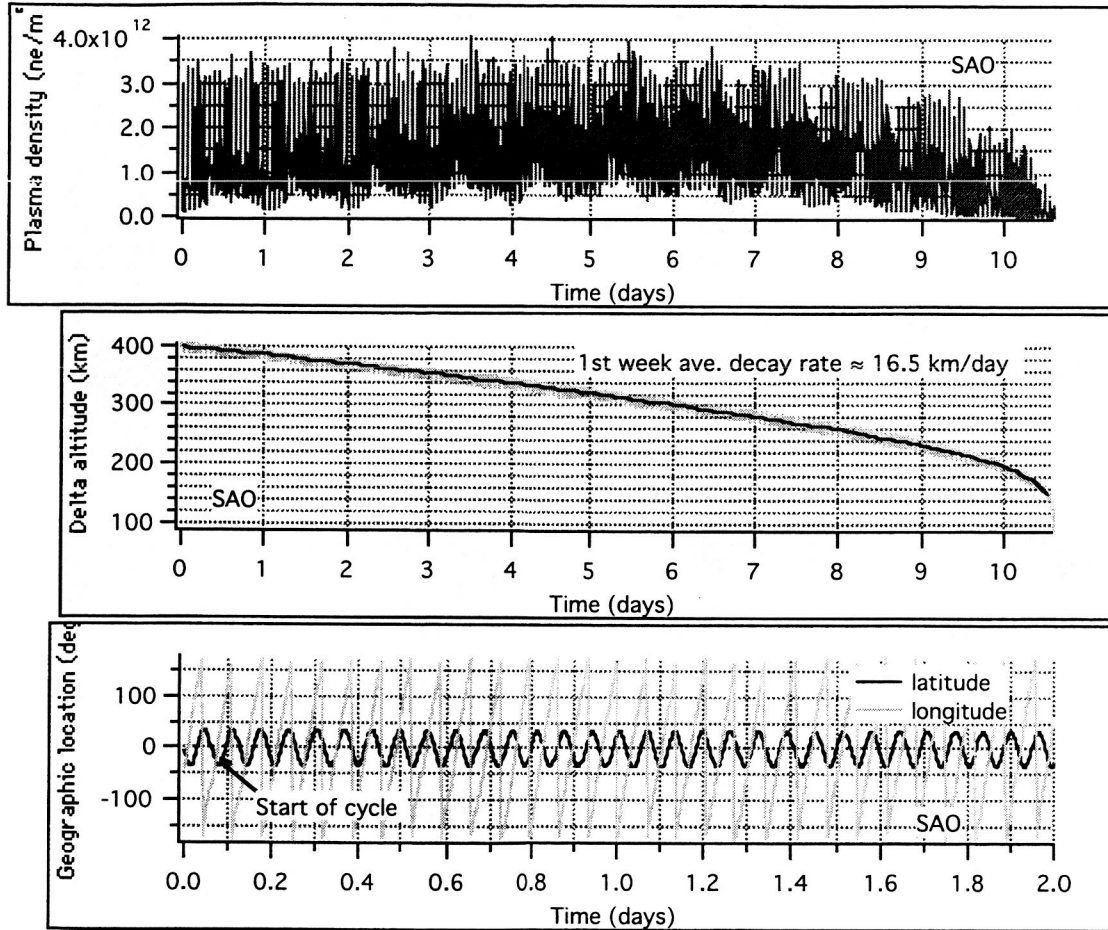


Figure 48 System decay and geographic position (latitude and longitude) for double the nominal plasma density on 16 August 2001.

ProSEDS 265 ohm@20 C, 400x400km, no plasma, day launch, 16 August 2001

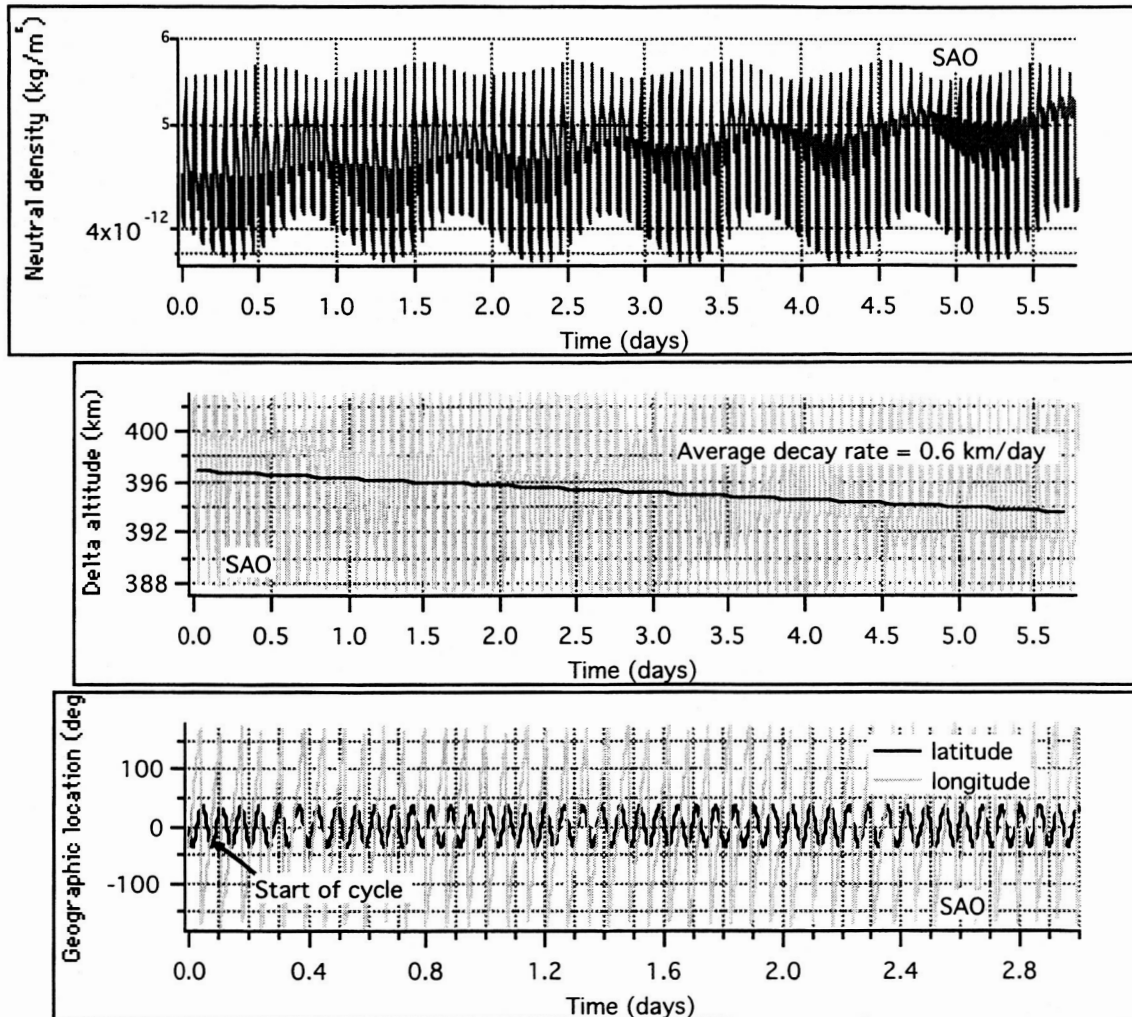


Figure 49 System decay and geographic position (latitude and longitude) without any electrodynamic forces for a launch on 16 August 2001.

8.3 Concluding Remarks

The postponement of the mission to August 2001 does not change substantially the dynamics of ProSEDS with respect to cases with earlier launch dates. The 1st day decay rate, however, is reduced by about 11% (with respect to a launch in August 2000) due to the reduced plasma density and the increase in the number of orbits on the primary operating cycle. The reduced plasma density is a consequence of the launch date moving away from the peak of the solar cycle 23 that occurred in April-June 2000. With the launch date being postponed even further, the decay rate and the average current available for recharging the secondary batteries will be further reduced.

The present estimates of the orbital decay rate during the 1st day of the mission are 9.4 km/day and 10 km/day for day and night launch, respectively. The estimates of the average current, for ProSEDS operating on the secondary cycle, are 0.8 Amp and 0.85 Amp for a day and night launch respectively with the average computed over the entire secondary cycle. When the average is computed over the *battery charging portion* only of the secondary cycle, then the average current values are 1.5 Amp and 1.6 Amp for a day and a night launch, respectively.

Conservative estimates of ProSEDS position error with respect to the nominal trajectory were also computed for two extreme cases of no current and excessive current due to an (artificial) doubling of the plasma density. After one day of mission elapsed time, the magnitude of the position errors are about 648 km (lag) and 232 km (lead), for the two case above, with respect to the nominal position. The position errors grow approximately linearly with time.

9. UPDATED DEPLOYMENT CONTROL PROFILES AND SIMULATIONS

9.1 Introduction

The ProSEDS control law consists of three distinct modes of operations which are activated during the deployment of the three different tether sections. The non-conductive 10-km-long Dyneema tether is deployed according to the SEDS-II feedback-feed-forward control law. During the deployment of the 4.9-km conductive wire, the brake is simply kept at a constant, low value (typically a fraction of a turn) in order to limit the deployment velocity. During the deployment of the 205-m (the value was increased from the original 160 m) insulated tether section, the brake is commanded to follow a time-based profile to slow down the deployment velocity at the end of the tether.

As explained in more details previously, the control law utilizes a set of control parameters and a reference table that provides the feedforward information to the first portion of the control law. The feedback, then, adjust the nominal fed forwarded brake profile based on the errors of the actual length and speed with respect to the nominal length and speed profiles.

The second and third portions (for the CCOR wire and insulated section deployment) are open-loop control. The second portion is a tension-offset control in which the brake is kept constant at a low value of turns simply for increasing the tether tension and reduce the maximum exit velocity. The wire is coated with a fairly delicate coating that can be rubbed off by excessive friction. Consequently, it is not possible to utilize a feedback control that ramps the brake up and down. The offset value of the brake utilized during this portion is a constant value in the range 0.5-0.8 brake turns.

In the third portion of the control law, the brake is made to follow an open loop rampup-constant-rampdown profile. This control law acts on a 205-m-long section of the tether with a quick rampup phase. Because of the absence of a sensor that measure the exit velocity directly in the SEDS hardware, the velocity must be computed numerically from a noisy signal and then filtered to make it usable for a feedback control law. This process is actually used in the first portion of the control law where a delay in the computation of the velocity does not affect the performance of the controller. Due to the shortness of the reaction time in the third portion of the control law, there is not enough time to obtain a filtered value of the velocity especially at a time when the noise from the tether length information is very high. Consequently, we opted for an open-loop control during this

phase and we shaped the slow down profile in such a way that it is rather tolerant of changes in the friction characteristics of the tether.

9.2 Friction parameters

We rewrite in the following the frictional tension model (derived originally by J. Carroll) of the tether and its parameters because, based on analysis of deployment test data, the brake effect had to be modeled differently, as shown in the following:

$$T = \left(T_0 + I \cdot \rho \cdot \dot{L}^2 \cdot A_{rel}^E \right) \cdot k^{2\pi f n effe} \cdot e^{f|\theta_0 - \theta|} \quad (6)$$

In equation (6), the term in round parenthesis is the frictional model of the tether/deployer as before (see also Ref. ¹⁴). The first exponential function with base k is the new model of the brake and the second exponential function with base e models the tether exit guide (unchanged). The model parameters are:

A_{rel}	=	$1 - A_{sol} \cdot L / L_{fin}$
A_{sol}	=	annulus solidity of tether
L	=	length of tether deployed
L_{fin}	=	final length of tether
B	=	$2\pi f n$ (n is the number of tether turns wrapped around the brake post)
T_0	=	minimum tension
ρ	=	linear density of tether
I	=	inertia multiplier
\dot{L}	=	tether exit speed
ϑ	=	tether's exit angle with respect to the local vertical
ϑ_0	=	tether deployment null angle (orientation of the longitudinal axis of deployer with respect to the local vertical)
f	=	friction coefficient
n	=	number of brake turns
$effe$	=	brake effectiveness coefficient
k	=	base of the brake power law

where k and $effe$ are new parameters. The values of the tether friction parameters obtained from the deployment tests on ground of a development tether and two prototype flight tethers (MAO Tether, Tether-A and Tether-B) resulted in the following values:

Dyneema (cleaned)

T_0	= spectra minimum tension	= $4 + 15L/L_F$ mN
ρ	= spectra linear density	= 0.15 kg/km
I	= inertia multiplier	= 2.5
f	= spectra friction coeff	= 0.19
E	= area exponent	= -0.4
effe	= brake effectiveness	= 0.8
k	= base of brake law	= 1.7
AnSol	= annulus solidity	= 0.2 (for $L_F = 10$ km)

Wire (CCOR)

T_0	= wire minimum tension	= 75 mN
ρ	= wire linear density	= 2.0 kg/km
I	= inertia multiplier	= 3.3
f	= friction coeff	= 0.25
E	= area exponent	= -0.6
effe	= brake effectiveness	= 1.2
k	= base of brake law	= 2.72
AnSol	= annulus solidity	= 0.947 (from 1.25km -> 6.25km)

Insulated (Kevlar overbraided)

T_{min}	= insulated minimum tension	= 350 mN
ρ	= insulated linear density	= 3.17 kg/km
f	= friction coeff	= 0.22
I	= inertia multiplier	= 2.5
E	= area exponent	= -0.6
effe	= brake effectiveness	= 0.9
k	= base of brake law	= 2.72
AnSol	= annulus solidity	= 0.947

The friction parameters of the entire tether (with the three different sections) are utilized to derive the reference table, that is, the reference deployment profile and a brake profile for the entire tether. The brake actuation is then adjusted by the feedback control law during the deployment of 10-km Dyneema portion while the reference brake profile is followed (without adjustments) during the wire and insulated portions of the tether.

9.3 Control parameters

Extensive simulations (numbering in the few hundreds) with a simplified yet accurate computer code are utilized to define and check the control parameters set with the goals of reducing the system libration and the exit speed at the end of deployment and making the control law fairly robust with respect to changes in the friction coefficients.

The present values of the control parameters for ProSEDS are shown in the following. These values may be updated if new results from the deployment tests require it.

```

----- CONTROL PARAMETERS (Ref#55) -----

```

No.	PARAMETER	VALUE (Units)	Type
1.	c	0.125	Filter coefficient
2.	K1	0.002 (1/Turn)	TurnCount Gain
3.	DZTC	5 (Turn)	TurnCount Deadzone
4.	TCELIM	3000 (Turn)	Max. TurnCount Error
5.	K2	0.4 (s/Turn)	TurnCountRate Gain
6.	DZTCR	0.1* (Turn/s)	TurnCountRate Deadzone
7.	TCRELIM	5 (Turn/s)	Max. TurnCountRate Error
8.	WAILP	3	WrapIncrement UpperLimit
9.	TBD s	65535 (s)	Time after which BIAS is applied
10.	BIAS	0 (Turn)	BrakePost Bias
11.	WACL P	6 (Turn)	WrapAdjustment UpperLimit
12.	TCBS	18000 (Turn)	Turns Count Brake Stop (pertinent to SEDS-II)
13.	A1	0.724	Coeff_1 in Variable Gains

14. A2	2.82E-6	Coeff_2 in Variable Gains
15. STOPDEPLOY	65535 (s)	Time for brake ramping up at end of deployment (pertinent to SEDS-II)
16. TCDUTY	13900 (turns)	End of 50% duty cycle
17. TURNBRAKE0	14160* (turns)	ramp down brake to WIREBRAKE
18. WIREBRAKE	0.5 (BrakeTurn)	BrakeTurns during CCOR deployment
19. RAMPUP	25890 (turns)	Start of slowdown procedure
20. QUITLAWBACKUP	14320(turns)	ramp down brake in case of Counter-A or -B failure
21. BRSD	1.5 (BrakeTurns)	Max brake turns during slow down
22. TBD(15)	14.2 (sec)	Time to rampup brake from WIREBRAKE to BRSD
23. TIMECFAIL	120 (sec)	Time of no update of Counter-C to declare the Counter-C failed
24. TIMEDUTY	3300 (sec)	time-based equivalent of TCDUTY
25. TIMEQUERY	4170 (sec)	the software interrogates the BES** if Counter-C had failed
26. TIMERAMPNOBES	4230 (sec)	Time-based start of slowdown procedure if the BES was declared failed

 *Values per ECR SAO-001
 **BES = brake enable switch

9.4 Reference tables

The desired final state at the end of deployment is for the system to be aligned and swingless with respect to the local vertical with a residual longitudinal velocity greater than 3 m/s before the beginning of the insulated portion of the wire (last 205 m of tether). The residual velocity is then reduced by a final activation of the brake immediately after the exiting of the insulated wire is sensed.

Several constraints are imposed to the minimization routine used to derive the reference profile mostly aimed at obtaining a reference brake profile that does not force undesired

situations during deployment. The exit velocity is constrained to be above about 2 m/s during deployment of the non-conductive tether and above 3 m/s during deployment of the wire. The velocity limitations ensure that the satellite has enough kinetic energy to overcome unexpected discontinuities along the tether. A constraint function that penalizes the trajectories with rate values smaller than the predetermined minimal rate values is used in the minimization process to achieve this goal as explained earlier.

The two new reference profiles (out of a large numbers of trials) that have been thoroughly developed and analyzed are the Ref#47 and Ref#55 as follows:

Ref#47 is based on the friction characteristics and spooling of the development tether and it was derived for an orbital altitude of 400 km.

Ref#55 is based on the friction characteristics of the MAO tether and spooling characteristics expected of the F-2 tether (which were extrapolated by Tether Applications from the spooling of the F-1 tether) and it was derived for an orbital altitude of 360 km.

Reference Profile #47

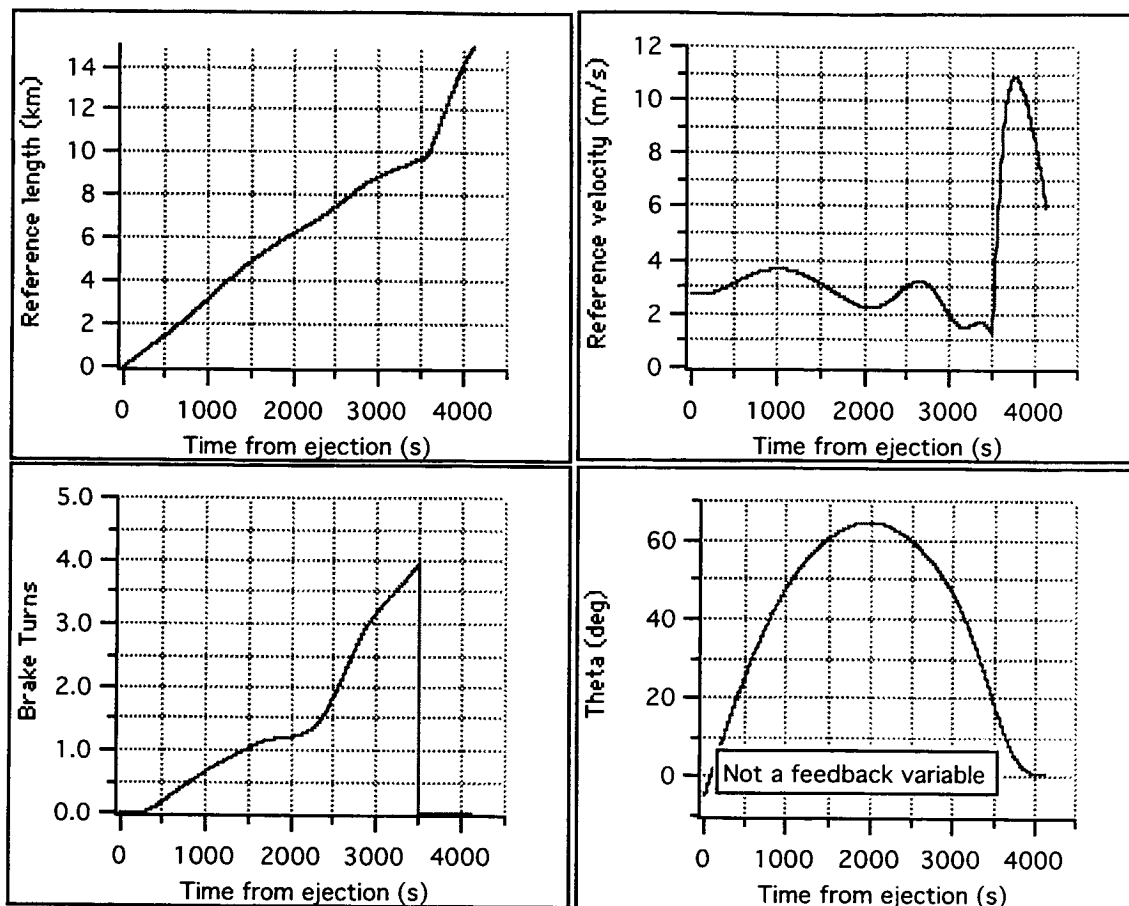


Figure 50 Reference profile Ref#47 (without slow down maneuver)

Reference Profile #55

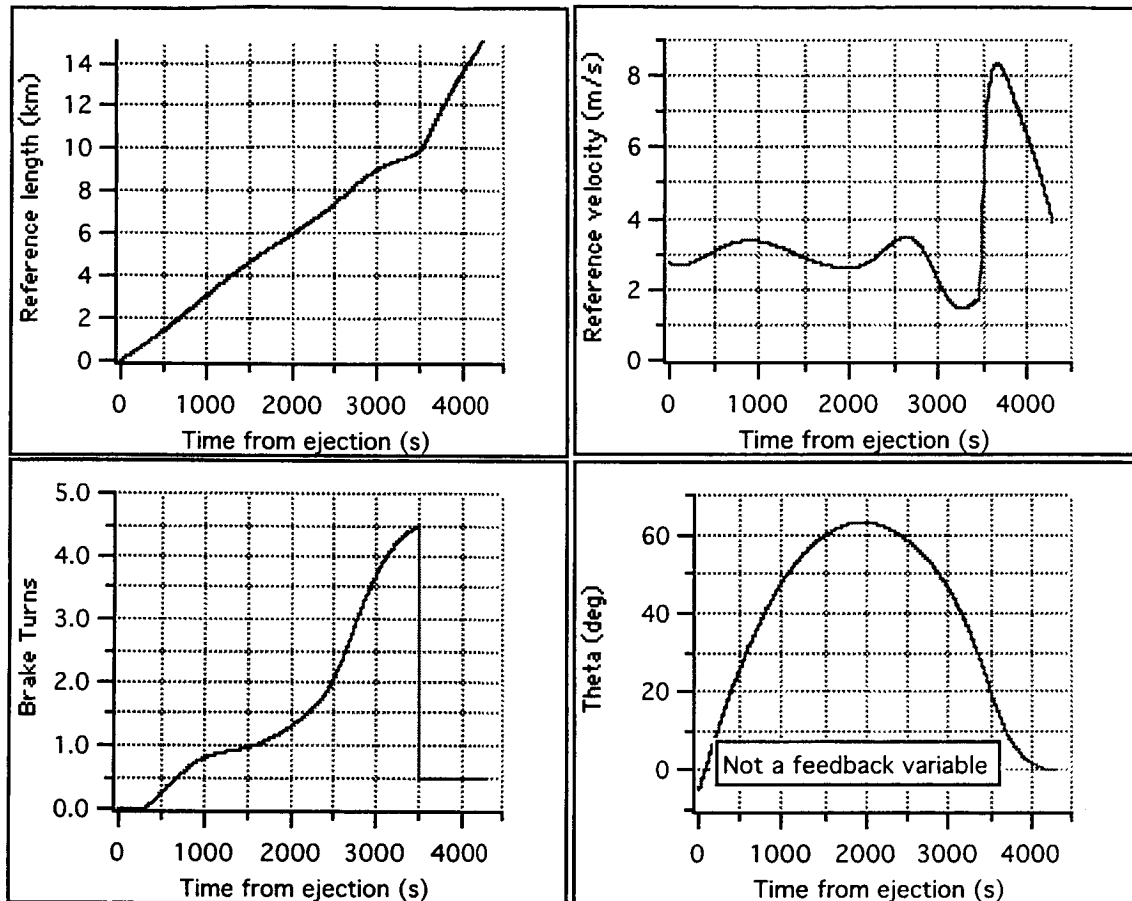


Figure 51 Reference profile Ref#55 (without slow down maneuver)

The most recent parameters adopted for deriving the latest reference profiles are as follows

Orbital and ejection parameters

Orbit: 400x400 km (for Ref#47)

Orbit: 360x360 km (for Ref#55)

Orbital inclination: 36 deg

Ejection velocity = 2.74 m/s

Ejection angle = 5 deg (forward of LV with an upward deployment)

System parameters

Satellite mass = 21.4 kg

Delta-II Mass = 994 kg

Tether lengths: 10 km Dyneema, 4.85 km CCOR and 205-m insulated

Table 8 Characteristics of selected reference profiles

Profile	ΔV (m/s)	T_0/T_{wire} (mN)	Orbit (kmXkm)	Friction characteristics	Spooling
#47	2.8	10/100	400x400	Dev. tether	Dev. tether
#55	2.8	10/75	360x360	MAO	F-2 (estim.)

Table 8 shows key characteristics of the two new reference profiles. Simulation results of ProSEDS deployment for Ref. #55 are shown in Figs. 52-54 for different values of the minimum tension of the Dyneema tether. The dynamic response is well within the required 20 deg maximum residual amplitude required for ProSEDS.

Ref#55, $T_{ref} = 10\text{mN}$, $T_{min} = 0\text{mN}/100\text{mN}$, $\Delta V = 2.74\text{ m/s}$, Brake $1.5t/0.07v$ -Ins205m

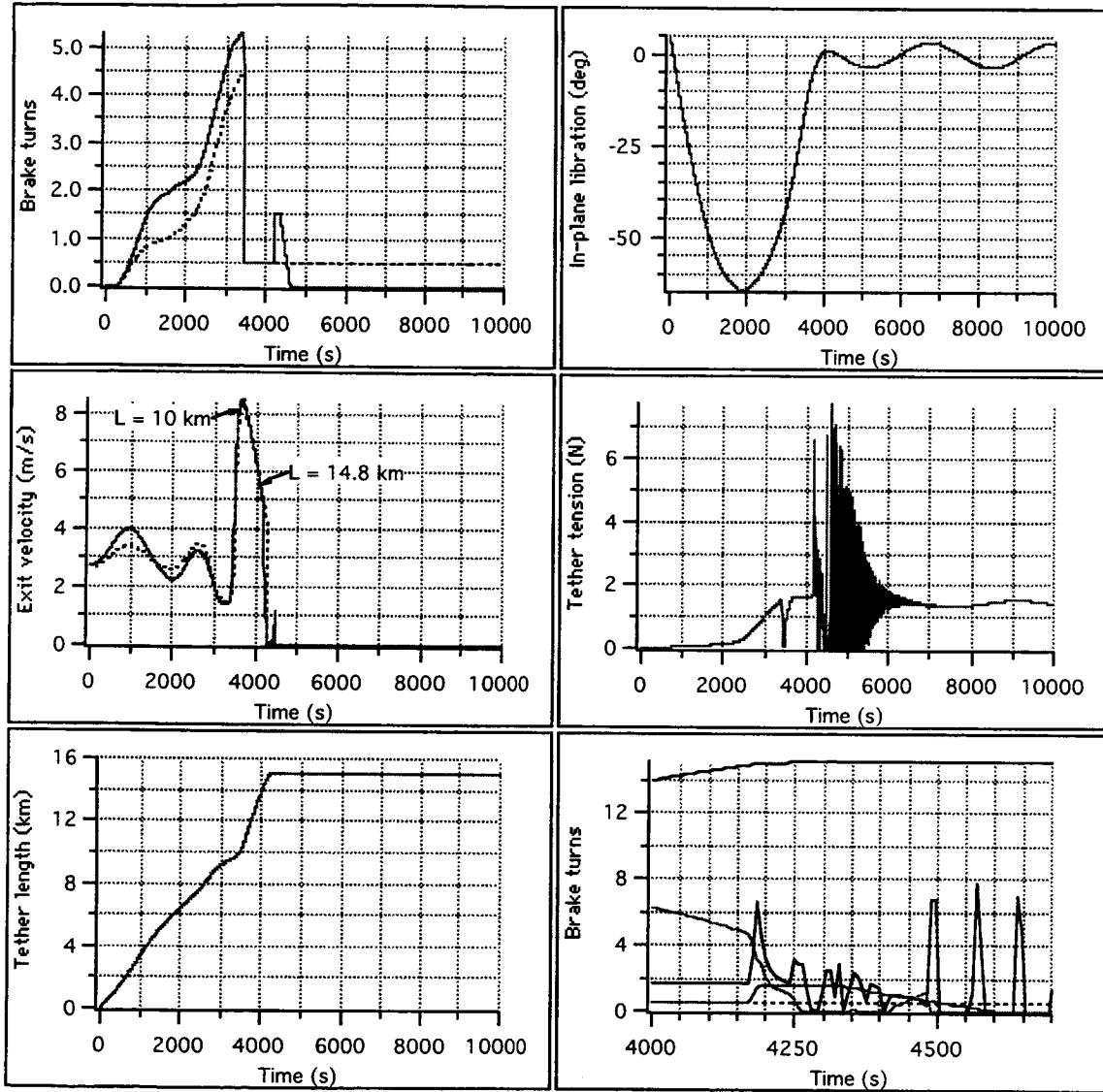


Figure 52 Deployment dynamics for Ref#55 for $T_0 = 0\text{ mN}$

Ref#55, $T_{ref} = 10\text{mN}$, $T_{min} = 10\text{mN}/100\text{mN}$, $\Delta V = 2.74\text{ m/s}$, Brake $1.5t/0.07v$ -Ins205m

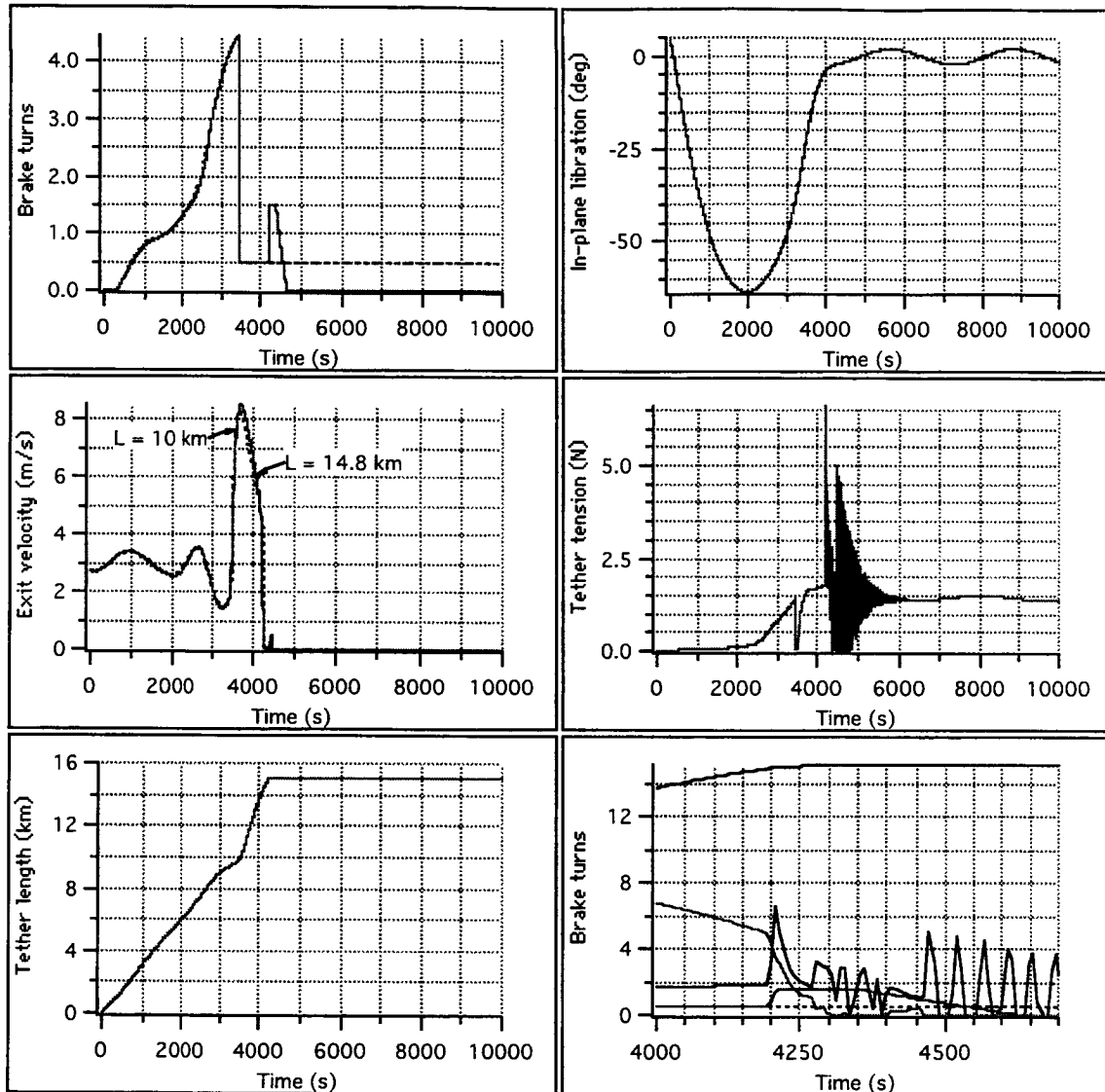


Figure 53 Deployment dynamics for Ref#55 for $T_0 = 10\text{ mN}$ (nominal)

Ref#55, $T_{ref} = 10\text{mN}$, $T_{min} = 20\text{mN}/100\text{mN}$, $\Delta V = 2.74\text{ m/s}$, Brake $1.5\text{t}/0.07\text{v-Ins205m}$

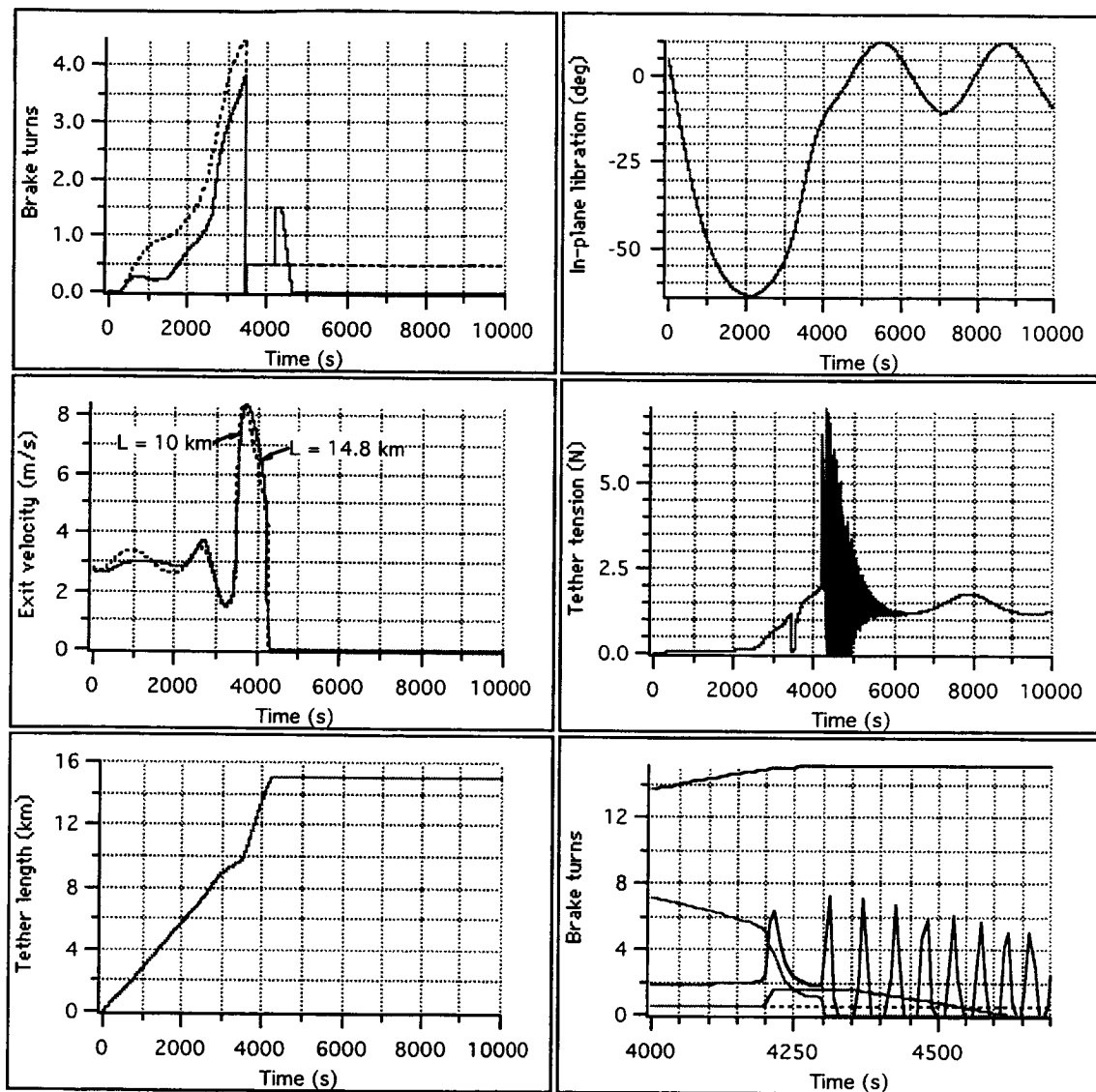


Figure 54 Deployment dynamics for Ref#55 for $T_0 = 20\text{ mN}$

Figure 55 shows the amplitude of the residual libration at the end of deployment vs. the minimum tension T_0 of the Dyneema tether for the selected profiles. The final libration amplitude is very sensitive to the leader tether T_0 and it is quite insensitive to the value of the wire T_{wire} . Values of T_{wire} of 50-300 mN have been explored with very good deployment dynamics. Values as high as 500 mN are tolerable for the minimum tension of the wire.

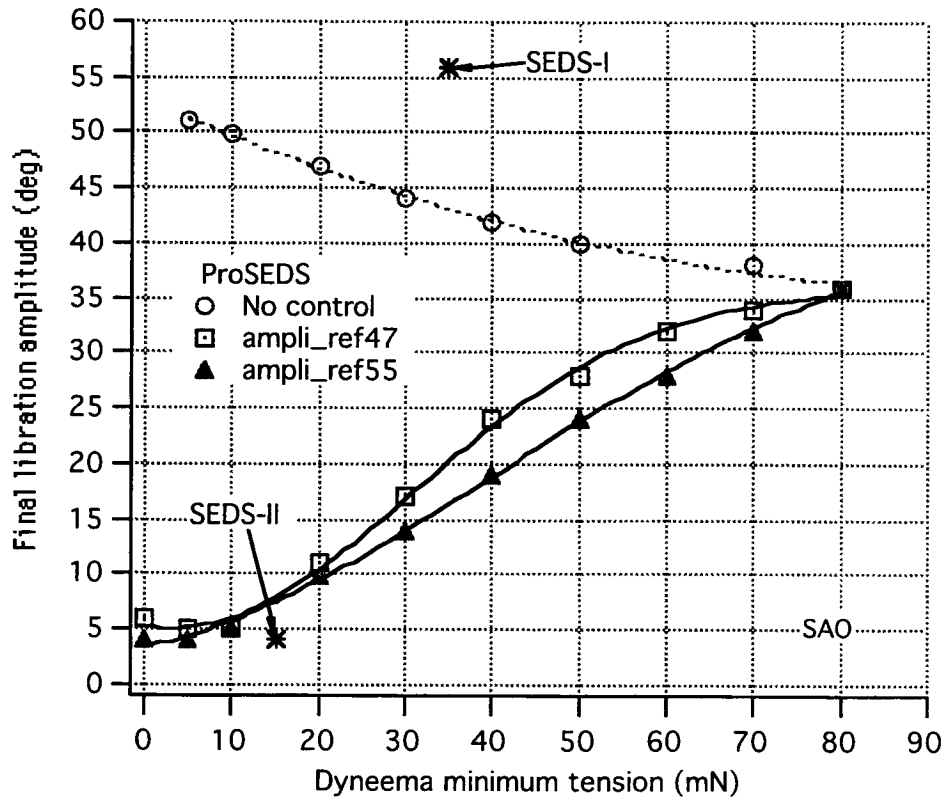


Figure 55 Final libration amplitude vs. T_0 for selected deployment profiles

9.5 Validation process

Hi-Fi ProSEDS deployment verification

The numerical simulations of ProSEDS deployment (Ref#47) were run using SAO's high-fidelity code MASTERDEP. MASTERDEP is a modified version of our simulator MASTER with the added capability of handling deployment of a massive tether. The results were compared to the DUMBBELL numerical code and they generally agree. Noticeable differences were found when the dynamics of the wire, not simulated by dumbbell, was a driver. Namely, the lateral modes excited by the deployment (e.g. Coriolis) caused the tether to bow and the pre-selected brake was too low to be able to control the final velocity. The problem, however, was solved by applying a moderate brake during the CCOR wire deployment and the results are presented in the following.

The reference deployment profile is ProSEDS Ref#47. MASTERDEP simulates the two end-platforms and tether with nine lumps. The system is acted by gravity ($J_0 + J_2$), aerodynamic drag and tether tensions (Spring-dashpot system). The system orbits the earth at 400 Km of altitude.

The following simulations are shown in the following (Figs. 56-69):

- a. Nominal Deployment (ProSEDS Ref#47 assumes 10 mN as minimum tension)
- b. Minimum tension = 5 mN
- c. Minimum tension = 20 mN

Case a: Nominal Dyneema minimum tension, $T_0 = 10$ mN. Unlike for the reference profile, the brake is set to 0.5 turns during wire deployment

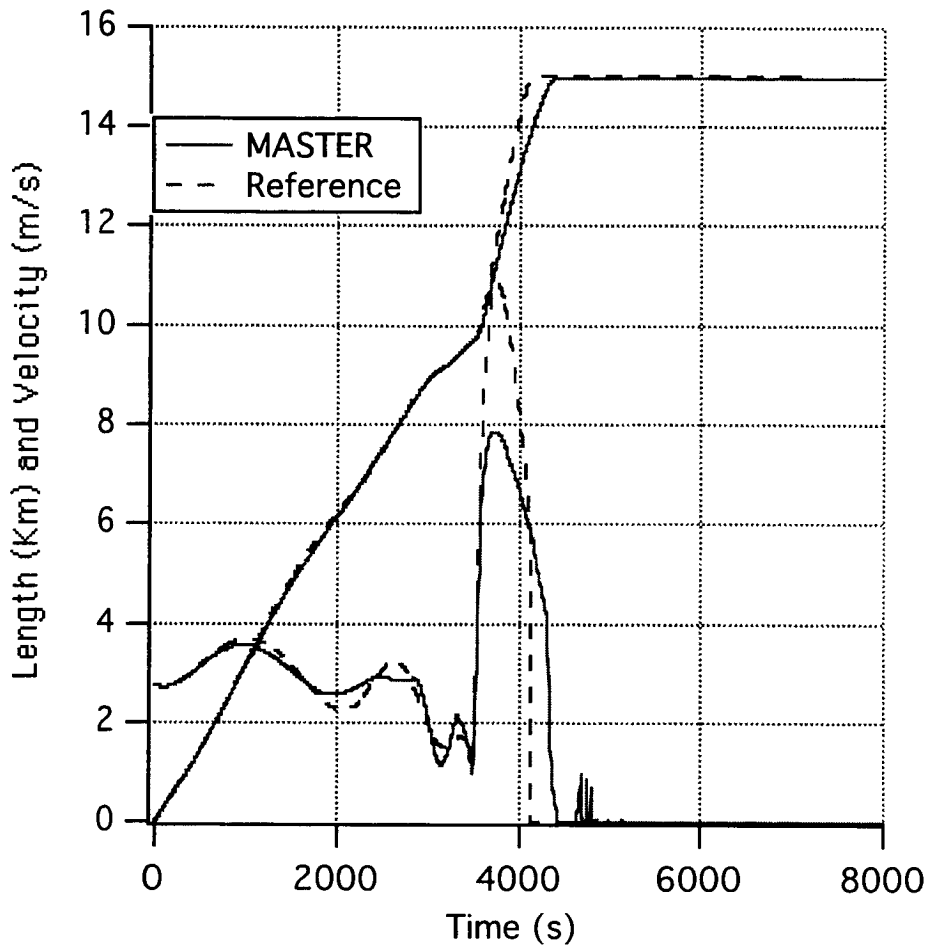


Figure 56 Nominal minimum tension $T_0 = 10$ mN

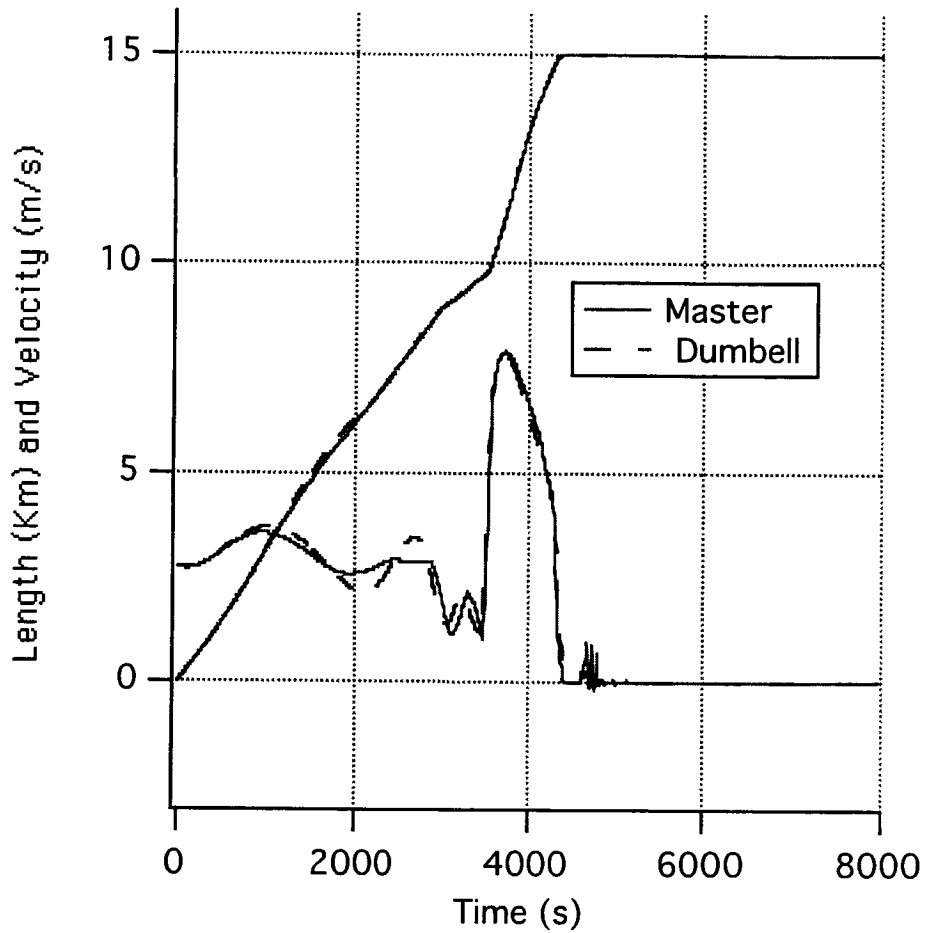


Figure 57 Nominal minimum tension $T_0 = 10$ mN (MASTER vs. DUMBELL)

The agreement between dumbbell and multimass MASTER simulations is quite good. The lateral dynamics however plays a role in the differences between the results of the programs. Large bowing produces travelling waves along the tether when braking is applied. The bowing can be minimized (as done here) by applying a moderate brake during wire deployment.

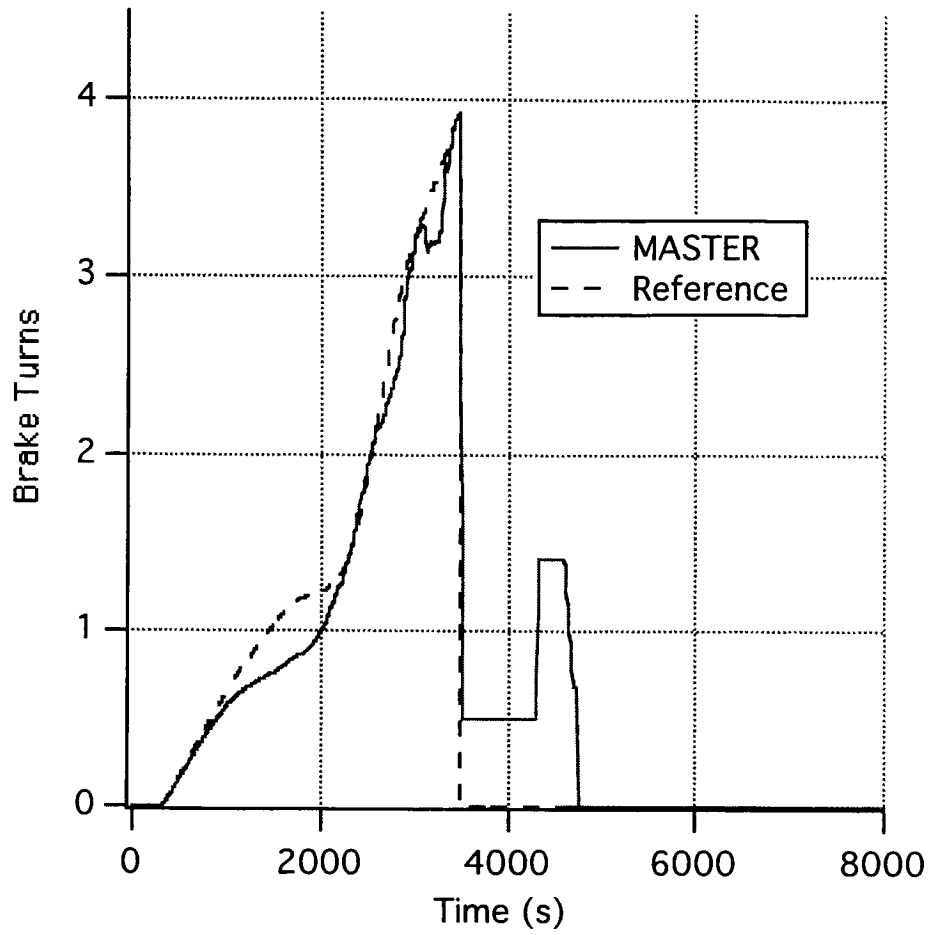


Figure 58 Nominal minimum tension $T_0 = 10$ mN

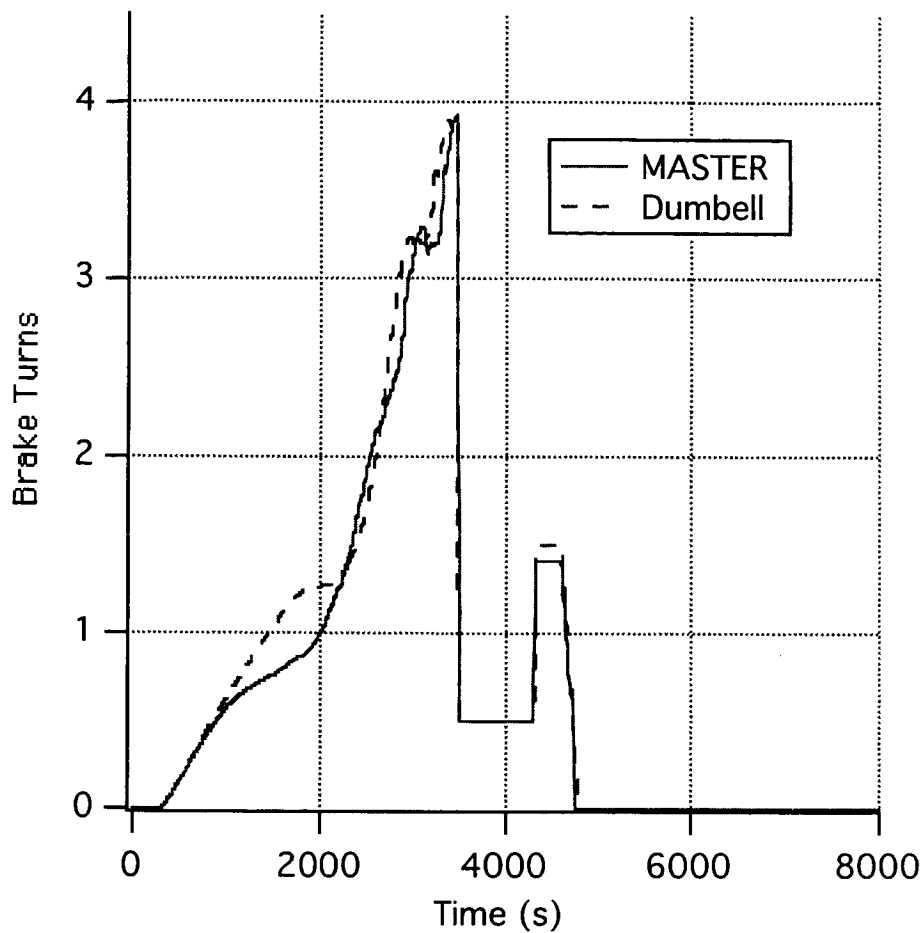


Figure 59 Nominal minimum tension $T_0 = 10$ mN

We applied a 0.5 turns of brake during wire deployment (starting at about 4000 s) to limit the magnitude of the bowing caused by the Coriolis force. The last portion of the control law (during deployment of the insulated wire) is used to bring the end-mass to a smooth stop. Values between 1.2 and 1.7 brake turns (for the constant-brake plateau) have been used without noticeable differences. A value of 1.4 turns was adopted for Ref#47.

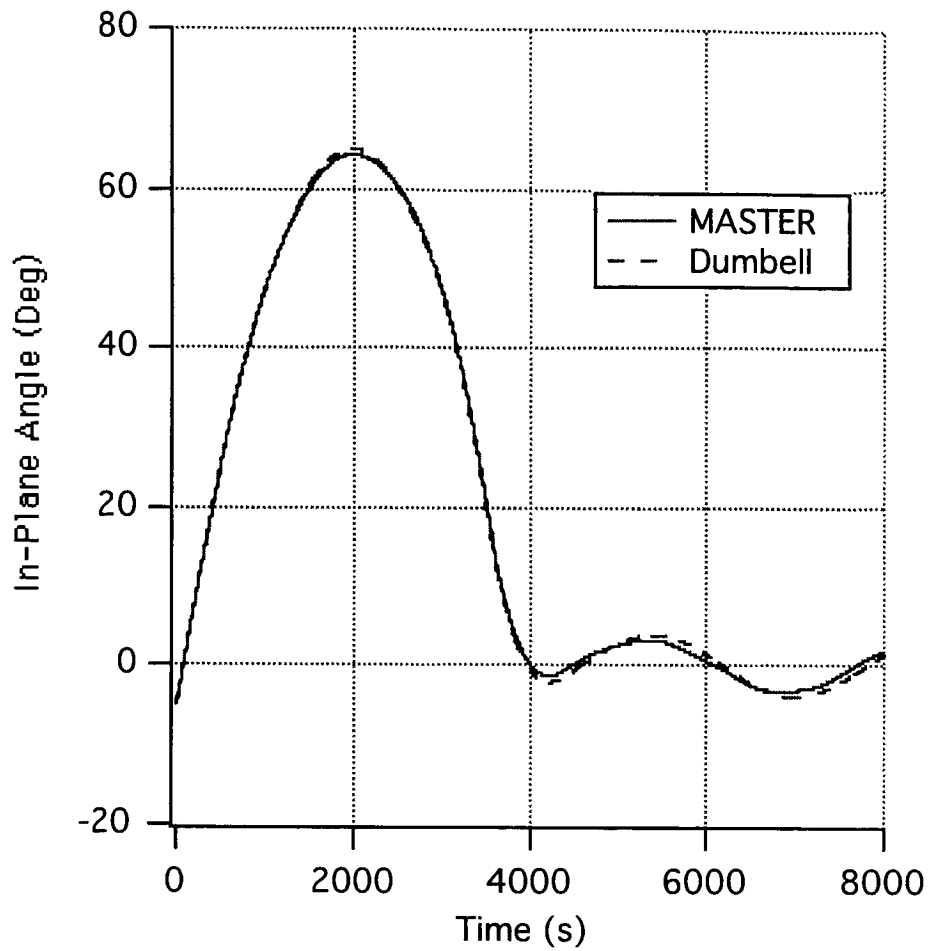


Figure 60 Nominal minimum tension $T_0 = 10$ mN

The in-plane angle is similar both in amplitude and in phase to the simplified simulation (DUMBELL). A final libration amplitude of less hat 10 deg has been reached.

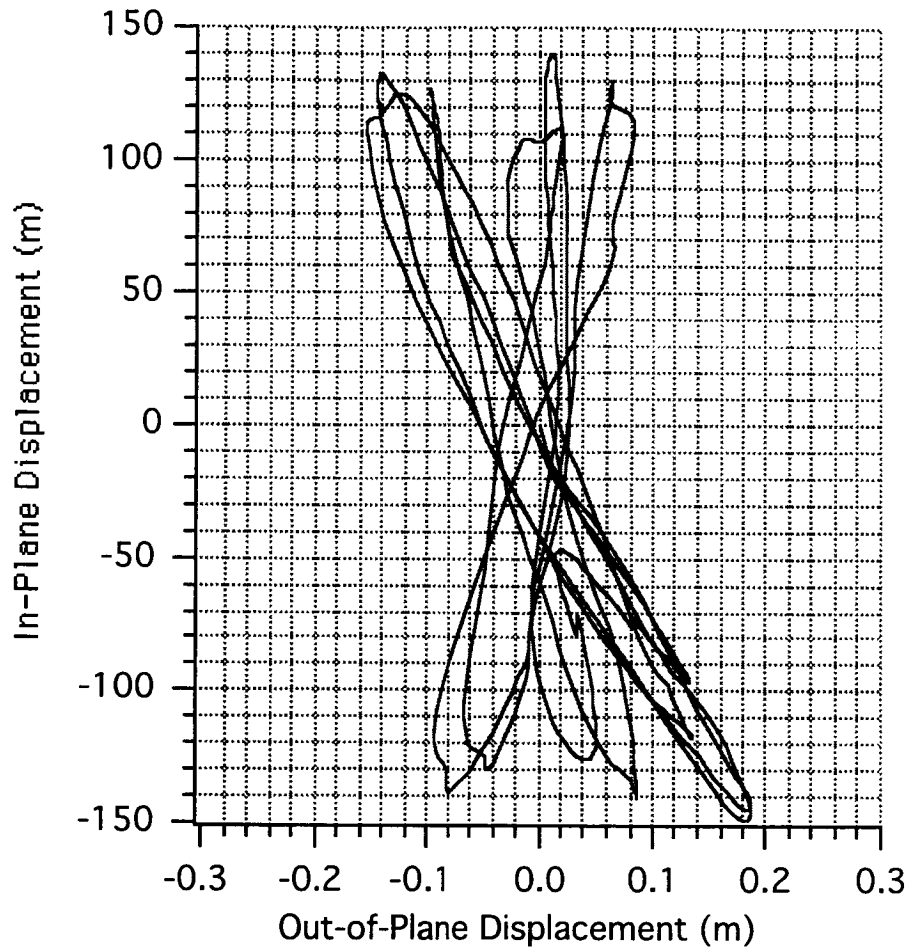


Figure 61 Nominal minimum tension $T_0 = 10$ mN

The lateral dynamics is mainly in-plane and it is limited to a few hundred meters. The out-of-plane dynamics is almost negligible during deployment.

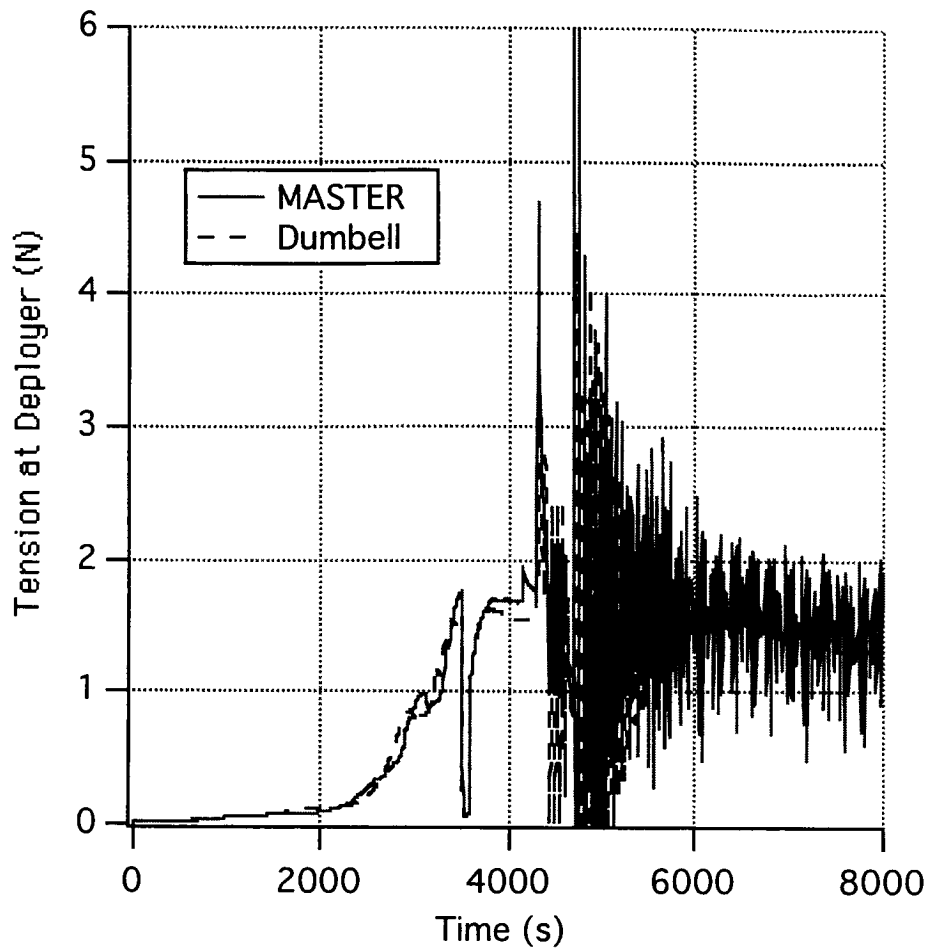


Figure 62 Nominal minimum tension $T_0 = 10 \text{ mN}$

The tether tension is similar during deployment. The rebound phase differs in variations because of the tether's higher longitudinal modes.

Case b: Dyneema minimum tension = 5 mN

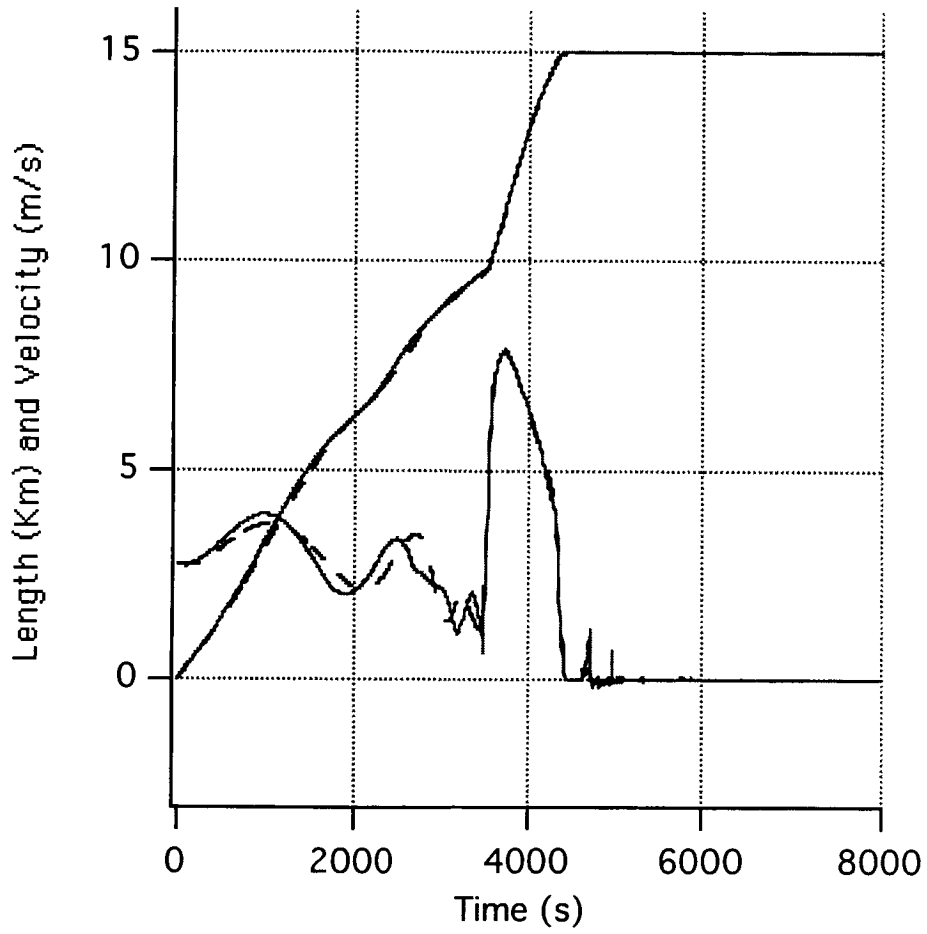


Figure 63 Minimum tension $T_0 = 5$ mN (MASTER vs. DUMBELL)

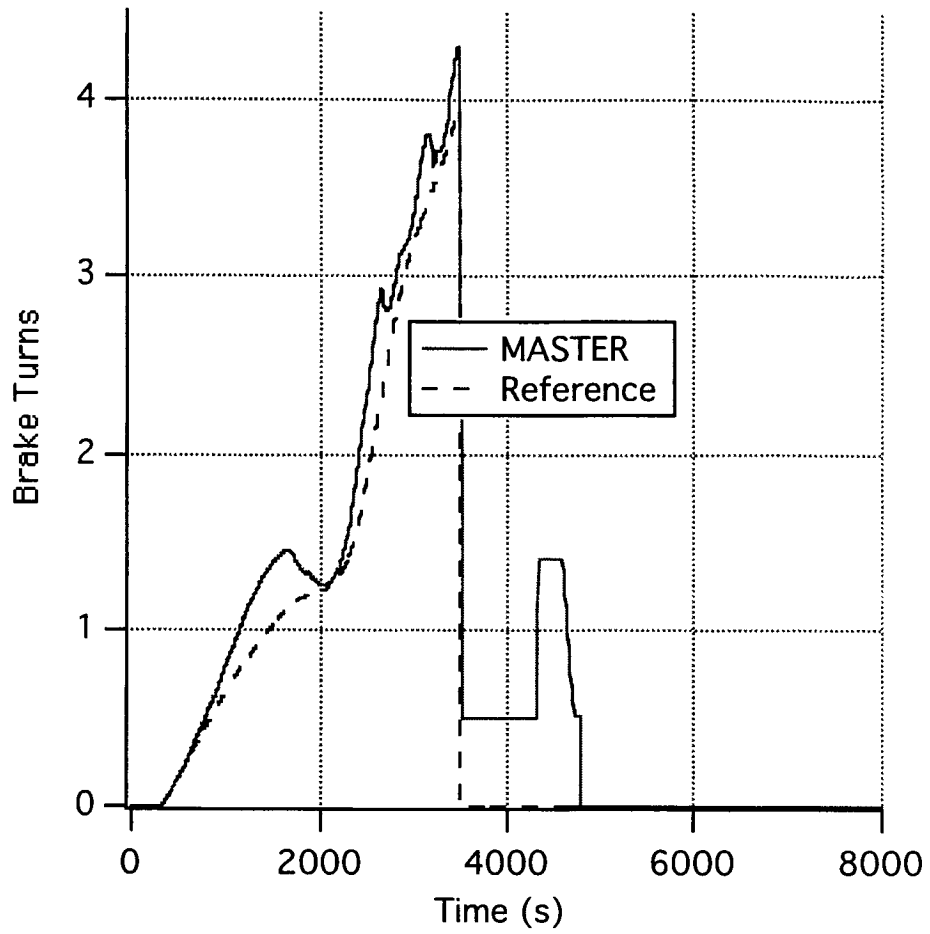


Figure 64 Minimum tension $T_0 = 5$ mN

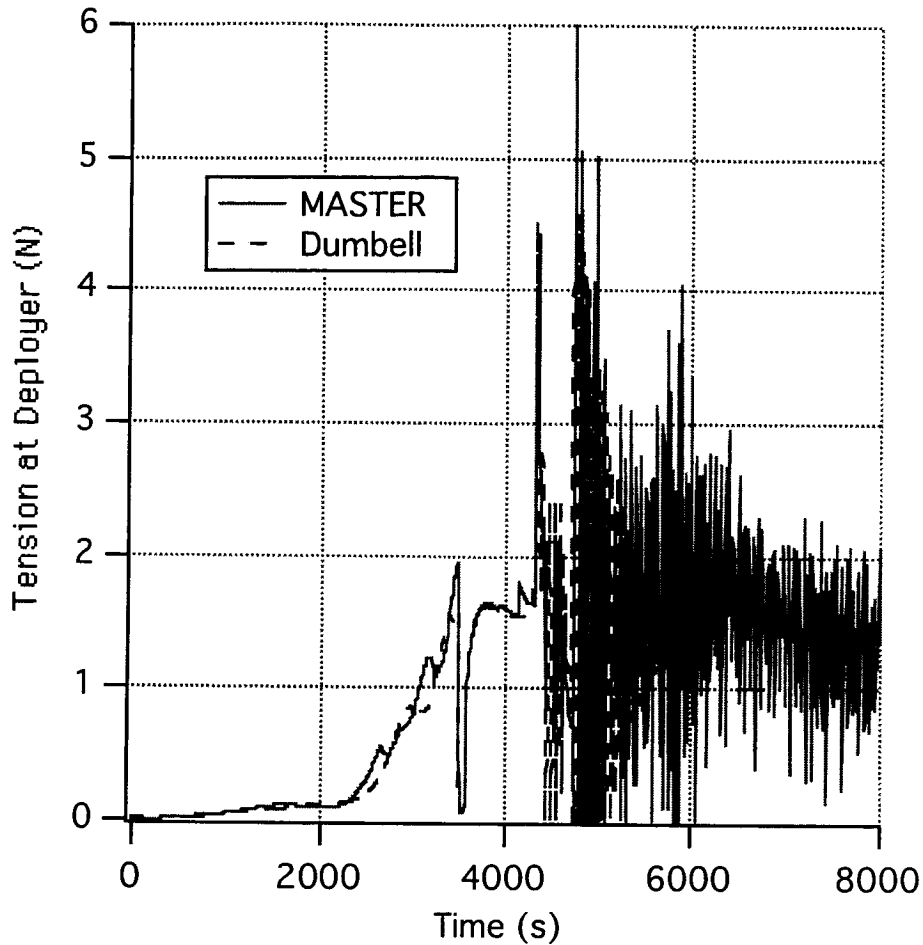


Figure 65 Minimum tension $T_0 = 5 \text{ mN}$

No dramatic changes can be noticed from case a. However, given a smaller tension in the deployment, the brake is about 1/2 turn larger than for the DUMBELL simulations. The in-plane libration (not shown here) has the same amplitude of the simplified simulations with a slight change of phase. Tension and lateral displacement are not reported for the sake of brevity and they do not show any peculiarities.

Case c: Dyneema minimum tension = 20 mN

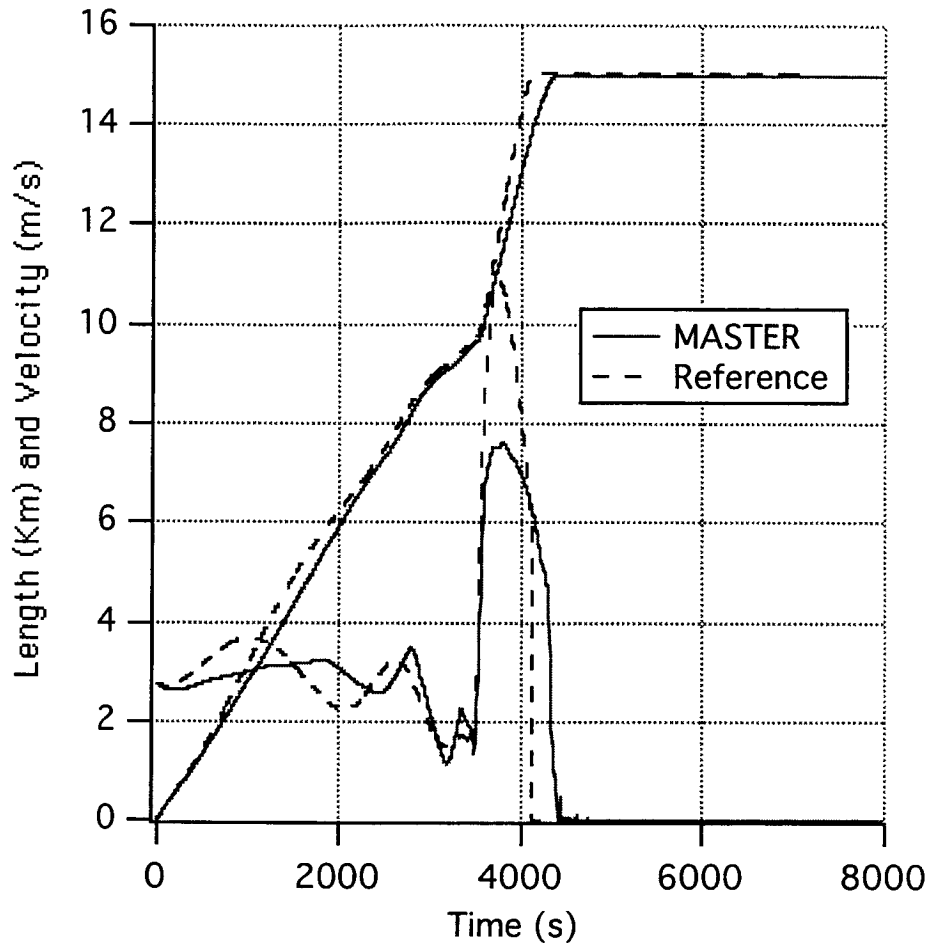


Figure 66 Minimum tension $T_0 = 20$ mN

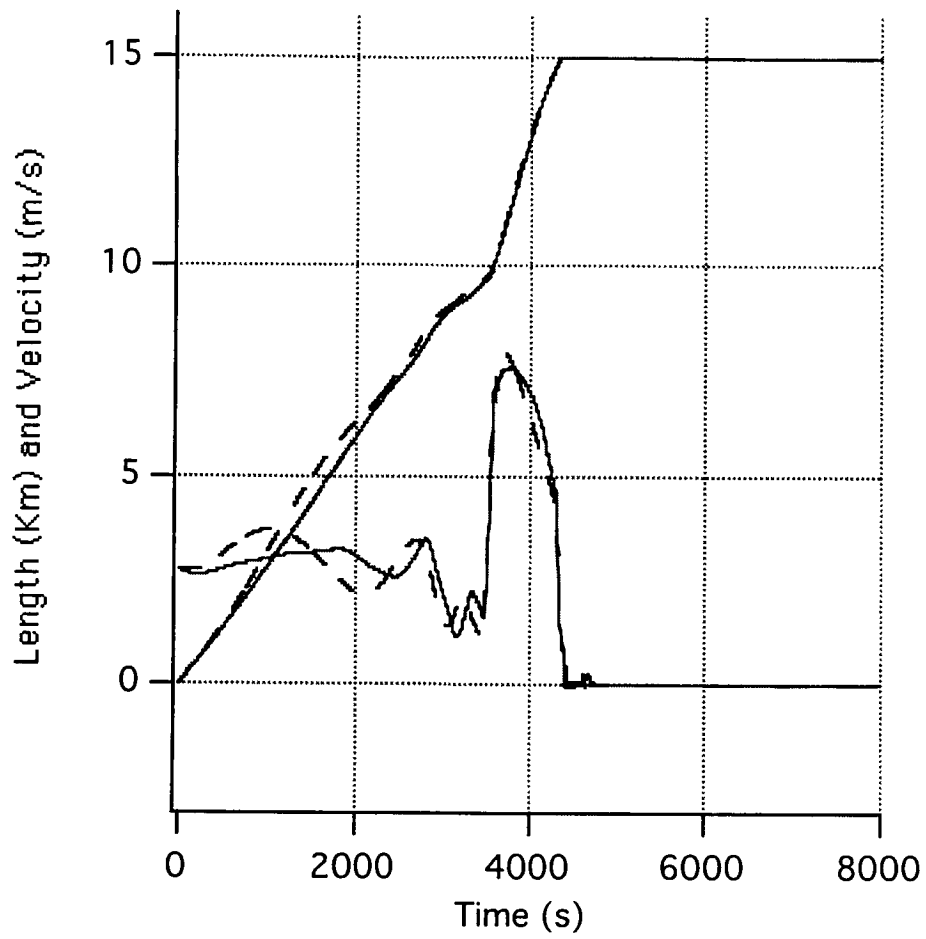


Figure 67 Minimum tension $T_0 = 20$ mN (MASTER vs. DUMBELL)

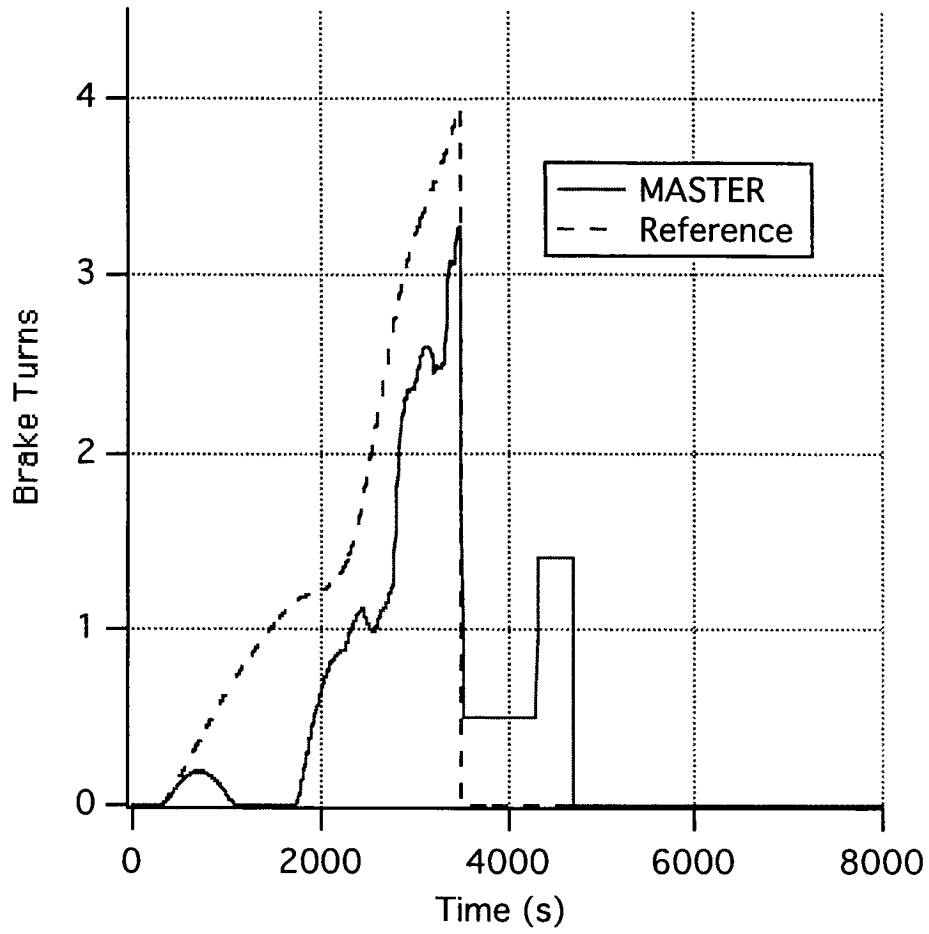


Figure 68 Minimum tension $T_0 = 20$ mN

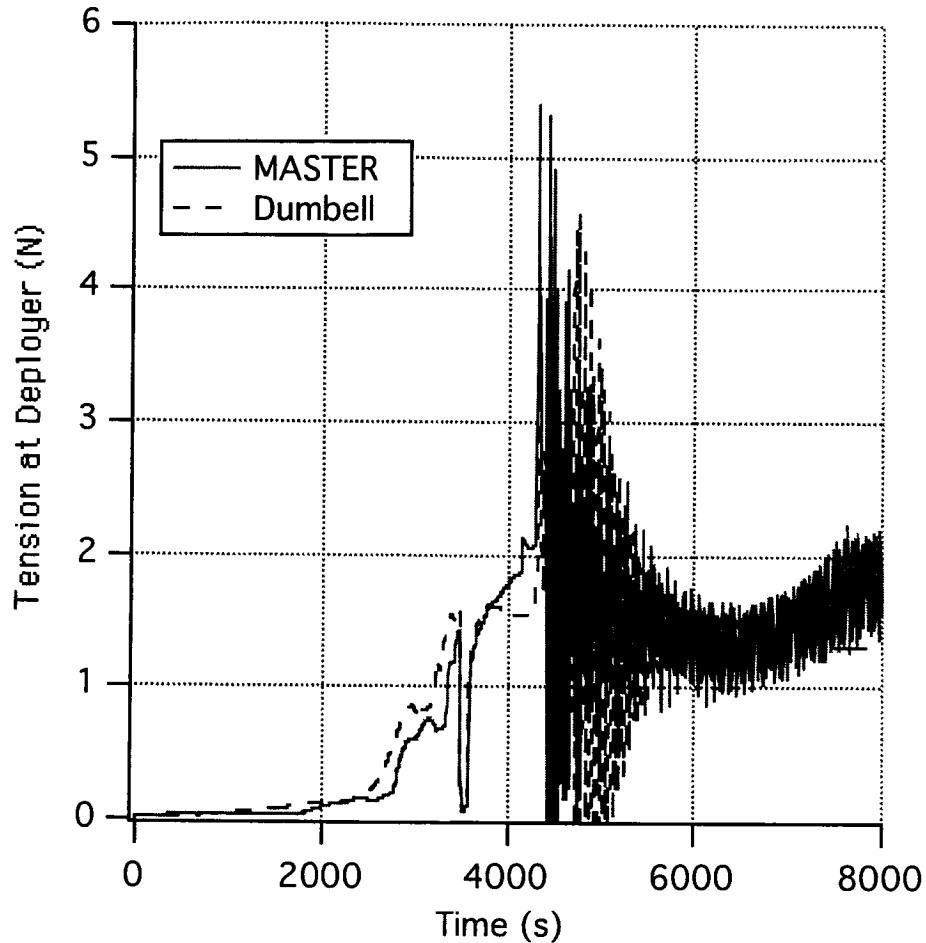


Figure 69 Minimum tension $T_0 = 20$ mN

Also in this case no noticeable changes can be seen from case a. The libration is a few degrees higher with a more pronounced change in the phase angle. Tension and lateral displacement are not reported for the sake of brevity and do not show any peculiarities.

In all three cases the control law has shown robustness to deploy 15 km of tether and bring the endmass to a smooth stop with small tension variations and rebound velocity. In all three cases the lateral dynamics has been limited by the brake action. The final libration is about 10 degrees or less in the minimum tension range of $5 \text{ mN} < T_0 \leq 20 \text{ mN}$.

Deployment without braking

The following run (Figs. 70-71) simulates ProSEDS dynamics when the brake is not activated. The tether is fully deployed but the rebound is quite significant (~5 m/s final deployment velocity).

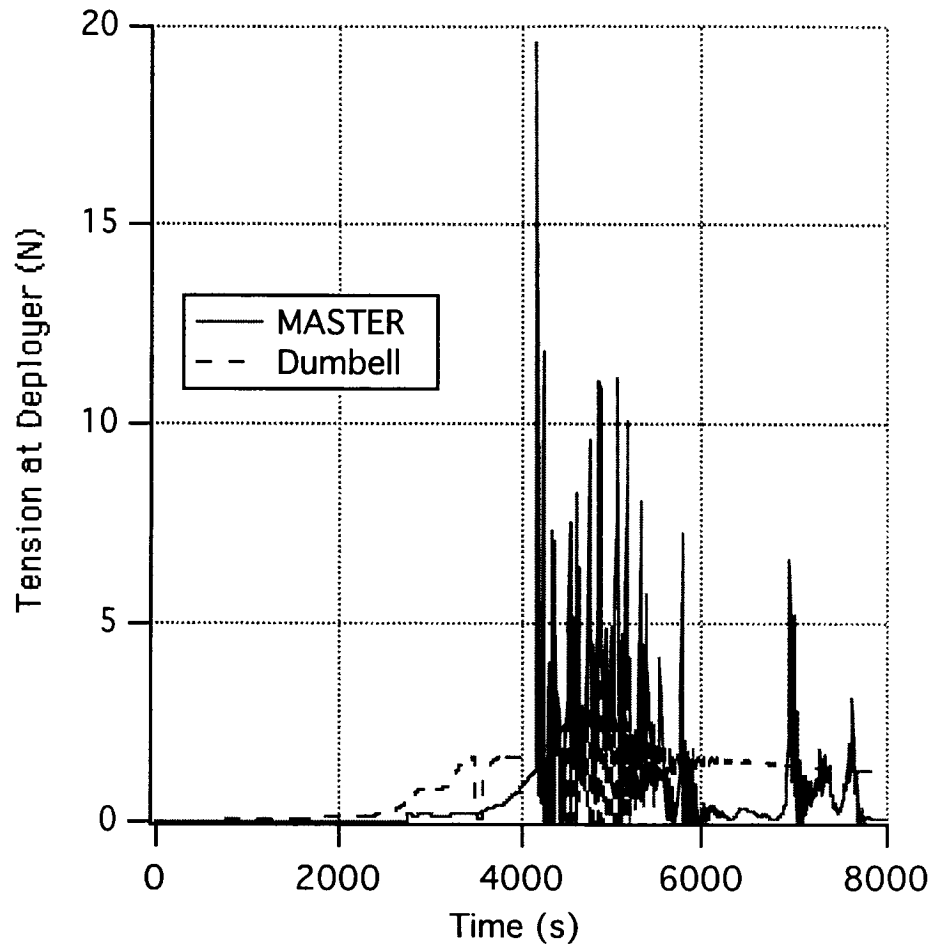


Figure 70 No brake is activated throughout deployment

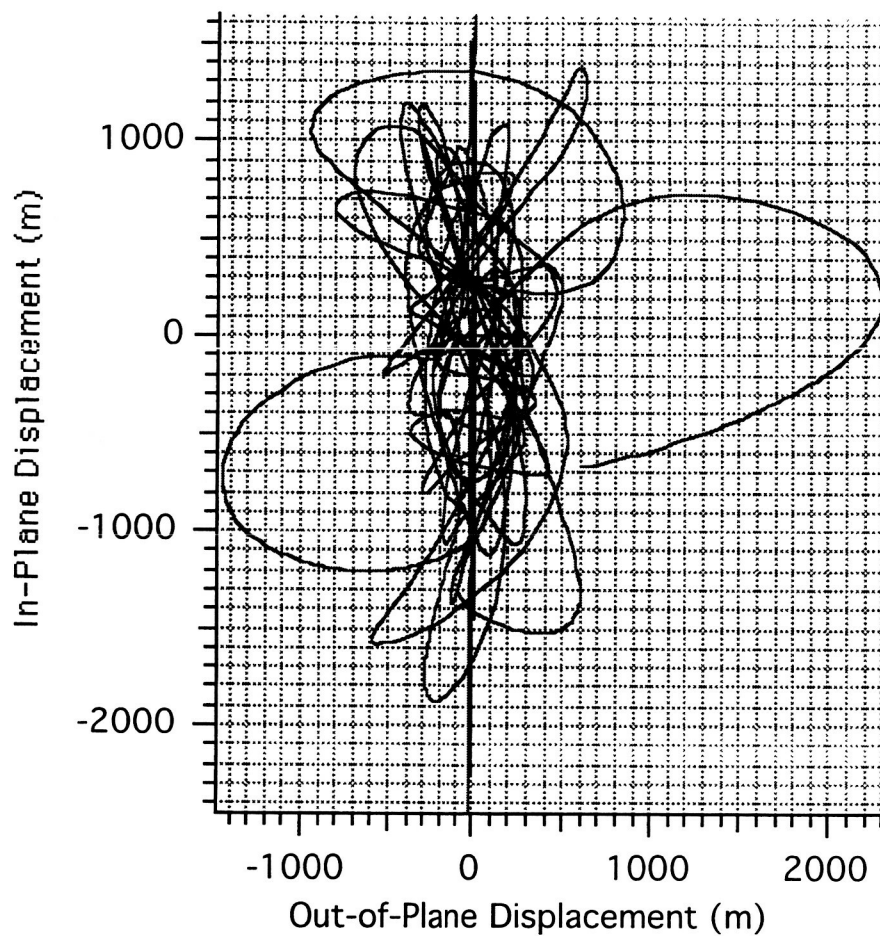


Figure 71 No brake is activated throughout deployment

The final libration is about 60 degrees since the brake was not activated. The tension reaches a maximum of 20 N during rebound and the lateral dynamics is highly excited with amplitudes of the order of a few kilometers both in-plane and out-of-plane.

Off-nominal Inertial Multiplier of Conductive Wire

No significant differences have been found from the baseline case when the brake is functioning and the inertia multiplier of tether conductive part is changed from 3 (nominal) to 2.5 and 3.5 (see Figs. 72-81).

A final in-plane angle slightly less than the baseline is reached when the multiplier is 2.5. Tension and in-plane motion of the mid-tether point are similar to the baseline.

On the other hand when the multiplier is 3.5, the deployment is similar to the baseline, though larger tension variations at the end suggest a larger final velocity. These variations and the associated peaks are within the desired bounds.

Inertial Multiplier of Conductive Wire = 2.5

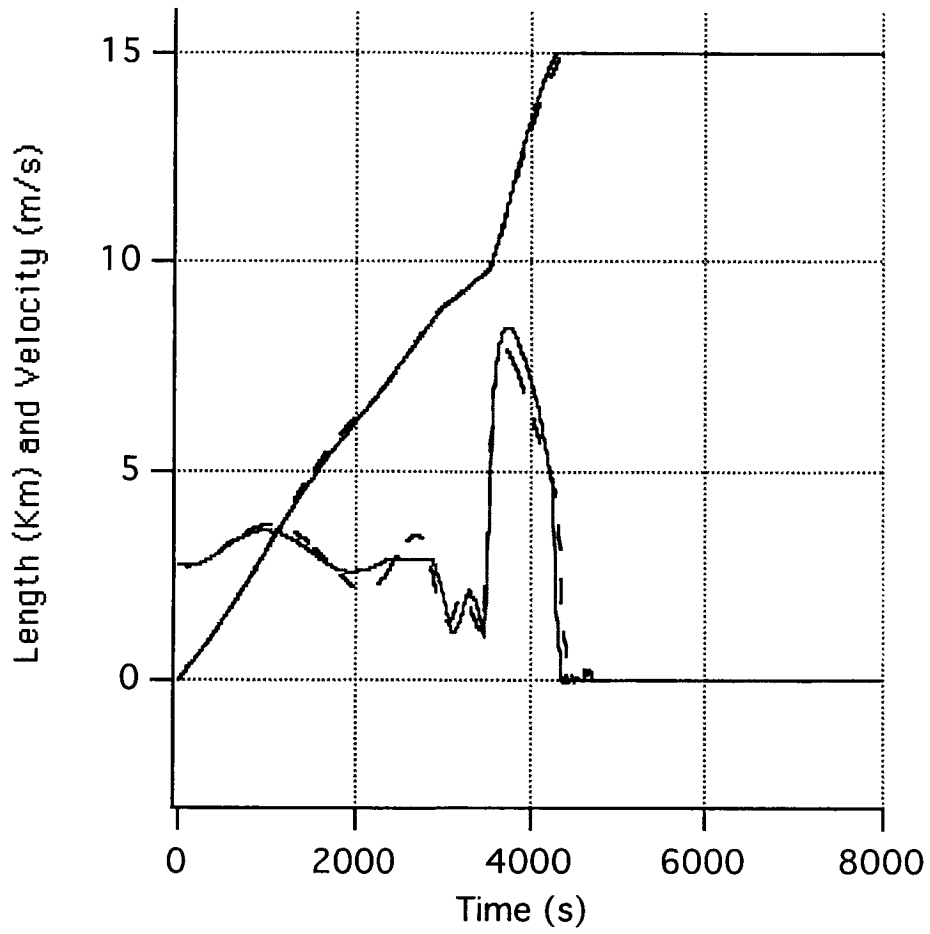


Figure 72 Wire inertia multiplier = 2.5

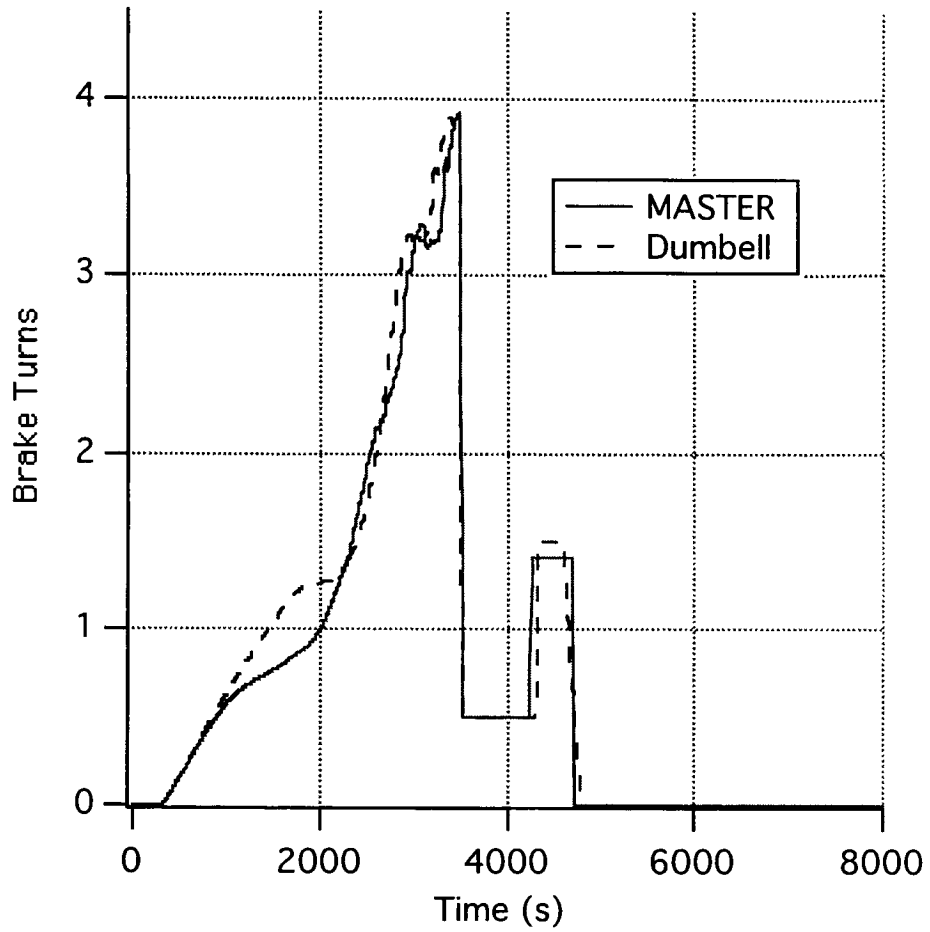


Figure 73 Wire inertia multiplier = 2.5

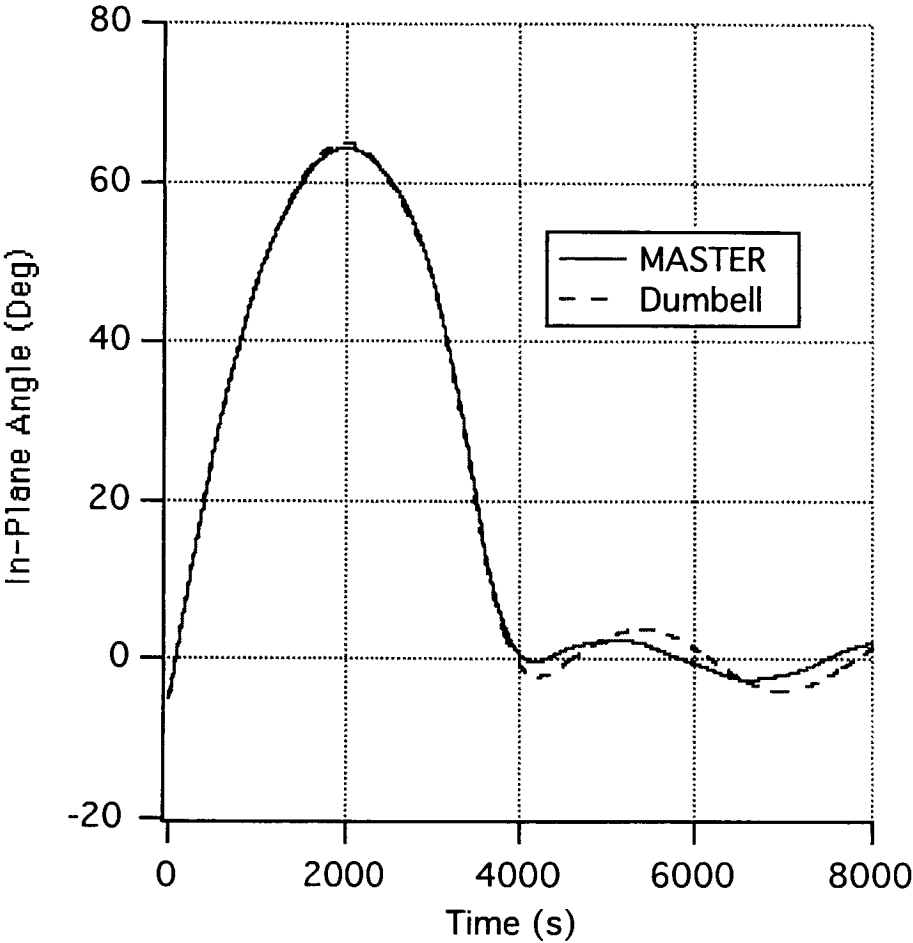


Figure 74 Wire inertia multiplier = 2.5

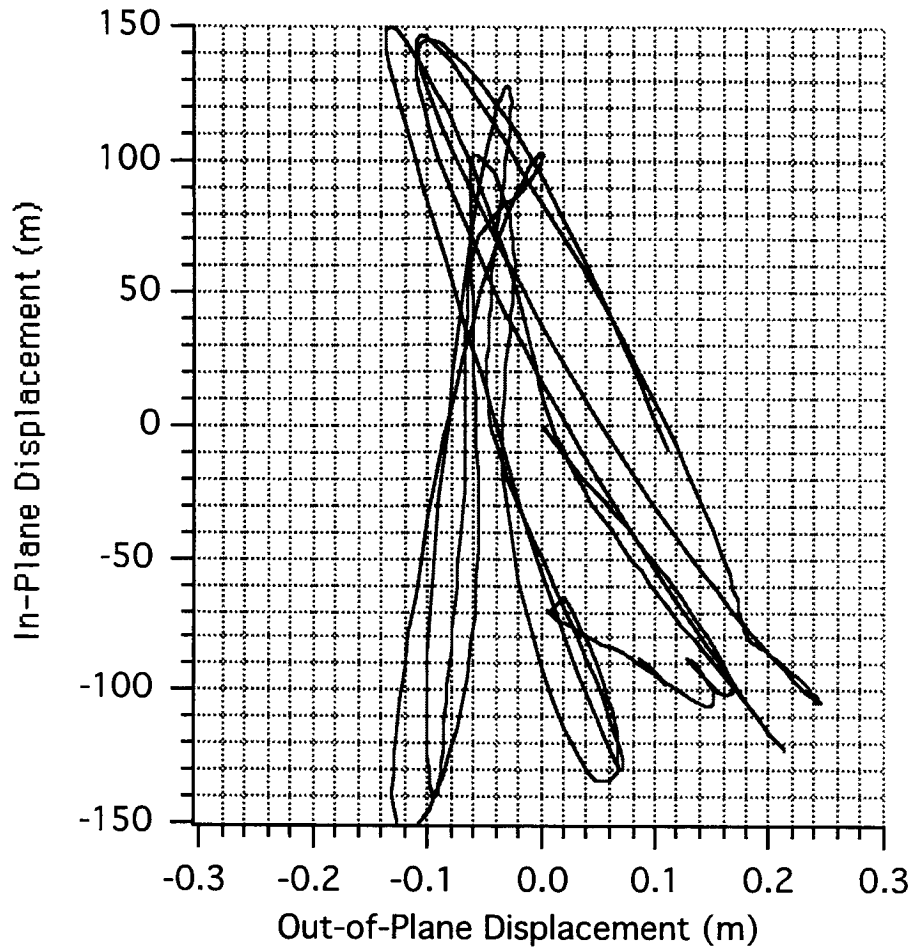


Figure 75 Wire inertia multiplier = 2.5

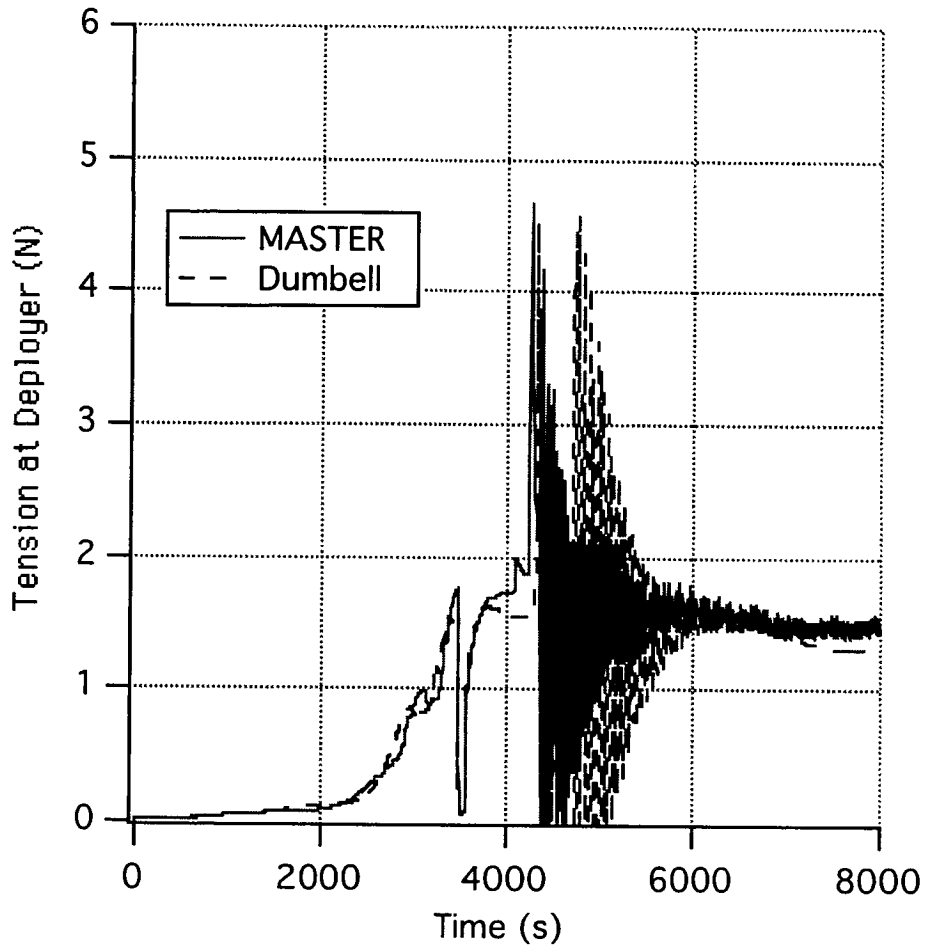


Figure 76 Wire inertia multiplier = 2.5

Inertial Multiplier of Conductive Wire = 3.5

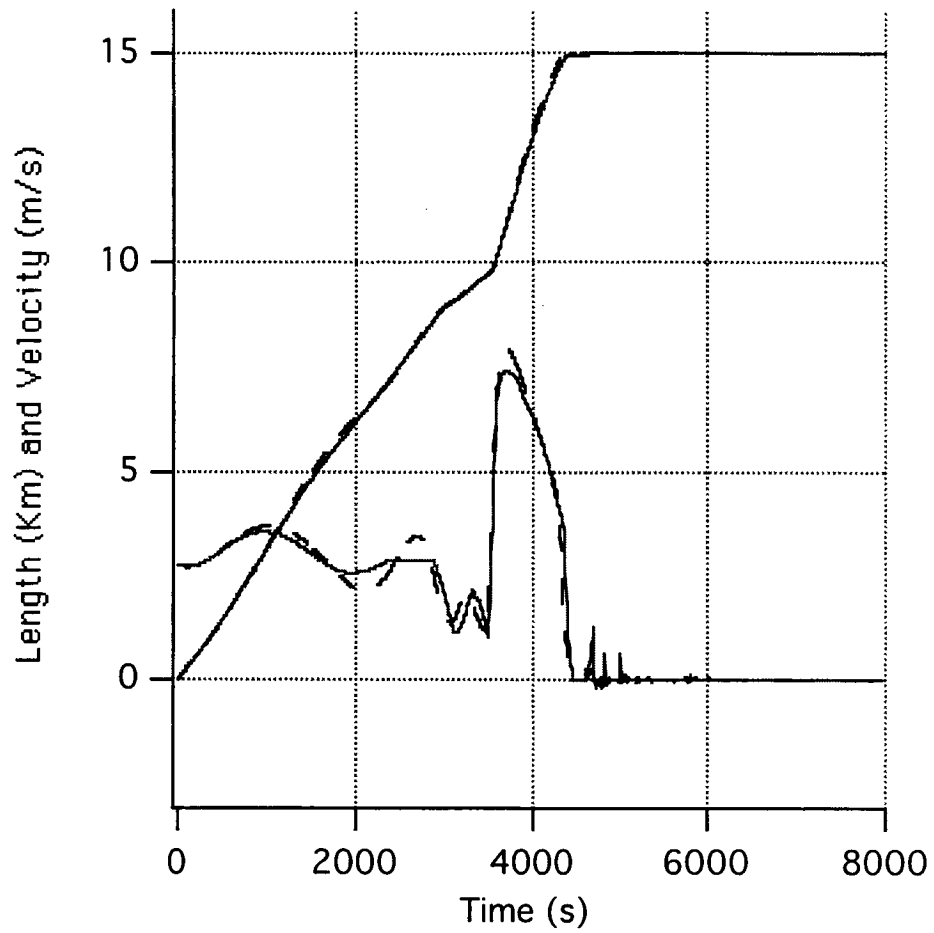


Figure 77 Wire inertia multiplier = 3.5

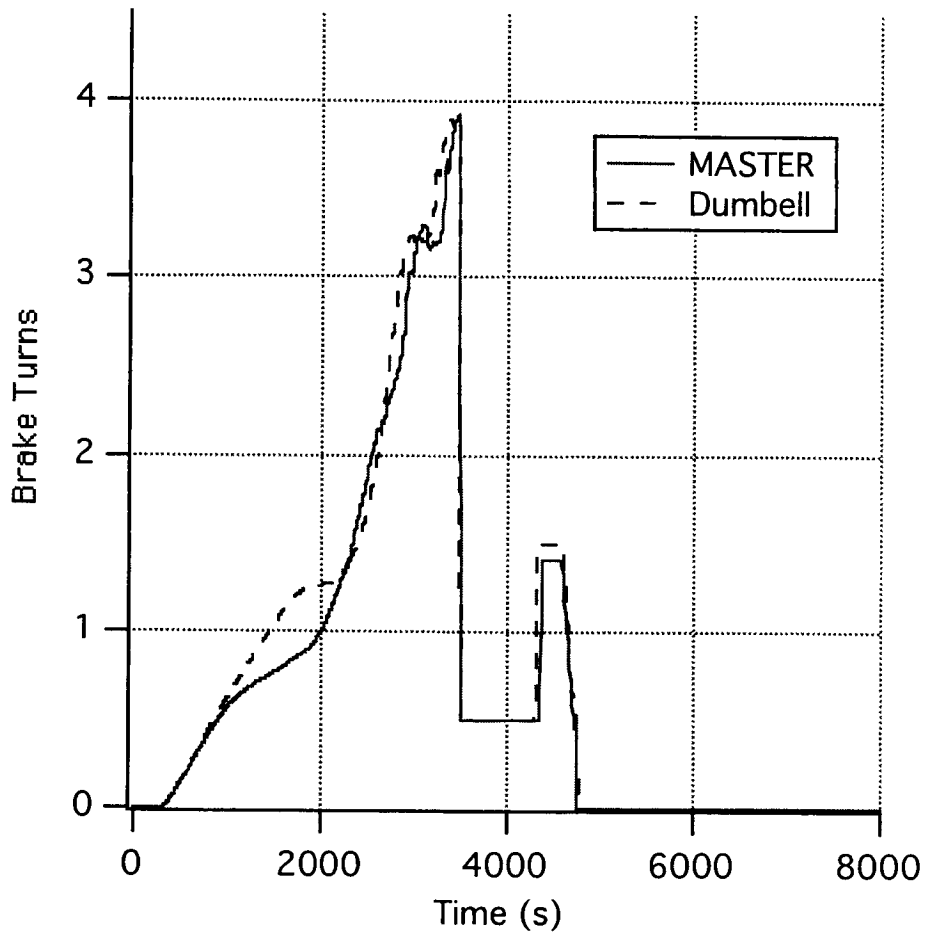


Figure 78 Wire inertia multiplier = 3.5

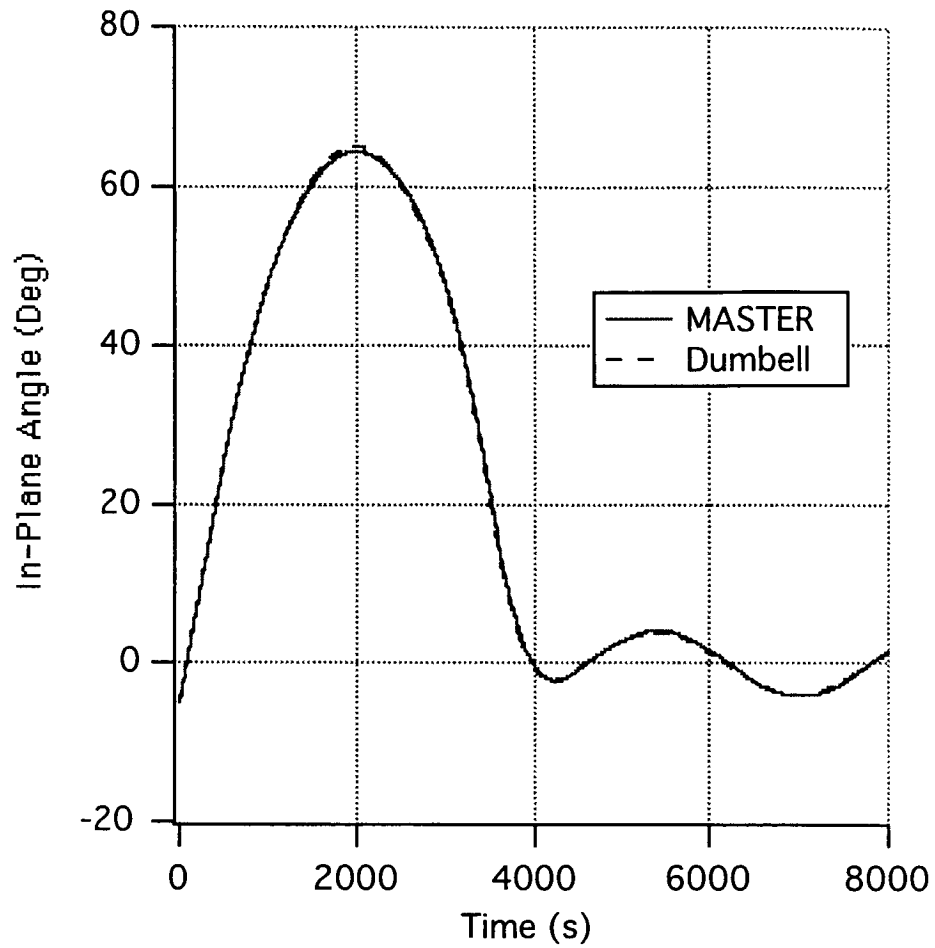


Figure 79 Wire inertia multiplier = 3.5

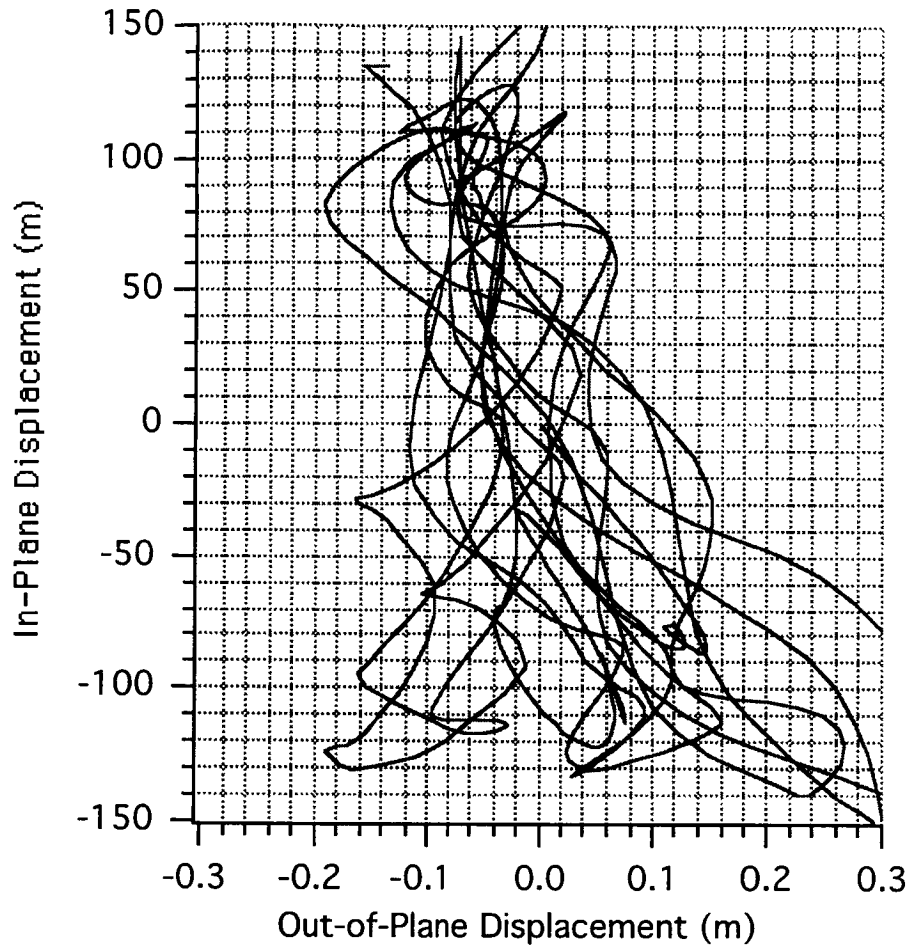


Figure 80 Wire inertia multiplier = 3.5

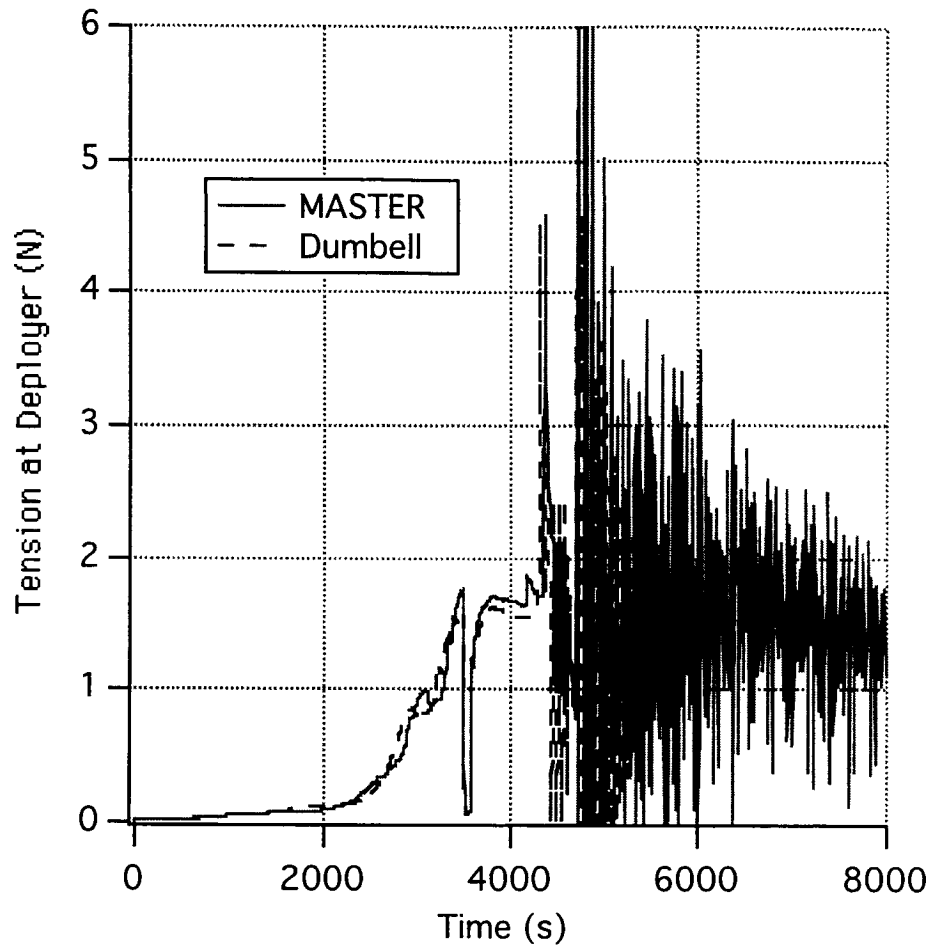


Figure 81 Wire inertia multiplier = 3.5

9.4 Concluding Remarks

The simplified simulation code DUMBELL is adequate to describe the overall dynamics of ProSEDS during deployment. The more refined (and much more CPU intensive) MASTERDEP code is strictly necessary to analyze particular features like the lateral (string-like) dynamics of the tether. Examples are deployment of the wire at very high velocity with consequent large bowing of the tether and the damping of the oscillations at the end of deployment due to tether rebounds and transfer of energy from the well-damped longitudinal modes to the lightly-damped lateral modes.

10. UPDATED REFERENCE MISSION

10.1 Introductory Remarks

The performance of ProSEDS will be assessed on the basis of the decay rate of the Delta stage which is affected (for a given tether design) by the plasma conditions at mission time. The launch date of ProSEDS has changed throughout its development with the latest launch date being in the Summer of 2002. Moreover, the modes of operation of the tether current (i.e., the operating cycle) have also changed, as explained later on, resulting in a strongly increased decay rate.

10.2 New Mission Parameters and Current Operating Cycles

The ProSEDS mission had some notable changes in terms of launch date, starting altitude and current operating cycle. The launch date was moved to the Summer of 2002, the starting altitude was decreased from 400 km to roughly 360 km and the secondary operating cycle (with 80-s period) now consists of 50-s battery charging and 30-s shunt mode (see Fig. 83). The original primary cycle (with 60-s period as shown in Fig. 82) is utilized during the first 5 orbits while the secondary cycle is utilized thereafter.

The reference mission for the scheduled launch date of July 25th, 2002 is analyzed in the following. The new launch date impacts the system performance because the current in the tether is a function of the plasma density which, in turn, is a function of the solar activity. Consequently, the electrodynamic drag force and the reentry time change because of the changed plasma conditions. We are presently in solar cycle 23 with the solar activity going down towards a minimum of activity currently estimated to happen around the years 2007-2008. More importantly the ProSEDS tether current operating cycle has been changed. The older cycle consisted of 7 orbits of primary operating cycle followed by a secondary cycle. The old secondary cycle consisted of 35-s open circuit mode, 5-s resistor mode, 5-s shunt mode and 35-s battery charging mode. The new secondary operating cycle consists of 30-s shunt mode and 50-s battery charging mode. This change has a positive effect (as shown later on) on the decay rate of the orbit because there are no periods in the secondary operating cycle in which the tether current is off (open circuit mode) or severely limited (high resistor mode).

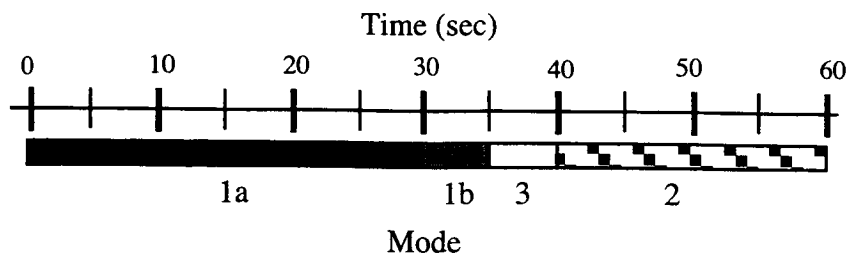


Figure 82 Operating cycle #1 (60-sec cycle) - Operation on Primary Battery

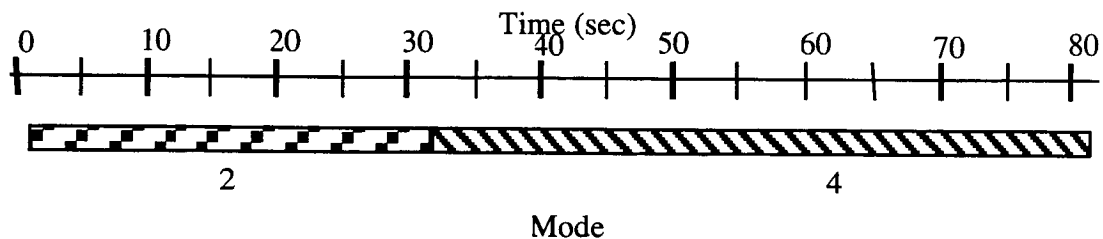


Figure 83 New operating cycle #2 (80-sec cycle) - Operation on Secondary Battery

Mode 1a is open circuit, plasma contactor OFF

Mode 1b is open circuit, plasma contactor ON

Mode 2 is SHUNT mode

Mode 3 is RESISTOR mode

Mode 4 is BATTERY CHARGE mode

Operating cycle #1 is on primary battery (first 5 orbits)

New operating cycle #2 is on secondary battery (after the first 5 orbits)

In the following, we show the results of the new reference mission simulation. The initial conditions and orbital parameters assumed for the reference simulation are as follows:

Launch date and time:

25 July 2002; UTC = 00:15:00 hr:min:s (at first perigee pass)

Orbital elements (from Boeing):

Semimajor axis = 6736.556794 km

Eccentricity = 0.001305

(Initial orbit approx: 350 km x 367 km, with respect to a spherical Earth)

Inclination = 35.363 deg

Right Ascension (RAAN) = 60.296 deg

Argument of perigee = 289.996 deg

Simulation started at first perigee pass, i.e., true anomaly = 0

Environmental conditions:

Nominal solar activity (50% percentile): Rz = 94 (SunSpot Number); IG = 132 (Ionospheric Global Index); F10.7 = 141 (radio flux), Ap = 15 (geomagnetic index).

System parameters:

Satellite mass = 21.4 kg;

Delta mass = 994 kg

Tether mass = 10-kg wire and 1.5-kg Dyneema

Wire external diameter = 1.2 mm

Dyneema average cross section: ~1.2mm x 0.2mm

Tether optical properties:

Dyneema: $\alpha_s = 0.1$, $\epsilon_{IR} = 0.5$;

C-COR coated wire: $\alpha_s = 0.9$, $\epsilon_{IR} = 0.8$.

Tether mechanical properties: EA = 15,000 N; E'A \approx 2000 Ns.

Wire ohmic resistance = 250 ohm at 20 °C

Electrical operating cycle:

The primary cycle is activated at Delta Time = 12,666 s which corresponds to 4700 s after simulation start (when ProSEDS is off the coast of Brazil). The secondary cycle is activated after 5 orbits, i.e., at about 32,200 s after simulation start.

Results of the new reference mission simulation are shown in the following figures. Although these results have been computed for July 25, 2002, they are also valid throughout the Summer of 2002 because the ionospheric indexes change only a little over those months as explained in the next subsection.

ProSEDS 250 ohm@20 C, 350x367km, nom. solar, UTC = 00:15:00,25 July 2002

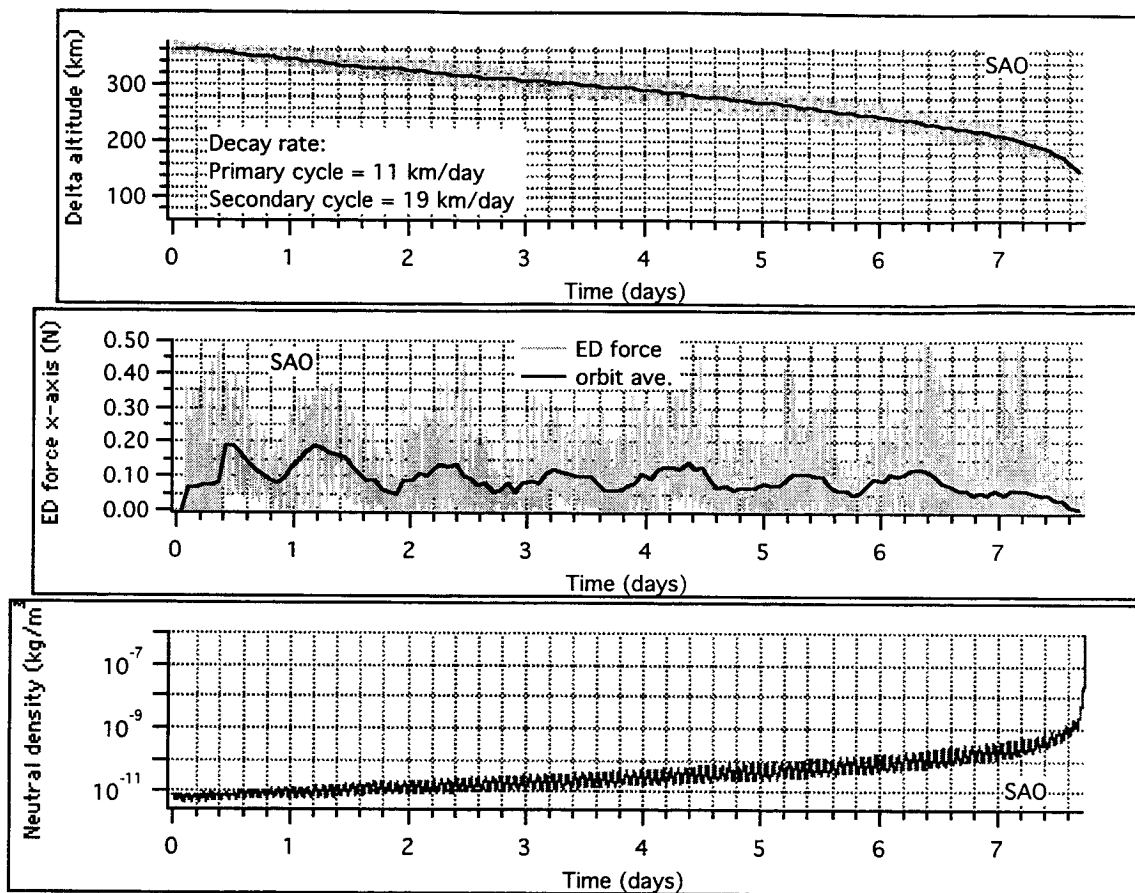


Figure 84 Simulation results for Summer 2002 launch; nominal solar condition

ProSEDS 250 ohm@20 C, 360km, double plasma, 00:15:00UT, 25 July 2002

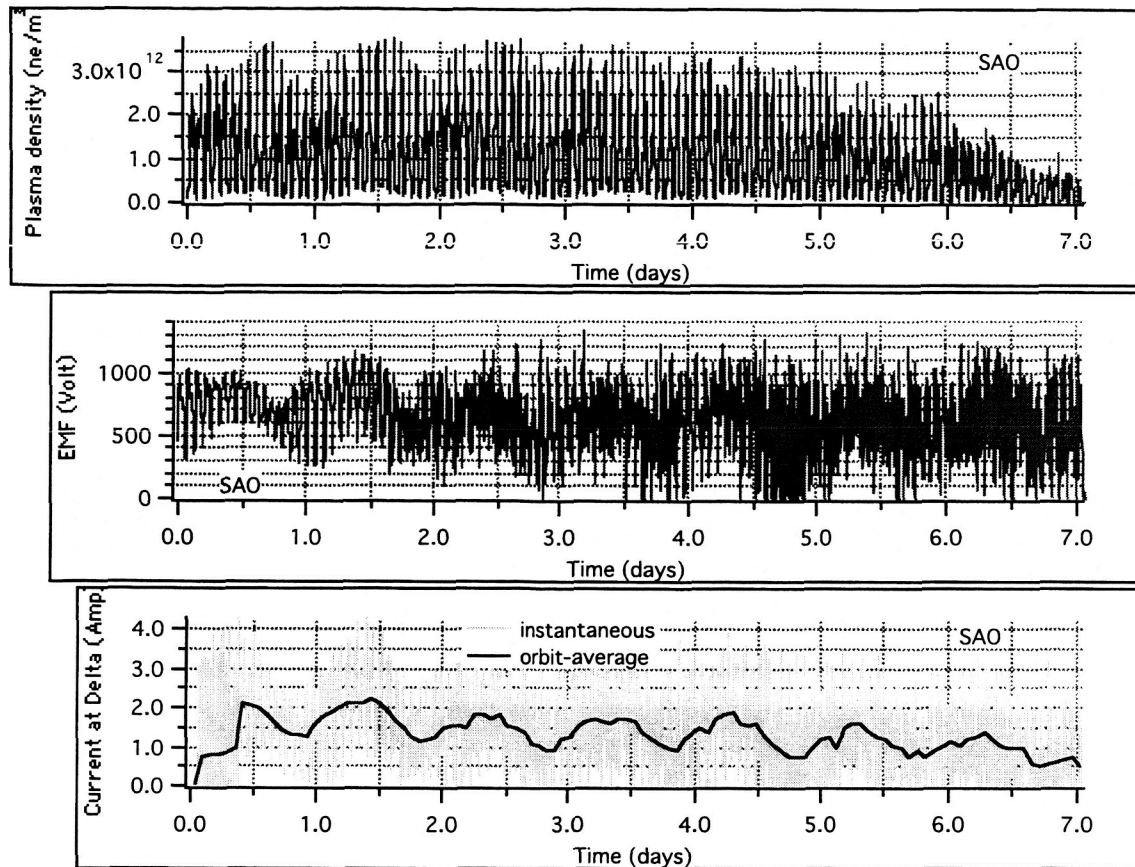


Figure 92 Results for Summer 2002 launch, plasma density twice nominal

ProSEDS 250 ohm@20 C, 360km, double plasma, 00:15:00UT, 25 July 2002

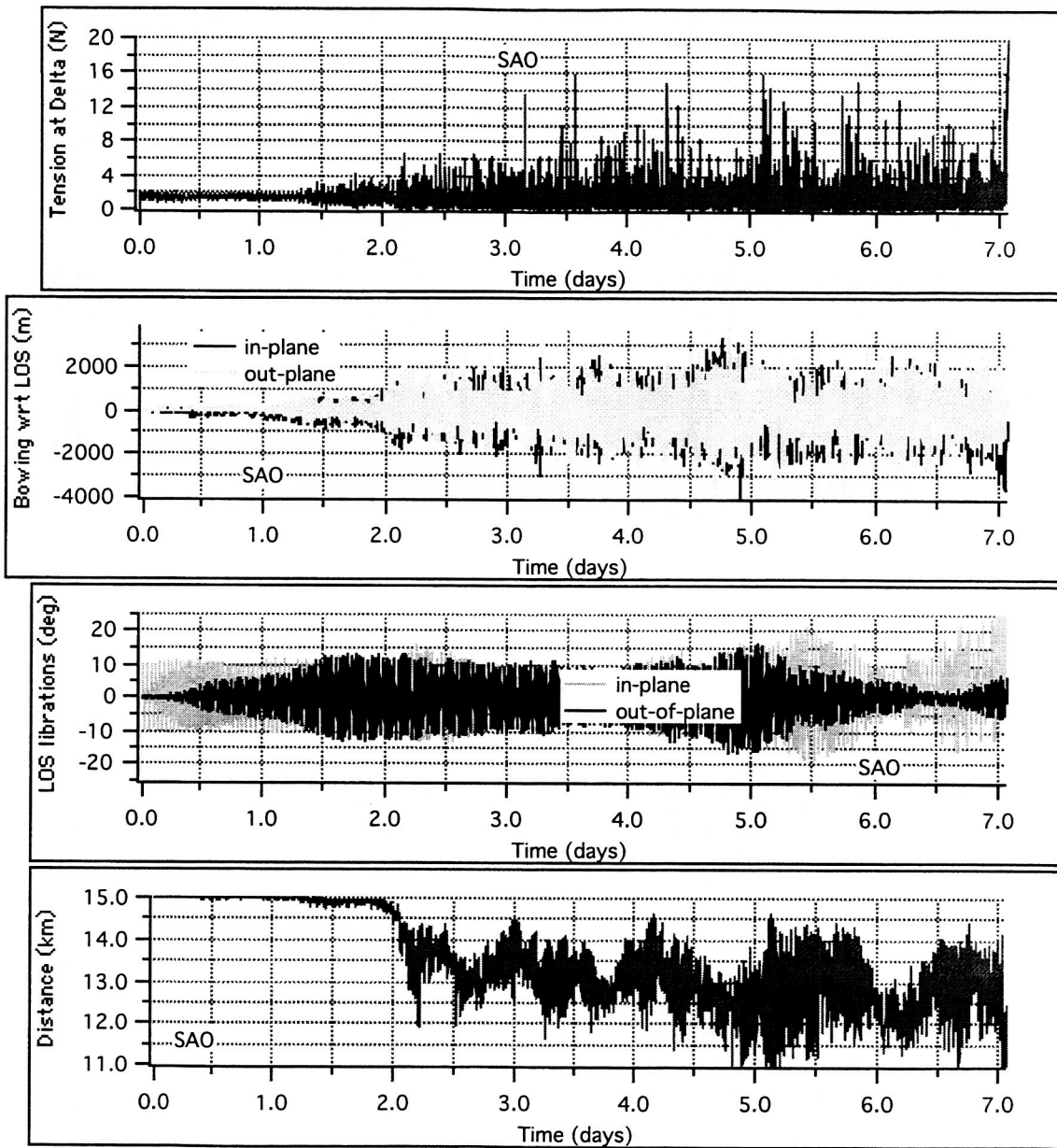


Figure 93 Results for Summer 2002 launch, plasma density twice nominal

ProSEDS 250 ohm@20 C, 350x367km, nom. solar, UTC = 00:15:00, 25 July 2001

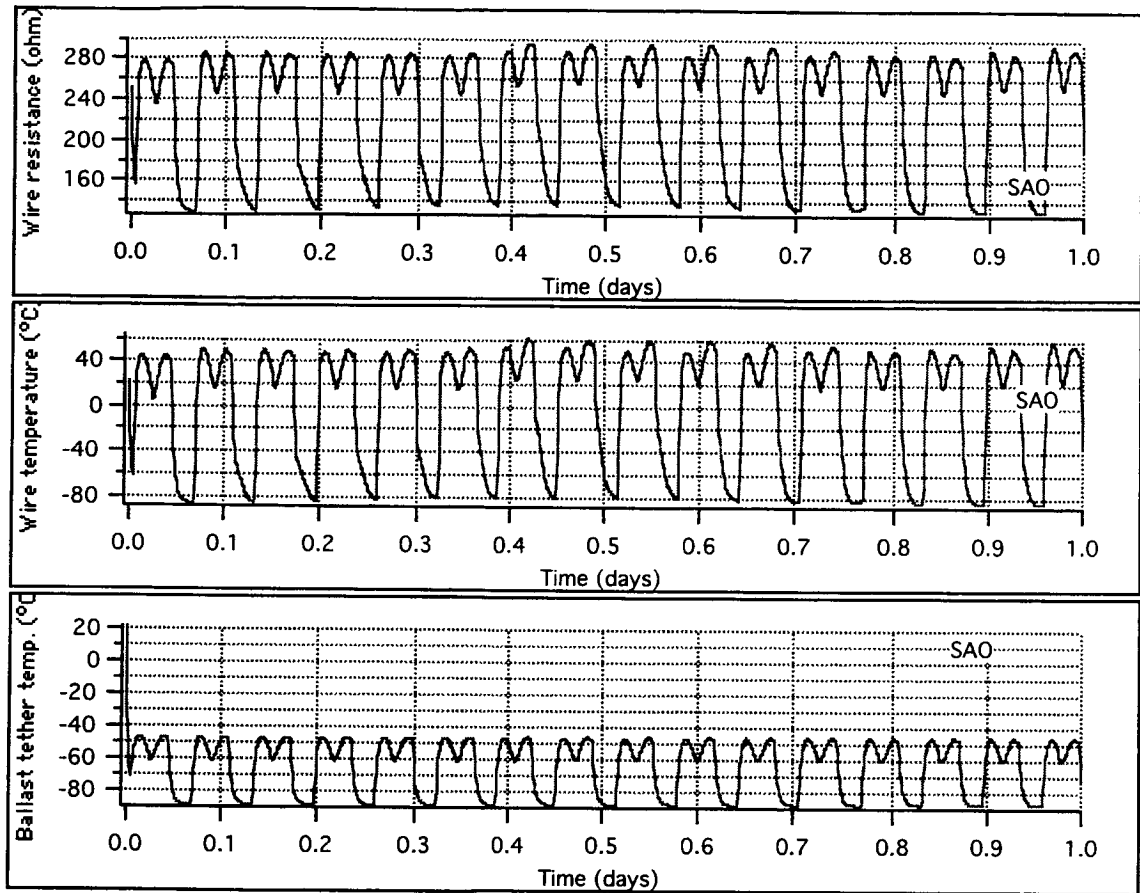


Figure 87 Simulation results for Summer 2002 launch; nominal solar condition

ProSEDS 250 ohm@20 C, 350x367km, nom. solar, UTC = 00:15:00, 25 July 2002

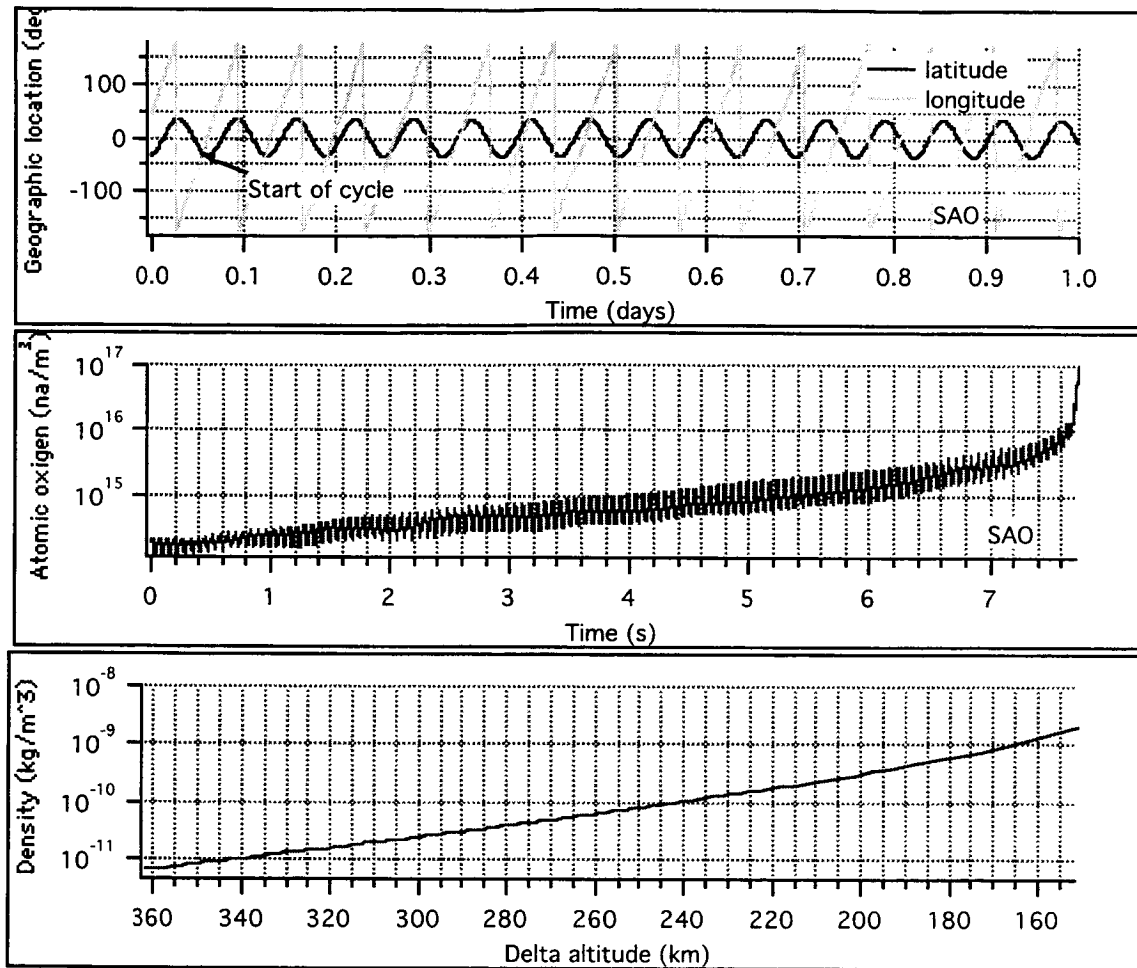


Figure 88 Simulation results for Summer 2002 launch; nominal solar condition

The results show that the new secondary operating cycle almost doubles the decay rate of ProSEDS with respect to previous scenarios. The system dynamics is also more strongly excited with the excitation increasing steeply after one day in orbit. The excitation is the result of a complex skip-rope motion in which the in-plane and out-of-plane motion are coupled as was studied in Refs. ¹⁵. The most noticeable indicator of this motion is the distance from the Delta to the end mass which is plotted in Figure 86. The fact that this distance does not go to zero suggests that the motion is not a planar motion but rather a coning motion resulting from a coupling between the in-plane and out-of plane degrees of freedom. The system dynamics is quite strong as it can be seen from the figure. The tension spikes in the tension plot result from recoiling after the tether has lost tension while there was a substantial shortening of the distance between the end mass and the Delta. The system, however, remains stable and it never topples over. The out-of-plane libration amplitude builds up to somewhat less than 30° at around 5.5 days and then decreases again; most likely because of an energy transfer between degrees of freedom.

If the tether were to remain intact (neglecting the effect of atomic oxygen and possibly a fatal micrometeoroid impact) the Delta stage would reenter the atmosphere before 8 days. However, this situation is only theoretical because the atomic oxygen will chew the Dyneema tether before the system encounters the dense atmosphere. The area below 250 km is where the Dyneema degradation due to atomic oxygen will become strong. The Dyneema tether will likely fail below that altitude, leaving the electrodynamic system in an uncertain state of functionality. Consequently, the rate of decay will slow down significantly after the tether severance with respect to the simulated decay rate that does not take a possible tether cut into account.

10.3 Applicability of results to later launch dates

We are presently in the solar cycle 23 during which the solar activity peaked in April-June 2000. Consequently, the solar activity and the plasma density (that is a function of the solar activity) will decrease over the next few years. The plasma density in the International Reference Ionosphere (IRI95) model is a function of two solar indexes (other than the point location): the Sun spot number (R_z) and the Ionospheric global index (IG). Figure 89 shows the prediction of the Sun spot number for this solar cycle and the next inclusive of high (95% percentile) and low (5% percentile) predicted values. Figure 90 shows the only available prediction of the Ionospheric global index (IG).

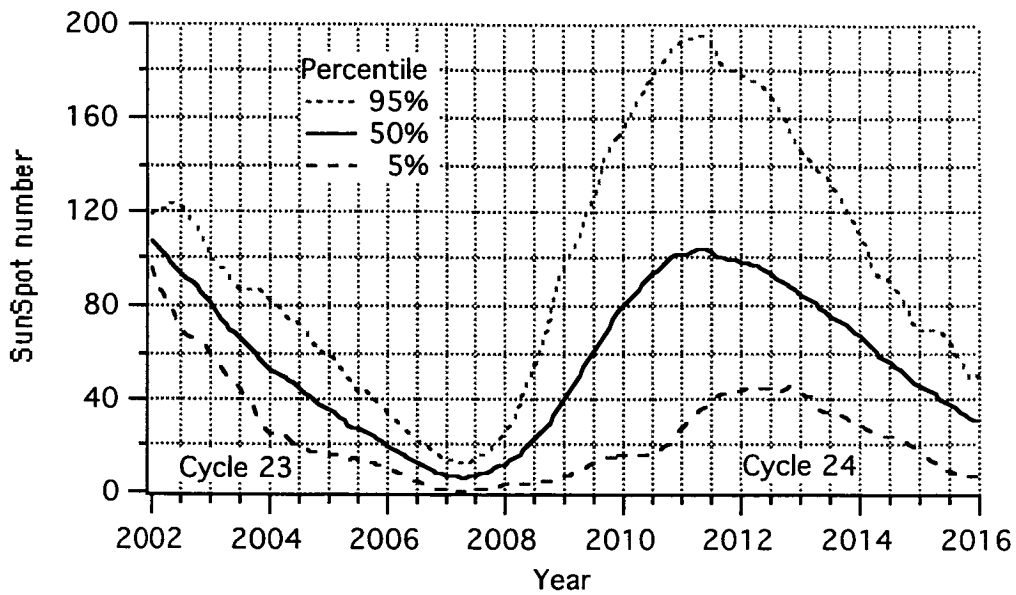


Figure 89 Sunspot number predictions [NASA MSFC]

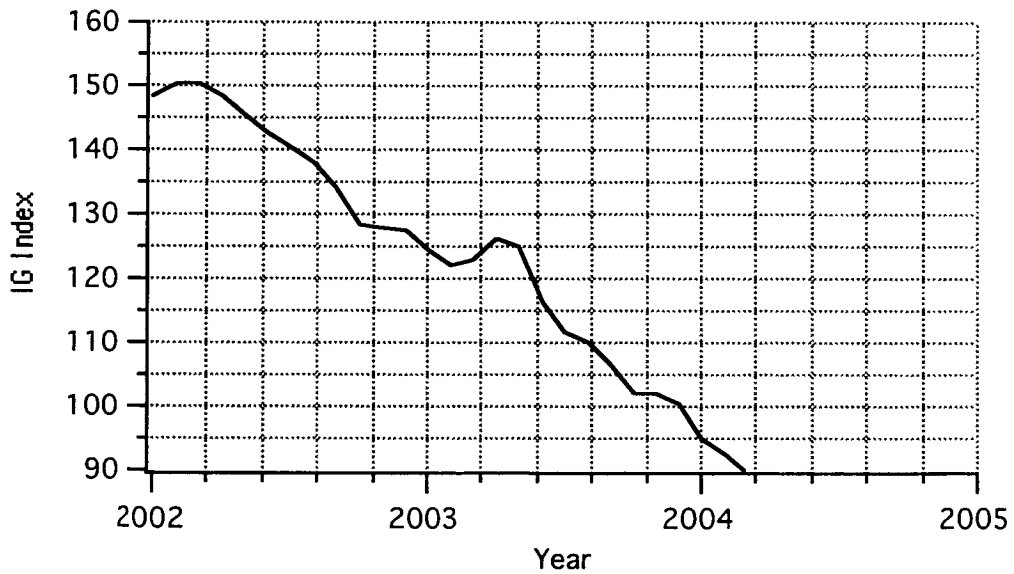


Figure 90 Ionospheric Global Index (IG) prediction [Rutherford Appleton laboratory]

The change of these two indexes over the 3 months of the Summer 2002 is fairly moderate and consequently the result of the July 25th simulation are valid in good approximation throughout the Summer of 2002.

10.4 Extreme electrodynamic forcing

For the purpose of evaluating the system behavior and stability under maximum forcing of the electrodynamic drag a case was run for a plasma density that is (artificially) twice the plasma density under nominal conditions for the Summer of 2002.

The double plasma density increases the decay rate to 23 km/day averaged over six days of secondary cycle operation. Figures 91-95 show the response of the system under these extreme conditions of plasma density. It is notable that the decay rate does not double with respect to the baseline case thanks to the ability of the bare tether to adjust in part to changing plasma conditions.

The dynamic response of the system is stable. The growth of the in-plane libration is actually less than for nominal solar conditions. The higher growth of the in-plane libration in the nominal case was likely due to a transfer of energy from the out-of-plane to the in-plane degrees of freedom as it can be inferred from Figure 93. This points again to the strongly non-linear characteristics of this system dynamics. The loss of tether tension most likely plays a key role by changing the phase relationship among degrees of freedom and forcing terms after the tether rebound and consequently transferring energy from some oscillations to others in a fairly random fashion.

The conclusion is that the overall system stability is not impaired by a doubling of the plasma density even for a launch in the Summer 2002.

ProSEDS 250 ohm@20 C, 360km, double plasma, 00:15:00UT 25, July 2002

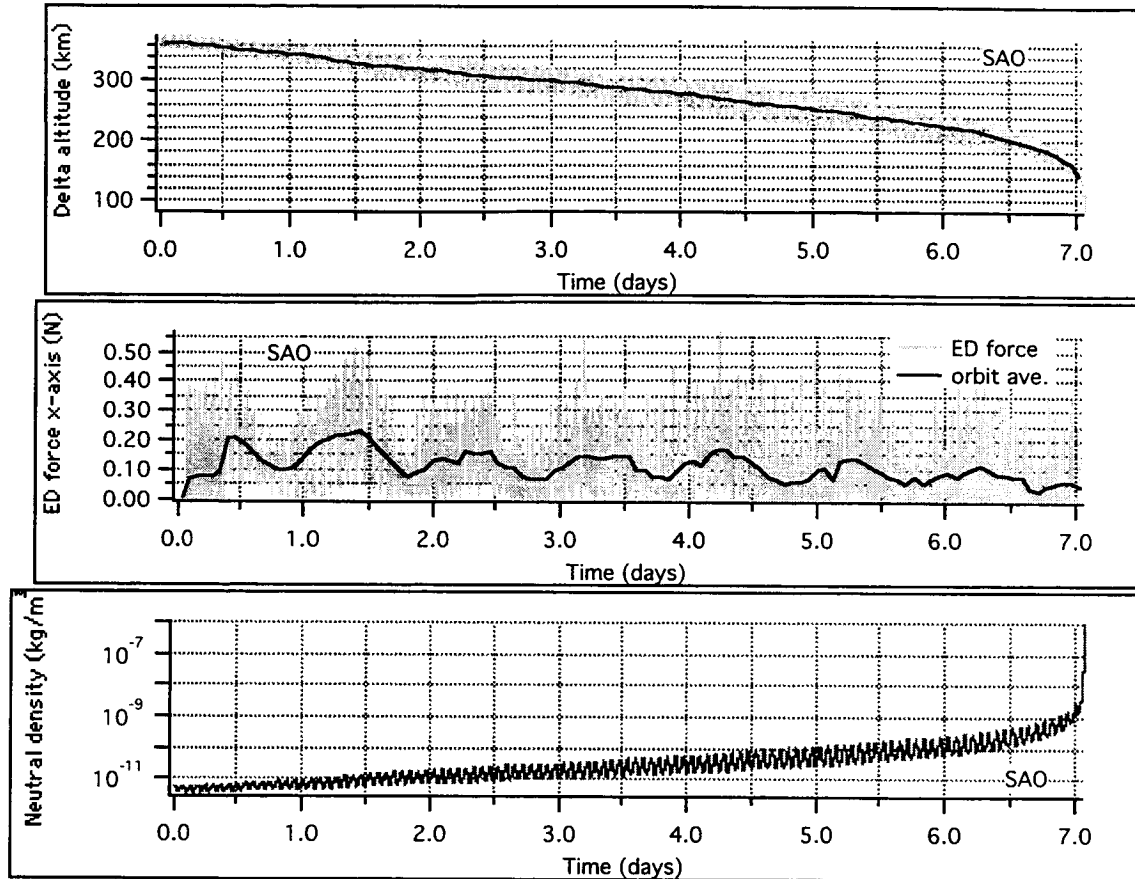


Figure 91 Results for Summer 2002 launch, plasma density twice nominal

ProSEDS 250 ohm@20 C, 360km, double plasma, 00:15:00UT, 25 July 2002

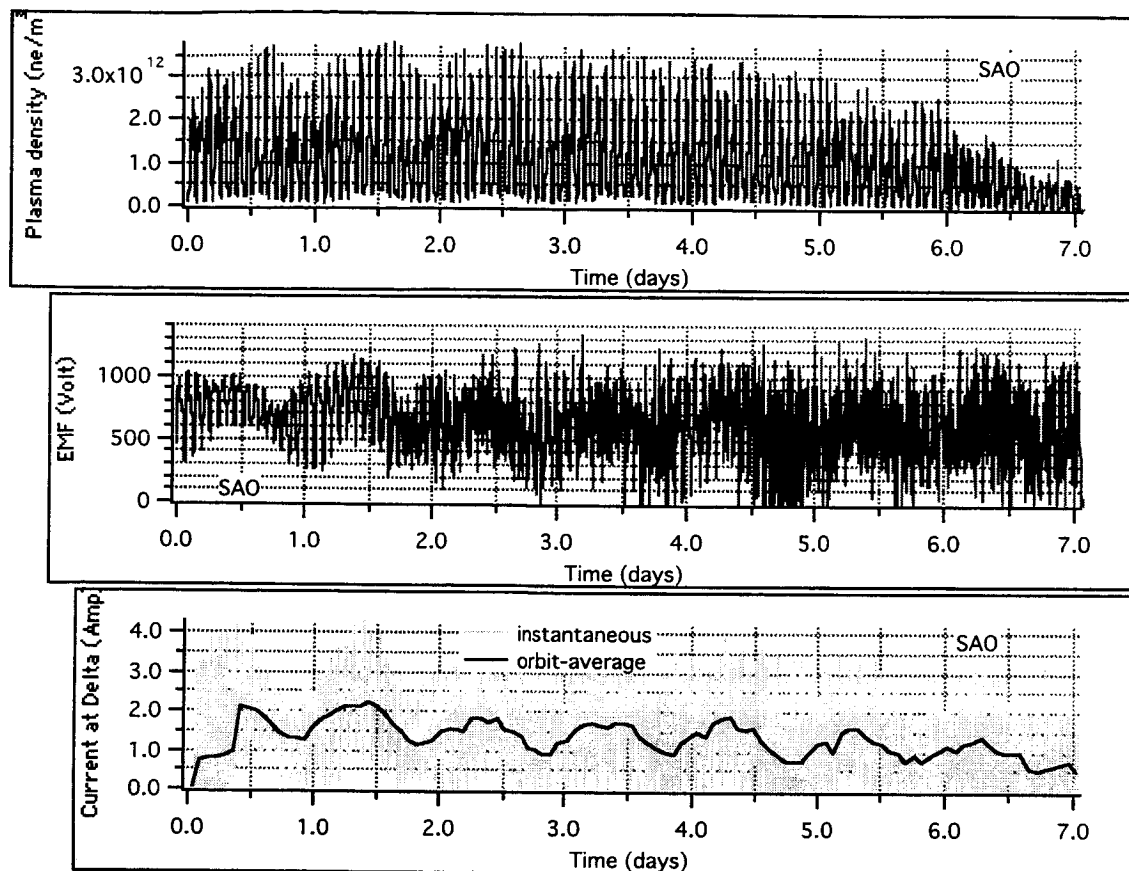


Figure 92 Results for Summer 2002 launch, plasma density twice nominal

ProSEDS 250 ohm@20 C, 360km, double plasma, 00:15:00UT, 25 July 2002

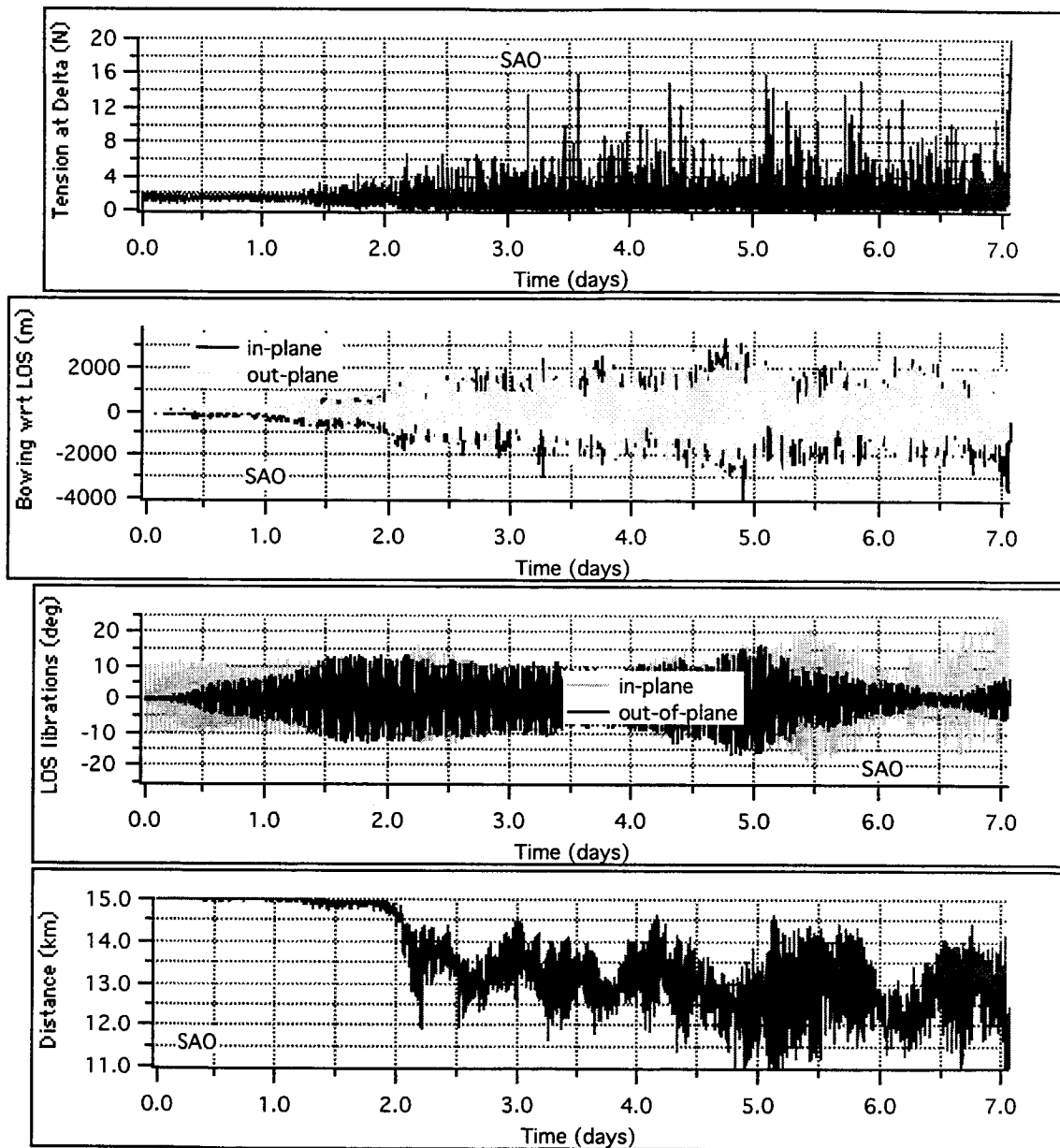


Figure 93 Results for Summer 2002 launch, plasma density twice nominal

ProSEDS 250 ohm@20 C, 360km, double plasma, 00:015:00T, 25 July 2002

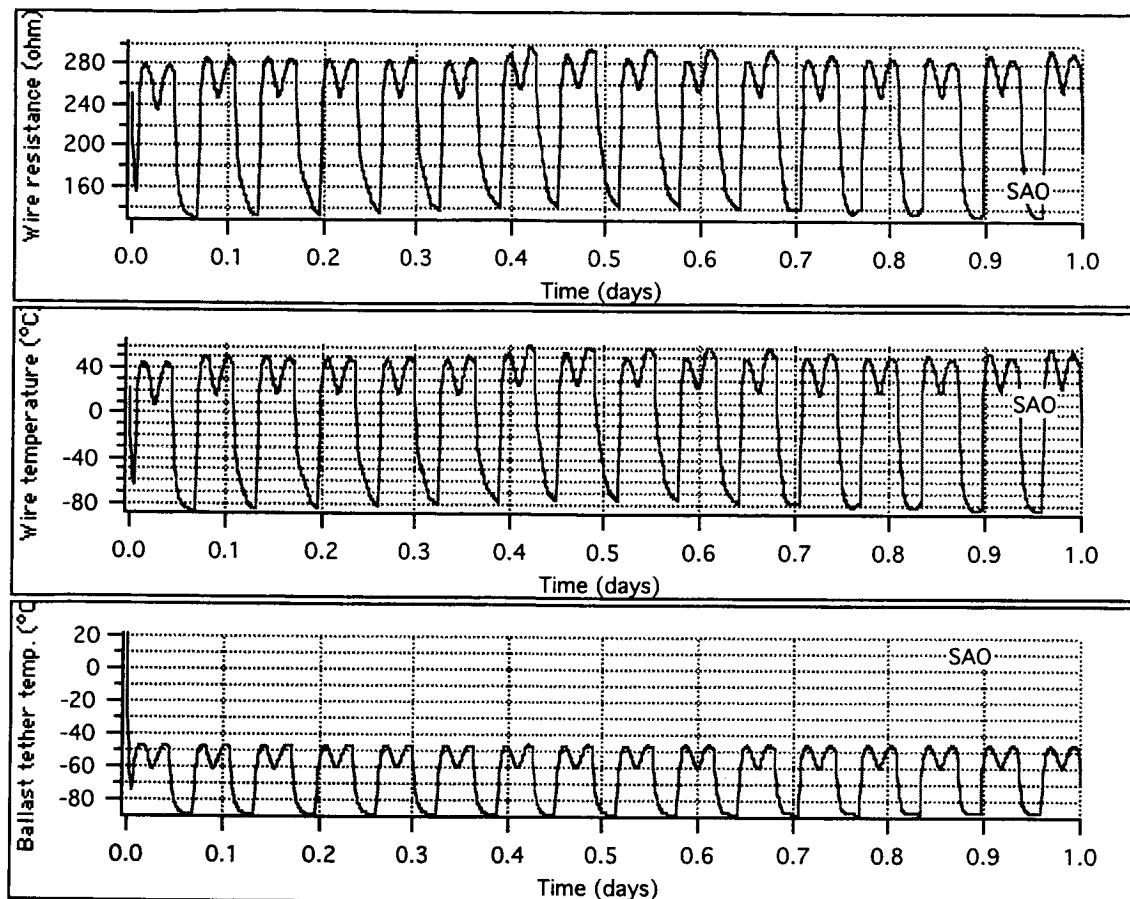


Figure 94 Results for Summer 2002 launch, plasma density twice nominal

ProSEDS 250 ohm@20 C, 360km, double plasma, 00:15:00UT, 25 July 2002

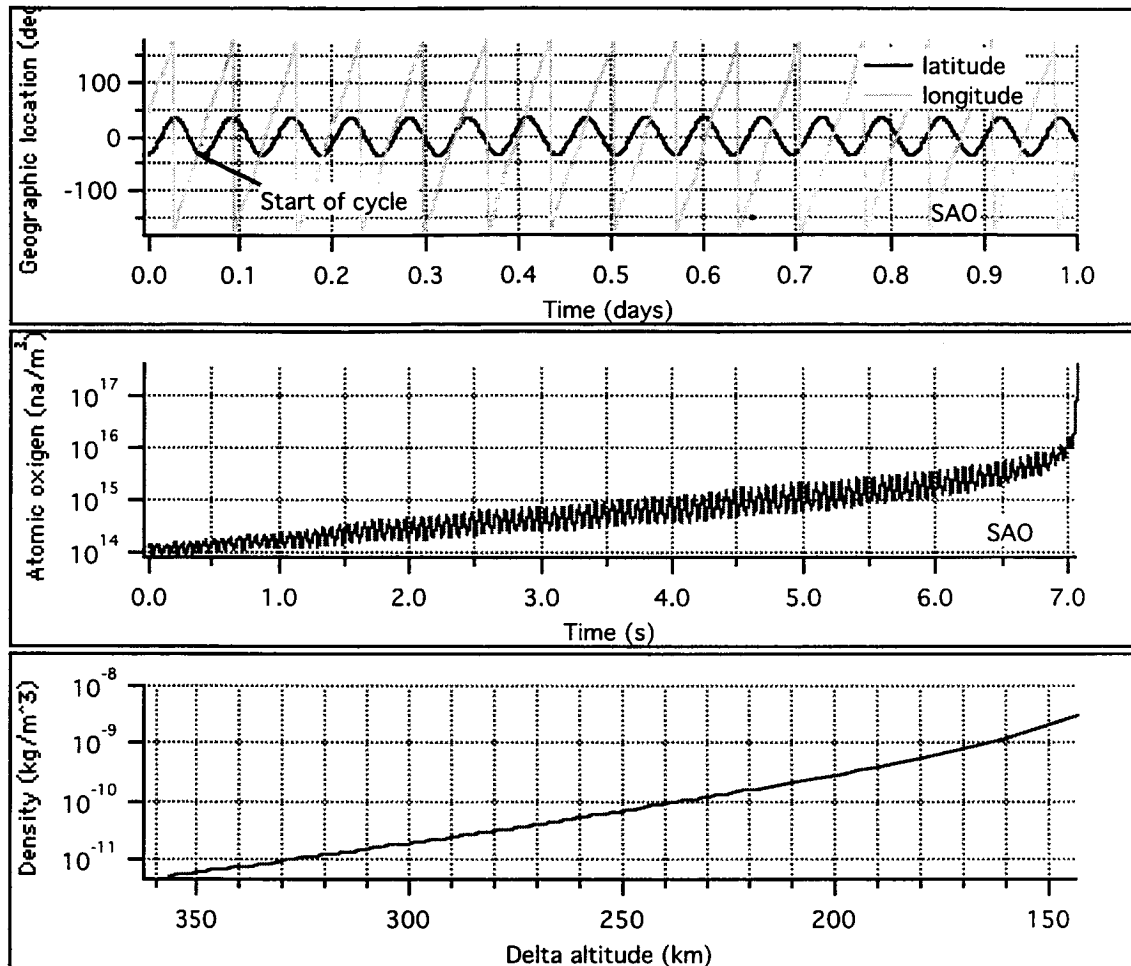


Figure 95 Results for Summer 2002 launch, plasma density twice nominal

10.5 Concluding Remarks

The changes in the operating cycles and most notably the elimination of the open-circuit mode during the 80-s cycles have changed the decay rate and dynamic response of ProSEDS. The present estimates of the orbital decay rate for a launch on July 25th, 2002 are 11 km/day while operating the 60-s cycle (for 5 orbits) and 19 km/day while operating the 80-s cycle during the remainder of the mission but before the neutral drag overpowers the electrodynamic drag. The decay rates estimates are valid with good approximation for any launch date during the Summer of 2002 because the estimated ionospheric and solar indexes that drive the plasma density vary only moderately over the three-month Summer period.

An extreme case with a plasma density twice as high as for nominal solar conditions was run to check the dynamical stability of the system. The decay rate increases only by 20% with respect to the nominal case thanks to the characteristic of the bare-wire anode to adjust to variations of the plasma density. The dynamics of the system remains stable.

11. EVALUATION OF POWER DELIVERED BY THE TETHER

11.1 Introduction

The elimination of the open-circuit mode in the 80-s operating cycle changes the amount of electrical energy available to recharge the battery. As a matter of fact, the change in the operating cycle increases the time spent in battery charging mode (i.e., mode 4) from the previous 35 s to 50 s per cycle. Moreover, the value of the tether resistance of the flight tether is lower (250 ohm at 20 °C) than the value of 265 ohm (at 20 °C) utilized in the previous estimates of the current produced by the tether. Consequently, a new estimate of the tether current during battery charging was carried out as shown in the following.

11.2 Numerical Results

The estimate of the tether current produced during battery charging was computed for minimum solar activity conditions predicted for July 2002. The minimum solar conditions, corresponding to a 5% percentile probability, provide a conservative estimate of the tether current (and consequently power) available to recharge the secondary batteries. All other orbital and system parameters are the same of the reference mission described in Section 10 of this report. Figure 96 shows the instantaneous tether current during battery charging (mode 4) and the 12-hour running average of the current. The average is computed over the mode-4 period of 50 s and not over the overall cycle of 80 s.

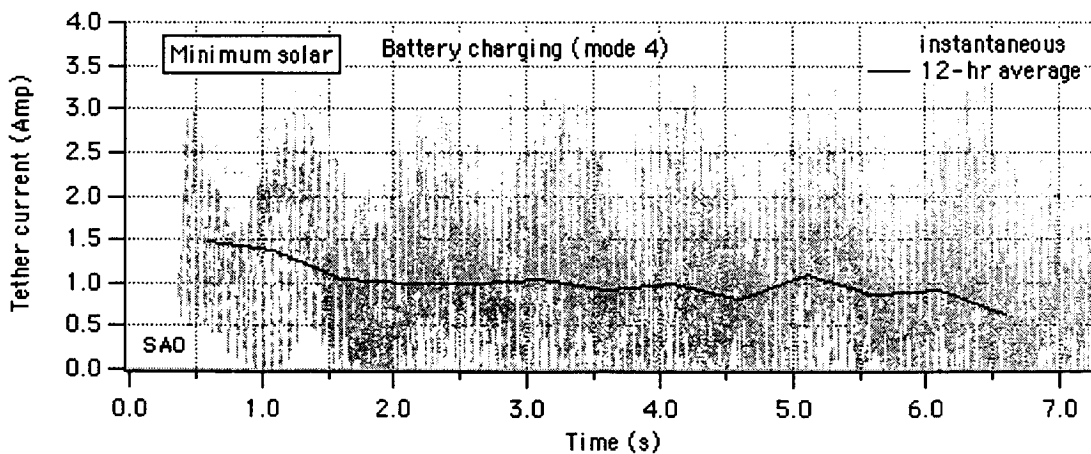


Figure 96 Tether current during battery charging mode: instant value and 12-hour average

The average value of the current is 1.33 Amp during the first day while the peak value of the current is 3.71 Amp. The corresponding values for nominal solar conditions (the plot is not shown) are 1.42 Amp for the average and 3.85 Amp for the peak value during the first day. The average value of the current decreases by roughly 30% after 1.5 day mostly due to tether dynamics.

Although the average values of the current during battery charging are similar to those computed for earlier launch dates, the net advantage of the new 80-s cycle is that the electrical energy provided by the tether (during normal battery charging operation) is higher because mode-4 is now 50-s long as opposed to 35 s for the older version of the cycle.

11.3 Concluding Remarks

The change in the 80-s operating cycle has improved the power budget for ProSEDS because of the longer time spent in battery-charging mode (mode 4). The estimate of the average current for the first day of operation in battery charging mode is 1.33 Amp for minimum solar conditions with the average computed over the 50-s battery charging mode. The estimated average value for nominal solar conditions is 1.42 Amp. The average values decrease by roughly 30% after 1.5 day due to system dynamics.

The value of the average current is similar to what was computed for the previous launch dates. However, the total electrical energy available for battery charging (during normal battery operation) is better than with the older 80-s cycle because the battery charging mode is now 50-s long as opposed to 35 s.

12. DEPLOYMENT CONTROL PROFILE REF. #78 AND SIMULATIONS

12.1 Introduction

We recall here that the ProSEDS control law consists of three distinct modes of operations which are activated during the deployment of the three different tether sections. The non-conductive 10-km-long Dyneema tether is deployed according to the SEDS-II feedback-feed-forward control law. During the deployment of the 4.85-km conductive wire, the brake is simply kept at a constant, low value in order to limit the deployment velocity. During the deployment of the 215-m (final value based on the flight tether characteristics) insulated tether section, the brake is commanded to follow a time-based profile to slow down the deployment velocity at the end of the tether. A more detailed description of the control law and the tether tension model was given previously.

12.2 Friction model

The updated values of the friction parameters obtained from the deployment tests on ground of the F-1 tether are as follows:

Author: E.C. Lorenzini (SAO)

Latest Friction Parameters of the F-1 flight tether

The reference values of the tension parameters for the ProSEDS tension model are listed in the following. These values, which are from the F-1 deployment tests, were adopted for deriving Reference Profile #78.

Flat Dyneema (cleaned)

T_{min}	= spectra minimum tension	= 18 mN
Den	= spectra linear density	= 0.2 kg/km
I	= inertia multiplier	= 2.5
f	= spectra friction coeff	= 0.16
E	= area exponent	= -5.0
effe	= brake effectiveness $Turn^{effe}$	= 1.2
AnSol	= annulus solidity	= 0.2 (for $L_f = 10km$)

K = base of braking power law = 1.7

Wire (CCOR)

T_{min} = wire minimum tension = 150 mN
den = wire linear density = 1.935 kg/km
I = inertia multiplier = 2.5
f = friction coeff = 0.24
E = area exponent = -0.65
Effe = brake effectiveness Turn^{effe} = 1.7
AnSol = annulus solidity = 0.947
K = base of braking power law = 2.72 (= e)

Insulated (Kevlar overbraided)

T_{min} = insulated minimum tension = 300 mN
den = insulated linear density = 3.176 kg/km
f = friction coeff = 0.21
I = inertia multiplier = 1.7
E = area exponent = -0.65
Effe = brake effectiveness Turn^{effe} = 0.9
AnSol = annulus solidity = 0.947
K = base of braking power law = 2.72 (= e)

Subsequent tests of the F-1 run in hot and cold conditions validated most of the values of the friction parameters with the exception of the minimum tether tension which is more sensitive to temperature variations and, even more importantly, to the amount of residual sizing agent in the non-conductive tether (level of cleanliness). The flight tethers have all been cleaned in order to provide values of the minimum tension below 20 mN. However, the control law is tested (as shown later on) also for much higher values of the minimum tension. The typical range of variation of the non-conductive tether minimum tension is assumed conservatively to be in the range 5mN-30mN which are the limit values measured

during the deployment tests of the many tethers developed for ProSEDS (and not just the F-1).

The friction parameters of the whole tether (with the three different sections) are utilized to derive the reference table, that is, the reference deployment profile and a brake profile for the whole tether. The brake actuation is then adjusted by the feedback control law during the deployment of 10-km Dyneema portion while the reference brake profile is followed (without adjustments) during the wire and insulated portions of the tether.

12.3 Flight reference table

Several new reference tables were derived for the deployment control law as tether friction data became available during the year from the deployment tests and spooling data from Tether Applications, Inc. We will not describe here all the new updates but rather concentrate on the *flight reference profile (Reference #78)*.

The process for deriving the reference profile is an optimization process that aims at minimizing a cost function which encapsulates the departure of the final dynamic state from the desired state. The desired final state at the end of deployment is for the system to be aligned and swing less with respect to the local vertical with a residual longitudinal velocity greater than 3 m/s before the beginning of the insulated portion of the wire (last 215 m of tether). The residual velocity is then reduced by a final activation of the brake immediately after the exiting of the insulated wire is sensed.

The flight reference table was derived based on the friction data of the F-1 tether deployment test at room temperature and for a minimum tether tension equal to 20 mN. This minimum tension is slightly higher than the 18 mN measured in that deployment test but the 20 mN value provided a reference profile with better features (e.g., smoothness of the deployment velocity and progressive ramping up of the brake) than what could be obtained with the 18 mN value. The friction data from the room temperature test were preferred to the hot and cold test data because the deployer will be close to room temperature at the start of deployment.

The most recent parameters adopted for deriving the flight reference profiles are as follows:

Orbital and ejection parameters

Orbit: 360X360 km

Orbital inclination: 36 deg

Ejection velocity = 2.74 m/s

Ejection angle = 5 deg (forward of LV with an upward deployment)

System parameters

Satellite mass = 21.4 kg

Delta-II Mass = 994 kg

Tether lengths: 10132 m Dyneema, 4865 m CCOR and 215-m insulated

Tether length is then converted to tether turns (and velocity to turn rate) which are the variable utilized by the control law. Consequently, two tethers appear very similar to the control law if the number of turns of the three segments are about the same. The following files (supplied by J. Carroll, Tether Applications, Inc.) provide the spooling data for the F-2 and F-3 tethers, respectively

F-2 flight tether spooling

Tether Applications, Inc.

Here are the quadratic equations for the Kevlar+Dyneema, CCOR, and overbraided insulated wire. The values are derived from the turns and estimated as-deployed lengths at various points in the winding, including the estimated effects of Dyneema creep during bakeout, and the temperature and tension differences between winding and deployed conditions. (The deployed tension is assumed to be ~1.3 newtons.) The "L" in meters and "T" (in core turns) for each segment start at zero when that segment starts deploying.

Quadratic length formula for PROSED19 winding of F-2 tether:

Noncond: 10132 meters; 14733 turns; $L = 0.72822 * T - 2.75E-6 * Sqr(T)$
 C-COR: 4865 meters; 11037 turns; $L = 0.64497 * T - 18.5E-6 * Sqr(T)$
 Insul: 215 meters; 1108 turns; $L = 0.2339 * T - 36E-6 * Sqr(T)$.

The F-2 non-conductive tether is 5 turns & 92 meters longer than F-1. The F-2 wire is 138 turns shorter but 12 meters longer than F-1. Most of these differences are due to the increased bulk of the longer overbraid on F-2, and the fact that we needed about the same wire length but the same # of Dyneema turns.

Meters	Turn#	Transition
0	0	Outer Kevlar tie-down
20	28	End of Kevlar leader (start of Dyneema)
5562	7872	Near the middle of the Dyneema
10132	14733	Start of wire (end of Dyneema)
12705	19328	Near the middle of the wire
14334	23384	Parallel/criss-cross winding transition
14997	25770	Start of overbraided insulated wire
15012	25835	Brake turn (second of two to deploy)
15212	26878	Termination pin at base of core

F-2 cross-straps and key transitions (m) from inner termination pin:

Meters	CoreTurn	Feature
0	0	Termination pin at base of deployer
200	1043	Brake enable sensor hole
215	1108	End of overbraided insulated length.
257	1287	1 (inboard cross-strap; rest are spaced 321m apart)
578	2507	2
900	3559	3
1221	4484	4
1542	5331	5
1863	6119	6
2184	6853	7
2505	7547	8
2826	8206	9
3147	8835	10
3469	9438	11
3790	10015	12
4111	10572	13
4432	11110	14
4753	11631	15
5074	12136	16 (outboard cross-strap)
5080	12145	End of wire (7 wires tuck into core, 1" apart)

F-3 flight tether spooling data

End-to-End Description of Flight Winding of F-3 (PROSED21)

Joe Carroll
Tether Applications, Inc.
Winding dates: March 18-19, 2002
Post-wind handling finished March 21, 2002

Notes on winding:

F-3 quadratic length formulas (winding PROSED21):

Non-conduct: 10167 meters; 14730 turns; $L = 0.73029 * T - 2.72E-6 * Sqr(T)$
C-COR wire: 4870 meters; 11042 turns; $L = 0.64642 * T - 18.6E-6 * Sqr(T)$
Insul wire: 214 meters; 1103 turns; $L = 0.2337 * T - 36E-6 * Sqr(T)$.

For comparison, here are the formulas for F-2 and F-1:

F-2 quadratic length formulas (winding PROSED19):

Non-conduct: 10132 meters; 14733 turns; $L = 0.72822 * T - 2.75E-6 * Sqr(T)$
C-COR wire: 4865 meters; 11037 turns; $L = 0.64497 * T - 18.5E-6 * Sqr(T)$
Insul wire: 215 meters; 1108 turns; $L = 0.2339 * T - 36E-6 * Sqr(T)$.

F-1 quadratic length formulas (for first winding, PROSED15):

Non-conduct: 10040 meters; 14728 turns; $L = 0.7215 * T - 2.70E-6 * Sqr(T)$
C-COR wire: 4894 meters; 11350 turns; $L = 0.6378 * T - 18.2E-6 * Sqr(T)$
Insul wire: 174 meters; 933 turns; $L = 0.2201 * T - 36E-6 * Sqr(T)$.

Tether mass/length:

Kevlar: 2.10g/m
Dyneema: 0.150g/m
CCOR: 1.92g/m
InsWire: 3.25g/m

Transition locations for F-3 (PROSED21):

As wound:		As deployed:		
MetW	Core	Meters	Turn#	Transition
30917	26875	0	0	Outer Kevlar tie-down
30878	26849	19	26	End of Kevlar leader (start of Dyneema)
19596	19008	5577	7867	Stop mid-Dyneema (0.2% longer in orbit)
10278	12145	10167	14730	Start of wire (end of Dyneema)
5072	7556	12741	19319	Stop mid-wire (wire=0.07% shorter)
1777	3497	14371	23378	Parallel/criss-cross transition
430	1103	15037	25772	End of overbraid wrap-splice
402	1044	15051	25831	Brake turn (second of two to deploy)
0	0	15251	26875	Termination pin at base of core

Turn differences of F-2 (PROSED19) and F-1 (PROSED15 & PROSED18) from F-3:

F-2	F-1#1	F-1#3	Transition
+3	-2	+76	Start of wire (end of Dyneema)
+6	-233	-154	Parallel/criss-cross transition
-2	+306	+453	End of overbraid wrap-splice
+4	+102	+228	Brake turn (second of two to deploy)
+3	+136	+272	Termination pin at base of core

Basis of length estimates:

Estimated as-deployed length per turn of TAI metwheel (491.066mm/turn w/o tether) 496.5 mm for insulated overbraided tether & 20m Kevlar leader (same as as-wound) 494.5 mm for C-COR-coated conductive tether (this is 0.07% shorter than as-wound) 492.6 mm for flat 13x100 Dyneema braid (this is 0.2% longer than as-wound)

Winding temperature range: ~21-23C

Winding tension (lengths were measured at these tensions):

13-16 newtons for parallel winding

12, 10.5, 9, 7.5, and 10 newtons for CC patterns #1-5.

Explanation of adjustments from as-wound to as-deployed conditions:

Assume Dyneema creep during bakeout reduces its tension to as-deployed tension.

Assume Kevlar has equilibrium post-deployment tension of ~1.3 newtons

Modulus of long segments (C-COR and Dyneema) is ~12000-15000 newtons.

Assume Dyneema and CCOR are 225K and 300K in orbit; CTEs are -28ppm/K and 0ppm/K. Thus Dyneema should be ~0.2% longer; CCOR ~0.07% shorter, deployed vs. wound.

F-3 Cross-strap locations (from start of winding):

MetWhl	CoreTurn	Meters	Gap
530W	1311.1C	262	262
1179W	2524.4C	584	321
1828W	3572.4C	905	321
2477W	4495.5C	1226	321
3127W	5343.7C	1547	322
3777W	6131.4C	1869	321
4426W	6866.1C	2190	321
5076W	7559.4C	2511	321
5725W	8217.9C	2832	321
6373W	8846.7C	3153	321
7023W	9447.5C	3474	321
7672W	10024.0C	3795	321
8322W	10578.9C	4116	321
8970W	11115.3C	4437	321
9619W	11633.7C	4758	321
10267W	12136.6C	5078	320

The differences in turns of the F-2 from the F-3 are less than 6 turns which makes them almost perfectly alike to the control law. The reference profile (Ref. #78) works equally well for the F-2 and F-3 flight tethers. This reference profile, shown in Figure 97, has several good features as follows: (a) the exit velocity changes smoothly during the Dyneema deployment and it does not deep down to low values; (b) the brake increases monotonously from zero to its maximum value; and (c) the libration angle is very close to zero at the end of deployment (for reference conditions). This reference profile when combined with the control law provides a final libration amplitude which is quite insensitive to variation of the Dyneema minimum tension and other friction parameters as it will be shown later on. The reference table for Ref. #78 is tabulated in Ref.¹⁶ (Annual Report#3 of this grant).

Reference Profile #78

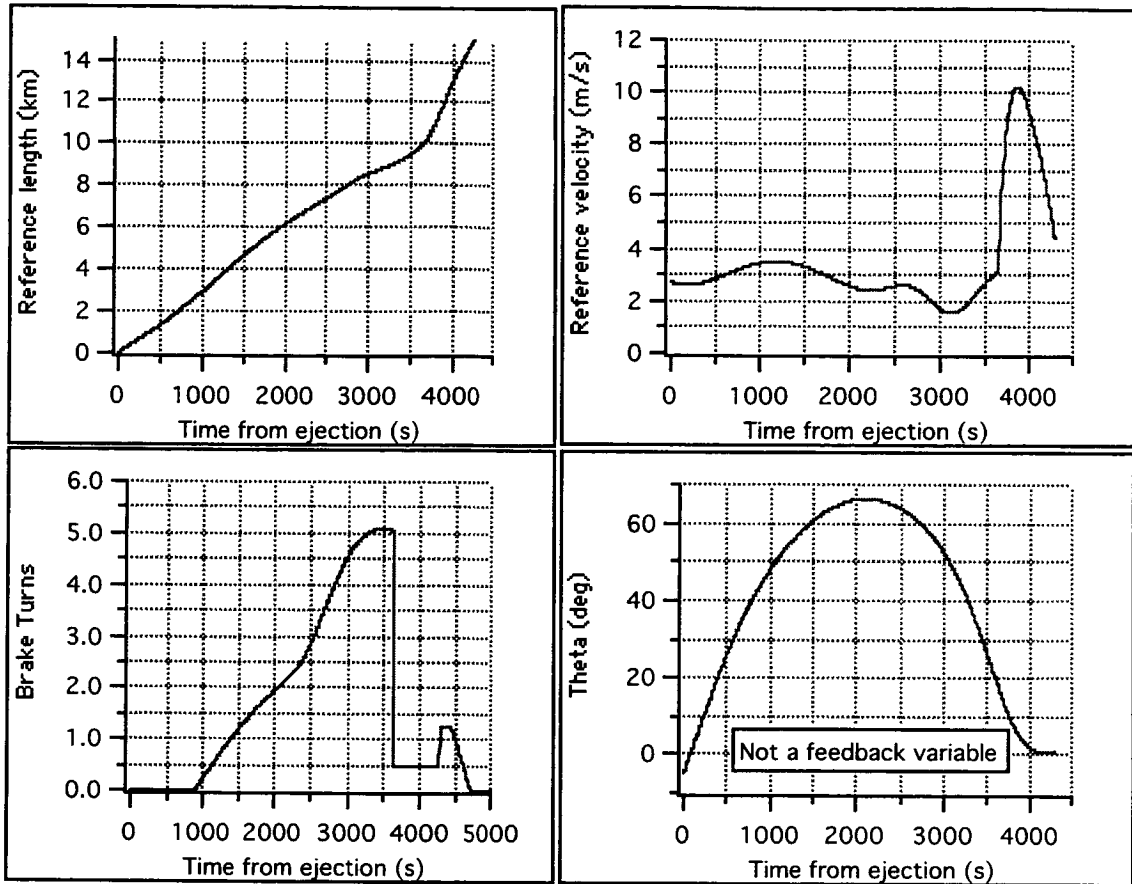


Figure 97 Control law Reference Profile #78

12.4 Flight control law backup modes and parameters

The control law not only provides the logic for controlling deployment under perfect functionality of the sensors. It also has a set of backup modes to circumvent or mitigate the effects of possible failures or malfunctions of the deployer sensors. The sensors in question are the two turn counters (Counter-A and Counter-B) which measure the number of tether turns that have been deployed. In standard operation, the output of the two turn counters is combined to produce a software turn count Counter-C which is unaffected by double counts. In case of failure of one of the turn counter, Counter-C is bypassed and the still functioning turn counter is utilized by the sensor logic. However, when only one turn counter is working there is an over count of the number of turns that has to be accounted for by the control law when transitioning from one tether segment to the next. Also, if both turn

counters fail, the control law logic sets the feedback to zero and utilizes exclusively the reference profile to drive deployment (this is one additional advantage of having the feed-forward profile in the control law). Similarly, there are two levels of backup for the actuation of the slow-down maneuver that starts at the beginning of the insulated tether portion (last 215 m of tether). The slow-down maneuver is activated, in standard operation, by the turn counter. In case of the two turn counters failing, there are two level of backup as follows: the first one is provided by the brake enabler switch which senses the beginning of the insulated wire, and the second is provided by time.

The control parameters define the standard operation of the control law and also the activation of the backup modes. The parameters controlling the standard operation are taken from the SEDS-II control set with a few adjustments aimed at improving the robustness of the control law to variations of the friction parameters. The control parameters that define the control modes corresponding to transitions from one tether segment to the next and the parameters that define the backup modes have been added to the original control set of the SEDS-II control law. The complete set of the updated control parameters for Reference Profile #78 are shown in Table 9.

Table 9 Updated control parameters for Reference Profile #78

Values of control parameters for ProSEDS Ref#78 (F2 & F3 tethers). Issued on April 5, 2002; revised on July 23, 2002.

----- CONTROL PARAMETERS (REF. #78) -----			
No.	PARAMETER	VALUE (Units)	Type
1.	c	0.125	Filter coefficient
2.	GTC	0.002 (1/turn)	TurnCount Gain
3.	DZTC	5 (turn)	TurnCount Deadzone
4.	TCELIM	3000 (turn)	Max. TurnCount Error
5.	GTCR	0.4 (s/turn)	TurnCountRate Gain
6.	DZTCR	0.1 (turn/s)	TurnCountRate Deadzone
7.	TCRELIM	5 (turn/s)	Max. TurnCountRate Error
8.	WAILP	3	WrapIncrement UpperLimit
9.	TBD s	65535 (sec)	Time after which BIAS is applied
10.	BIAS	0 (turn)	BrakePost Bias
11.	WACLP	6.5 (turn)	WrapAdjustment UpperLimit
12.	TCBS	18000 (turn)	Turns Count Brake Stop (SEDS-II law)
13.	A1	0.724	Coeff_1 in Variable Gains
14.	A2	2.82E-6	Coeff_2 in Variable Gains
15.	STOPDEPLOY	65535 (sec)	Time for brake ramping up to max. value at end of deployment (SEDS-II law)
16.	TCDUTY	13560 (turn)	End of 50% duty cycle
17.	TURNBRAKE0	14265 (turn)	RampDown brake to WIREBRAKE
18.	WIREBRAKE	0.5 (turn)	BrakeTurns during CCOR deployment
19.	RAMPUP	25835 (turn)	Start of slowdown procedure

20. QUITLAWBACKUP	14400	(turn)	Ramp down brake in case of CounterA or B failure
21. BRSD	1.25	(turn)	Max brake turns during slow down
22. TBD(15)	20	(sec)	Time to rampup brake from WIREBRAKE to BRSD
23. TIMECFAIL	120	(sec)	Time of no update of CounterC to declare the CounterC failed
24. TIMEDUTY	6080*	(sec)	Time-based equivalent of TCDUTY
25. TIMEQUERY	6832*	(sec)	The software starts interrogating the BES if CounterC has failed
26. TIMERAMPNOBES	6894*	(sec)	Time-based start of slowdown procedure if the BES was declared failed

*These values of parameters assume a SMET = 2640 sec at endmass separation (parameters revised on July 23, 2002)

Notes:

BES = brake enable switch

SW = flight software

SMET = secondary mission elapsed time

12.5 Sensitivity of control law to friction parameters

Deployment trajectory is mostly influenced by the tether tension profile during the early part of deployment. The physical explanation for this behavior is that small changes in the tether changes alter the dynamics the most when the external forces (i.e., the gravity gradient) are small, that is, at short tether lengths.

The deployment test data show that the range of variation of most of the friction parameters are smaller than $\pm 20\%$. The minimum tether tensions of the Dyneema and the CCOR wire are the exception. The value of the Dyneema minimum tension in particular changes by a few folds across the many tether samples tested. The CCOR minimum

tension, besides being less variable than the Dyneema, has an almost negligible effect on the libration amplitude at the end of deployment.

The minimum tension of the ProSEDS Dyneema tether (which dominates the final state at the end of deployment) has already been measured in deployment ground tests under different temperatures to vary between 5mN and 30 mN for all the tether samples tested with a smaller range of variation for the F-1 tether. Consequently, the control law must provide a residual libration at the end of deployment of less than 20° (as specified by the mission requirements) within the measured range of variability of the minimum tension.

The control law with Reference #78 can tolerate without a significant decay in performance a value of the non-conductive tether minimum tension between 5 mN and 30 mN. For $30 \text{ mN} < T_0 < 60 \text{ mN}$, the libration at end of deployment increases above 10° but still below 20°. For $T_0 \geq 80 \text{ mN}$, the deployment stops at a distance of about 500 m because of excessive friction and without any role being played by the control law. The critical value of 80 mN for the minimum tension is determined by the ejection velocity which with the present ejection system is equal to 2.74 m/s.

Figure 98-100 show details of the deployment dynamics for values of the minimum Dyneema tension for $T_0 = 5 \text{ mN}$, 10 mN, and 20 mN (reference value), respectively. Figure 101 shows the effect on the control law and deployment dynamics of a noisy tether tension on the deployment dynamics (for $T_0 = 20 \text{ mN}$). A $\pm 50\%$ white noise has been added to the tether tension. The figure shows that the control law is capable of handling the high noise level with ease. The brake actuation is still smooth and the deployment dynamics is negligibly affected by the noise. The final libration amplitude is unaffected by the white noise.

Ref#78, $T_{min} = 5\text{mN}/150\text{mN}$, $\Delta V = 2.74\text{ m/s}$, Brake 1.25/20s

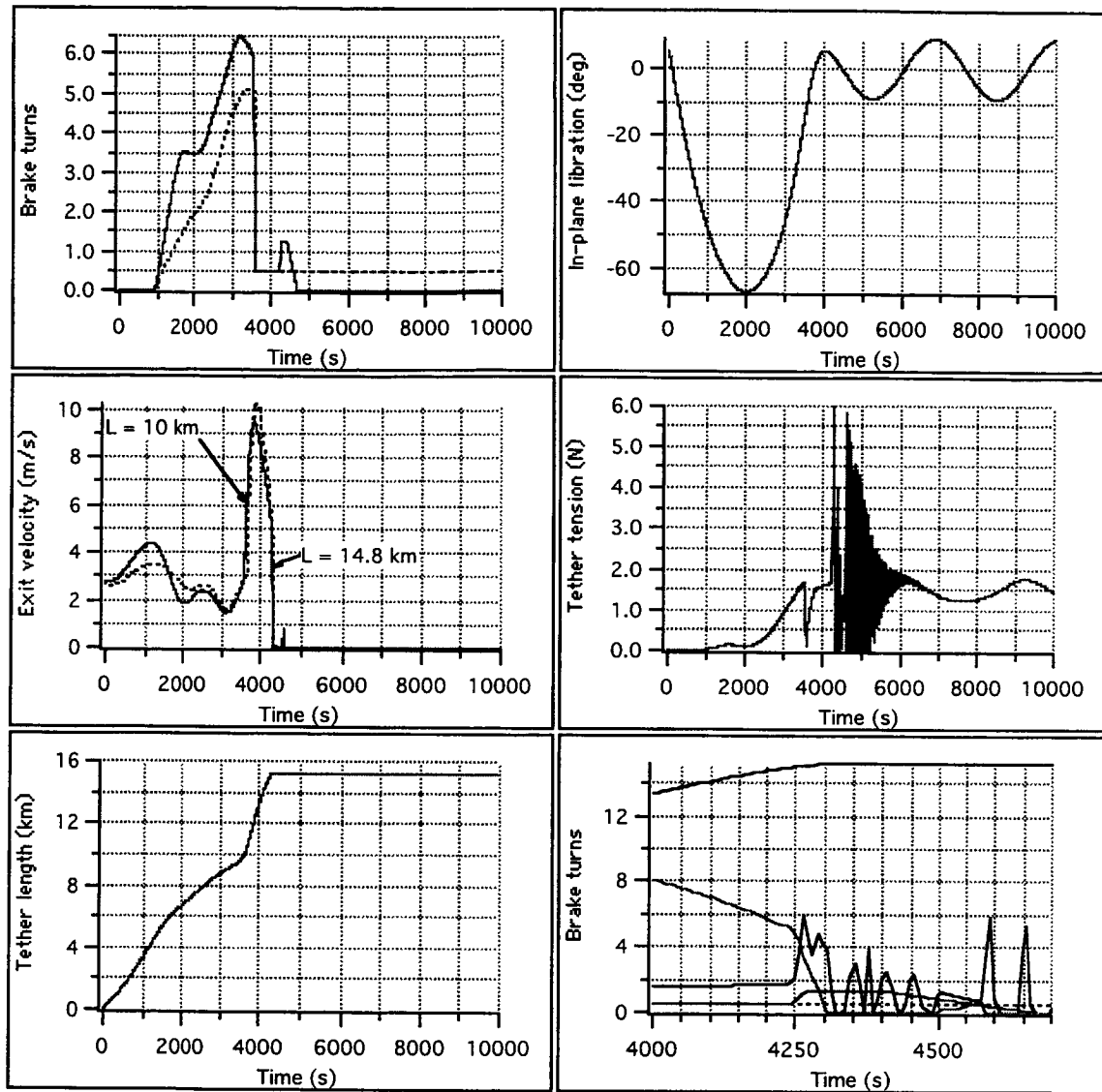


Figure 98 Deployment dynamics for Ref#78 and $T_0 = 5\text{ mN}$

Ref#78, $T_{min} = 10mN/150mN$, $\Delta V = 2.74$ m/s, Brake 1.25/20s

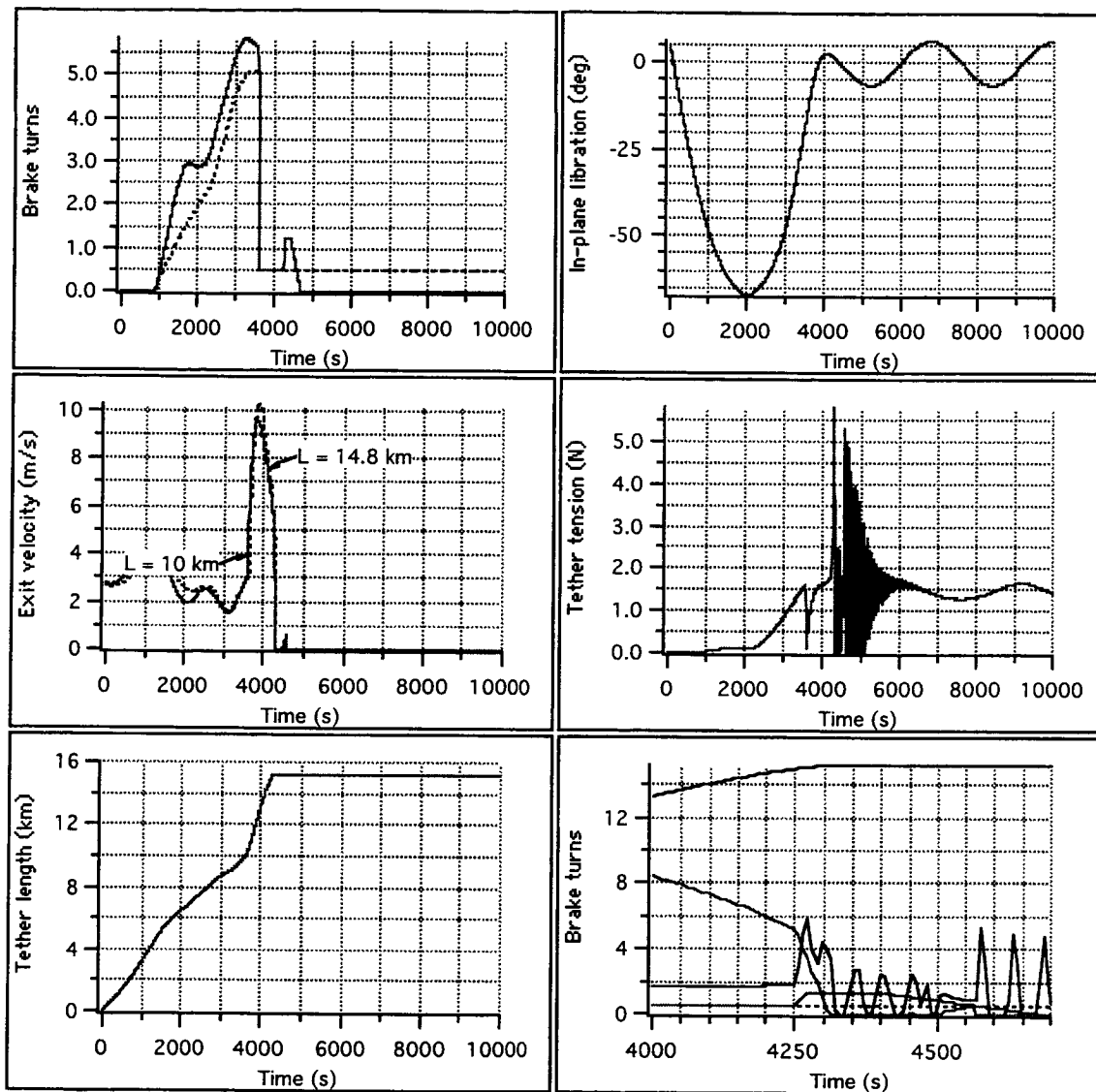


Figure 99 Deployment dynamics for Ref#78 and $T_0 = 10$ mN

Ref#78, $T_{min} = 20\text{mN}/150\text{mN}$, $\Delta V = 2.74 \text{ m/s}$, Brake 1.25/20s

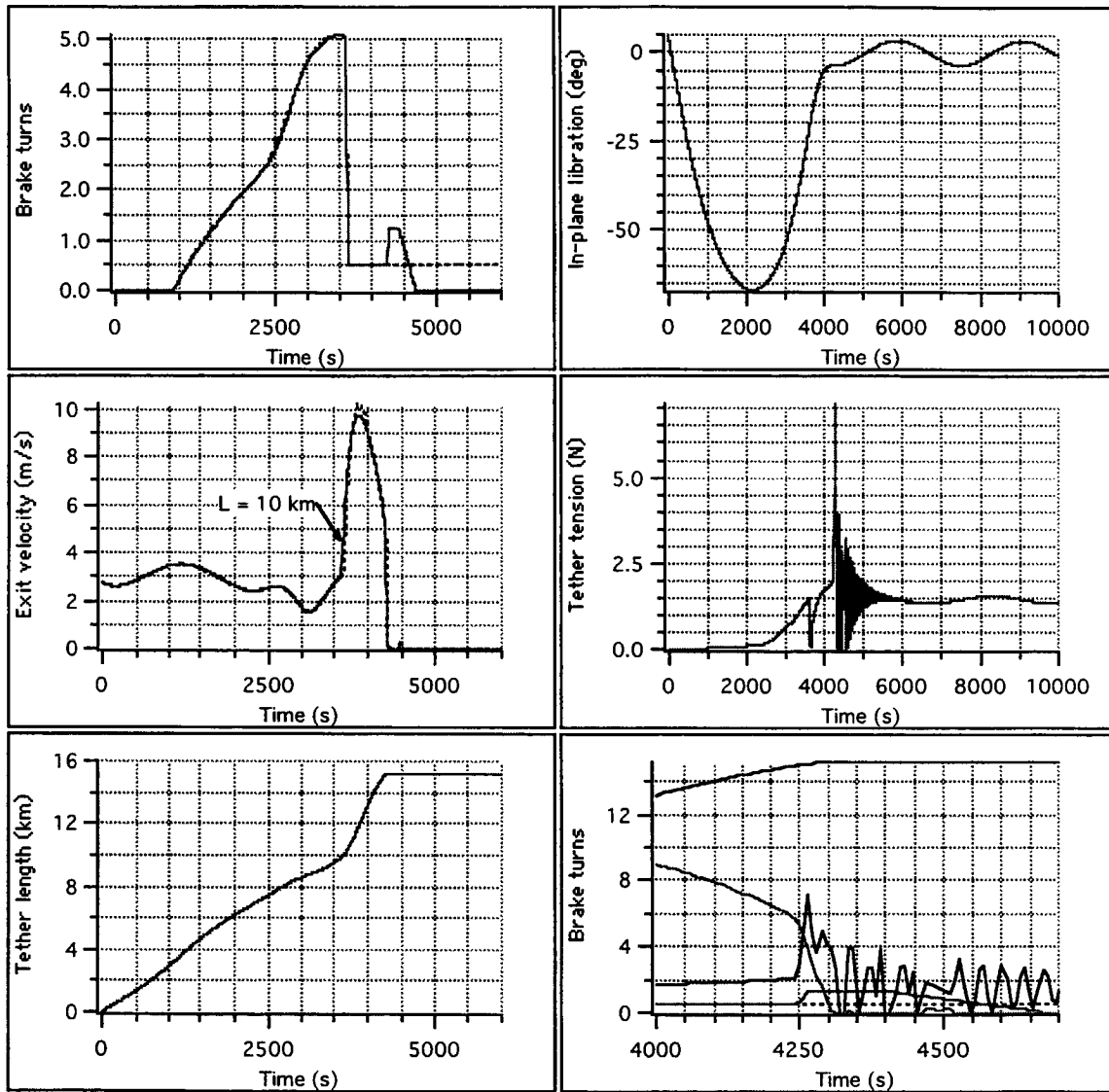


Figure 100 Deployment dynamics for Ref#78 and $T_0 = 20 \text{ mN}$ (reference)

Ref#78, $T_{min} = 20\text{mN}/150\text{mN}$, $\Delta V = 2.74 \text{ m/s}$, $\pm 50\%$ White Noise

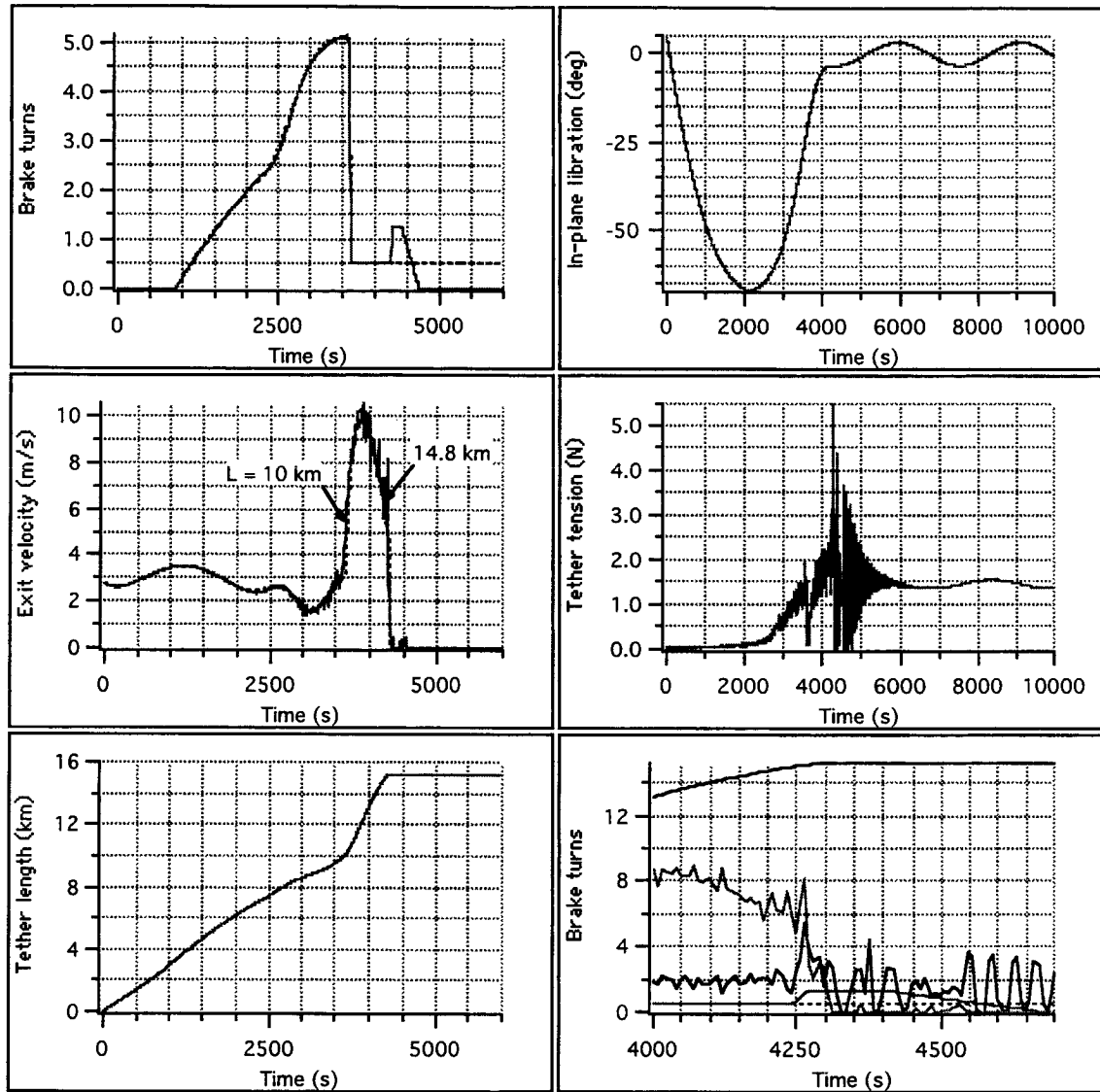


Figure 101 Deployment dynamics for $T_0 = 20 \text{ mN}$ with $\pm 50\%$ tension white noise

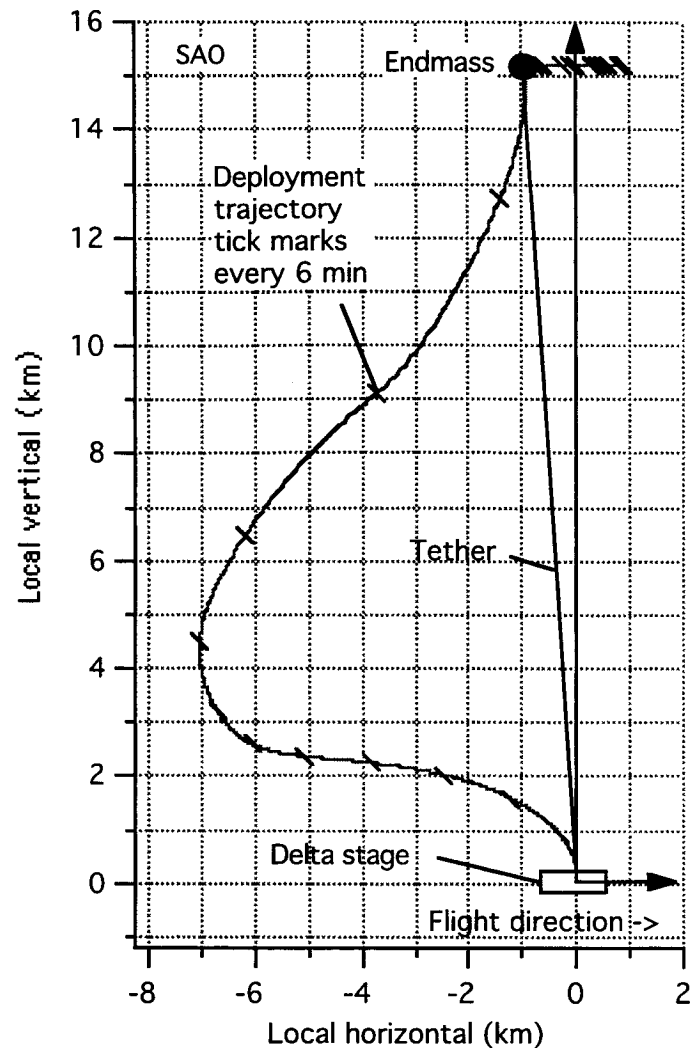


Figure 102 Deployment trajectory of the endmass with respect to the Delta stage

Figure 102 depicts the deployment trajectory of the endmass with respect to the Delta stage for the reference case of $T_0 = 20$ mN. The tick marks along the trajectory are every 6 minutes. The CCOR wire starts deploying at about the point where the tick mark caption is pointing. Figure 103 shows the amplitude of the residual libration at the end of deployment vs. the minimum tension T_0 of the Dyneema tether for Ref. #78. The figure also shows the libration amplitude without deployment control and the representative points of the SEDS-I and SEDS-II missions. The final libration amplitude is sensitive to the Dyneema tether T_0 and it is quite insensitive to the value of the wire minimum tension T_{wire} . Values of T_{wire} of 50-300 mN have been explored with very good deployment dynamics. Values as high as 500 mN are tolerable for the minimum tension of the wire.

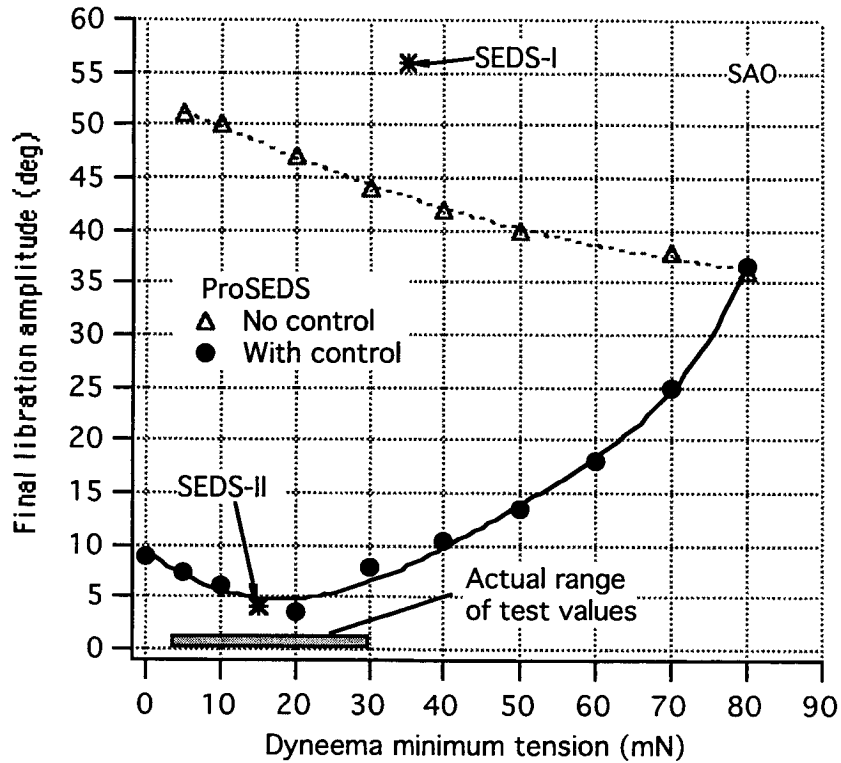


Figure 103 Final libration amplitude vs. T_0 with control (Ref. #78) and without control

12.6 Concluding remarks

The deployment control law in combination with Reference Profile #78 is robust with respect to changes of the most influential and uncertain friction parameters. A number of backup modes have been built into the control logic to circumvent (or mitigate) the effects of the possible failure of one (or two) turn counters. The control law meets the requirement of a final libration smaller than 20° over the measured values of the friction parameters with a positive safety margin.

13. KALMAN FILTERS FOR MISSION ESTIMATION

13.1 Introduction

As part of the data analysis effort, SAO has focused on the following objectives:

- a. Characterization of the system decay (semi-major axis and rates)
- b. Estimation of the Average Current (for decay and EM modeling)
- c. Estimation of Delta Rotation Rates (Magnetometer calibration and Instrument Readings)
- d. Estimation of Skip Rope Motion (produced by deployment and built up during mission)

Two extended Kalman Filter estimators have been developed to address the objectives.

13.2 Magnetometer data Kalman filter

KAL Mag - Uses magnetometer data and a reference magnetic field (IGRF) to estimate:

- a. Bias, on each axis, due to uncalibrated residual magnetic fields and those generated during the flight from currents.
- b. Rotation rates of Delta stage (yaw rotation about the tether axis)
- c. Skip-rope motion (Frequency analysis and estimation of amplitude)

An FFT pre-processor estimates the yaw rate (highest amplitude) and one user-defined frequency (e.g. skip-rope frequency). A pre-calculated IGRF field data, inertial components and modulus, is supplied for the time readings of the magnetometer.

Each magnetometer component is decomposed into a constant bias and a series of sinusoids with known frequency and unknown random-walk amplitudes.

The software works in conjunction with the IGOR data analysis and display software package. It has been designed to process data in real-time, making it suitable during the ProSEDS flight. The program can also be run backwards in order to provide a smoothed estimate of the parameters in the post-processing phase.

The software is very robust and has been tested with SEDS-I data, where the constant bias affecting the magnetometer was calculated after the flight with a least-squares estimator. Moreover, SEDS-I reached a very low perigee (~180 km) and a FFT analysis revealed that the tether lateral modes had been excited to hundreds of meters. Once the skip-rope modulated by the Delta rotation is estimated, the amplitude can be computed by geometrical considerations. This part of the effort is still under study. The modeling of the process and measurement errors affect the calculation of the covariance. A normal distribution of the measurements, though simplified, seems appropriate for the effort.

We recommend an additional test by running SAO high-fidelity code MASTER and generating a magnetic field at the Delta stage due to the current cycle.

The estimated components of the bias are shown in Figure 104 and the estimated vs. measured magnetometer component (Y direction) is shown in Figure 105.

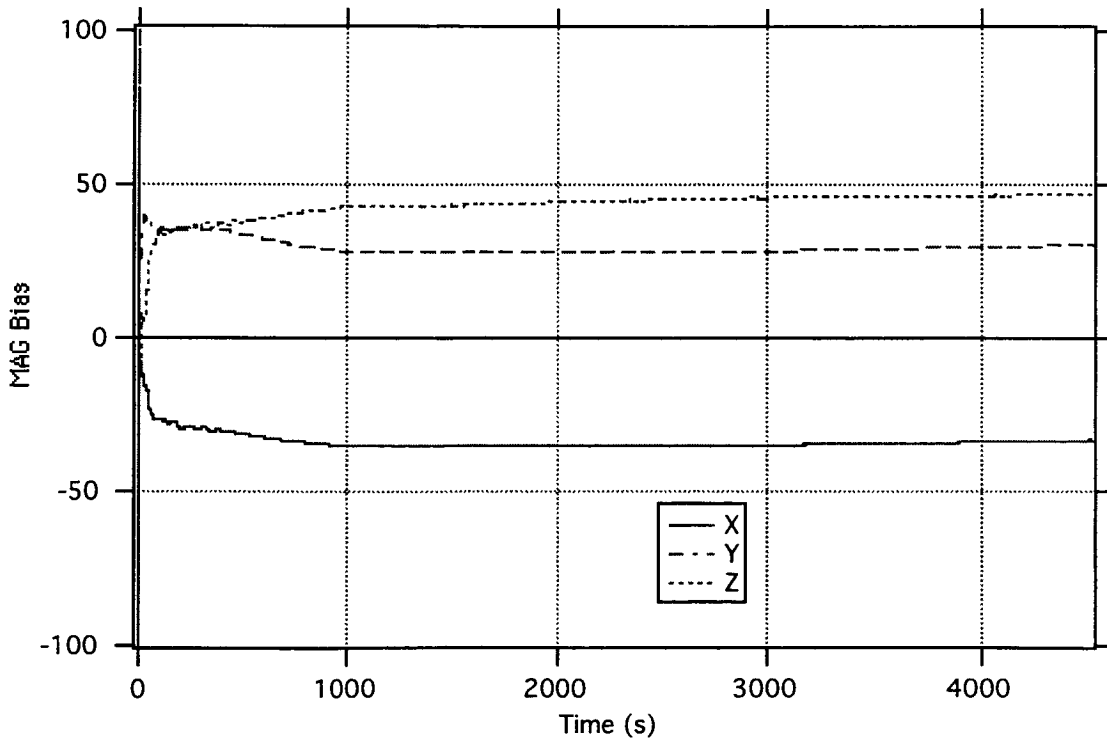


Figure 104 Estimated Bias Components (SEDS-1 Flight Data)

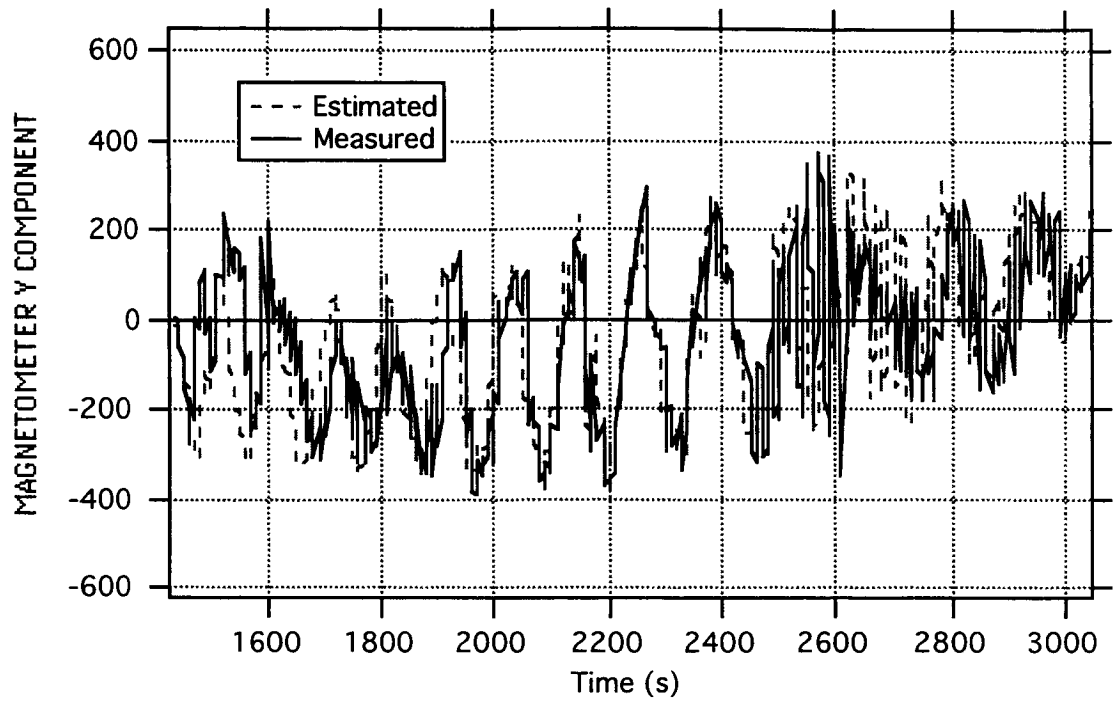


Figure 105 Magnetometer Y Component - Estimated vs. Measured (SEDS-I Flight Data)

13.3 Position/current data Kalman filter

KAL_Pos - Uses measured emf, current, position and velocity of Delta Stage to estimate:

- e. Semi-major axis and decay rate
- f. Average current
- g. Angle between local vertical and magnetic field.

GPS continuous observations of positions and velocity have been assumed during this phase. Ground-based tracking can also be used though the data would be sparsely distributed and the software should be modified accordingly. Another alternative is to check whether position-only information yield acceptable results. This possibility, however, has been briefly explored and needs further refinement.

The angle between the local vertical and the Earth's magnetic field is also estimated, because being part of the Lorentz force term, can yield information on the librations of the tether with respect to the local vertical.

The software assumes that the average current is a known fraction of the current measured at the Delta stage plus a small linear correction estimated by the filter.

All the parameters to be estimated are modeled as random-walk processes. An estimate of the magnitude of the magnetic field must be provided in input.

This software also runs on a Power Mac with a G3 processor and IGOR software for display and data analysis. Though robust, this filter needs an accurate set of initial conditions. The measurement and process errors are very sensitive to parameters' correlation so a more accurate modeling of the process could be necessary.

Data produced by MASTER simulations were used to test KAL_Pos.

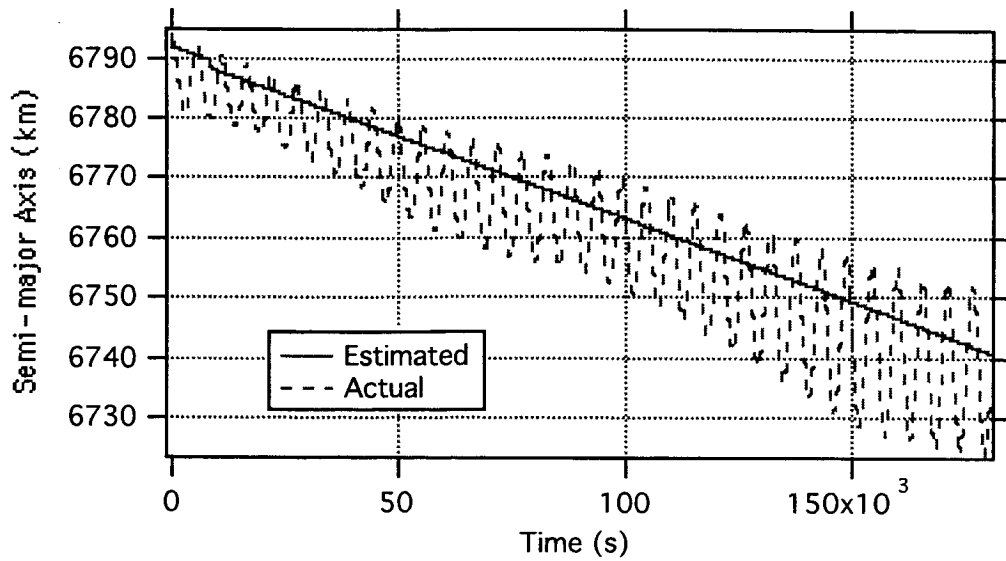


Figure 106 Estimated vs. Actual Proseds Semi-major Axis (MASTER simulation)

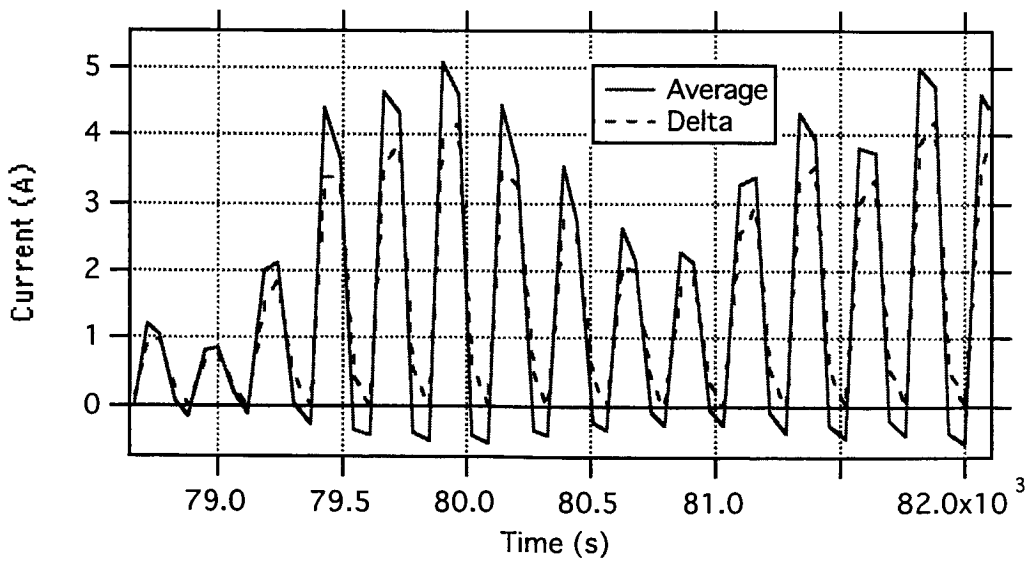


Figure 107 Estimated Average vs. Current Measured at Delta (MASTER simulation)

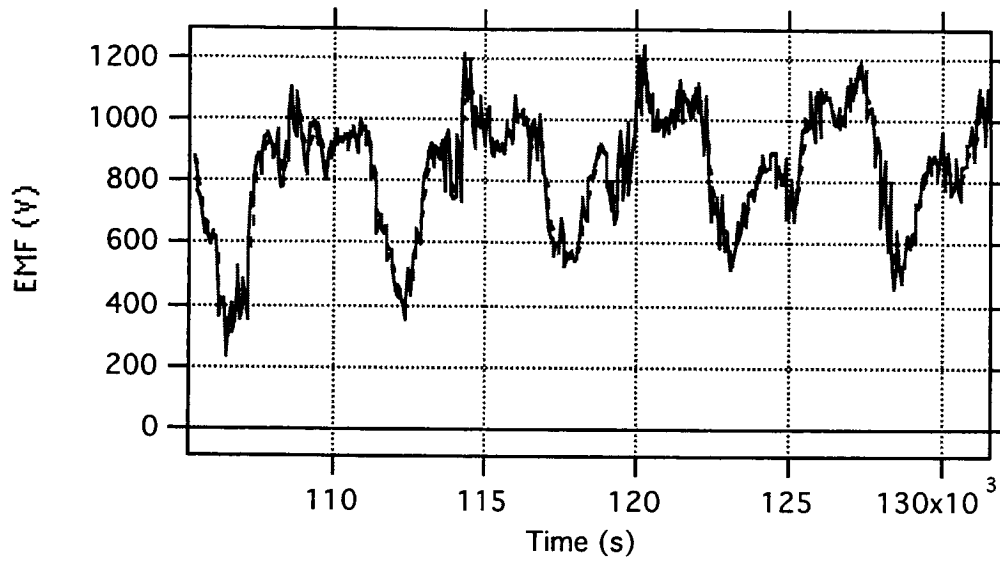


Figure 108 Estimated Proseds EMF (MASTER simulation)

14. ANALYSIS/ESTIMATION OF DEPLOYMENT FLIGHT DATA

14.1 Introduction

The performance of the deployment control law in terms of final libration (and other dynamic variables) can be assessed from the single data stream of the turn counter. In fact, from the (in-plane) libration equation it is possible to see that in the absence of strong external forces (other than gravity gradient forces) the libration state of the system can be extracted from the knowledge of the tether length and speed profiles. Since deployment takes place almost exclusively on the orbital plane, knowledge of the in-plane angle define the libration state of the system.

It is possible to construct an observer of the system libration based on the deployed tether length and exit speed. In the actual case, the only available information is the turn counter which provides the number of deployed tether turns. The tether turns must be first converted into tether length by utilizing the spooling relationship. The length data must be filtered with a low-pass filter before computing the exit speed because any small jump in tether length over a short time period will result in a big jump of tether rate when the speed is computed by numerical derivation.

Finally, the smoothed length and speed can be used as input to the deployment observer in order to compute tether libration and consequently reconstruct the deployment trajectory of the endmass and estimate the libration amplitude after the end of deployment when the attitude of the endmass has stabilized.

An alternative way to the deployment state estimation is to utilize position estimates from the GPS receivers on board the endmass and the Delta and derive the relative dynamics through differences of simultaneous position data. The GPS-method, however, is predicated on having the two signals available from the very beginning of deployment when the endmass is tumbling and prone to loosing the signal lock. The GPS method can be utilized more reliably to backup the estimate of the libration amplitude at the end of deployment.

14.2 Numerical results

In the following we will show results from the deployment observer (i.e., based on the turn counter estimation method). We take a noisy string of turn counter data from the deployment simulation shown in Fig. 109 (with $T_0 = 20$ mN and heavy white noise) and we prove that the deployment trajectory can be reconstructed and the amplitude of the final libration accurately evaluated by means of the process described previously.

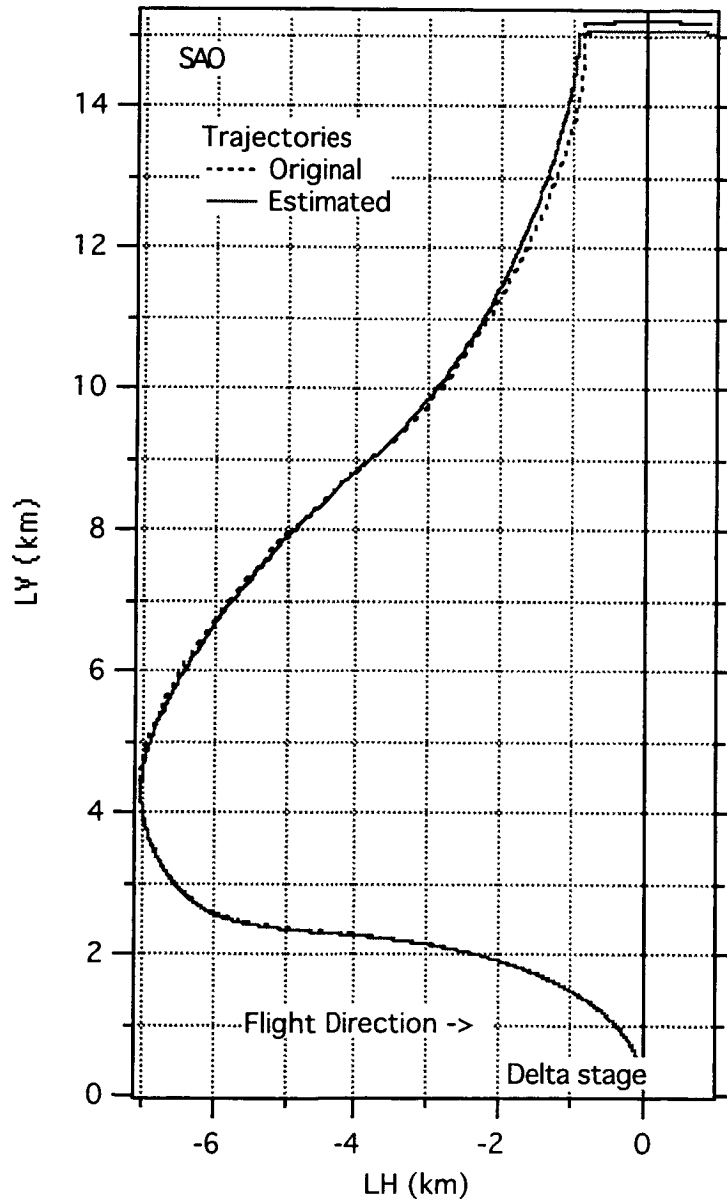


Figure 109 Deployment trajectory of endmass: estimated from noisy turn counter data (solid line); and original data (dotted line)

Figure 109 shows the deployment trajectory of the endmass with respect to the Delta stage estimated from noisy turn counter data (for $T_0 = 20$ mN) and the original trajectory computed from the simulated data. Clearly, the estimation software is capable of extracting the deployment trajectory from noisy turn counter data and of estimating accurately the libration amplitude at the end of deployment. This estimation software was also installed on the computer at NASA MSFC and it was run successfully twice during the mission operation simulations at the EDAC.

14.3 Concluding remarks

The estimation technique based on the data string provided by the turn counter is able to reconstruct the deployment trajectory and provide an accurate estimate of the amplitude of the libration at the end of deployment starting from noisy data. The advantage of this method is that it is based on one string of data that is readily available throughout deployment. The GPS data from both the Delta stage and the endmass can also be utilized to check the estimate of the libration after the end of deployment.

15. COMPARISON OF ED TETHERS AND ELECTRICAL THRUSTERS

15.1 Introduction

The basic figure of merit for a thruster is the ratio $M_d/F\tau$, which is the inverse of a velocity, and should be as small as possible¹⁷. Here, F is thrust, τ is duration of thrusting, and M_d is dedicated mass. For electrical thrusters, which would be natural competitors of tethers, M_d is made of propellant mass $\dot{m}_p\tau$ ($\dot{m}_p \equiv$ propellant flow rate) and tankage and plumbing mass ($\alpha\dot{m}_p\tau$); and from hardware related to the required electrical power W_e ,

$$M_d = \dot{m}_p\tau(1 + \alpha) + \beta W_e. \quad (7)$$

Typically, α is about 0.2, and β is about 6 kg/kW if just power processing unit and thruster need be considered and one order of magnitude greater if dedicated solar panels are required (Estes et al, 2000).

Introducing the specific velocity v_{sp} (specific impulse in velocity units, about 16 and 28 km/s for Hall and Ion thrusters respectively), one has $\dot{m}_p = F/v_{sp}$ and $W_e = Fv_{sp}/2\eta$ ($\eta =$ thruster efficiency = 0.5-0.65), and arrives at

$$\frac{M_d}{F\tau} = \frac{1 + \alpha}{v_{sp}} + \frac{\beta v_{sp}}{2\eta}. \quad (8)$$

Given a specific velocity, the ratio $M_d/F\tau$ approaches a limit minimum for long thrust durations, with a characteristic time $\tau \propto v_{sp}^2$. Duration, however, may need be restricted by a number of reasons. For each maximum allowed τ , there is an optimal specific velocity yielding a minimum in eqn. (7); as τ is allowed to increase, $v_{sp}(\text{opt})$ increases, resulting in a lower $M_d/F\tau$ minimum. In addition, given a total (mission) impulse $F\tau$, a maximum allowed duration determines a lower bound for thrust F .

15.2 Comparisons

Let us compare the extended-mission mass requirements of some typical electrical thrusters with that of bare-tether thrusters chosen to have equivalent average thrust. There are two cases to consider: the case where a dedicated solar power system is required, which would be the case for any kind of electrical orbit-transfer vehicle (a space “tug”); and the

case where the solar power system is already in place, with power available for thruster use, which might be the case for a Space Station drag-compensation system.

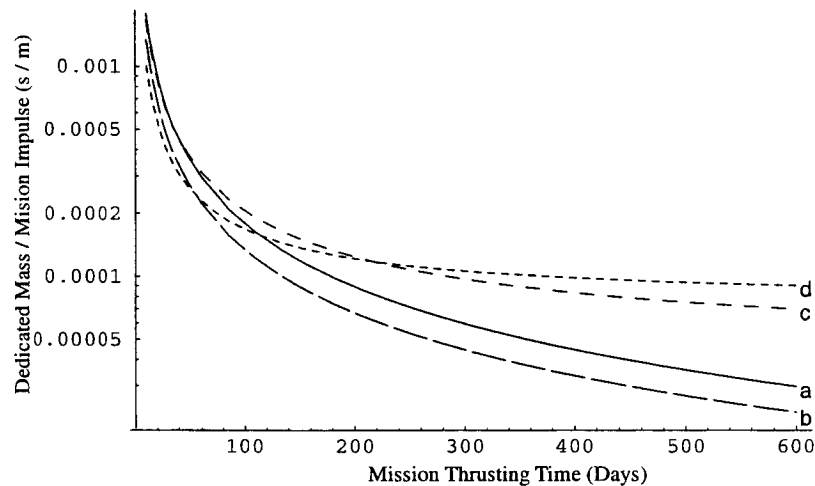


Figure 110 Comparison of EDT (a, b) and Electrical Thrusters (c, d) with Dedicated Solar Power System

Figure 110 shows the case where a dedicated power system is required. It plots $M_d/F\tau$ on a logarithmic scale for a range of mission (thrusting) times τ of 10 to 600 days. All systems are taken to have $\eta = 0.6$. Curves c and d correspond to electrical thrusters of $v_{sp} = 28$ and 16 km/s, respectively. The EDT systems were chosen to provide an average η of 0.6 over an altitude range of 300 to 800 km. Curve a is for a 30 kg tether (with $\alpha_t = 2$) and $W_e = 1$ kW. Curve b corresponds to the same tether but with $W_e = 2$ kW; it is seen to be better than either electrical thruster for mission times of roughly 50 days or more, while the upper EDT (1 kW) curve needs a mission time of over 120 days achieve that. Both of these times are well within the time required for either type of system to boost a large payload from one low Earth orbit to another orbit several hundred kilometers higher.

Multiple orbit transfers would, of course, take proportionally longer, and the time to return to lower orbit would also have to be taken into account. We note that by only considering powered thrusting, we have, so to speak, forced the EDT to fight with one hand tied behind its back, since the EDT does not require external power to descend to a lower orbit. An orbit-transfer vehicle would need to return to a lower orbit after taking a spacecraft to a higher one, and an EDT system could, if so designed, descend more quickly than its electrical thruster counterpart. This is a topic for later development. There are implicit

assumptions of system lifetimes and practicality of the systems which we note without further discussion.

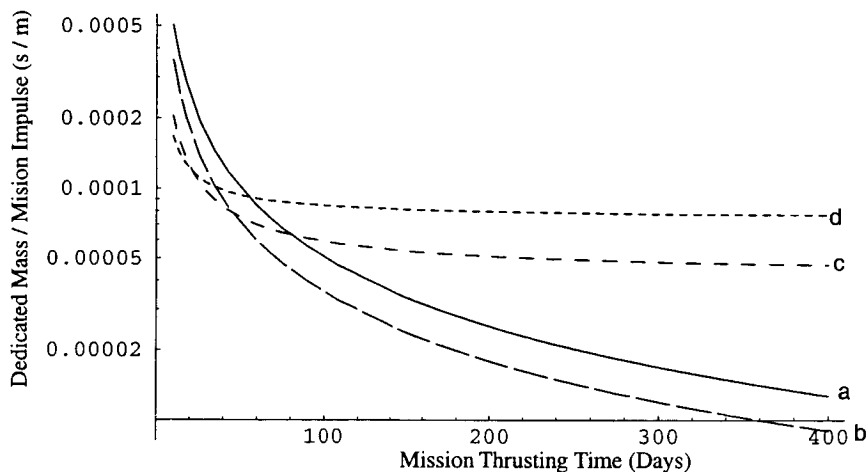


Figure 111 Comparison of EDT (a, b) and Electrical Thrusters (c, d) without Dedicated Solar Power System

As Figure 111 shows, for the case where abundant power is available without the need for a dedicated solar system, the EDT is clearly superior to the electrical thrusters for mission lifetimes somewhat shorter than for the case when a dedicated system is required. All parameters for the electrical thrusters c and d are the same as for Fig. 110, except for β . The tethers have a mass of 70 kg, and the assumed operating power is 5 kW for curve a and 10 kW for curve b. Thus, as previously noted (Estes et al., 2000), EDT would be attractive for International Space Station (ISS) reboost, assuming power were available from the Station.

15.3 Conclusions

In terms of total mass required for the mission, EDT thrusters are superior to electrical thrusters for mission thrusting times of 50-100 days or more both in the case of dedicated solar panels and the case when power is available without the need for a dedicated system. The advantage becomes greater as the mission time increases because of the comparatively insignificant use of gas by the EDT systems. Since an EDT tug would require no electrical power to descend, one could be designed to improve the mass to mission impulse ratio by descending at a rate faster than it ascends in the electrically powered mode, thus increasing its advantage over electrical thrusters.

16. DYNAMICS ANALYSIS FOR MISSION STARTING AT LOWER ALTITUDE

16.1 Introductory remarks

After the Shuttle Columbia accident in February 2003, the Space Station (ISS) can no longer be refueled as frequently as desired and, consequently, its ability to move in orbit is diminished. The Space Station office has become very sensitive to the issue of a tethered satellite that will be flying for several days at an latitude close to the ISS altitude. The launch of ProSEDS, manifested for 29 March 2003 has been postponed (one month ahead of the event) pending an analysis of lowering substantially (ie, by 100 km) the initial orbital altitude of ProSEDS. The following is an analysis of the effect of such altitude reduction on ProSEDS dynamics and decay performance.

16.2 Dynamics Analysis

The results of simulations for ProSEDS starting from a 260-km orbital altitude are shown here. Nominal values of the ionosphere and atmospheric densities were assumed as predicted by the IRI95 and MSIS86 models for a launch at 22:00:00 GMT on March 29, 2003. Figure 112 shows the orbital decay of the Delta stage of ProSEDS with ED and atmospheric drag while Figure 113 shows the decay for atmospheric drag only (with the tether fully deployed but not generating current).

In summary, the atmospheric drag plays a rather significant role in this altitude region. In fact, the atmospheric drag is comparable to the ED drag (see Figure 114). The instantaneous value of the ED drag can exceed the value of the atmospheric drag but its orbital average is mostly lower than the atmospheric drag with the exception of a brief period of time (see Figure 115).

Finally, Figures 116 and 117 show the neutral density of the atmosphere and the atomic oxygen (AO) vs. time during ProSEDS decay when both ED and atmospheric drag are present. One issue that needs to be evaluated is the time needed for the AO to erode the Dyneema tether during this orbital decay profile.

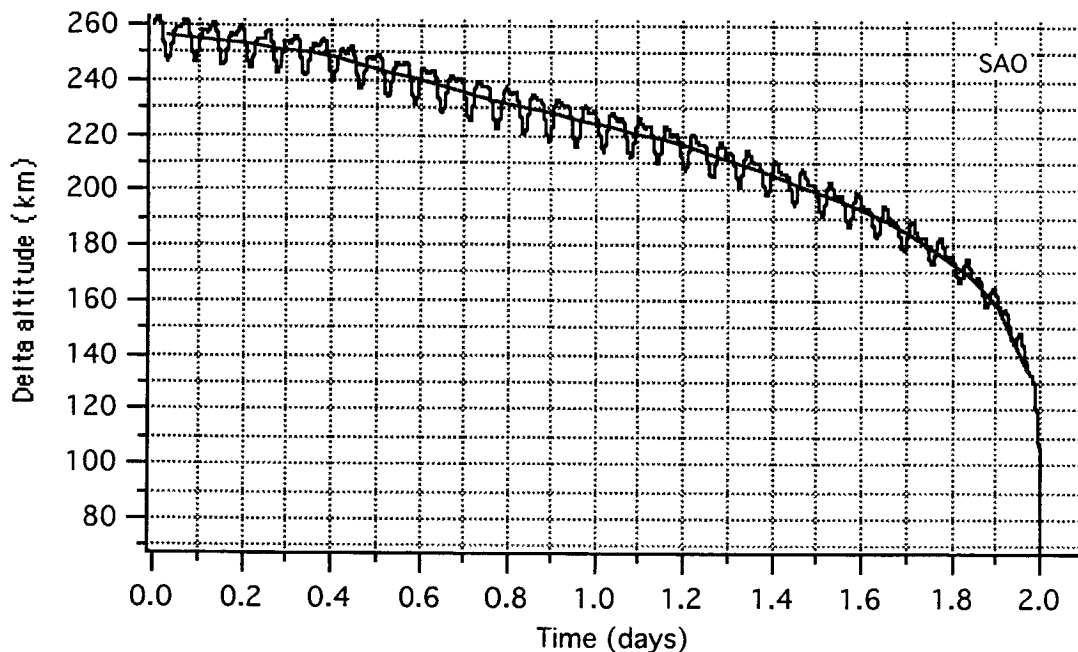


Figure 112 ProSEDS decay with atmospheric and ED drag

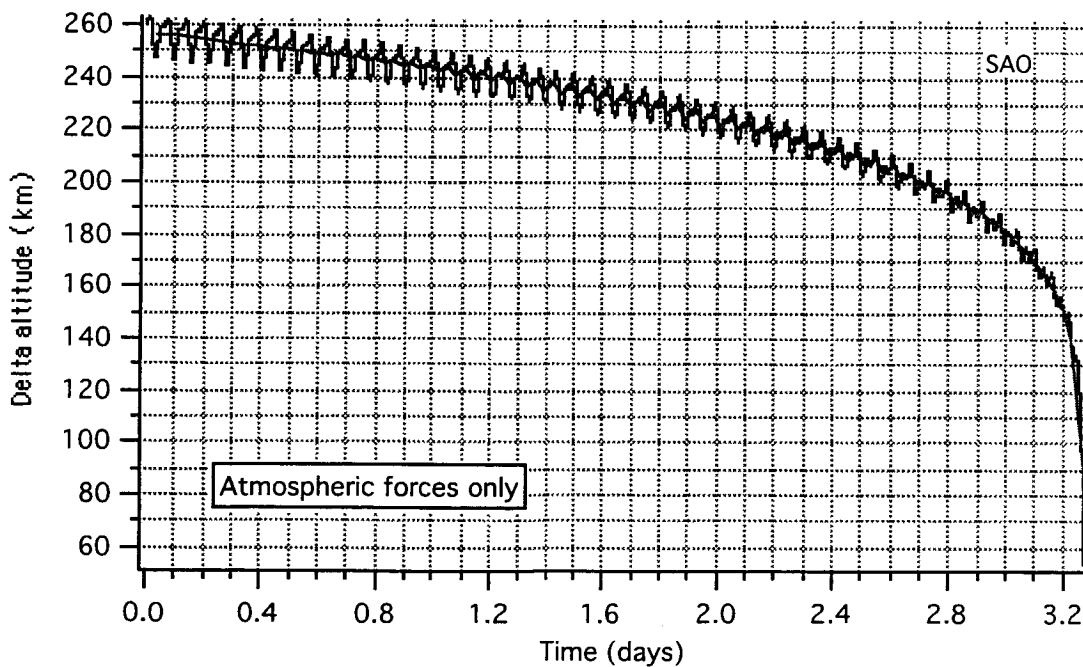


Figure 113 ProSEDS decay with atmospheric drag only

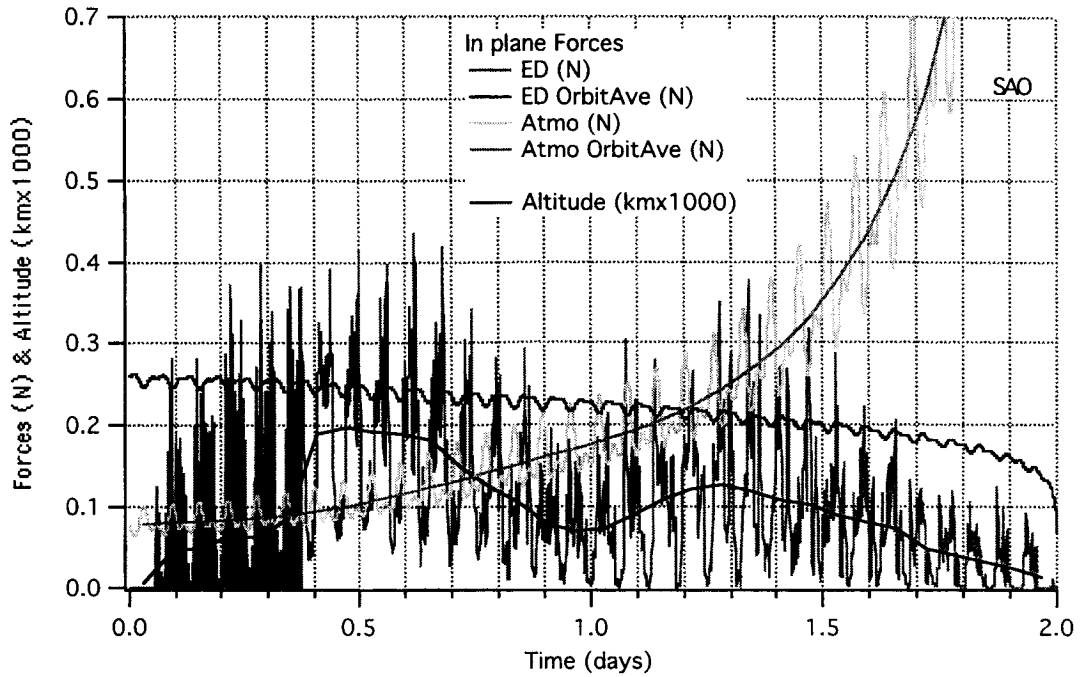


Figure 114 Comparison of atmospheric and ED forces acting on ProSEDS

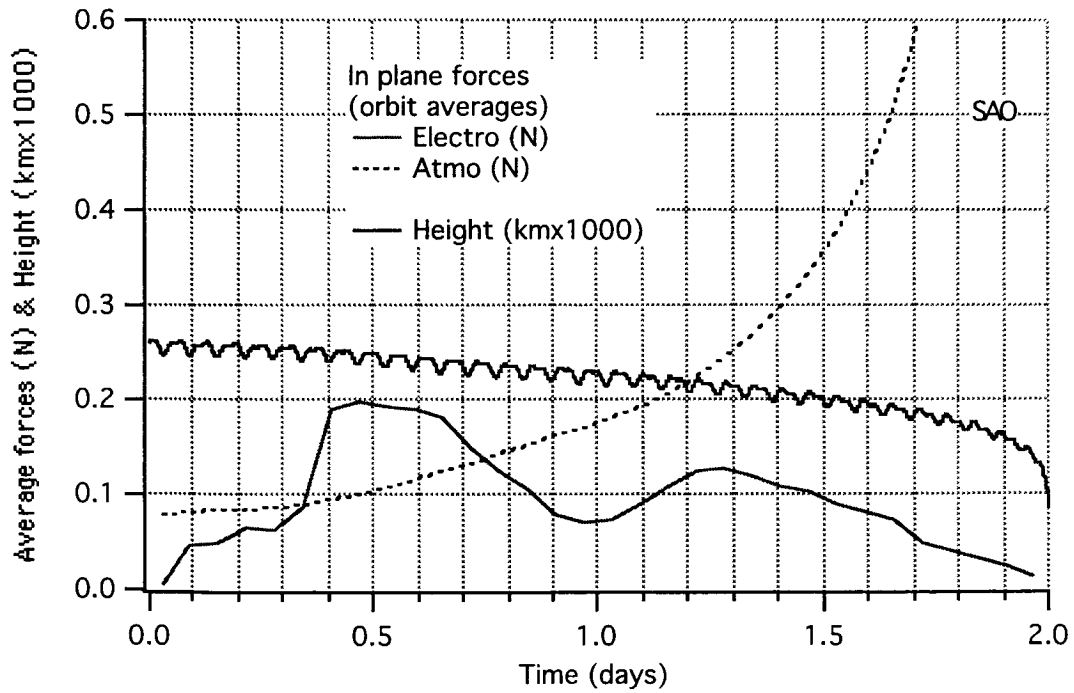


Figure 115 Comparison of orbit-average atmospheric and ED forces on ProSEDS

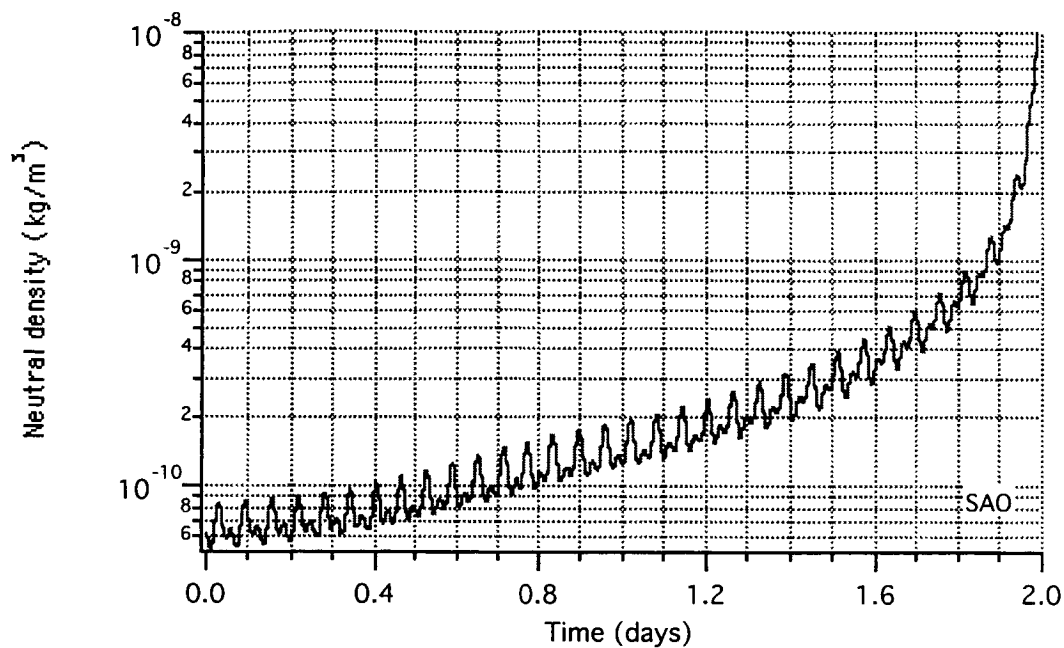


Figure 116 Neutral density vs. time

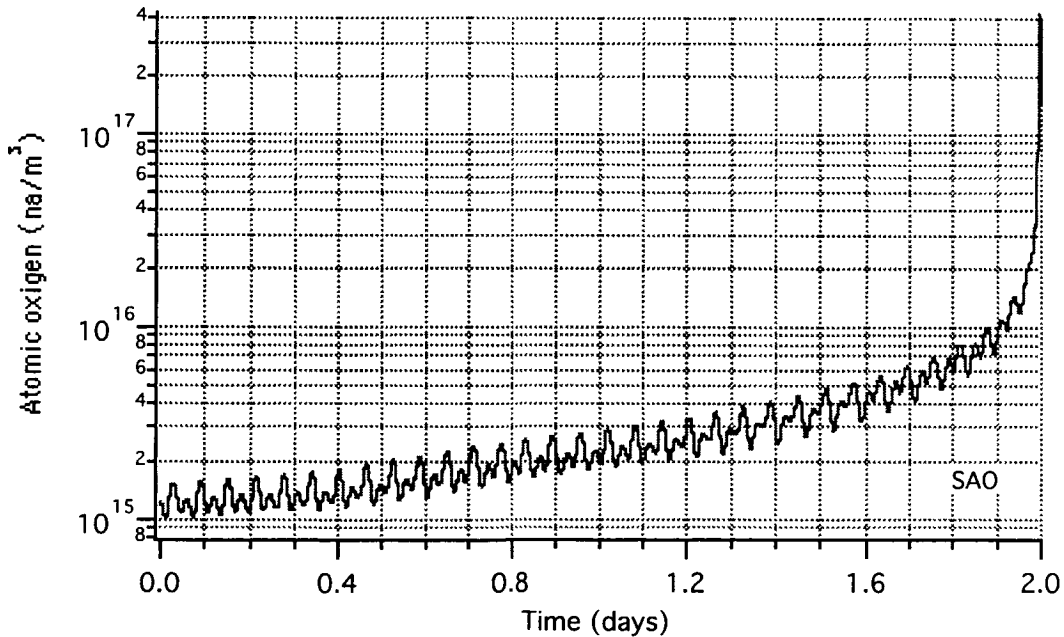


Figure 117 Atomic oxygen vs. time

16.2 Concluding Remarks

A reduction of the starting orbital altitude from 360 km to 260 km will change the relative contributions of electrodynamic and neutral drag forces to the decay rate. The overall decay rate will be still substantial and well above the value established in the mission success criteria. However, about one half of the decay rate can be attributed to neutral drag at this low altitudes and the other one half to electrodynamic forces.

17. DEPLOYMENT PERFORMANCE AT A LOWER ALTITUDE

17.1 Deployment Analysis

We have analyzed the impact of a starting altitude at 260 km on the deployment of ProSEDS. The control law and control parameters are those utilized for the original starting altitude at 360 km. Simulations have been run to estimate the impact of the lower altitude on the performance of ProSEDS deployment control law without any modification to the control law.

The final libration amplitude at the end of ProSEDS deployment is required to be less than 20 deg with respect to the local vertical. This goal is attained by utilizing a feedback control law that controls the tether during the 10-km-long Dyneema tether. The brake is then kept constant at half a turn during the CCOR deployment in order not to damage the CCOR coating while limiting the deployment velocity. Before the end of deployment, when the insulated portion starts deploying, the brake is ramped up to decrease the deployment speed. Finally, the brake is slowly removed to let any remaining tether coils out of the deployer canister.

The control law is derived from the law successfully utilized to deploy SEDS-II. As it was investigated for SEDS-II the deployment final libration is mostly sensitive to the shape of the exit velocity profile during the early part of deployment, that is, for ProSEDS during the deployment of the Dyneema portion. The libration amplitude is insensitive to changes in the profile during the latter part of deployment (i.e., the CCOR portion). The deployment control law adjusts the brake in order to force the tether length and velocity to follow pre-computed reference profiles that would provide a very small final libration amplitude under reference conditions. The actual deployment velocity depends on the frictional force acting on the tether as it moves through the deployer. This force depends on a set of friction parameters.

The most uncertain and also influential parameter (during the early and critical phase of deployment) of the tension model is the minimum tension T_0 . The minimum tension of the ProSEDS non-conductive tether has been measured throughout the many deployment tests on the ground to vary between 5 mN and 30 mN depending on temperature and cleanliness of the tether.

Figure 118 shows the amplitude of the residual libration at the end of deployment vs. the minimum tension T_0 of the Dyneema tether for the flight profile of Ref. #78 and starting altitudes of 360 km and 260 km. The figure also shows the final libration that ProSEDS

would attain without control and the representative points from the SEDS-I and SEDS-II flights. The final libration amplitude is sensitive to the Dyneema tether T_0 and it is insensitive to the value of the wire T_{wire} .

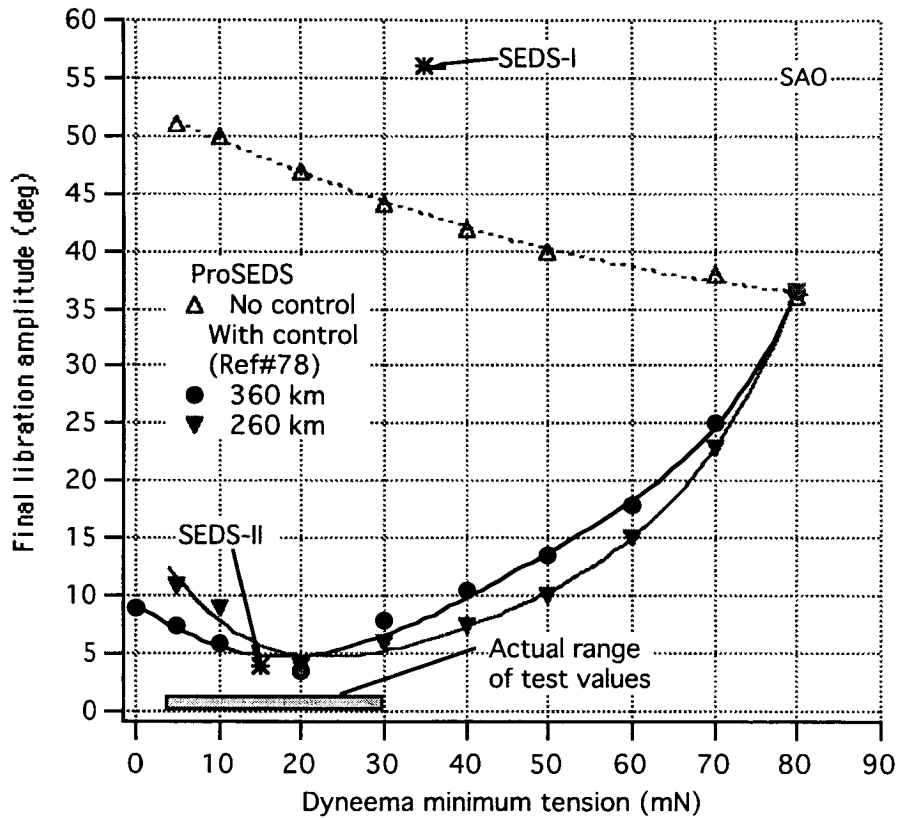


Figure 118 Final libration amplitude vs. Dyneema minimum tension

The differences in performance between starting altitudes of 360 km and 260 km are not substantial. A starting altitude of 260 km implies a somewhat larger final amplitude (than starting at 360 km) for $T_0 < 20$ mN (the reference value for the control law) and somewhat smaller values of the final libration amplitude for $T_0 > 20$ mN.

17.2 Concluding Remarks

The deployment control law meets the requirement of a final libration amplitude of less than 20 deg over the experimentally-measured range of the Dyneema minimum tension of 5 mN and 30 mN with a substantial margin even for a starting altitude of 260 km. The performance decays substantially only for values of T_0 above 60 mN. For $T_0 \geq 80$ mN, the deployment stops prematurely because of excessive tether friction and without any role being played by the control law.

18. SATELLITE ORBIT AFTER TETHER CUT

18.1 Introductory remarks

The ProSEDS tether has about 1% probability of being cut by M/OD per day in its present length of 15 km with the probability decreasing proportionally to tether length. A cut will increase the apogee height of the satellite (with some tether attached to it). A simple formula can be used to obtain an approximate value of the orbital height increase by multiplying by 7 the distance between the center of mass (CM) of the cut portion and the CM of the system before the cut. The presence of a tether in-plane libration can then increase or decrease the orbital height of the satellite if the cut occur during the prograde or retrograde phase of the libration. In addition, if the starting orbit is slightly elliptic, then the location of the system along the orbit affects the distance between the separating bodies. An increased separation being obtained for a cut at perigee and a decreased separation distance for a cut at apogee. In formulas, the maximum separation distance between the two bodies can be expressed (in approximation) as follows:

$$\Delta H_{cm} = [7 \pm 4\sqrt{3} \sin(\bar{\theta}) \pm 8e] L_{cm} \quad (9)$$

where ΔH_{cm} is the maximum separation between the CMs of the two separating bodies, $\bar{\theta}$ is the amplitude of the in-plane libration, and e is the orbital eccentricity. The first plus sign in eqn. (9) is for a cut during a prograde libration and the second plus sign for a cut at perigee. Conversely, the first minus sign is for retrograde libration and the second for a cut at apogee.

It is clear that many parameters influence the final orbit after cut: (a) position of the satellite along the orbit (if the orbit is not perfectly circular); (b) phase of the in-plane libration; and (c) location of the cut along the tether which determines the CM location of the departing body. In the next section we will show results from numerical simulations of specific cases of tether cuts.

18.2 Numerical cases

We used the tether simulator to run cases of tether cuts under realistic conditions. The system is initially at an altitude of 285 km (current estimate for the ProSEDS mission) and the tether is cut at the splice between the CCOR wire and the Dyneema (that is a worst case scenario). The system also has a small libration of a few degrees that is expected for a nominal deployment. We show in the following three representative cases for a perfectly

circular orbit (Figure 119), a cut at apogee (Figure 120) and a cut at perigee (Figure 121). The value of eccentricity adopted results in a difference height between apogee and perigee of about 11 km which is representative of ProSEDSs expected orbit.

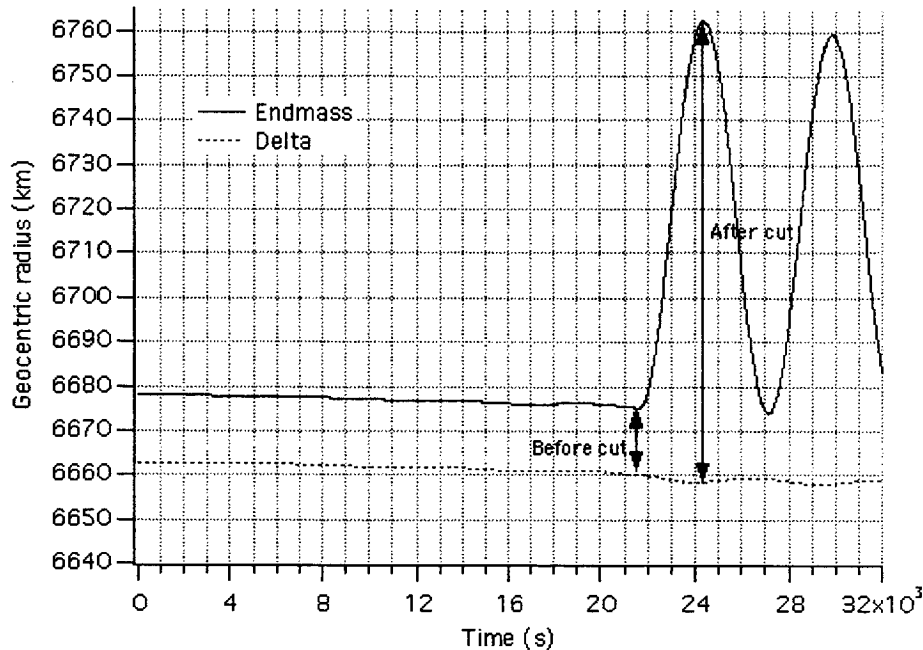


Figure 119 Effect of a tether cut for a circular orbit.

Because the eccentricity and the libration amplitude are small, the ratio between the separation distance between the CMs of the departing bodies before and at its maximum value after the cut follows pretty much the the 7-fold rule. From the point of view of the maximum altitude reached by the end-mass after the cut, the worst case situation would be for a cut at perigee with a perigee altitude at the same altitude of the circular orbit (unlike Figure 121 where the apogee altitude is at the height of the circular orbit). The differences are, however, relatively small considering the small eccentricity of the ProSEDS orbit. In summary, the expected maximum gain in height of the endmass after a cut with nominal amplitude of the in-plane libration is about 100 km. A different initial altitude does not affect the 7-fold rule for computing the relative separation after a cut.

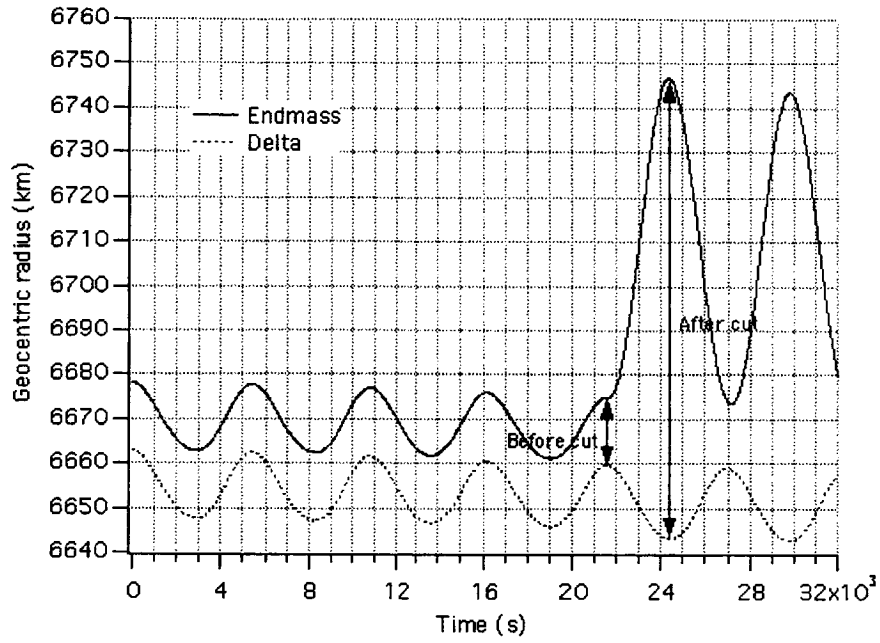


Figure 120 Effect of a tether cut at apogee for the max. expected eccentricity

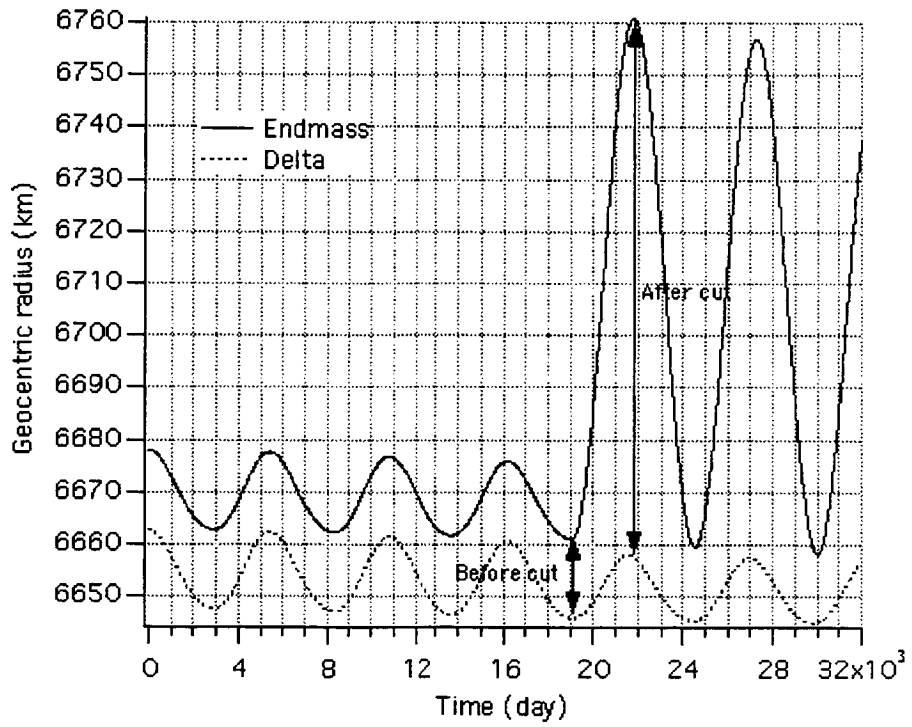


Figure 121 Effect of a tether cut at perigee for the max. expected eccentricity

18.3 Concluding remarks

The orbit of the end-mass after the cut is affected by several parameters: (a) position of the satellite along the orbit (if the orbit is not perfectly circular); (b) phase of the in-plane libration; and (c) location of the cut along the tether which determines the CM location of the departing body. Numerical simulations of ProSEDS tether cut for nominal libration amplitudes show an altitude increase of the apogee height of the end-mass of about 100 km with respect to the orbital altitude of the Delta stage. The expected eccentricity of the ProSEDS orbit is small and it plays a relatively small role in the maximum height reached by the endmass. Higher amplitude librations, due to off-nominal conditions, would significantly increase or decrease the maximum height reached by the endmass depending on whether the libration is prograde or retrograde at the time of cut.

19. DEPLOYMENT WITH SHORTER DYNEEMA TETHER LENGTH

19.1 Introductory remarks

The concern about a (very-remotely) possible interference between the Space Station and ProSEDS endmass after a (relatively-low-probability) tether cut has prompted the search for a reduction in the overall tether length. A system with a reduced length would sling the endmass up to a lower height after a cut and, consequently, ProSEDS could fly at a higher orbit without any possible interference with the ISS. The length reduction will be done on the Dyneema tether in order for the ED wire to produce the same ED force.

One issue related to reducing the length of the Dyneema is deployment control and the magnitude of the in-plane libration at the end of deployment. For reasons explained previously, deployment is controlled in a feedback fashion over the Dyneema portion of the tether only. A substantial reduction of the Dyneema tether leads to a reduced control authority during deployment and finally to a larger in-plane libration.

19.2 Deployment profiles for shorter tether lengths

We have derived preliminary deployment profiles for values of the overall tether length of 12 km, 11 km, 10 km and 8 km. Since the length of the ED bare wire and its insulated portion is about 5 km, the feedback control will be exercised over a Dyneema length of 7 km, 6 km, 5 km and 3 km, respectively.

The four preliminary profiles are shown in Figure 122 for $L = 12$ km, Figure 123 for $L = 11$ km, Figure 124 for $L = 10$ km and Figure 125 for $L = 8$ km. We call these profiles preliminary because they have not gone through the extensive analysis to test their robustness to changes in the friction parameters. Nevertheless, the profiles themselves were derived after extensive runs of the optimization routine with the goal of finding profile candidates able to minimize the in-plane libration at the end of deployment.

Clearly, the profile for 12-km tether length has an almost ideal response as it is capable of canceling out the in-plane libration amplitude at the end of deployment under reference conditions. A profile with these characteristics would be capable of providing a libration amplitude of a few degrees (like Ref. #78) in the presence of nominal perturbations.

Profiles for length shorter than 12 km have a poor response with large libration amplitudes at the end of deployment. All the deployment responses at length shorter than 12 km do not meet the requirement of a final libration less than 20°. Moreover, the control authority decreases for shorter tether length and, consequently, the ability of the control law to compensate for external perturbations or changes in friction parameters will be severely limited. Control laws for length shorter than 12 km will be sensitive to perturbations.

ProSEDS Deploy Reference: L = 12 km

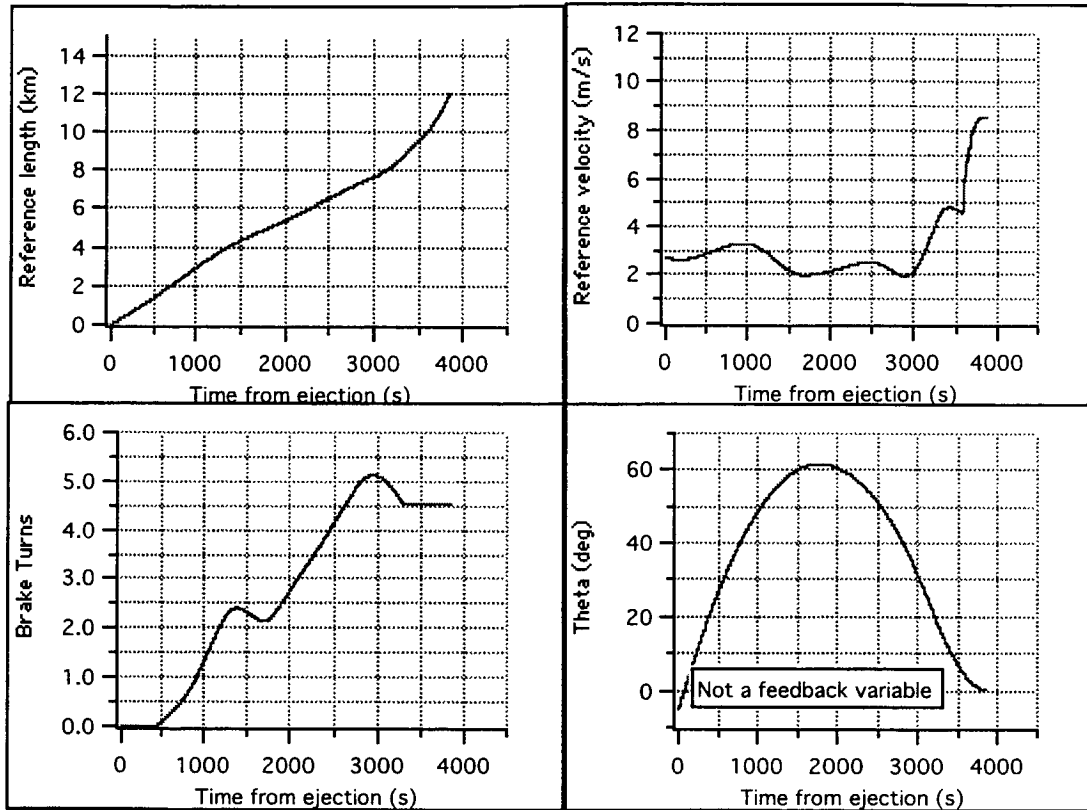


Figure 122 Deployment reference profile for an overall tether length of 12 km

ProSEDS Deploy Reference: L = 11 km

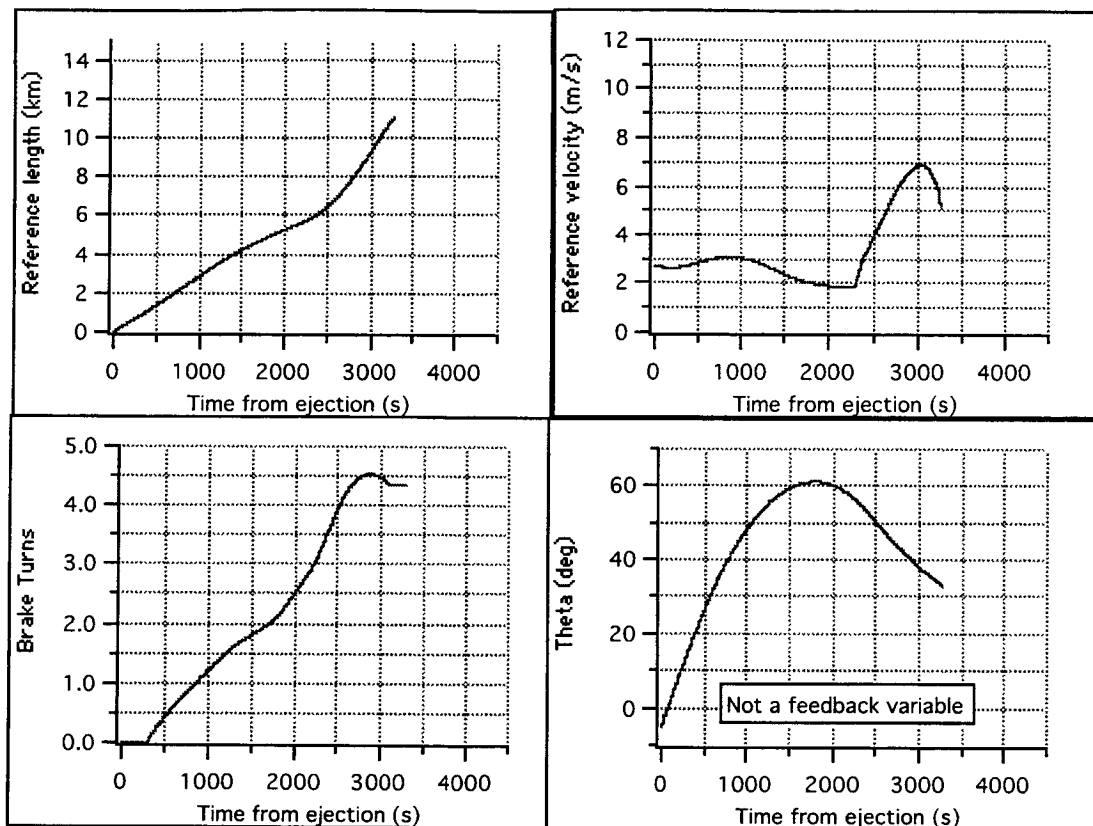


Figure 123 Deployment reference profile for an overall tether length of 11 km

ProSEDS Deploy Reference: L = 10 km

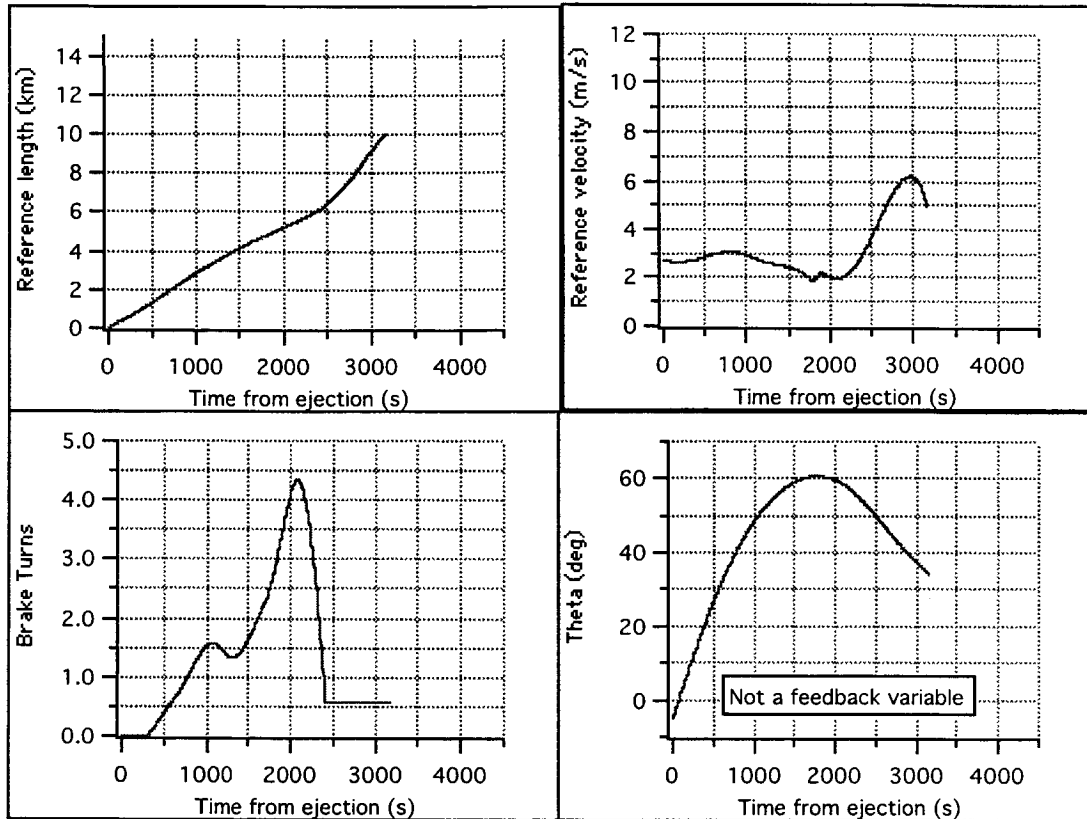


Figure 124 Deployemnt reference profile for an overall tether length of 10 km

ProSEDS Deploy Reference: L = 8 km

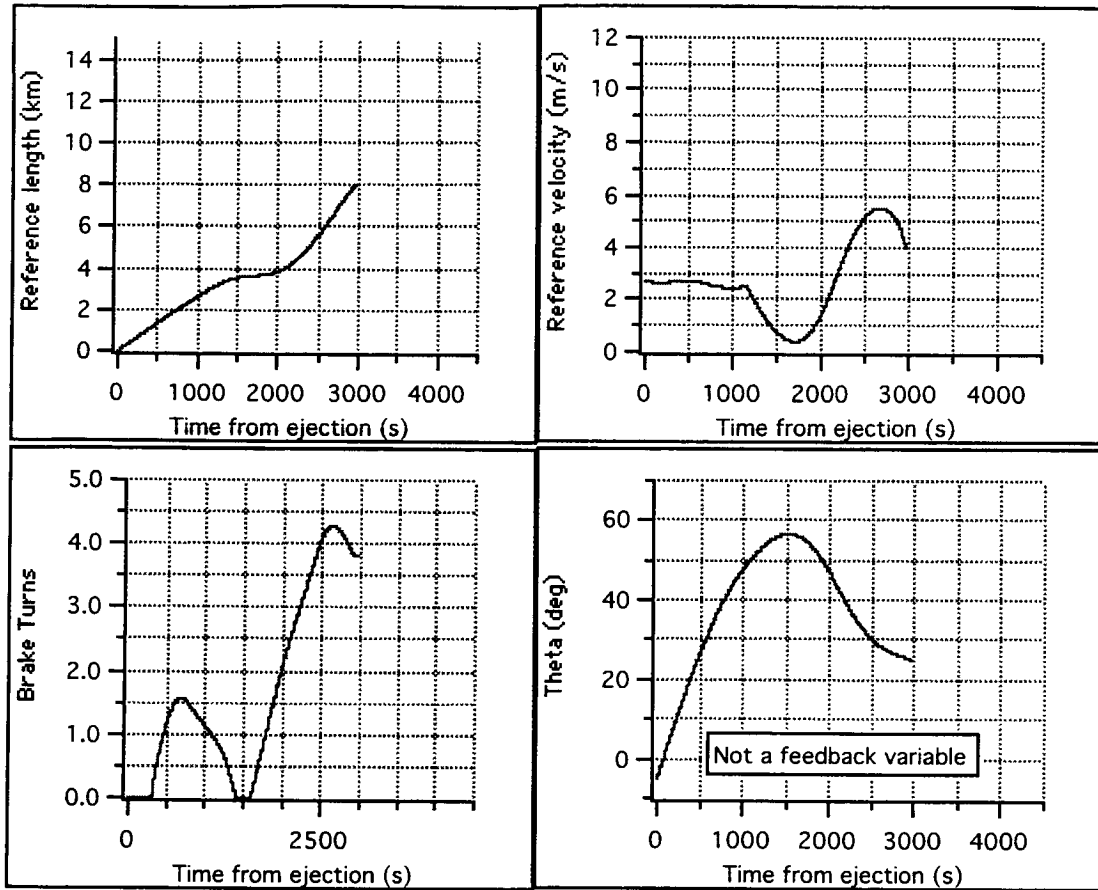


Figure 125 Deployment reference profile for an overall tether length of 8 km

19.3 Concluding remarks

A suitably-derived deployment profile will be able to handle deployment with satisfactory dynamics characteristics if the overall tether length is at least 12 km. For a tether length shorter than 12 km, we were not able to derive reference profiles capable of meeting the final libration requirement of an amplitude less than 20° . The dynamics response during deployment becomes less and less desirable as the overall tether length is reduced below 12 km.

20. INTERACTIVE SOFTWARE FOR ED TETHERS

20.1 Goals

One of the tasks undertaken by SAO was to develop an interactive computer program for the Windows operating system that would allow the user to obtain a quick estimate of the performance obtainable by bare tether propulsion systems for various applications in low Earth orbit, both orbit raising and lowering.

20.2 Brief Description

The software has been designed with the aim of allowing for experimentation in tether system design with quick feedback to the user on how changing various system parameters (length, collecting surface, tether material, tether geometry, available power, etc.) affect system performance under various environmental conditions. In addition, the user can use the software to get a good idea how the system would perform for different missions in which the environmental conditions vary during the mission, as, for example, the average plasma density decreases when the system moves above the F-layer of the ionosphere. The window in which the user defines the EDT system is shown below in Figure 126.

Those parameters that the user can adjust (i.e., tether length, insulated length, etc.) are shown with white backgrounds. The dependent variables have gray backgrounds. The mode in this example is deboost, and the tether geometry is cylindrical. The system is shown schematically in the right hand portion of the window. The lower part of the system is where electrons are expelled (hollow cathode), and the tether is shown as a vertical line. The insulated part of the tether is indicated on the screen by a difference in color, seen as a lighter shade of gray in the figure. The tether system display adjusts to changes the user makes in the fraction of the tether that is insulated.

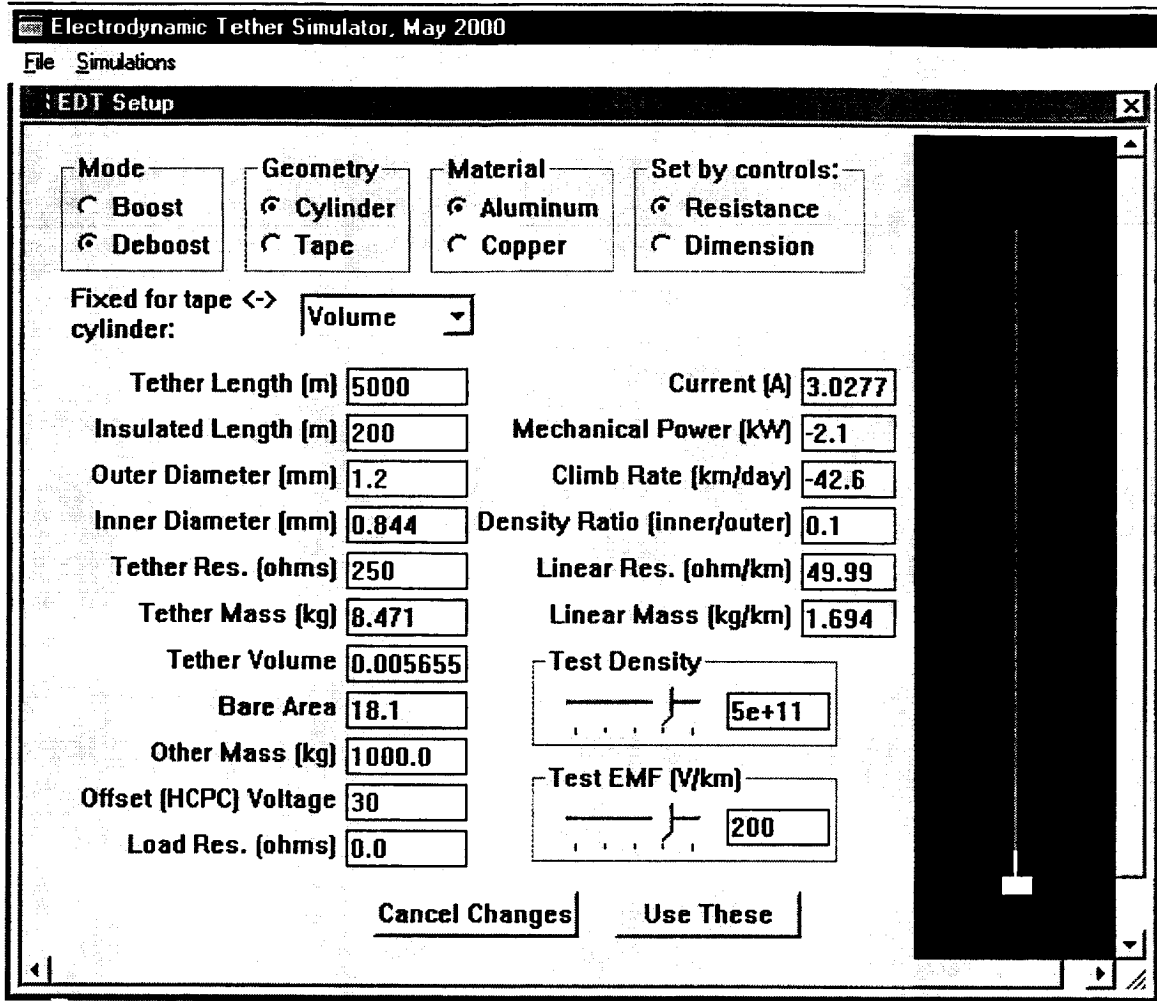


Figure 126 The simulation setup window for defining the system.

The system shown in the example is quite similar to that of ProSEDS, as the conductive part of the tether (chosen to be Al) is a cylindrical shell filled with a nonconductive material. Since the “Set by controls” option (upper right) has been set to “Resistance”, the user can directly set the tether resistance, and the inner diameter of the conductive adjusts to obtain that resistance (if possible). The tether mass is also automatically recalculated and displayed. More importantly, the collected current reaching the platform (lower end in this case), the mechanical (thrusting) power, and the climb rate this corresponds to for the chosen total tether system plus payload mass are all recalculated for the chosen test density and test motional emf. This is done assuming OML collection by the bare part of the tether.

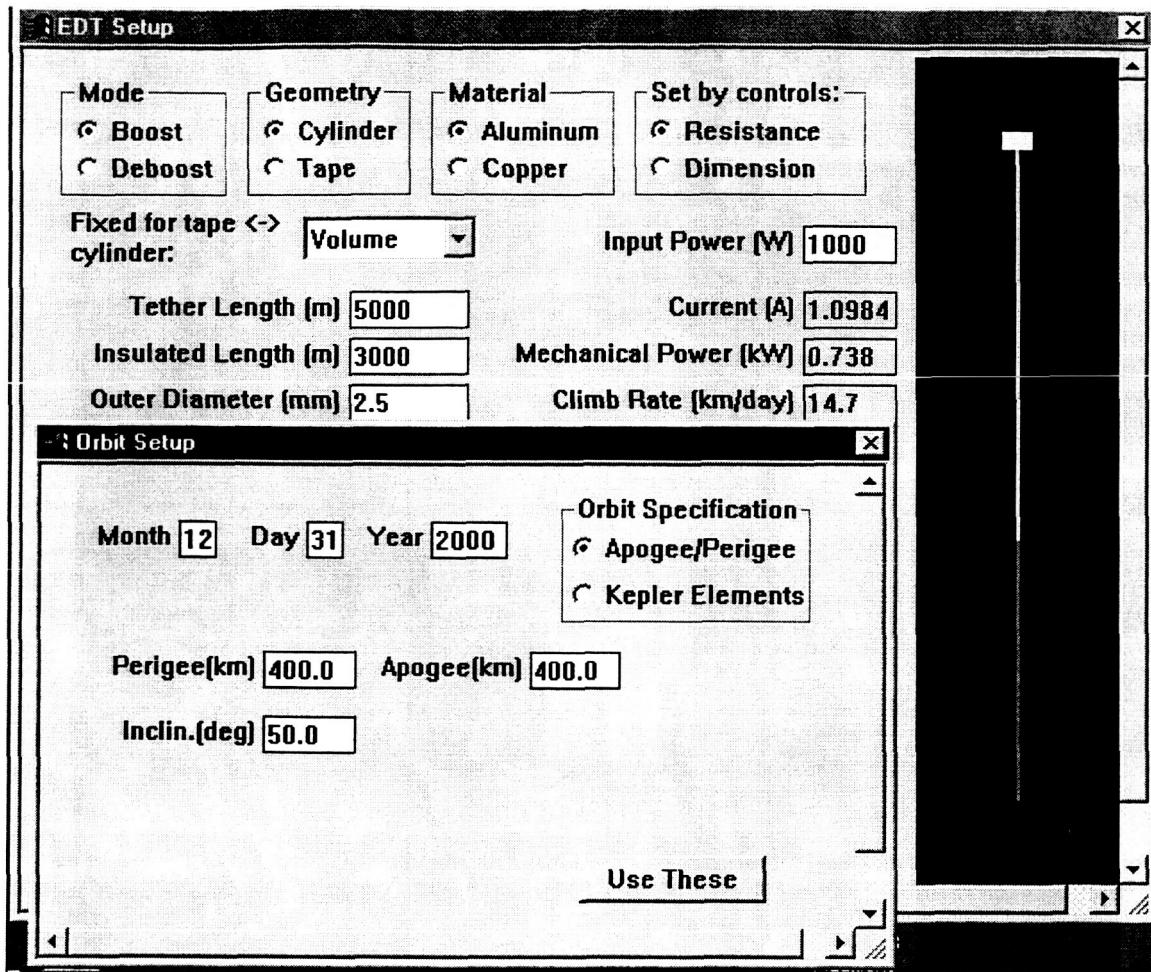


Figure 127 Starting orbit setup window with boost system setup in background.

Even taken by itself, this interactive window can be a useful tool for system design, since the test densities and motional emf values can be varied over a wide range. The user can take the simulation further, however, by actually following the progress of the system with a payload as it moves from one orbit to another. In this case, the starting orbit and date are needed, and there is another setup window that allows the user to specify these. This is shown in Figure 127. Note that in the background of this figure a boost system setup is partially visible. For a boost system an additional parameter, the input power is needed, shown as 1 kW in the figure. The diagram of the system shows the tether deployed downward, and the climb rate is positive. The date is of secondary importance, but it does enter into the plasma density calculations (through solar activity level) used for the simulation. The orbital parameters may be specified in more detail (full Kepler element set) if desired, but the set shown in the figure should be adequate in most cases for getting a reasonable idea of system performance.

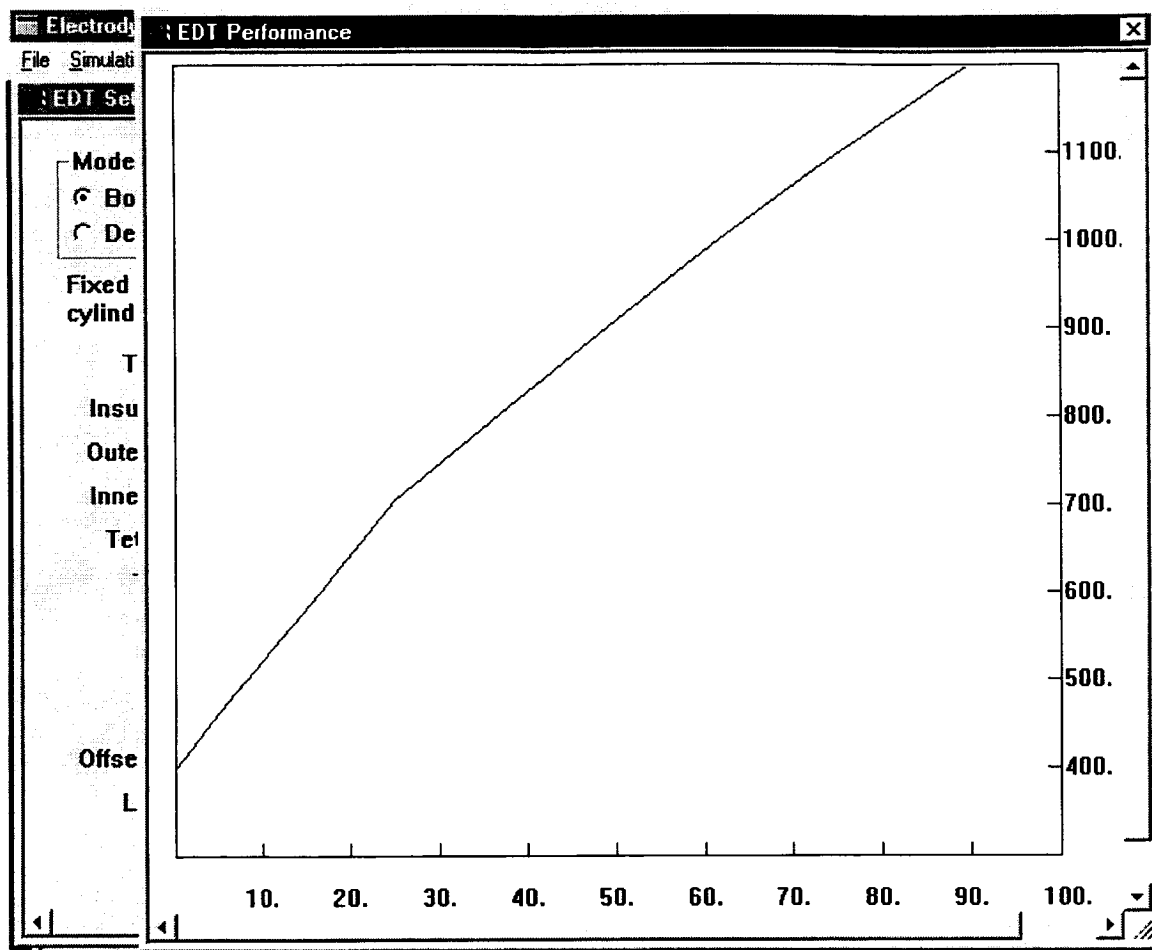


Figure 128 An orbit raising simulation showing altitude in km versus days.

Once the system and starting orbit have been defined by the user by means of the windows shown in Figure 128 and Figure 129, a simulated orbital change can be calculated and displayed. Figure 128 shows the progress of a boost system taking a payload to an orbital height of 1200 km, starting at 400 km. The height in km is shown on the vertical axis, while the time in days is shown on the horizontal one. Note that the climb rate slows above 700 km in the figure. The simulation is done in the following way. Two complete revolutions are made starting with the input initial orbit, and the average climb rate, which varies with the plasma density and motional emf encountered along the orbit, is calculated in this period. This rate is used to advance the system to an orbit 100 km higher and the process is repeated at intervals of 100 km until the desired altitude is reached. Multiple simulation runs can be made and shown on the same plot to compare different systems or the performance of the same system under different conditions (starting orbit and/or date).

20.2 Delivered Software

The interactive computer program for the Windows operating system that allows the user to obtain a quick estimate of the performance obtainable by bare tether propulsion systems for various applications in low Earth orbit, for both orbit raising and lowering, was delivered to NASA/MSFC in December 2001. The use of the software was demonstrated by Robert Estes to NASA/MSFC personnel in January 2001 to the satisfaction of the customer.

20.3 Brief Description of Final product

The software was designed with the aim of allowing for experimentation in tether system design with quick feedback to the user on how changing various system parameters (length, collecting surface, tether material, tether geometry, available power, etc.) affect system performance under various environmental conditions. In addition, the user can use the software to get a good idea how the system would perform for different missions in which the environmental conditions vary during the mission, as, for example, the average plasma density decreases when the system moves above the F-layer of the ionosphere. The window in which the user defines the EDT system is shown below in Figure 129 for a typical deboosting operation and in Figure 130 for a typical boosting operation.

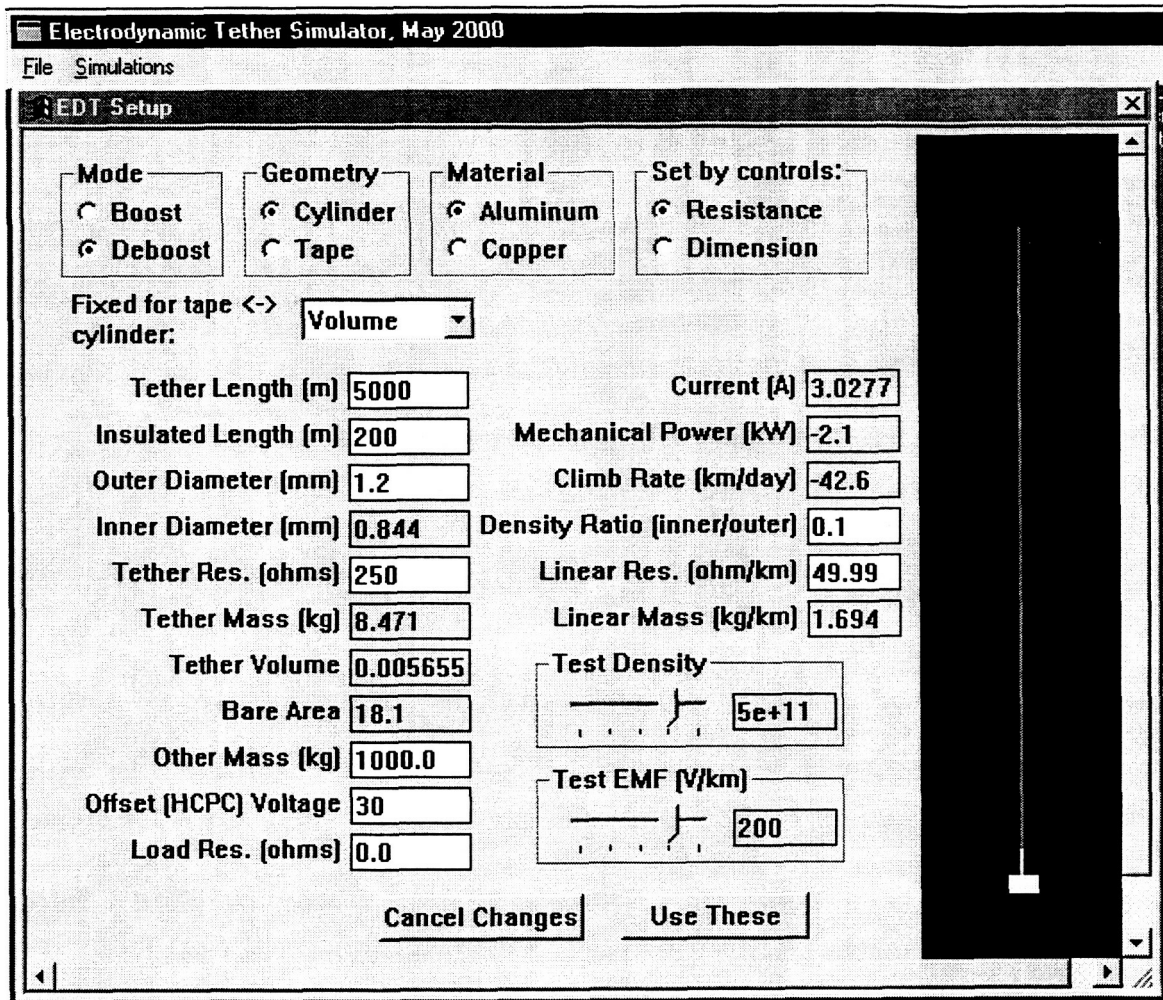


Figure 129 The simulation setup window for defining the system.

Even taken by itself, this interactive window can be a useful tool for system design, since the test densities and motional emf values can be varied over a wide range. The user can take the simulation further, however, by actually following the progress of the system with a payload as it moves from one orbit to another as described in the previous subsections.

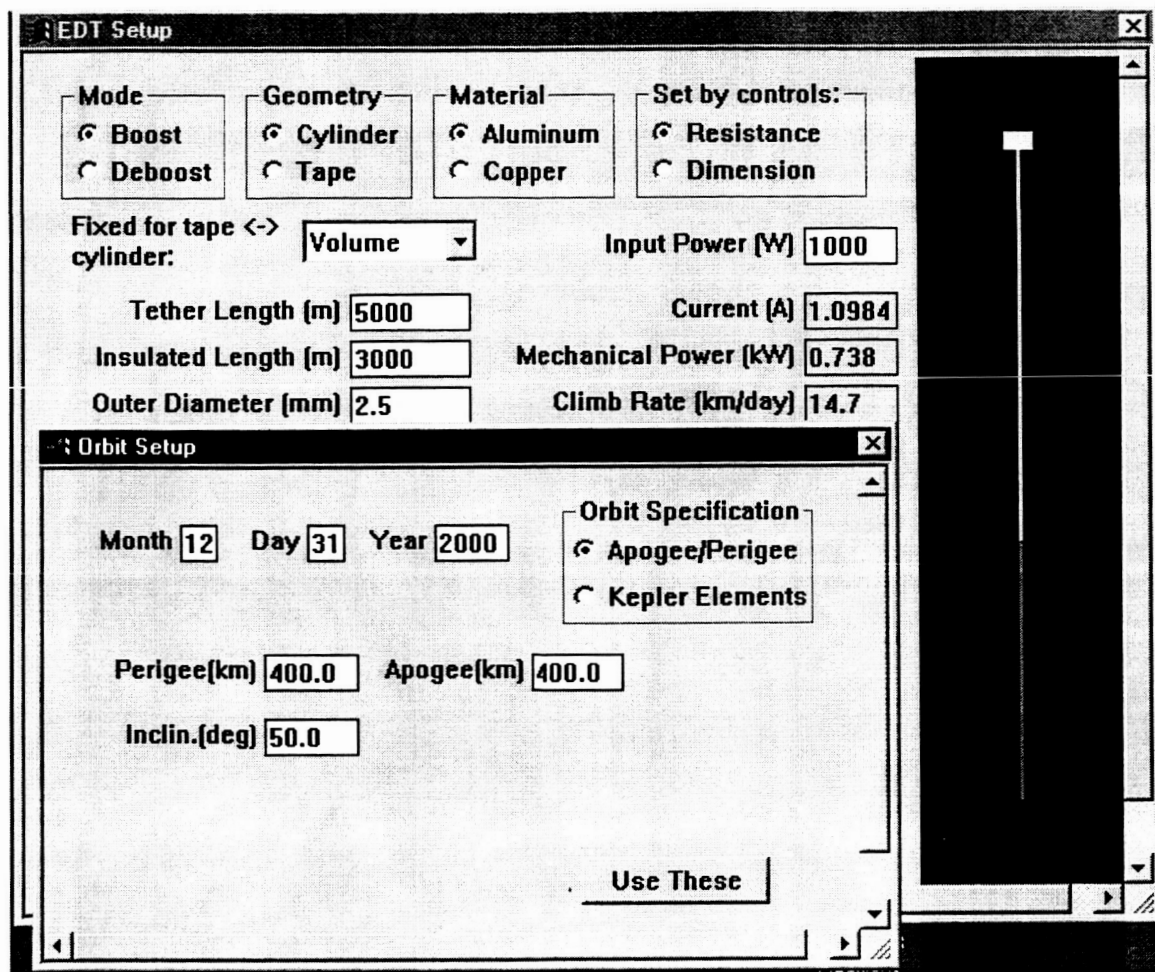


Figure 130 Starting orbit setup window with boost system setup in background.

Based on the parameters selected the software can run simulations of an EDT (assumed aligned with the local vertical) that climbs or descends starting from a specified orbit. The simulation is done in a piece-wise fashion by successive altitude intervals in order to expedite the run.

Multiple simulation runs can be made and shown on the same plot to compare different systems or the performance of the same system under different conditions (starting orbit and/or date). The results can be displayed either as the heights of the apogee and perigee vs. time or as the semi-major axis vs. time. This software tool is user friendly, quick to execute, and results are rather accurate. The only substantial difference from a full-blown simulator is that this software assumes the tether to be straight and along the local vertical as it neglects the tether dynamics.

PAPERS PUBLISHED OR PRESENTED AT CONFERENCES

A list of papers related to this Grant published in peer-reviewed Journals (underlined) and in Conference Proceedings is as follows:

1. Lorenzini, E.C., R.D. Estes, M.L. Cosmo and J. Pelaez "Dynamical, Electrical, and Thermal Coupling in a New Class of Electrodynamical Tethered Satellites." Advances in the Astronautical Sciences, Vol. 102, pp. 1333-1344, *Spaceflight Mechanics 1999*.
2. Gilchrist, B.E., Les Johnson, Sven G. Bilen, Enrico Lorenzini and Nestor R. Voronka, "System Considerations of Electrodynamical-Tether Propulsion Technology and Future Plans." *Procs. of the International Propulsion Technology Conference*, Japan 1999.
3. Johnson, L., B. Gilchrist, R.D. Estes, E.C. Lorenzini, "Overview of Future NASA Tether Applications." Advances in Space Research, Vol. 24, No. 4, pp. 1055-1063, 1999.
4. Johnson, L., R.D. Estes, E.C. Lorenzini, M. Martinez-Sanchez and J. Sanmartin, "Propulsive Small Expendable Deployer System Experiment." Journal of Spacecraft and Rockets, Vol. 37, No. 2, pp. 173-176, 2000.
5. Estes, R.D., E.C. Lorenzini, J. Sanmartin, J. Pelaez, M. Martinez-Sanchez and L. Johnson, "Bare Tethers for Electrodynamical Spacecraft Propulsion." Journal of Spacecraft and Rockets, Vol. 37, No. 2, 205-211, 2000.
6. Pelaez, J., E.C. Lorenzini, O. Lopez-Rebollal and M. Ruiz, "A New Kind of Dynamic Instability in Electrodynamical Tethers." The Journal of the Astronautical Sciences Vol. 48, No. 4, 449-476, 2000.
7. Estes R.D. and E.C. Lorenzini, "Performance and Dynamics of an Electrodynamical Tether." *Proceedings of the AIAA 38th Aerospace Sciences and Exhibit*, Reno, Nevada, 10-13 January 2000, Paper AIAA 2000-0440, AIAA, Washington, DC.
8. Sanmartin, J., R.D. Estes, E.C. Lorenzini, "Efficiency of Different Types of ED-Tethers." *Proceedings of Space Technology & Applications International Forum (STAIF-2001)*, Albuquerque, NM, 11-15 February 2001.

9. Estes, R.D., J. Sanmartin, E.C. Lorenzini, "Short Tethers for Electrodynamic Thrust." *Proceedings of Space Technology & Applications International Forum (STAIF-2002)*, Albuquerque, NM, 3-7 February 2002, AIP publication.
10. Pelaez, J., M. Ruiz, O. Lopez-Rebollal, E.C. Lorenzini and M.L. Cosmo, "Two-bar Model for the Dynamics and Stability of Electrodynamic Tethers." *Journal of Guidance, Control and Dynamics*, Vol. 25, No. 6, 1125-1135, 2002.
11. Cosmo, M.L., J. Ashenberg and E.C. Lorenzini, "Modeling and estimation of ProSEDS decay." *Procs. of 13th AAS/AIAA Space Flight Mechanics Meeting*, Paper AAS 03-216, 9-13 February 2003, Ponce, Puerto Rico.
12. Lorenzini, E.C., K. Welzyn, M.L. Cosmo, "Expected deployment Dynamics of ProSEDS." *Procs. of 39th AIAA/ASME/SAE/ASEE Joint Propulsion Conference*, July 20-23, 2003, Huntsville, Alabama.
13. Sanmartin, J., E.C. Lorenzini, R.D. Estes, M. Charro, M.L. Cosmo, "Analysis of ProSEDS Test of Bare-Tether Collection." *Procs. of 39th AIAA/ASME/SAE/ASEE Joint Propulsion Conference*, July 20-23, 2003, Huntsville, Alabama.
14. Johnson, L., Gilchrist, B., Lorenzini, E., Stone, N. and Wright, K. "Propulsive Small Expendable Deployer System (ProSEDS) experiment: Mission Overview and Status." *39th AIAA/ASME/SAE/ASEE Joint Propulsion Conference*, Huntsville, Alabama, 20-23 July 2003, Paper AIAA-2003-5094.

REFERENCES

- ¹ J.R. Sanmartin, M. Manuel-Martinez, and E. Ahedo, "Bare Wire Anodes for Electrodynamic Tethers." J. of Propulsion and Power, Vol. 9, No. 3, 353-360, 1993.
- ² R.D. Estes, J.R. Sanmartin, and M. Martinez-Sanchez, "Performance of Bare-Tethers Systems Under Varying magnetic and Plasma Conditions." J. of Spacec. and Rockets, Vol. 37, No. 2, 197-204, 2000.
- ³ Estes, R.D., E.C. Lorenzini, J.R. Sanmartin, M. Martinez-Sanchez and N.A. Savich, "New High-Current Tethers: A Viable Power Source for the Space Station?," Smithsonian Astrophysical Observatory, White Paper, December 1995.
- ⁴ L. Johnson, R.D. Estes, E. Lorenzini, M. Martinez-Sanchez and J. Sanmartin "Propulsive Small Expendable Deployer System Experiment." J. of Spacec. and Rockets, Vol. 37, No. 2, 173-176, 2000.
- ⁵ R.D. Estes, J.R. Sanmartin, "Cylindrical Langmuir probes beyond the orbital-motion-limited regime." Physics of Plasmas, Vol. 7, No. 10, 4320-4325, 2000.
- ⁶ E.C. Lorenzini, R.D. Estes, M.L. Cosmo and J. Pelaez, "Dynamical, Electrical and Thermal Coupling in a New Class of Electrodynamic Tethered Satellites." *Advances in the Astronautical Sciences*, Spaceflight Mechanics 1999, pp. 1333-1344, American Astronautical Society 1999.
- ⁷ J. Pelaez, E.C. Lorenzini, O. Lopez-Rebollal and M. Ruiz, "A new kind of dynamic instability in electrodynamic tethers." Procs. of the 10th AAS/AIAA Space Flight Mechanics Meeting, Paper AAS 00-190, Clearwater, Florida, January 23-26, 2000.
- ⁸ J. Pelaez, M. Ruiz, O. Lopez-Rebollal, E.C. Lorenzini and M.L. Cosmo, "A two-bar model for the dynamics and stability of electrodynamic tethers." Procs. of the 10th AAS/AIAA Space Flight Mechanics Meeting, Paper AAS 00-188, Clearwater, Florida, January 23-26, 2000.
- ⁹ E.C. Lorenzini (PI), et al., "Analytical Investigation of the Dynamics of Tethered Constellations in Earth Orbit (Phase II)", NASA Final Report, Contract NAS8-36606, pp. 1-160, May 1994.
- ¹⁰ E.C. Lorenzini, S.B. Bortolami, C.C. Rupp and F. Angrilli, "Control and Flight Performance of Tethered Satellite Small Expendable Deployment System-II," J. of Guidance, Control, and Dynamics, Vol. 19, No. 4, 1148-1156, 1996.
- ¹¹ J. Glaese, R. Issa and P. Lakshmanan, "Comparison of SEDS-I pre-flight simulations and flight data" Paper AIAA 93-4766, Procs of AIAA Space Programs and Technology Conference, Huntsville, AL September 1993.
- ¹² J. Smith, NASA/MSFC, email communication, May 2001.
- ¹³ E.C. Lorenzini et al., "The Propulsive Small Expendable Deployer System (ProSEDS)." Annual Report #1, NASA Grant NAG8-1605, September 2000.
- ¹⁴ E.C. Lorenzini et al. "The Propulsive Small Expendable Deployer System (ProSEDS)." Annual Report #2, NASA Grant NAG8-1605, July 2001.
- ¹⁵ J. Pelaez, E.C. Lorenzini, O. Lopez-Rebollal and M. Ruiz, "A New Kind of Dynamic Instability in Electrodynamic Tethers." The Journal of the Astronautical Sciences Vol. 48, No. 4, 449-476, 2000.
- ¹⁶ E.C. Lorenzini et al. "The Propulsive Small Expendable Deployer System (ProSEDS)." Annual Report #3, NASA Grant NAG8-1605, July 2002.
- ¹⁷ J.R. Sanmartin, R.D. Estes, and E.C. Lorenzini, "Efficiency of Different Types of ED Tether Thrusters." Procs. of the STAIF-2001 Conference, Reno, Nevada, February 2001.